idc Machining Science.

The University Of Sheffield.

Tool Wear Characterisation and Parameter Optimisation in Micro-manufacturing Processes

By:

Lisa Alhadeff

November 2019

A thesis submitted in partial fulfilment of the requirements for the degree of Doctor of Philosophy

The University of Sheffield

Faculty of Engineering

Department of Mechanical Engineering

The highest forms of understanding we can achieve
are laughter and human compasssion.

— Richard P. Feynman

For David, who inspired me to become an engineer. It was an honour.

1967 - 2018

ABSTRACT

Increases in demand for miniaturised static parts, actuators and devices has presented challenges in machining; requiring fast advancement in the field. This work examines two processes: Wire Electrical Discharge Machining (WEDM), and micro-milling. While very different processes, both of these have in common the fact that their behaviour and the phenomena seen differ from those seen in conventional subtractive machining. Capability of machine tools has increased to allow highly intricate parts to be produced, but there are significant challenges in achieving excellent surface finish, geometrical accuracy and tool life.

WEDM is appropriate for cutting complex shapes without long set-up times, but cutting very thin workpieces represents difficulties in achieving stable machining, while the process results in a recast layer which can affect wear and transmission. This work focuses on investigating optimal parameters for machining micro-gears. This has traditionally been challenging because the limited area for spark generation between wire and workpiece leads to unstable machining, resulting in poor machining rate and surface finish. Investigations into significant machining parameters have taken place, followed by a feasibility study cutting brass gears of 0.3 mm thickness. The results indicate that the depth of the recast layer can be minimised while maintaining an acceptable Material Removal Rate (MRR), by considering gear geometry. This work suggests that WEDM is a valuable tool in prototyping miniature gears.

Micro-milling allows small, accurate parts to be produced, but micro-tools wear quickly and unpredictably, therefore tool wear is difficult to measure. This results in a high rate of tool changes and reduced productivity. A protocol for measuring tool wear has been produced to allow a common method to be used across research institutes. This presents a method for analysing and reporting micro-mill tool wear which will allow transfer between research institutions and industry, to extend tool life and improving process efficiency. This protocol has then been used to investigate tool coatings on the micro scale, and compare the tribological processes seen on micro-tools to their macro counterparts. This work has resulted in extended tool life for industrial micro-mills and has been applied to industrial situations.

PUBLICATIONS

Some ideas and figures have appeared previously in the following publications:

[1] L. Alhadeff, D. Curtis, M. Marshall, and T. Slatter. 'The Application of Wire Electrical Discharge Machining (WEDM) in the Prototyping of Miniature Brass Gears.' In: *Procedia CIRP* 77 (2018), pp. 642–645.

[2] L. Alhadeff, M. Marshall, and T. Slatter. 'Wear data for trials machining brass, titanium grade 2 and Hastelloy in order to characterize wear of micro-tools.' In: *Data in Brief* (2018).

[3] L. Alhadeff, M. Marshall, D. Curtis, and T. Slatter. 'Protocol for tool wear measurement in micro-milling.' In: *Wear* 420 (2019), pp. 54–67.

[4] L. Alhadeff, M. Marshall, and T. Slatter. 'Applying Experimental Micro-tool wear Measurement techniques to Industrial Environments.' In: *IMechE Part B* (Under Review).

[5] L. Alhadeff and T. Slatter. 'A Straightforward and Low-cost Pre-inspection Measurement Method for Small Gears.' In: *Manufacturing Letters* (2020).

[6] L. Alhadeff, M. Marshall, and T. Slatter. 'The influence of tool coating on the length of the normal operating region (steady-state wear) for micro end mills.' In: *Precision Engineering* (2019).

> *The rule is, jam to-morrow and jam yesterday – but never jam to-day.*
>
> — adapted by Lewis Carroll

ACKNOWLEDGMENTS

Acknowledgements go to the Engineering and Physical Sciences Research Council, for funding this research. Long may they continue to fund cutting-edge research.

I would like to thank my supervisors, Tom Slatter, David Curtis and Matt Marshall. Tom, for is overarching presence throughout the process, Dave, for his machining knowledge, and Matt for the contributions to publications, providing an alternative perspective.

It is worth mentioning numerous anonymous academics who have reviewed my work and provided constructive feedback. Whilst they are not known, this is the basis of progression in research. I would also like to Acknowledge Paul Rigden, Amber Bennett, Beth Cousins and Matt Young, without whom I could not have navigated the intricacies of the machining trial process; and Steve Neil for his long term commitment to collaboration and contributions to my research.

I am indebted to my parents for instilling in me a desire to succeed, but also to love, and to care about everything that I invest in, to Kate and Sophie, for being my team-mates through the good and the bad and to all six of my grandparents, whose unequivocal belief in my success is both terrifying and inspiring.

Finally, thank you to my husband, Alistair - the love of my life, who has provided unwavering support not just over the duration of my thesis, but for as long as I can remember.

CONTENTS

I INDUSTRIAL AND ACADEMIC MOTIVATION

1 INTRODUCTION 3
1.1 Research Motivation and Novelty . . . 3
1.2 Machining of Ferrous and Non-ferrous Materials . . . 4
1.2.1 Steel and its Role Herein . . . 5
1.2.2 Titanium in Aerospace and Medical Engineering . . . 5
1.2.3 Nickel Superalloys . . . 7
1.2.4 Brass and Bronze . . . 8
1.2.5 Aluminium . . . 10
1.3 Watches and Their Role as a Test-piece . . . 10
1.4 Aim and Objectives . . . 11
1.5 Limitations of Scope (for mechanical watches to be made in the UK) 12
1.5.1 Equipment Limitations . . . 12
1.5.2 Limitations in Funding . . . 12
2 LITERATURE REVIEW 13
2.1 Processes of Interest . . . 13
2.1.1 Working Principles of Wire Electrical Discharge Machining (WEDM) . . . 13
2.1.2 Important Parameters in WEDM . . . 16
2.1.3 Micro-milling Process . . . 18
2.1.4 Size Effect . . . 22
2.2 Current Research Trends in WEDM . . . 24
2.2.1 Process Outcomes . . . 24
2.2.2 Surface Finish . . . 25
2.2.3 White Layer . . . 30
2.2.4 Miniature Gears . . . 31
2.2.5 Directions in the Field and Research Gaps . . . 32
2.3 State-of-the-Art in Micro-milling . . . 33
2.3.1 Tool Wear . . . 34
2.3.2 Chip and Burr Formation . . . 35
2.3.3 Further Development of the Field . . . 35

II FUNDAMENTAL RESEARCH INTO PROCESSES

3 EXPERIMENTAL METHODS 39
3.1 WEDM . . . 39
3.1.1 Machining Process . . . 39
3.1.2 Analysis of Surface Finish . . . 40
3.1.3 Analysis of White Layer . . . 41
3.1.4 Profile Fidelity . . . 44
3.2 Micro-milling . . . 53
3.2.1 Machining Process . . . 53
3.2.2 Measurement of Tool Wear . . . 55
3.2.3 Measuring Cutting Forces . . . 56

4 OPTIMISING MACHINING PARAMETERS IN WEDM 57
4.1 Application of WEDM in Micromechanical Systems 57
4.2 Assessment of Capability for Producing Small Gears 58
4.2.1 Machining Process and Testing 59
4.2.2 Results and Discussion 61
4.2.3 Conclusions and observations for further trial considerations 68
4.3 Development of Optimum Machining Parameters 70
4.3.1 Introduction 70
4.3.2 Machining Process/Details of Experimentation 71
4.3.3 Results and Discussion 72
4.3.4 Conclusions 81
4.4 Multi-pass methods for Producing a High Quality Surface in WEDM 83
4.4.1 Existing Work 84
4.4.2 Machining Process 84
4.4.3 Results and Discussion 86
4.4.4 Conclusions 88
4.5 Viability of the WEDM for Prototyping Small Gears 89
5 DEVELOPMENT OF A PROTOCOL FOR MEASUREMENT OF MICRO-END-MILL TOOL WEAR 91
5.1 Introduction 91
5.1.1 Wear and wear measurement for micro-tools 92
5.1.2 A need for a common method 93
5.2 Preliminary Study 94
5.3 Development of a Protocol 96
5.3.1 Purpose 96
5.3.2 Definitions 97
5.3.3 Materials: using sliding distance as a measure of distance cut 97
5.4 Wear Measurement Protocol 98
5.4.1 Tool and Workpiece Preparation 98
5.4.2 Measurement of Tool 99
5.4.3 Measurement of Slot Profiles 99
5.4.4 Criteria for Tool Life 100
5.4.5 Test Procedure 101
5.4.6 Reporting of Results 102
5.5 Validation Tests 103
5.5.1 Materials and Method 103
5.5.2 Results 104
5.6 Reflection on Protocol 111
5.6.1 Improvement of new method over tool diameter 111
5.6.2 Efficacy of measuring slot profiles as a post-machining tool wear measurement technique 111
5.6.3 Sliding distance vs. Cutting distance 112
5.6.4 Direct tool measurement vs. Slot measurement 114
5.6.5 Rake face wear vs. Cutting Forces 114
5.6.6 Force Signature - uneven engagement of teeth 116
5.6.7 Mechanism of tool breakage 117

5.6.8 Considering alternative coatings: an early investigation into extending tool life through tool coatings 119
5.7 Conclusions 119
6 INVESTIGATING TOOL COATINGS AS A MEANS OF EXTENDING MICRO-END-MILL LIFE 121
6.1 Introduction 121
6.1.1 Definitions 121
6.1.2 Existing Studies into Tool Wear of Micro-milling 123
6.1.3 The use of Coatings in Macro- and Micro-milling 125
6.1.4 Expected Wear 128
6.1.5 Motivations for Current Work 129
6.2 Methodology 129
6.3 Results 132
6.3.1 Sources of Error 133
6.3.2 Comparison between TiB_2 tools and an AlTiN coating for CuZn38 brass 134
6.3.3 Comparison between AlTiN coated tools and TiAlN/TiSiN for cutting titanium grade 2 134
6.3.4 Comparison between AlTiN coated tools and AlTiCrN for cutting Hastelloy 135
6.3.5 Relative wear of AlTiN coated tools across materials 136
6.4 Discussion 137
6.4.1 Relationship between SSR and running in period as a measure of tool performance 137
6.4.2 Coating Performance and Wear for Brass 138
6.4.3 Coating Performance and Wear for Titanium 139
6.4.4 Coating Performance and Wear for Hastelloy 140
6.4.5 Differences between wear mechanisms seen in micro and macro 142
6.5 Conclusions 152
7 INVESTIGATING MODIFIED GEOMETRIES AS A MEANS OF EXTENDING MICRO-END-MILL LIFE 155
7.1 Edge Radius in Macro- and Micro-milling 155
7.2 Justification for Trial 157
7.2.1 Trial Design 157
7.3 Experimental Set-up 158
7.3.1 Measurements Taken 159
7.3.2 Analysis 159
7.4 Results 159
7.4.1 Titanium - Edge Radius Vs Sharp 159
7.4.2 Steel - Edge Radius Vs Sharp 160
7.4.3 Hastelloy - Edge Radius Vs Sharp 161
7.4.4 Cutting Forces - Feed Force 162
7.5 Discussion 162
7.5.1 Note on Quality of Results 163
7.5.2 Future Work 164
7.6 Conclusions 164

III RE-APPLICATION OF FUNDAMENTAL RESEARCH TO INDUSTRY

8 WEDM OF GEARS FOR MICROMECHANICAL WATCHES 167
8.1 Introduction 167
8.1.1 Aims 168
8.2 Experimental Procedures 168
8.2.1 Fixturing 172
8.2.2 Evaluation 172
8.3 Results and Discussion 173
8.3.1 Effects of Parameters on White Layer 173
8.3.2 Effects of Parameters on Surface Finish 176
8.3.3 Relationship between White Layer Depth and Surface Finish 181
8.3.4 Notes on White Layer Depth and Surface Finish across Tooth Geometry 181
8.4 Conclusions 182
9 APPLYING STRAIGHT CUT MEASUREMENTS TO INDUSTRIAL ENVIRONMENTS 185
9.1 Introduction 185
9.1.1 Fundamental Studies and Transfer to Industry 185
9.1.2 Tool Wear Measurement On- and Off-line 186
9.1.3 Tool Wear Measurement Protocol 187
9.1.4 Purpose of Work 190
9.2 Experimental Methods 190
9.2.1 Testing Process 192
9.3 Results and Discussions 193
9.3.1 Cutting Forces 193
9.3.2 Tool Wear 198
9.3.3 Industrial Outcomes 203
9.4 Conclusions 204
10 CONCLUSIONS 205
10.1 Introduction 205
10.2 Wire Electrical Discharge Machining - Key Outcomes and Conclusions 205
10.2.1 Outcomes 205
10.2.2 Academic Impact of Research into WEDM 206
10.2.3 Industrial Relevance and Impact of Research into WEDM . 206
10.2.4 Limitations 206
10.2.5 Future Work 207
10.3 Micro-milling - Key Outcomes and Conclusions 208
10.3.1 Outcomes 208
10.3.2 Academic Impact of Micro-milling Research 210
10.3.3 Industrial Relevance and Impact of Micro-milling Research 210
10.3.4 Limitations 210
10.3.5 Future Work 211
10.4 Formal Statement of Novelty 211

IV BIBLIOGRAPHY

BIBLIOGRAPHY 215

LIST OF FIGURES

Figure 0.1 The locations of catapaults centres in the UK xxxi
Figure 1.1 Primary and Secondary deformation zones in metal cutting. 6
Figure 1.2 Schematic of the tool showing rake face and flank, as well as rake angle. 9
Figure 1.3 Types of chip that occur when machining material: (a) - a continuous chip, which often occurs in ductile materials in low friction situations. (b) - a built-up-edge (BUE) chip, where a portion of the chip adheres to the rake face and is later deposited on the material surface. (c) - a discontinuous chip, which occurs in more brittle materials. (d) - a serrated, sawtooth or semi-continuous chip, where regions of high and low shear stress cause the chip to shear. 9
Figure 1.4 The typical geometry of a watch bridge 11
Figure 2.1 The spark gap is shown between the wire (small purple circle) and the workpiece (large blue circle). 14
Figure 2.2 The WEDM Setup. The water jet is used to feed the wire that comes from a roll, through the machine bed and to the rollers at the bottom. 14
Figure 2.3 The plasma theory for how an EDM works. The workpiece is shown at the bottom of the image, the wire is at the top. In this instance, the wire acts as the positive electrode. . . 15
Figure 2.4 Schematic of two EDM pulses. T_{on} denotes pulse-on time, T_{off} pulse off time, t_d ignition delay time, V_0 open circuit voltage, $\overline{VG}$ average machining voltage, t_r current rise time, t_f current fall time, i average discharge current and i_{max} maximum discharge current. 18
Figure 2.5 A milling tool with respect to the workpiece in axes x, y and z. 18
Figure 2.6 Schematic of a milling tool cutting a workpiece. 19
Figure 2.7 The two types of macro mill. Image Courtesy of Mano DIY parts (www.manomano.co.uk) 19
Figure 2.8 Down (Climb) milling and Up (conventional) milling. . . . 20
Figure 2.9 Four commonly used types of milling cut. 20
Figure 2.10 Typical geometry of a micro-milling tool. 21
Figure 2.11 (a) shows a macro-tool (zoomed out) and (b) shows a micro-tool (zoomed in). Although both tools have the same cutting edge radius at the start of machining, the cutting edge radius for the micro tool is typically much closer to the depth of cut than for the macro tool. 23
Figure 2.12 Grain sizes relative to tool size 24
Figure 2.13 Surface profile from which R_a value is obtained. 25
Figure 2.14 Path followed by wire for finish cut. 29

Figure 2.15 The trim cut reduces the white layer depth without cutting into the bulk material. 29
Figure 2.16 Gear Quality Measures: these include profile error, pitch error, lead error and runout. 31
Figure 3.1 | 1. Guard | 2. Wire | 3. Tension control | 4. Wire cutter (spark) | 5. Wire collection | 6. Lower tension control | 7.Wire spool | 8. Guide rollers | 9. Machine bed | 10. Dielectric fluid tank | 39
Figure 3.2 Clamping system for workpieces. | 1. Dial gauge for squaring workpiece | 2. Pre-drilled workpiece | 3. Clamps | 4. Water jet for threading | 40
Figure 3.3 Working principles of Alicona optical profilometers. . . . 41
Figure 3.4 An example of the crater-like structure observed after a cut with a WEDM. Each crater (highlighted in red) represents an area melted by a single spark. 42
Figure 3.5 Optical measurement of white layer depth, w_d. 43
Figure 3.6 Photos of a straight cut testpiece taken optically, and SEM micrographs of a straight-cut testpiece. 43
Figure 3.7 Profile errors, characterised by a deviation from the nominal profile. These increase noise. 44
Figure 3.8 Lead errors, a linear deviation along the face of the tooth. This affects load-carrying capacity. 45
Figure 3.9 Pitch error, the difference between nominal angular location and actual measured location. This affects motion transfer. 45
Figure 3.10 Runout, radial displacement of gear teeth which is cumulative across teeth. This affects motion transfer. 45
Figure 3.11 Thresholding with a red and green background. 51
Figure 3.12 Image analysis method for determining profile errors in gears. 52
Figure 3.13 (a) shows the workpiece mounted onto the load cell, (b) shows the slotting process that was carried out. 54
Figure 3.14 Measurement angle for tools in early studies. 55
Figure 3.15 Tools were measured face on (left) and side on (right) to determine wear. 56
Figure 3.16 Schematic of the force measurement setup 56
Figure 4.1 Clamping of the workpiece. 60
Figure 4.2 The yellow surface shows the machined part of the brass (the top and bottom faces of the gear are unmodified from the original gear blank). 60
Figure 4.3 The two possible errors in profile measured: missing material (a), and extra material (b). 62
Figure 4.4 Error in profile that occurs as gear falls from workpiece. . 63
Figure 4.5 Graphical representation of the profile error for a gear with pitch diameter 6 mm and 18 teeth. 63

Figure 4.6 The Coordinate Measuring Machine (CMM) image and Computer Aided Design (CAD) file overlaid. The CMM image is be identified by the burr on one of the teeth. . . . 64
Figure 4.7 Measurement of white layer using optical measurement software for a microscope with 50x magnification. 66
Figure 4.8 White layer plotted against position for three different gear teeth on 18 tooth gear. 67
Figure 4.9 White layer plotted against position for two different gear teeth on 12 tooth gear. 68
Figure 4.10 A normal Q-Q plot of standardised residuals shows that the data meets normality assumptions since the points fall along a straight line.. 74
Figure 4.11 A Pareto Plot of Main Effects. Factors which extend beyond the significance line (dotted) have a significant effect on R_a. 75
Figure 4.12 (a) shows a surface machined with a low IP, (b) shows a surface with a higher IP and (c) allows comparison between the two. It can be seen from the relative scales that craters machined with a higher IP are typically both deeper and wider. 76
Figure 4.13 $R_a$value for each gear at the two different levels of current (8 gears are machined per level). 77
Figure 4.14 Estimated marginal means to show interaction between IP and T_{off}. 77
Figure 4.15 Main effects plot for R_a. A steep gradient indicates a relationship between parameter and output. 78
Figure 4.16 A Pareto Plot of Main Effects. Factors which extend beyond the significance line (dotted) have a significant effect on R_a. 80
Figure 4.17 Main effects plot for R_a 80
Figure 4.18 Micro-cracking of the machined surface can be seen. . . . 81
Figure 4.19 The effect of carrying out a second, sub-wire-width pass without changing other parameters. Errors can be propagated from quoted calibration errors to be .approximately 0.3 µm. 83
Figure 4.20 Path followed by EDM for finishing cuts. 84
Figure 4.21 Cuts made with changing machining parameters. 85
Figure 4.22 Four-pass cutting of the workpiece. 86
Figure 4.23 Effects of parameters on surface finish. 87
Figure 4.24 Surface finishes with finishing passes. 88
Figure 4.25 Surface finish with finishing passes. The bars show the four passes: rough cut on the left hand side and subsequent passes moving rightwards. A smoother finish (lower R_a) can be seen with each pass. 88
Figure 5.1 Wear of 0.5mm micro-end-mills cutting CuZn38. The wear is given in terms of total reduction in diameter. 94
Figure 5.2 The two orientations in which tools were measured. . . . 95

Figure 5.3 An example of multiple types of wear occurring - here, VB and KT2 can be seen in purple, while CH and KT1 are seen in red, and VB is seen in blue. 95
Figure 5.4 Types of Wear - graphical representation. 96
Figure 5.5 Path taken by milling cutter with tool starting and finishing clear of the work piece. 98
Figure 5.6 Image of the workpiece sectiond perpendicular to direction of cut. Cross section of the slots machined can be seen. 100
Figure 5.7 Cross-section of slots machined measured using profilometer. 100
Figure 5.8 Slot profile measurement parameters. D_T represents total theoretical depth, D_A is actual measured depth. W_{BT} is the theoretical width of the base of the slot and W_B is the actual measurement. 100
Figure 5.9 Forces exerted on the micro end mill. 102
Figure 5.10 An example of the way in which results should be reported: the y-axis is represented both in terms of sliding distance and in terms of number of cuts. 103
Figure 5.11 Schematic of the force measurement setup. 104
Figure 5.12 Tool wear curve measured for face wear of tool used to machine Hastelloy C-276. Red points indicate how much smaller new tool is compared to manufacturer stated size 500 µm. Starting size is shown with dotted line. 105
Figure 5.13 The force signature for the tool used to machine Hastelloy C-276. 106
Figure 5.14 Tool wear curve measured for outside edge wear of tool used to machine Hastelloy C-276. The dotted horizontal line represents a baseline - tools were measured and discrepancy between actual size and manufacturer stated measurement. These points are differentiated as red. . . . 106
Figure 5.15 Tool wear curve measured for outside edge wear of tool used to machine Hastelloy C-276. Red points indicate how much smaller new tool is compared to manufacturer stated size of 500 µm. 107
Figure 5.16 Tool wear curve measured for face wear of tool used to machine Ti grade 2. Red points indicate how much smaller new tool is compared to manufacturer stated size 500 µm. Starting size is shown with dotted line. 108
Figure 5.17 Tool wear curve measured for outside edge wear of tool used to machine Ti grade 2. Red points indicate how much smaller new tool is compared to manufacturer stated size 500 µm. Starting size is shown with dotted line. 109
Figure 5.18 Tool wear curve measured for flank wear of tool used to machine Ti grade 2. Red points indicate how much smaller new tool is compared to manufacturer stated size 500 µm. Starting size is shown with dotted line. 109

Figure 5.19 Rake face wear for uncoated and coated tools used to machine brass. CF indicates catastrophic tool failure. Red points indicate how much smaller new tool is compared to manufacturer stated size 500 µm. 110
Figure 5.20 Tool wear curve measured using slot dimensions for Ti grade 2. 112
Figure 5.21 Possible sources of error when measuring slots. 112
Figure 5.22 Comparison between using sliding distance and cutting distance. 113
Figure 5.23 Relationship between tool and slot measurement. 114
Figure 5.24 Wear in relation to cutting forces for a tool used to cut Hastelloy C-276. 115
Figure 5.25 Wear in relation to cutting forces for a tool used to cut Ti grade 2. 116
Figure 5.26 The fit made using the second term of the Fourier series. . 116
Figure 5.27 Effect of runout is magnified for a smaller tools. 117
Figure 5.29 Chips produced in machining. 118
Figure 5.28 Grain sizes relative to tool size. 118
Figure 5.30 A serrated-type or discontinuous chip. 119
Figure 6.1 Wear curves of two different tools. 122
Figure 6.2 A schematic to show the relationship between position on tool wear curve and predictability of the tool's wear. The step function shows that predictability is either high or low, and occurs in the steady state region. It is longer for the tool with the black wear curve. 122
Figure 6.3 A schematic to show the relationship between position on tool wear curve and surface finish quality of machined part. The tool with the longer steady state region produces a good surface finish for much longer, as shown by the larger area under the curve. 123
Figure 6.4 Micro mill measured using an SEM in two orientations. Where tools were uncoated, abrasive wear dominated. . . 128
Figure 6.5 Example of the relatively large grain size in relation to tooth size end edge radius. 128
Figure 6.6 The tools were measured in the two orientations shown, with rake face and flank wear considered from the end-on perspective, and chipping considered from the side-on perspective. 131
Figure 6.7 Flank wear is denoted VB, while rake face wear is denoted KT. 132
Figure 6.8 If one or both teeth were lost, catastrophic failure (CF) was indicated. 132
Figure 6.9 Schematic of the UMT used to carry out pin-on-disc testing of the samples. 133
Figure 6.10 Tool wear plotted for tools used to machine brass with different coatings (TiB_2 and AlTiN). CF indicates catastrophic failure of the tool. 134

Figure 6.11 Rake face wear for tools used to machine titanium grade 2. TH coating is TiAlN/TiSiN. 135
Figure 6.12 Flank wear for tools used to machine titanium grade 2. TH coating is TiAlN/TiSiN. 135
Figure 6.13 Rake face wear for tools used to machine Hastelloy. TX coating is AlTiCrN. 136
Figure 6.14 Flank wear for tools used to machine Hastelloy. TX coating is AlTiCrN. 136
Figure 6.15 Relative rates of rake face wear for the three materials tested, with the original AlTiN coating. 137
Figure 6.16 Adhesion can be seen on the tool, especially in the form of adhered chips. There is also some sign of residual adhered material. 139
Figure 6.17 Three images of teeth: (a) and (b) are the front-on and side-on views for TH-coated tool, while (c) is the front-on view for an AlTiN coated tool. 140
Figure 6.18 Examples of micro-chipping to the coating, exposing the tool underneath (a). 140
Figure 6.19 (a) shows three different tools with interesting wear mechanisms. These can be seen zoomed in, in (b). 142
Figure 6.20 Friction coefficient for the four coatings over 1m of sliding distance. 143
Figure 6.21 Wear of AlTiN coated discs when rubbed in a reciprocating sliding motion. Observed optically after 2, 5, 10, 20 and 50 runs. Some types of wear are highlighted. 144
Figure 6.22 Wear to TiB_2 tools in the form of abrasion and chipping/notching. 145
Figure 6.23 Wear of discs coated with TiB_2 when rubbed in a reciprocating sliding motion. Observed optically after 2, 5, 10, 20 and 50 runs. Some types of wear observed are highlighted here. 146
Figure 6.24 Wear of discs coated with TiAlN/TiSiN when rubbed in a reciprocating sliding motion. Observed optically after 2, 5, 10, 20 and 50 runs. Some types of wear observed are highlighted here. 148
Figure 6.25 Wear of discs coated with AlTiCrN when rubbed in a reciprocating sliding motion. Observed optically after 2, 5, 10, 20 and 50 runs. Some types of wear observed are highlighted here 150
Figure 7.1 The two types of radii discussed herein are identified as (a) Corner Radius and (b) Edge Radius. 155
Figure 7.2 Types of cutting seen with tools with cutting edge radius for tools in the region where cutting edge radius is similar to cutting depth. 156
Figure 7.3 Depiction of stress distribution for (a) a sharp tool and (b) a tool with cutting edge radius introduced. 157
Figure 7.4 The two tools used in the investigation 158

Figure 7.5 (a) shows the workpiece mounted onto the load cell, (b) shows the slotting process that was carried out. 158
Figure 7.6 Orientations in which tools were measured. 159
Figure 7.7 Wear with sliding distance on the flank of the tools used to machine titanium. In both cases a long steady state region is seen and catastrophic failure is not reached. . . . 160
Figure 7.8 Wear with sliding distance on the rake face of the tools. . 160
Figure 7.9 Wear with sliding distance on the flank of the tools used to machine steel. The tool which does not have a designed edge radius wears much faster and fails catastropcially at less than 20 m of cutting in each case. 161
Figure 7.10 Wear with sliding distance on the rake face of the tools. . 161
Figure 7.11 Wear with sliding distance for the radiused tools. 162
Figure 7.12 Cutting forces plotted against sliding distance for three materials. In the case of steel and titanium, the cutting forces remain similar throughout tool life, while they increase linearly and plateau for two of the Hastelloy tools.162
Figure 8.1 A two-level factorial design. 170
Figure 8.2 Full factorial vs. half-factorial design. Measurements are made at the red circled points. 170
Figure 8.3 $\bar{x}_1$overlaps with $\bar{x}_2$, but $\bar{x}_3$overlaps with neither. 172
Figure 8.4 Fixture used to machine gears. 172
Figure 8.5 (a) an SEM image of the smaller grains in the white layer; (b) and optical image of the same. 173
Figure 8.6 Varying Surface Finish (SF) across tooth profile can be seen. Below the label 'Root' can be seen an apparently smoother surface than below either 'side' or 'top'. 173
Figure 8.7 Main effects and interactions plots for white layer depth at the root of the gear. 175
Figure 8.8 Pareto plot for significant parameters afecting white layer depth. 176
Figure 8.9 Highlighted in dark purple are (a) an example of the large irregular crater-like SF seen at the base of the teeth after the initial rough cut; (b) smaller and more regular craters visible after the finish cut. 177
Figure 8.10 Pareto plot and main effects plots for R_a and R_q. 178
Figure 8.11 Pareto plot and main effects plots for R_z. 180
Figure 8.12 Removal of only white layer using a skim cut. 181
Figure 8.14 For a smaller radius of cut (left), the craters overlap in such a way as to reduce overall surface roughness as compared to a larger radius (right). 182
Figure 8.13 (a) white layer depth for the top of a tooth (seen as smaller crystals in a slightly darker shade of grey); (b) white layer depth for the root of a tooth. 182
Figure 9.1 Commonly the mid-level TRLs are missing. Catapult centres help to bridge this gap. 186
Figure 9.2 Types of wear seen. 187

Figure 9.3 The two orientations in which tools were measured. 189
Figure 9.4 An example of the way in which results should be reported. 190
Figure 9.5 Depths to be cut for each feature. 191
Figure 9.6 Testpiece to be machined. 192
Figure 9.7 Workpiece mounted on force cell. 192
Figure 9.8 Mounting for force cell. 193
Figure 9.9 Cutting forces signatures for cuts 1 - 3 (see Figure 9.5) made with tools coated with TiB_2. 195
Figure 9.10 Cutting forces signatures for cuts 4 - 6 (see Figure 9.5) made with tools coated with TiB_2. 196
Figure 9.11 When the same cut (cut 3) is compared, differences in magnitudes of force can be seen. 197
Figure 9.12 Although there is suggestion of a wear curve in the raw data, the averaged data is not conclusive due to high uncertainty. 198
Figure 9.13 Comparison of face wear for uncoated and TiB2 coated tools. 199
Figure 9.14 Comparison of flank wear for uncoated and TiB2 coated tools. 200
Figure 9.15 Comparison of face wear for realistic cuts and straight slots. 202
Figure 9.16 Comparison of face wear for realistic cuts and straight slots, with error bounds shaded for clarity. 203

LIST OF TABLES

Table 0.1 Descriptions of TRLs taken from the catapault website. . xxx
Table 2.1 Significant Machining Parameters in WEDM 16
Table 2.2 Effect of altering different machining parameters in WEDM. Surface finish is typically measured using $R_a$values, where a smaller value denotes a better surface finish. 26
Table 3.1 Analytical methods for checking gears for form errors, and their relative uses, advantages and disadvantages. . . 48
Table 3.2 Analytical methods for checking gears for position errors, and their relative uses, advantages and disadvantages. . . 49
Table 3.3 Chemical composition of Titanium grade 2 (with major elements in **bold**). All alloying elements are an upper limit. 54
Table 3.4 Chemical composition of Hastelloy C-276 (with major elements in **bold**). 54
Table 3.5 Chemical composition of Hastelloy C-276 (with major elements in **bold**). 54
Table 4.1 Sizes and modules of gears produced. 59
Table 4.2 Profile Errors for Different Gears 61
Table 4.3 Profile roughness measurements across four different teeth. 65
Table 4.4 Mean white layers for the five teeth measured. The difference between minimum and maximum for each measurement indicates that white layer is highly variable for the set of parameters used. 66
Table 4.5 Parameters used to investigate WT, LQ, IP and T_{off}. A full factorial design was used. 71
Table 4.6 Mean and standard deviations of $\mathrm{R_a}$ and white layer for each gear machined. The parameters used to machine each gear can be identified by the run order of each gear as seen in Table 4.8. 73
Table 4.7 Parameters used for rough and finishing cuts. 85
Table 4.8 Parameters used to cut testpieces. 86
Table 5.1 Nomenclature used in this chapter. 91
Table 5.2 Types of wear: classification. 95
Table 5.3 Parameters used in machining. These were chosen based on manufacturer recommendations and titanium grade 2 was based on titanium alloys while Hastelloy was based on nickel alloys. 104
Table 6.2 Coating material properties datasheet as provided by the tooling manufacturer, ... 130
Table 6.1 Coatings used for each material and measurement intervals.130
Table 6.3 Machining parameters used to machine the three materials tested. These were consistent across different coatings. . . 130
Table 6.4 Calculated ratio of SSR to RIP for milling tools. 138
Table 7.1 Number of slots cut before measurement for each material.158

Table 8.1 The full factorial experimental parameters. 169
Table 8.2 The three rough cut parameter sets used. 169
Table 8.3 Experimental design techniques used to investigate Wire Electrical Discharge Machining (WEDM) parameters. 171
Table 8.4 The ratio of white layer to surface roughness parameters R_a and R_z was used to indicate relative thickness of white layer to surface roughness. 181
Table 9.1 Materials used, and coating used to machine each of these. 191
Table 9.2 Speeds and feeds used for machining each material. 191

NOMENCLATURE

$\varnothing$	Wire diameter, the diameter of the wire used
M_{His}	Machining history, whether roughing or finishing passes have taken place
R_a	A meaure of surface finish, determined by the arithmetic mean of the absolute values of vertical deviation from the mean line through the profile
T_{off}	Pulse-off time, the time period in which the pulse is low, or off. During this time no discharging occurs
T_{on}	Pulse-on time, the length of a machining pulse
V_s	Servo speed, the speed of an advancing axis during machining operations
C	Capacitance of pulse-generating circuit, measured capacitance of the pulse-generating circuit
Chemical affinity	The tendency of a material to react to the cutting tool due to chemical similarities between the two
Difficult-to-machine	Materials which have a low machinability, i.e. cannot be cut without difficulty
IP	Peak current, the maximum current that passes through the electrodes each pulse
LQ	Dielectric flow rate, the rate at which dielectric fluid is circulated around the tank
Pulse Energy	The energy of a pulse during WEDM. Determined by a number of input parameters
SV	Servo reference voltage, controls gap width
VG	Gap voltage, the voltage across the distance between the wire periphery and workpiece
WO	Wire offset, this is equal to wire radius plus electrical discharge gap
WS	Wire speed, the rate at which the wire is fed from the spool through the machine
WT	Wire tension, tension in the wire electrode

ACRONYMS

AMRC	Advanced Manufacturing Research Centre
ANOVA	Analysis of Variables
BSE	Backscattered Electron
BUE	Built-up Edge
CAD	Computer Aided Design
CMM	Coordinate Measuring Machine
COF	Coefficient of Friction
DAQ	Data Acquisition
DOE	Design of Experiments
DXF	Drawing Exchange Format
EDM	Electrical Discharge Machining
MRR	Material Removal Rate
MQL	Minimum Quantity Lubrication
OD	Outside Diameter
RIP	Run-in Period
SE	Secondary Electron
SEM	Scanning Electron Microscope
SF	Surface Finish
SSR	Steady-state Region
WC	Tungsten Carbide
WEDM	Wire Electrical Discharge Machining

AUTHOR'S NOTE

This work has taken place in part at the Advanced Manufacturing Research Centre (AMRC), of one of the UK's network of Catapault centres. The purpose of the catapault centres is to drive innovation in the UK by linking fundametal research to industrial applications. This can be described by Technology Readiness Levels (TRLs). The TRL of a piece of research indicates how close to full industrial application a piece of technology is, and the TRL scale consists of 9 points (described in Table 0.1). This scale has also been adapted for manufacturing.

The UK has numerous catapault centres divided into groups ranging from medical through renewable energy to transport systems. The AMRC is part of the High Value Manufacturing (HVM) catapault, whose aim is to provide economic growth through high-value specialist machining capabilities unique to the UK. The locations and descriptions of catapaults and their relevent areas is given in Figure 0.1. To help describe the contribution of this thesis to the catapault aims, technology readiness levels are given for each body of experimental work.

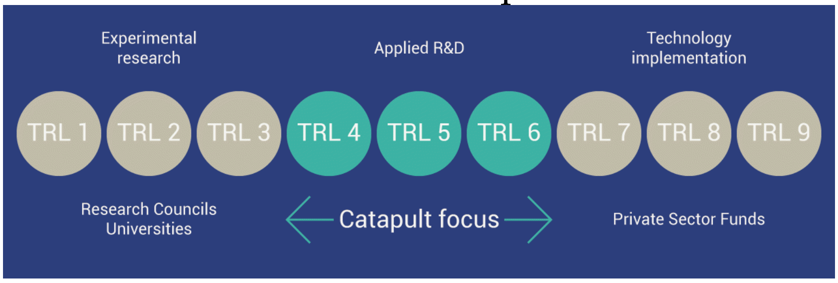
Experimental research
Applied R&D
Technology implementation
TRL 1
TRL 2
TRL 3
TRL 4
TRL 5
TRL 6
TRL 7
TRL 8
TRL 9
Research Councils Universities
Catapult focus
Private Sector Funds

TRL	Description
1	Basic principles observed and reported: scientific principles investigated
2	Technology concept and/or application formulated: Practical applications of principles considered, possibly only speculatively
3	Analytical and experimental critical function and/or characteristic proof of concept: Laboratory validations of technological predictions
4	Component and/or breadboard validation in laboratory environment: technology is tested and validated in a laboratory
5	Component and/or breadboard validation in relevant environment: Technology tested in a simulated enviroment
6	System/subsystem model or prototype demonstration in a relevant environment: Technology tested in a high-fidelity laboratory environment or simulated operational environment
7	System prototype demonstration in an operational environment: system prototype in an operational environment
8	Actual system completed and qualified through test and demonstration: technology proven to work under expected conditions. Often final stage of development
9	Actual system proven through successful mission operation: Actual application of the technology in its final form and under real-life conditions

Table 0.1: Descriptions of TRLs taken from the catapault website.

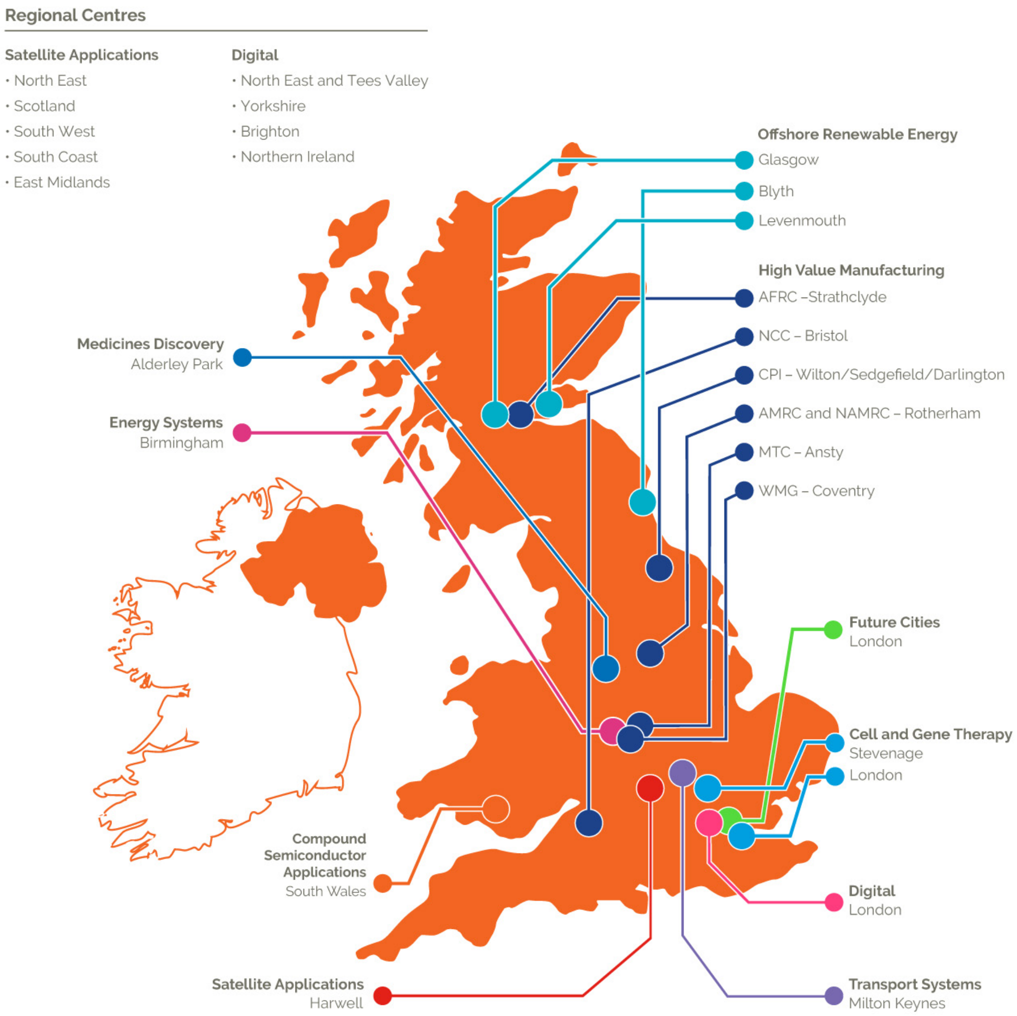
Regional Centres
Satellite Applications
• North East
• Scotland
• South West
• South Coast
• East Midlands
Digital
• North East and Tees Valley
• Yorkshire
• Brighton
• Northern Ireland
Offshore Renewable Energy
Glasgow
Blyth
Levenmouth
High Value Manufacturing
AFRC –Strathclyde
NCC – Bristol
CPI – Wilton/Sedgefield/Darlington
AMRC and NAMRC – Rotherham
MTC – Ansty
WMG – Coventry
Medicines Discovery
Alderley Park
Energy Systems
Birmingham
Future Cities
London
Cell and Gene Therapy
Stevenage
London
Compound Semiconductor Applications
South Wales
Digital
London
Satellite Applications
Harwell
Transport Systems
Milton Keynes

Figure 0.1: The locations of catapaults centres in the UK

Part I

INDUSTRIAL AND ACADEMIC MOTIVATION

This thesis is split into three parts: Part I - Industrial and Academic Motivation; Part II - Fundamental Research into Processes; and Part III - Re-applications of Fundamental Work to Industry. Due to the breadth of an investigation into multiple machining processes that lend themselves to micromachining, this allows a coherent pathway for research that is primarily motivated by academic need and secondarily motivated by industrial need. Part I sets the scene, with a description of the industrial and academic motivations, which determine the project aims. Part II describes fundamental research into the machining processes investigated. Part III then re-applies this work to a more industrial context, ensuring the validity of the research from Part II in a real-world environment, and considering the implications of this work for industry.

1

INTRODUCTION

1.1 RESEARCH MOTIVATION AND NOVELTY

Changing industrial landscapes have driven strategic shifts in research motivations since 1970 [1]. Severe economic recession combined with increasingly competitive exports [2] has meant that both emerging and advanced countries in Europe can no longer compete with the large-scale market. At the same time, environmental concerns, political agendas and sustainability legislation has added variables to the manufacturing problem [3]. A possible solution to this problem is to generate high-value exports through specialist and high-value manufacturing.

The UK Engineering and Physical Sciences Research Council has developed the "Manufacturing the Future" theme to fund the development of high-value and specialist manufacturing to help solve both economic and practical challenges to the UK currently and in the future.

With industries such as aerospace, automotive and others involved in advanced manufacturing calling for more affordable, light-weight composite materials, this creates a significant market growth opportunity for those who are able to take advantage, e.g. civil aerospace employs over 230,000 people in the UK alone. Increasing miniaturization of devices in the electronics, medical, dental, chemical and aerospace industries highlights a key area of "advanced" manufacturing - that of scaling parts whilst maintaining high quality and production rates.

Micro-milling has emerged as one of the most popular processes for manufacturing small components because it is capable of rapidly producing high integrity parts. It is widely used in the medical and aerospace sectors, and in fields where miniaturised machine elements are commonplace such as watchmaking; optics and electronics; miniature heat exchangers or fuel injectors; and micro-mould manufacturing [4]. Although micro-milling is relatively commonplace, research into this process is typically applied and in comparison to its macro-scale contemporary, micro-milling is poorly understood. Little optimisation of the process has taken place, as described in Chapter 5, and understanding of the process behaviour limits intelligent process design. Research into the way that tools wear and the dynamic behaviour of the tools and centres are priorities in terms of improving process efficiency, the former of which is investigated herein. In the context of this work, micro tools are defined to have a diameter of less than 1000 μm, while small or meso-parts have size less than 1 cm.

Only after an understanding of the wear patterns and mechanisms has been reached can optimisation take place. A relatively small base of research has taken place in micro-milling, typically focussing on geometry of tools [5–8] or to a lesser extent coatings, based on the premise that this technique is used on the macro scale [7–11]. Even here, results have a large variety of process inputs and outputs and a lack of unified measurement methods make it impossible to compare studies [12]. To appropriately compare different studies and apply the results to design of tools and industrial processes, a standard protocol needs to be defined [13]. It is intended that this novel wear measurement protocol should facilitate faster development of micro-milling. Furthermore, tool coatings that have not previously been investigated for micro-milling will be investigated to characterise wear curves in greater detail than has previously been carried out. This work represents, for the first time, a comparison between fundamental tool wear studies and tool wear observed when producing testpieces representative to micro-industrial parts. This delivers a novel perspective on tool wear and facilitates the integrating of existing micro-milling research into industry.

Wire Electrical Discharge Machining (WEDM) is a similarly growing process. Its ability to cut complex shapes with high quality surface finish and little-to-no finishing lends it to high-cost parts such as those used in jewellery, medicine and dentistry [14]. Furthermore, since the process is largely independent of material properties, it can be used to produce such shapes from materials that are traditionally difficult-to-machine [15].

Due to the complexity of machining and the huge number of input variables [16], WEDM presents an optimisation problem: parameters that tend towards a good surface finish tend towards a slower machining rate, and vice-versa. In addition, different WEDM machines have different characteristics and so traditionally machining characteristic tables are dependant on the manufacturer and model of WEDM and are based purely on experimentation, which makes them hard to transfer to other set-ups [17]. Thus much of the work on WEDM is subjective and depends on the machining set-up. Although it has use in prototyping and high-value, high-precision parts, the technology is held back by slow machining times. There is value in looking for techniques which can speed up machining times while maintaining a decent surface, building on work that has been carried out using multiple passes [18, 19] and applying this to novel and more complex geometries. To enable quick measurement of gears an original method for measurement will be designed, which will reduce measurement times and costs.

1.2 MACHINING OF FERROUS AND NON-FERROUS MATERIALS

This work is carried out in conjunction with the University of Sheffield's Advanced Manufacturing Research Centre. As such, it is prudent to introduce the basics of machining here. Machining refers to successively cutting (often by shearing) material away from a solid block of material. The work carried out over this course of this thesis focusses on subtractive manufacturing, in which the behaviour and properties of the materials being machined significantly affects the outcome.

Machinability is a property which describes the ease with which a particular material can be machined, and a typical criterion for measuring this is the machining cost per part [20]. At any scale, machinability of a material carries a significant weight when choosing a material. However, for technical or small parts, a material's machinability can eliminate possible manufacturing processes. Another key issue is chemical affinity: This describes the tendency of the cutting tool to react with the material that it is cutting [21].

1.2.1 *Steel and its Role Herein*

Steel was chosen for this work as a comparative metal: its use in engineering components is extensive and its various grades lead to its application in almost every industry: medical, aerospace, chemical, construction and more. The metals used in this research typically have more specialist applications but more importantly titanium and nickel alloys are classified as "difficult-to-machine". At the opposite end of the scale, brass is often easy to machine and does not represent therefore the average machining life of a tool. As with any machining process research, it is helpful to have a reference to determine whether the tools simply perform well in the context of these materials or would be likely to perform well across the board.

1.2.2 *Titanium in Aerospace and Medical Engineering*

Titanium typically exhibits excellent corrosion resistance [22] even in seawater both in its pure and alloyed forms [23]. Other desirable properties of titanium for watchmaking as well as other industry are its non-magnetic characteristics and chemical inertness, which make it appropriate for medical use. Commercially pure titanium is much softer than alloyed titanium but has lower strength [20]. One of the primary barriers to using titanium is its classification as a difficult-to-machine material (this is synonymous with hard-to-cut and difficult-to-cut) [20]. This term describes materials whose cutting results in high rates of tool wear and failure, and high machining costs. There are three primary reasons that titanium presents itself as difficult-to-machine: Poor thermal conductivity, low modulus of elasticity and high chemical reactivity.

Since titanium has poor thermal conductivity, any heat generated during machining is not dissipated quickly from the cutting zone, so the tool-workpiece interface gets very hot [24]. This adversely affects tool life [25]. At the same time, titanium maintains its high strength at high temperatures which opposes chip formation [26].

The low modulus of elasticity of titanium (≈ 113 GPa) results in a greater deformation [23] under the same cutting forces than other materials. Upon cutting, the workpiece is deflected by the tool, which causes the cutting edge of the tool to rub against the surface [20]. Rather than shearing, rubbing occurs, and the friction creates high temperatures. The resultant "bouncing" action [27] from this elastic deflection causes chatter [24]. This leads to poor surface finish, dimensional errors and accelerates tool wear [28].

Though titanium is relatively inert at low temperatures, it becomes highly reactive at temperatures above 500°C, which results in an interaction between the tool and the workpiece. Conventional tool materials (high speed steel (HSS) and tungsten carbides) have a high affinity with titanium [29] which causes chips to weld to the tool tip. This results in chipping of tool edges, and

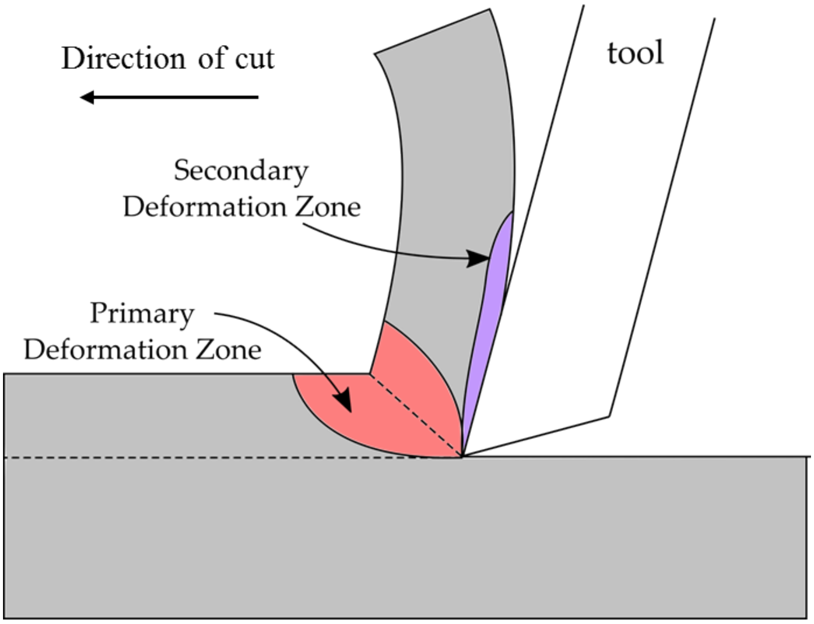

Figure 1.1: Primary and Secondary deformation zones in metal cutting.

premature tool failure [24]. Titanium and its alloys react with most materials at temperatures exceeding 500°C [25]. The corrosion resistance and high strength at high temperatures make titanium a much more appropriate material than steel for extreme engineering applications.

1.2.2.1 *Chip Formation*

Chips formed by machining titanium are often discontinuous (serrated) [27]. The plastic deformation in the primary deformation zone (see Figure 1.1) results in serrated chips across which the strain is not evenly distributed [30]. Another way to explain the process of chip formation is adiabatic shear theory: a thermoplastic instability occurs along the chip, from tool chip to free surface, causing material from one side of the instability to be extruded into shape. The result is a saw-tooth chip in which stress is not evenly distributed (as seen in Figure 1.3). Barry et al. [31] observed that at very small cutting depth, a continuous chip forms. As cutting speeds increased, saw-tooth segments formed which were evidence of ductile fracture. It was also seen that at high temperatures the chip and tool welded, and this increased with cutting speed.

1.2.2.2 *Tools and Tool Wear*

The serrated chips formed in titanium machining cause the rake face and the flank of the tool to wear. The rake face of the tool is directly in contact with the workpiece and therefore experiences high temperatures and adhesion to chips which results in both chemical wear and adhesive wear. Meanwhile, the flank is worn both by direct contact with the workpiece in the case of shoulder or slot milling, and also as chips travel up the tool flutes. The wear generally occurs quickly as the high localised temperatures in the region of the cutting edge result in chemical diffusion and adhesion to the workpiece or chips. One of the reasons for increased tool wear is that the bottom of the chip moves very slowly along the tool face, and so heat is transferred into the chip which enables the tool and chip to interact chemically [30]. Studies into machining with titanium have identified the following requirements from tools [25]:

1. Tool materials should maintain hardness at high temperatures.
2. Tools should have good chipping resistance.
3. Tools must demonstrate toughness and fatigue resistance under cyclic machining forces (as chips are often segmented).
4. Tool materials should have low chemical affinity with titanium, as this reduces the probability of tool-workpiece reactions.
5. Tools should have excellent compressive strength.
6. Tools should have excellent thermal conductivity so that heat generated can be drawn away from the cutting zone.

If titanium is machined with conventional tools, the wear rate increases rapidly with cutting speed. It is difficult to exceed a cutting speed of 60m/min [32]. Lopez et al. found that within this range, a speed of up to 60m/min was achievable for tungsten carbides but only 30m/min for HSS tools [33]. As a result of this and the above criteria, HSS is not suitable where the cutting speed exceeds 30m/min, as at these speeds the high temperatures dramatically reduce hardness. Many harder tools have a high chemical affinity at higher temperatures and are thus unsuitable [27]. Ezugwu et al. suggest the use of tungsten carbide (WC) tools for many machining situations, as almost all materials react chemically with titanium when temperatures exceed 500°C [25]. Another issue with tool wear relates once again to the reactivity of titanium at high temperatures: chips which have welded to the tool chip can lead to chipping and hence premature tool failure.

1.2.3 *Nickel Superalloys*

A superalloy is a metallic alloy which can be used at high temperatures, even up to and over 70% of the absolute melting temperature. Superalloys can be based on iron, cobalt or nickel, and nickel is often the primary choice in aerospace engineering.

Although Nickel superalloys have the ability to be used at very high temperatures, they can also be used at cryogenic or room temperatures and are thus appropriate for applications with variable temperatures [34]. Nickel Superalloys are used in industries such as aerospace, marine, nuclear and chemical due to their excellent corrosion-resistance and their superior mechanical properties [35]. However, they are notorious for being difficult-to-machine due to high temperatures, adhesive and diffusion wear, and the formation of a Built-up Edge (BUE) [36]. Nickel superalloys present further complexity in small-scale machining as burring and crystal irregularities lead to regular catastrophic fracture of the tools. These high tool fracture rates lead to poor machining efficiency, increased costs and difficulties predicting machining times. The alloy used in this work, alloy C-276 has applications in chemical exhaust processing and similarly corrosive environments for producing heat exchangers or pollution control - such as flue desulphurisation systems or fans/fan housings. These applications lend to its use in the Chemical Processing, Aerospace and Pharmaceutical industries.

1.2.4 *Brass and Bronze*

Brass and bronze are favoured in micromechanical, electrical or jewellery industries due to the ease with which they can be machined [37], and their relatively elastic properties. Brass typically produces a continuous chip when it is machined and it is thus important to consider chip removal mechanisms[38]. Brass is stronger than pure copper and more corrosion resistant, making it an appealing alternative [39].

Aluminium bronze is more difficult to machine than brass (its machinability is about 20% of that of brass) [40]. The dominant tool wear effect is that the cutting edge becomes dulled, and a notch forms on the leading edge of the tool during cutting [41]. However, aluminium bronze can be milled at high speeds, using a small radial depth of cut at low surface speeds (less than 15 m/min). Aluminium bronzes are relatively hard and have similar machining properties to high grade steel. They generally require a smaller rake angle (angle of the cutting tool relative to the workpiece, see Figure 1.2) than machining more ductile alloys would [42], but can be milled at speeds of up to 61m/min and feeds of 0.25 to 0.56 mm/rev using end-mills. An important consideration when milling aluminium bronzes is temperature, and coolants should be used to prevent unwanted temperature effects (increased wear, for example). Many aluminium bronzes form short, serrated or curled chips [42].

Another issue when machining bronze is adhesion [43]: this can cause a built-up edge chip (BUE) to form on the tool (see Figure 1.3). The extent to which this occurs is dependant on the chemical affinity of the workpiece to the tool.

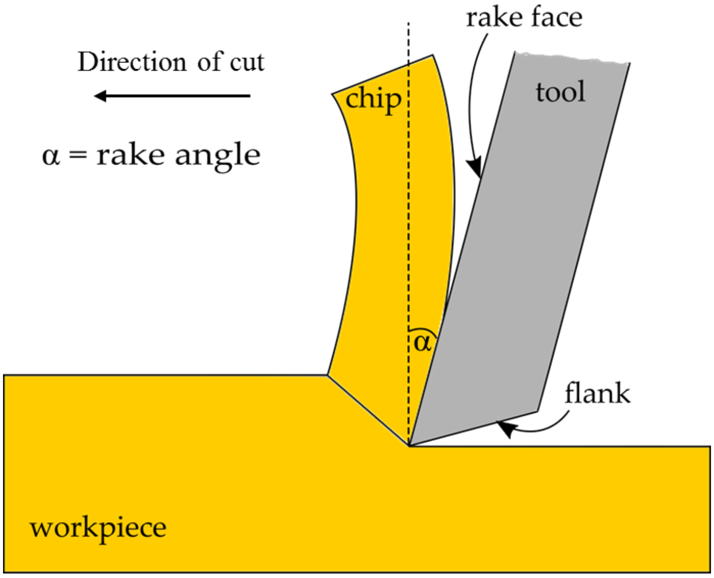
rake face
Direction of cut
chip
tool
α = rake angle
α
flank
workpiece

Figure 1.2: Schematic of the tool showing rake face and flank, as well as rake angle.

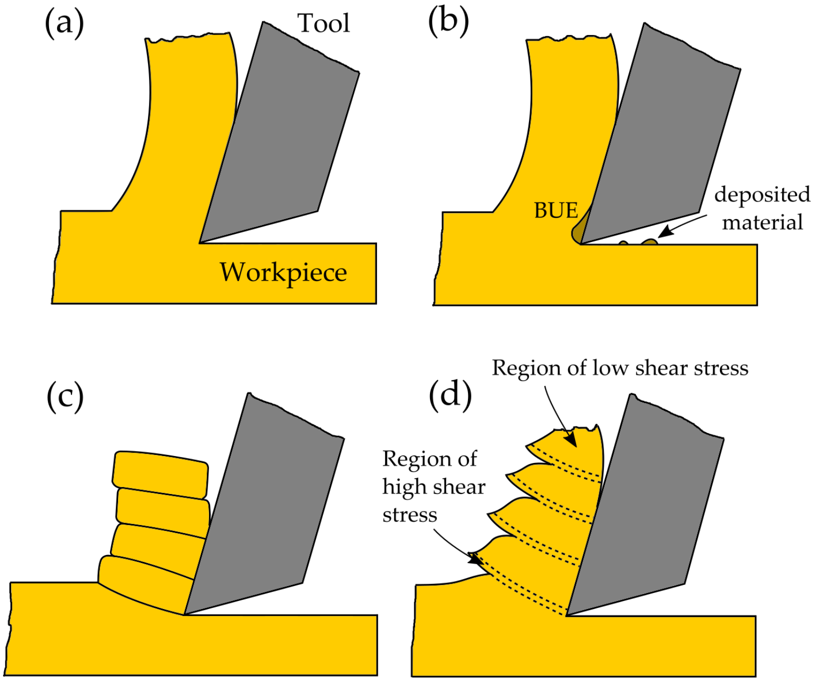
(a)
Tool
Workpiece
(b)
BUE
deposited
material
(c)
(d)
Region of low shear stress
Region of
high shear
stress

Figure 1.3: Types of chip that occur when machining material: (a) - a continuous chip, which often occurs in ductile materials in low friction situations. (b) - a built-up-edge (BUE) chip, where a portion of the chip adheres to the rake face and is later deposited on the material surface. (c) - a discontinuous chip, which occurs in more brittle materials. (d) - a serrated, sawtooth or semi-continuous chip, where regions of high and low shear stress cause the chip to shear.

1.2.5 *Aluminium*

Aluminium rates very highly in terms of machinability, and because the melting point of aluminium is low (659°C), temperatures reached in cutting are not high enough to damage high-speed steel (HSS) tools. Typically, tool wear when machining aluminium is seen on the flank of tools [38]. Aluminium alloys often require lubricants or cutting fluids as chips have a tendency to stick to the tool rake face [44]. Damage to tools is commonly caused by the formation of a BUE and an adhesion layer on the tool [45, 46]. Because aluminium has a high coefficient of thermal expansion[47], the absorption of heat causes deformation which makes the process inappropriate for situations where tight tolerances are specified [46, 48] and puts the workpiece at risk of welding to the tool. Furthermore, dry machining reduces surface quality.

Rather than dry machining, lubrication using Minimum Quantity Lubrication (MQL) improves temperature cycling during cutting [48]. The low melting point and high coefficient of expansion of aluminium make maintaining tolerances difficult without sufficient lubrication (and thus cooling). Because end milling is an intermittent cutting process, the tool tip dramatically changes temperature levels over short timescales (from approximately cold to 300°C) which further supports the need to use appropriate cooling.

The plasticity of aluminium is one of the major causes of high friction and strong adhesion with tool materials [49] and geometries. This is because it contributes this to the formation of a BUE which causes high cutting forces and poor surface finish and reduces tool life. Sandvik [47] recommend using a sharp cutting edge, and suggest that the welding along the cutting edge is due to the abrasive nature of aluminium causing localised burning. This is caused by a near-instantaneous heat build up, and should be counteracted in milling processes using spray mist coolant for efficient cooling. Cutting fluids should also contain additives that will suppress the formation of aluminium oxides [50].

1.3 WATCHES AND THEIR ROLE AS A TEST-PIECE

This work is in part sponsored by the Bremont Watch Company, a small independent British watch company established in 2002. Their interest in a research project has arisen from changes in the mechanical watch part supply chain, which has led to the need for autonomy in the production of their watches.

The relationship with Bremont inspired the consideration of several components of watches as appropriate test pieces around which to base this work. Two parts of a typical mechanical watch were considered: one moving, and one static. This provides a reflection of a wide range of engineering products. Watch gears were considered, to give a micromechanical context to this work, while watch bridges were considered to give a number of common features found in typical micro components.

A watch bridge is a small plate used to hold watch gears in place on the watch main plate. The main plate must be flat and resistant to mechanical

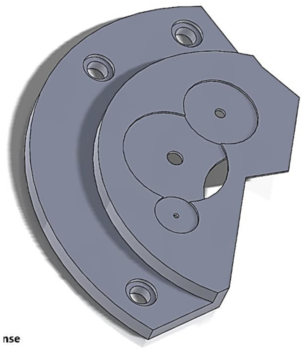

Figure 1.4: The typical geometry of a watch bridge

warping to ensure that the wheels in gear trains are correctly aligned [51]. As with machining of other micro-parts such as dental implants or miniature pump systems, it is required that parts are machined with minimal residual stresses. A typical watch bridge will contain machined features such as pockets, holes, bosses and steps (see Figure 1.4), making it an ideal test part.

Watch gears are typically manufactured from brass, and mesh with small hardened steel pinions. Brass is used due to its ability to self-lubricate in a system where liquid lubrication is not possible due to the high surface tensions of the lubricants used [52]. Miniature gears are commonly used in micromechanical systems and are difficult to manufacture due to their complex geometries. Methods for manufacturing such parts are often mass-production such as stamping, or large batches using a hobbing process. It is clear that there is a need for a smaller-scale process which can be used in system prototyping.

1.4 AIM AND OBJECTIVES

The project aims to develop advanced manufacturing operations and improve process outcomes for small static and micro-mechanical parts in terms of material removal rate and surface finish and quality, and tool wear reduction. It is intended that the research findings with both contribute to the manufacturing the future strategy and help to bridge the gap between university research and industrial applications. This will be achieved using the following key objectives:

1. Thorough literature research into a number of material removal processes that have been identified as being important in developing micromachining technology.

2. Development of a reliable tool measurement methodology to unify research into micro-milling tool wear and measurement therein, thus enabling more collaborative work and sharing of results/building on existing research to increase common understanding.

3. Using the tool measurement methodology, develop and test coatings to extend useful tool life.

4. Testing of machining parameters in WEDM to speed up production times while maintaining part quality, thereby improving one of the most significant difficulties to WEDM being more widely employed in manufacturing.
5. Application of Parameter testing in WEDM to production of micromechanical parts.
6. Using the research methodology developed to investigate factors that affect tool wear curves in micro-milling; specifically novel coatings and use of different geometries.
7. Applying the research to an industrial context using a standard testpiece which include many common micro-milling processes found in the chemical (miniature pumps), micro-mechanical (gears), dental (implants) and aerospace (micro-electronics and micro-channels for aerospace).

1.5 LIMITATIONS OF SCOPE (FOR MECHANICAL WATCHES TO BE MADE IN THE UK)

There are some constraining aspects that will limit the scope of this research. These fall under the categories of Equipment Limitations and Limitations in Funding. Where relevant, solutions to limitations are suggested.

1.5.1 *Equipment Limitations*

Typically, spindle speeds for micro-milling tools recommended by manufacturers are in the region of 100,000 revolutions per minute. The machining centre available at the AMRC is capable of achieving spindle speeds of only 50,000 RPM. However, this results in greater stresses on the tools, and the machining parameters must be altered from manufacturer recommendations which are based on significant testing. In addition, the best method for lubricating tools in micro-milling applications is MQL [9] or mist lubrication. This has not been possible with the system available at the AMRC.

The final issue causing significant disruption to research was the loss of the WEDM machine that had been used as the basis for all research and trial design. Based on the equipment available at the AMRC and the research gaps identified in micro-milling, it was clear that there was scope for significant research into micro-milling. Therefore micro-milling has made up much of the main body of the PhD rather than attempting to source an alternative WEDM machining centre.

1.5.2 *Limitations in Funding*

Machining time is expensive, costing over £800 for a single day of research. This meant that preliminary testing to optimise machining parameters had to be minimised, limiting the optimisation which resulted in higher than desirable tool breakage rates. Similarly, number of tools tested was limited by funding.

2

LITERATURE REVIEW

2.1 PROCESSES OF INTEREST

This section describes the processes of interest in the development of micromachining processes: Wire Electrical Discharge Machining (WEDM) and micromilling, as justified in Section 1.1. A general review of the state-of-the-art is carried out following a technical description of each process. More focussed literature is critically reviewed in experimental chapters, in the context of the work carried out.

2.1.1 *Working Principles of Wire Electrical Discharge Machining (WEDM)*

Machining can be divided into two categories: conventional and non-conventional. In conventional machining processes, such as milling and turning, material is removed by mechanical force through plastic or brittle failure of the material [53]. Where this is not the case, the process is defined as non-conventional. Electrical Discharge Machining (EDM) is a non-conventional machining process [16] since material is removed using thermal and electrical, rather than mechanical, energy [54].

WEDM is a special case of electrical discharge machining, whereby the electrode is a wire that is continuously fed through the machine [16].

WEDM uses a controlled spark erosion to remove material from the workpiece. A series of repeated electrical discharges cause a spark to jump between the tool electrode (in this case a wire) and the workpiece [55]. This distance between the wire periphery and the workpiece is referred to as the spark gap (Figure 2.1).

The sparks cause localised melting [56]. The molten material is then flushed away by some means (usually dielectric fluid, although dry-EDM uses high velocity gas [57]). Since the electrode on a WEDM is not rigid, it must be kept under tension. This is achieved by a series of pulleys and rollers as depicted in Figure 2.2. Wire tension is an important machining parameter and basic guidelines are often specified by the manufacturer of the machine [58]. Unlike traditional EDM, WEDM does not require elaborate pre-shaped electrodes [16], and very small corner radii and intricate shapes can be achieved [59]. The electrode is also continuously replaced, which means that electrode wear is of little significance as compared with traditional EDM[60].

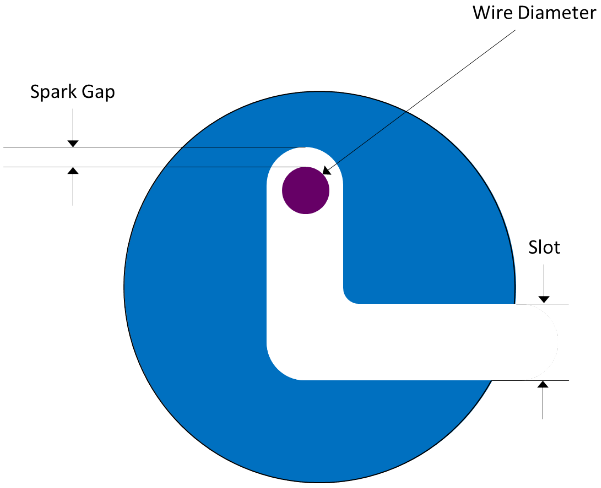

Figure 2.1: The spark gap is shown between the wire (small purple circle) and the workpiece (large blue circle).

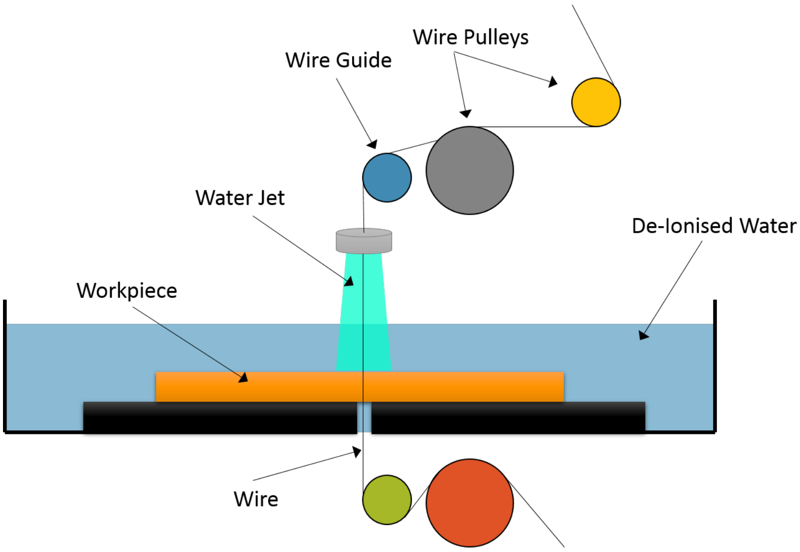

Figure 2.2: The WEDM Setup. The water jet is used to feed the wire that comes from a roll, through the machine bed and to the rollers at the bottom.

The method of material removal is described in more detail using Figure 2.3. Initially, a potential difference is applied between the wire and workpiece (A) [61]. This potential can vary between 40V and 400V depending on requirements [62]: less than 40V is not advisable since to generate enough electric field strength for dielectric breakdown to occur the gap would have to be very small relative to the wire diameter. Chips would be hard to flush out and wire breakage more likely [63]. On the other hand, a higher peak voltage decreases Material Removal Rate (MRR) [64].

Following the application of a potential difference, dielectric breakdown occurs at the smallest distance between wire and workpiece. This causes the voltage to drop and the current to rise. Current is allowed to flow in the gap due to the ionisation of the dielectric, and a plasma channel is formed. The higher current flowing gives rise to a strong magnetic field (B).

The magnetic field creates an ionised plasma channel which results in localised heating. As the area involved is small, the resultant temperature rise is very large (up to 12, 000 °C) and the workpiece melts in this area [65] (C). After the discharge has taken place, the current and voltage are turned off, and the plasma implodes as a result of the pressure from the surrounding dielectric (D). This draws the molten material into the dielectric, flushing it away from the workpiece and leaving a crater [66].

The dielectric used has important consequences for the machining, and typically de-ionised water is used as the dielectric in WEDM. This fulfils three roles: firstly, it prevents electrolysis from occurring, which would allow current to flow freely between the wire and workpiece, preventing sparks from occurring [60] or would resulting in premature discharge [67]). Secondly it flushes molten material from the workpiece to prevent re-solidifying of the material [68]. Finally, the dielectric cools the wire and workpiece [67].

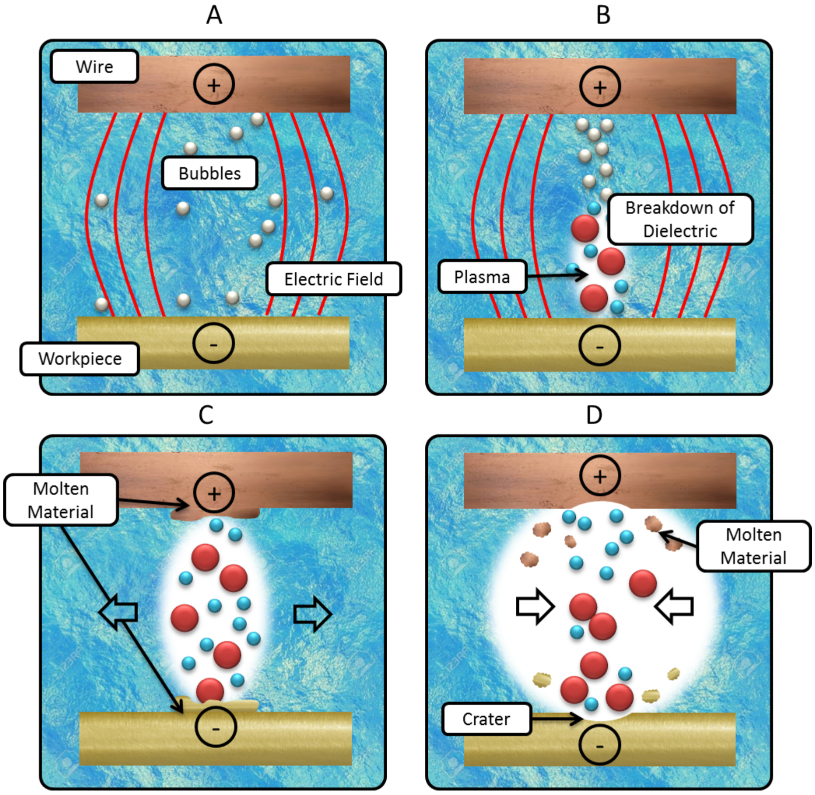

Figure 2.3: The plasma theory for how an EDM works. The workpiece is shown at the bottom of the image, the wire is at the top. In this instance, the wire acts as the positive electrode.

Since WEDM does not use mechanical energy to remove material from the workpiece, the process is relatively free of forces and is largely independent of the mechanical properties of the workpiece [69]. This allows extremely hard-to-machine materials to be machined [70], and eliminates mechanical stresses, chatter and vibration problems [16]. Residual stresses cannot be completely avoided, however, and can occur due to the melting and re-solidifying of material, especially where cooling and heating is non-uniform [70], which can plastically deform structures [69].

2.1.2 *Important Parameters in WEDM*

One of the major difficulties in machining using WEDM is the sheer number of machining parameters involved [16]. The WEDM process consists of a complex series of physical occurrences, each of which is influenced by some or all of the possible parameters [71]. Machining characteristic tables are not transferable between manufacturers [17].

Table 2.1 details the most significant common machining parameters that have been researched in the last 20 years. Discharge energy is the most important factor affecting surface finish in WEDM. This is influenced by parameters such as discharge current, gap voltage [71], pulse duration, pulse-on time and peak current [72, 73]. Unfortunately, Surface Finish (SF) and MRR are contradictory in nature so although a high MRR and good SF (or low R_a value) are desirable, optimisation must take place to achieve a compromise [71]. Generally speaking, a higher discharge energy results in larger craters which causes a poorer SF [74–76] but a higher MRR [72].

Pulse energy, E, can be described as

$$E = \int_{0}^{t_0} u(t)i(t)dt \tag{2.1}$$

where $t_0$is discharge duration, $u(t)$ is discharge voltage and $i(t)$ is discharge current. E is pulse energy [76].

Table 2.1: Significant Machining Parameters in WEDM

Parameter	**Symbol (used herein)**	**Units (typical)**	**Definition**
Pulse-on Time	T_{on}	µs	The time during which the machining is performed [77].
Pulse-off Time	T_{off}	µs	The time period in which the pulse is low, or off (Figure 2.4). During this time no discharging occurs.
Servo Speed	V_s	mm/min	Controls the speed of an advancing axis during machining operations [78].
Servo Reference Voltage	SV	V	Controls gap width [54]. With increased servo voltage, gap width is increased [79].

Machining Voltage (or Gap Voltage)	VG	V	The voltage across the distance between the wire periphery and workpiece [68].
Peak Current	IP	A	The maximum current that passes through the electrodes each pulse [68].
Wire Speed (or Wire Feed Rate)	WS	m/min	The rate at which the wire is fed from the spool through the machine.
Wire Tension	WT	gm^{-2}	The tension applied to the wire electrode [80].
Dielectric Flow Rate (or flushing pressure)	LQ	L/min or bar	The rate at which dielectric fluid is circulated around the tank [68].
Type of Dielectric			This influences its conductivity.
Machining History	$\mathrm{M}_{\mathrm{His}}$		This describes the conditions used to machine previously, and should be known if roughing passes have taken place [17].
Type of pulse-generating circuit			AC or DC, has an effect on machining [75].
Capacitance of pulse-generating circuit	C	F	The measured capacitance of the pulse-generating circuit.
Polarity Effect			This determines whether the wire is the anode and the workpiece the cathode (conventional or positive polarity) or vice versa (reverse or negative polarity) [69].
Wire Diameter	Ø	mm	The diameter of the wire used.
Wire Offset	WO	mm	Wire radius plus electrical discharge gap [81].

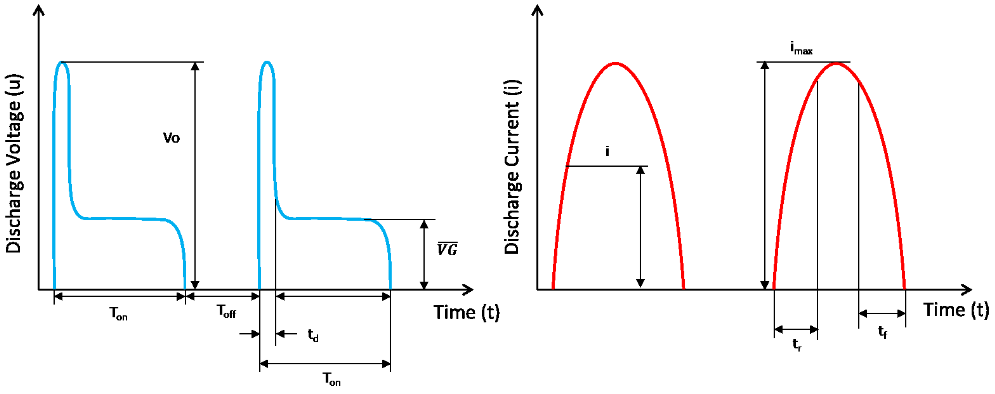
Discharge Voltage (u)
Vo
$\overline{VG}$
T_{on}
T_{off}
t_d
T_{on}
Time (t)
Discharge Current (i)
i_{max}
i
t_r
t_f
Time (t)

Figure 2.4: Schematic of two EDM pulses. T_{on} denotes pulse-on time, T_{off} pulse off time, t_d ignition delay time, V_0 open circuit voltage, $\overline{VG}$ average machining voltage, t_r current rise time, t_f current fall time, i average discharge current and i_{max} maximum discharge current.

2.1.3 *Micro-milling Process*

Milling is a standard machining process which is commonly used for metal-cutting Groover [82]. It is a subtractive process: that is, it removes material from the workpiece such that the resulting shape meets geometrical requirements [83]. The cutting tool rotates and cutting teeth shear material (Figure 2.5). Typically, the tool will rotate about the Z-axis, where the axes are shown in Figure 2.5.

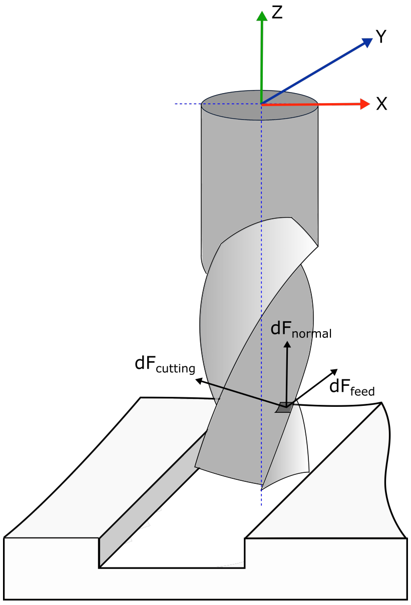
Z
Y
X
dF_{normal}
$dF_{cutting}$
dF_{feed}

Figure 2.5: A milling tool with respect to the workpiece in axes x, y and z.

The tool rotates, and cutting teeth shear the material (Figure 2.6). The tool can have either solid teeth (Figure 2.7a) or inserts (Figure 2.7b).

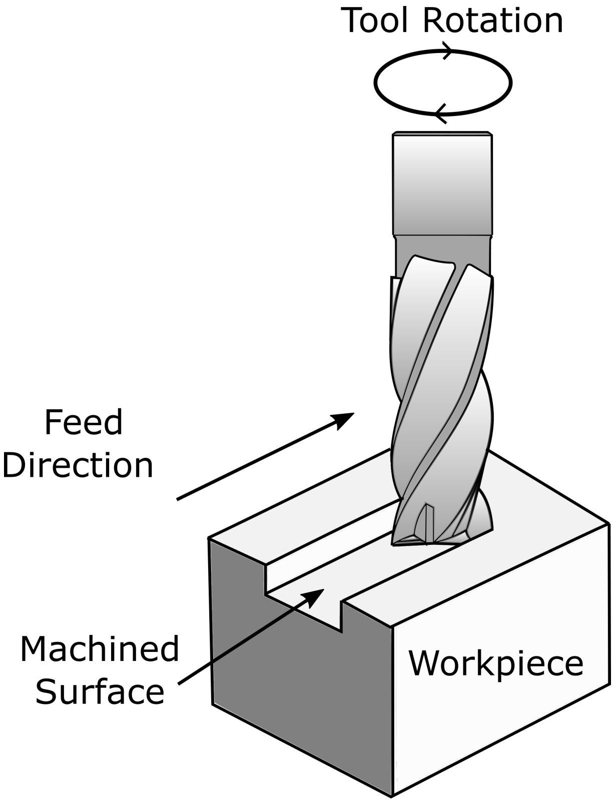

Figure 2.6: Schematic of a milling tool cutting a workpiece.

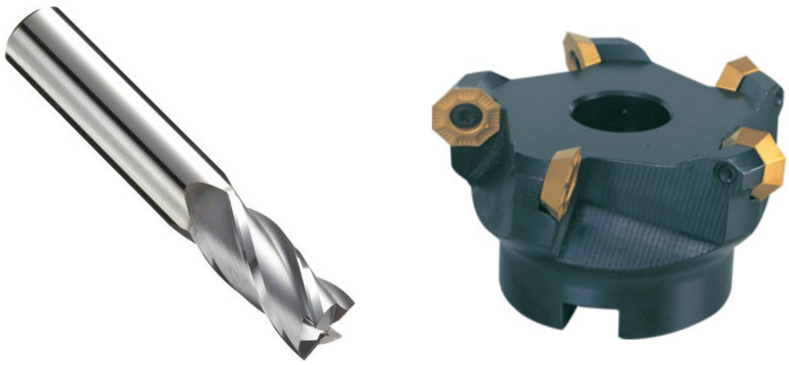

(a) A solid-toothed mill.

(b) A mill with inserts.

Figure 2.7: The two types of macro mill. Image Courtesy of Mano DIY parts (www.manomano.co.uk)

When a milling tool cuts, it may cut in two possible directions: with the direction of teeth (down, or climb milling), or against the direction of the cutting teeth (up, or conventional milling). This is shown in Figure 2.8. This has a significant effect on the outcome of the process: down milling results in a gradual reduction of chip width along the cut, which reduces rubbing and burring. Large chip thicknesses achieve stable machining, and cutting forces pull the workpiece into the cutter. However, the machine needs to offset backlash on the table. Up milling, on the other hand, results in a chip with zero starting thickness which increases along the cut. Because the cutting edge is forced into the cut, friction can cause rubbing and burnishing, high temperatures and work hardening of the surface. However, impact forces are lower which can be useful for delicate tools.

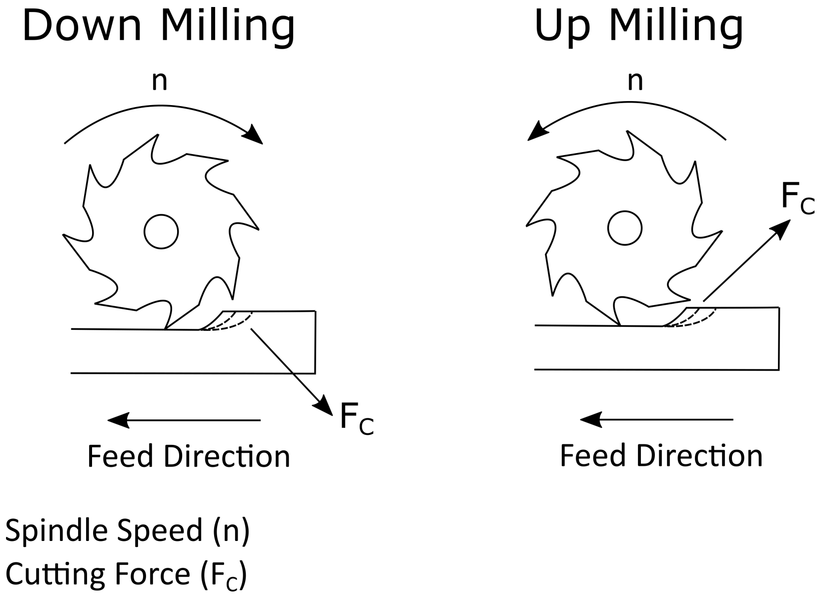
Down Milling
Up Milling
n
n
F_C
F_C
Feed Direction
Feed Direction
Spindle Speed (n)
Cutting Force (F_C)

Figure 2.8: Down (Climb) milling and Up (conventional) milling.

Milling is extremely versatile and tools can be used to cut in a number of ways. Four common cut types used here are side milling, face milling, slot milling and plunge milling (Figure 2.9) Side milling machines the edge part of a surface, face milling machines the top face, slot milling machines between two edge surfaces such that a two-toothed tool would have both teeth in contact with the side at one, and plunge milling feeds axially along the Z-axis. Slot milling has primarily been used for the duration of this work, with the exception of a validation study which uses all four types of milling.

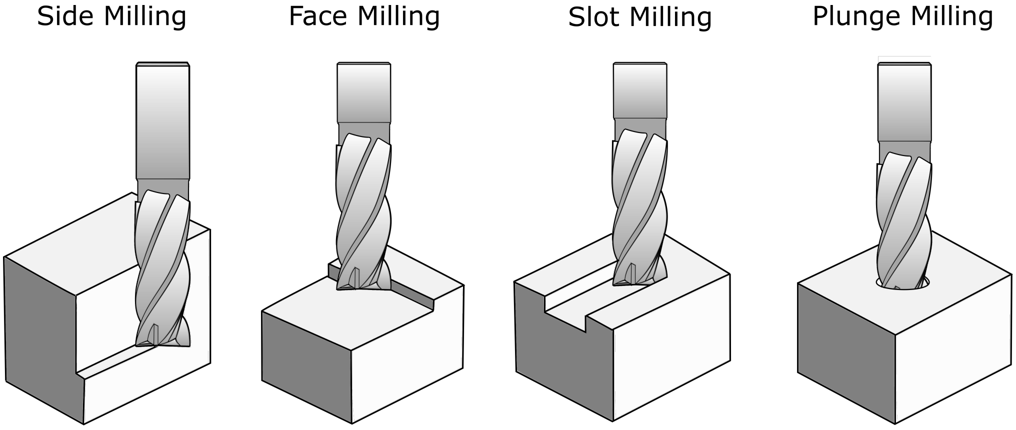
Side Milling
Face Milling
Slot Milling
Plunge Milling

Figure 2.9: Four commonly used types of milling cut.

There are several common types of cut achieved with a milling cutter, of which four are of relevance here: side, face, slot and plunge milling (Figure 2.9). Milling tools are designed with certain geometries and coatings to achieve the best possible tool life and finish. A particularly important element in milling tool design is the number of teeth: generally speaking, a lower number of teeth is used for roughing operations while more teeth result in a smoother surface finish (see equation 2.2), where R_a is surface roughness, $f_z$and z are feed per tooth and number of teeth respectively, R is cutter radius and $+$ and $-$ refer to up and down milling) [84]. However, an increased number of teeth can result in increased temperatures and reduced tool life [85].

$$R_a = \frac{f_z}{32\left(R \pm \frac{f_z z}{\pi}\right)} \tag{2.2}$$

Micro-machining can be defined as the use of mechanical tools which have geometrically defined cutting edges, to manufacture features which have dimensions in the order of micrometres ($1 \times 10^{-6} - 999 \times 10^{-6}$m) [86]. Micro-milling can be considered a subsection of micro-machining and, as with all micro-machining, produces very different results to conventional machining. This is due to a combination of physical phenomena which are referred to as the *size effect* (discussed in Section subsection 2.1.4). Micro-milling tools are all "solid tools", as they are too small for inserts, and often have a two- or four-tooth geometry, as illustrated in Figure 2.10. Two-tooth mills have more flute space between teeth. This is especially important for micro-milling tools which are very small and for which chip removal is a problem, A two-toothed mill allows for more chip carrying capacity, especially in softer materials where material adhesion can be a problem. Four flute mills can be used for finish-milling since faster feed rates can be used and more teeth result in improved surface finish [84]. However, chip removal can be problematic [87].

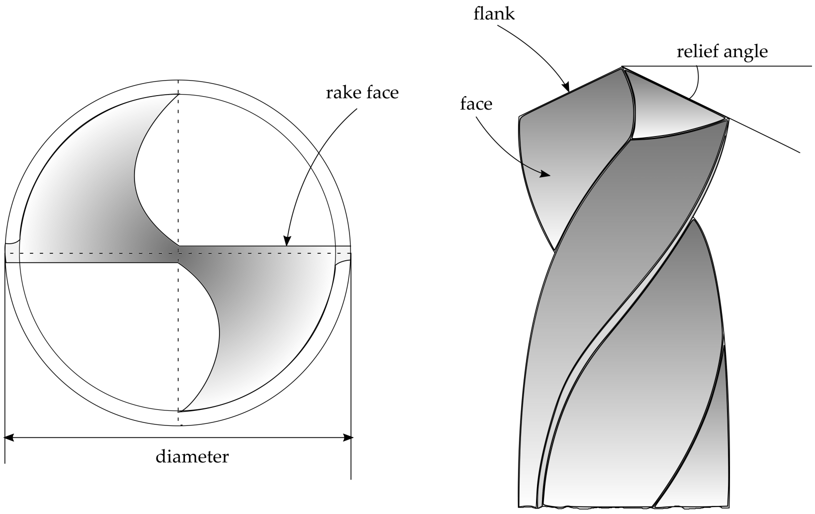

Figure 2.10: Typical geometry of a micro-milling tool.

Though micro-milling appears to be a scaled-down version of macro-milling, the size effect (subsection 2.1.4) leads to challenges in measuring tools and predicting wear behaviour.

2.1.4 *Size Effect*

The size effect is defined by Mian et al. as

> "The phenomenon whereby the uncut chip thickness to levels below the cutting edge radius, or grain size of the workpiece material begins to influence workpiece material deformation mechanisms, chip formation and flow" [88].

Micro-milling can be considered a subsection of micro-machining and, as with all micro-machining, produces very different results to conventional milling. There are several reasons for this [89], the first being that, relatively speaking, tools can appear blunt from the point of view of the workpiece material. If the depth of cut is much smaller than the cutting-edge radius, the result is a negative rake angle (Figure 2.11) and high cutting forces. The tool is likely to rub along the surface of the workpiece and burnish it, rather than cutting it. Another problem is that due to their diameter, even fine-grained micro-milling cutters generally have low stiffness and poor resistance to fracture [90] and so it can be difficult to study them for extended periods of time as the tools can fracture before significant wear has taken place [91].

Finally, although on a macro-scale a polycrystalline structure appears homogeneous, at the micro-scale grain sizes are relatively large when compared to the size of the tool (Figure 2.12) and thus machining forces can be hugely variable [92].

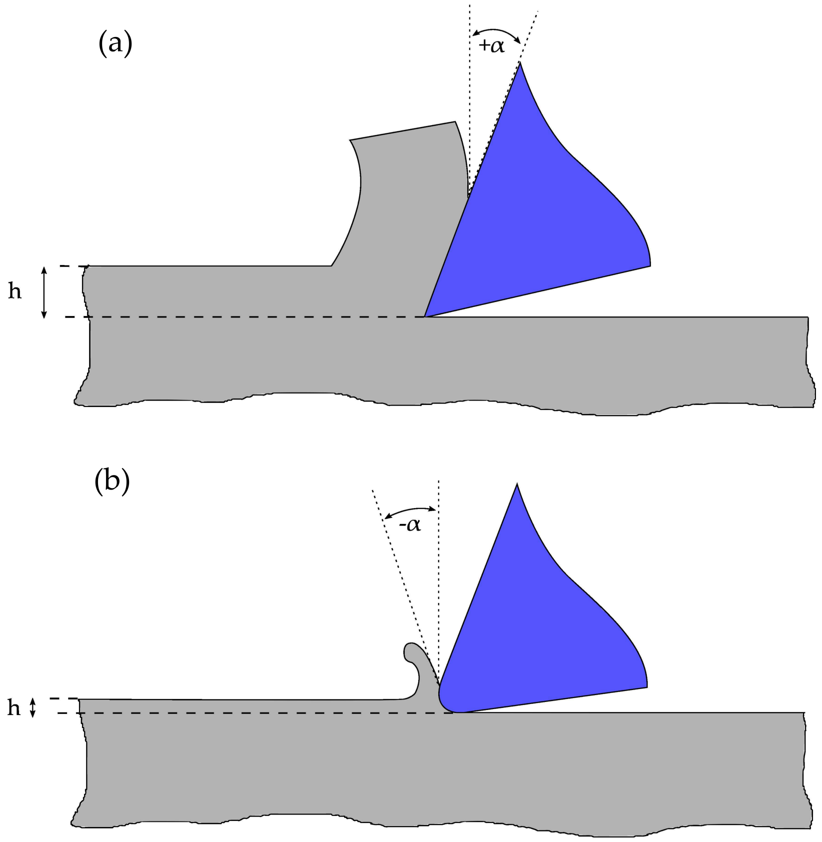

Figure 2.11: (a) shows a macro-tool (zoomed out) and (b) shows a micro-tool (zoomed in). Although both tools have the same cutting edge radius at the start of machining, the cutting edge radius for the micro tool is typically much closer to the depth of cut than for the macro tool.

These issues combine to create a phenomenon known as the size effect. The result is that that conventional macro-mechanics cannot be used to describe the system as simply reducing the scale does not produce a representative model. The result is that that conventional macro-mechanics cannot be used to describe the system as simply reducing the scale does not produce a representative model and thus a significant body of research in the field is dedicated to investigating the material removal mechanisms, dynamics and wear mechanisms of micro-milling.

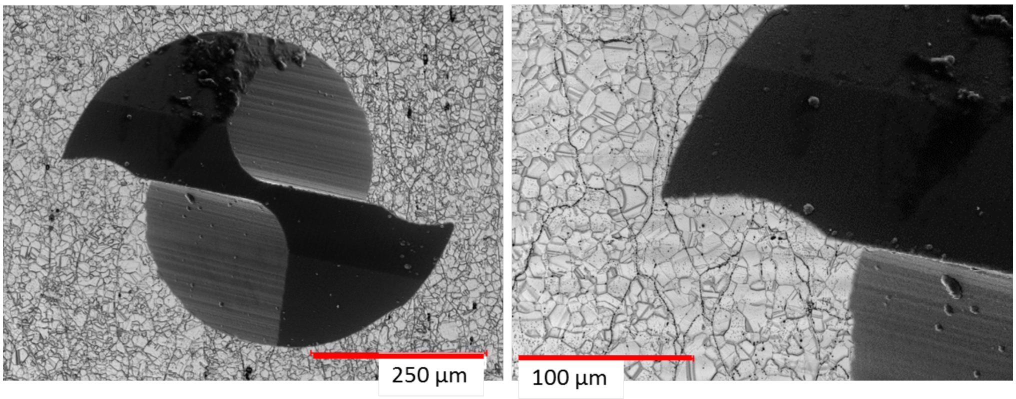

Figure 2.12: Grain sizes relative to tool size

.

2.2 CURRENT RESEARCH TRENDS IN WEDM

The characteristics of WEDM described make it a candidate for producing high-quality micro and micromechanical parts that require little or no finishing or polishing which reduces processing time [93]. A review has been carried out detailing work undertaken in recent years on achieving a high quality surface finish using WEDM, both through altering of parameters and through carrying out finishing cuts. Work to characterise the white layer and identify its cause has also been considered, with a brief discussion on the machining of ceramic materials using WEDM which supports it's versatility as a process.

White layer describes the region of material that has been structurally modified by heat [94] This results in increased surface roughness and also alters the hardness of the material, reducing the fatigue strength and modifying the wear properties of the part.

This gives a context for the research that has taken place herein into optimising process outcomes which has ultimately led to development of manufacturing methods for producing miniature gears.

2.2.1 *Process Outcomes*

As with conventional machining processes, MRR and SF are commonly chosen as process outcomes when machining. In addition, white layer is an important process outcome. This is discussed further in subsection 2.2.3.

Because it has negative effects structurally and in terms of surface quality, it is important to minimise white layer. Similarly, surface roughness is often undesirable in parts as it indicates quality of part (for example, minimal surface cracking, low friction properties) while a high MRR is desirable because the viability of any machining process is limited by the time it takes to machine a single part.

Finally, geometrical accuracy is important when machining small parts for the chemical processing, medical or aerospace industries where tolerances are small. A combination of these process outcomes provides the basis for most WEDM studies.

2.2.2 *Surface Finish*

As described in 2.2.1, pulse energy ultimately has the greatest effect on surface roughness in WEDM. However, as this is dependent on various parameters, there is no one way to optimise this. There are two primary methods employed to optimise surface finish: altering parameters alone, and carrying out multiple passes. Typically, an R_a value is used to compare surface finish between machined surfaces. This is defined as the arithmetic mean of the absolute values of vertical deviation from the mean line through the profile (Figure 2.13, Equation 2.3).

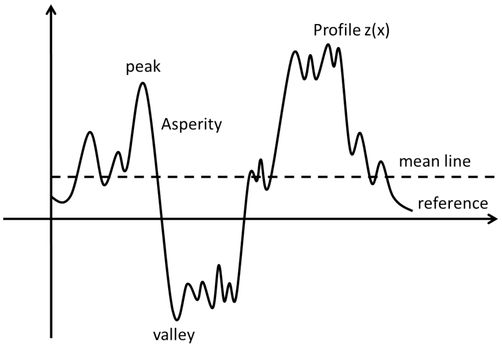

Figure 2.13: Surface profile from which R_a value is obtained.

The advantages of using this value are the ability of many types of measurement instrument to calculate this and its standardisation across industry. On the other hand, it provides a directional result. However, theoretically a WEDMed surface is directionally homogeneous, mitigating this to some extent.

$$R_a = \frac{1}{L} \int_0^L |z - m| \, dx \tag{2.3}$$

2.2.2.1 *Improving Surface Finish by Altering Parameters*

Significant work has taken place since the inception of WEDM to investigate the effects of the various machining parameters on the surface finish that can be achieved. The parameters investigated include all of those detailed in Table 2.1, and a summary of the effects of changing the process parameters is given in Table 2.2. Supporting studies for the conclusions described are indicated in the "relevant studies" column. Typically, due to the physical nature of the process, studies are in agreement as the sparking behaviour of a WEDM is the same across machines. However, it is noteworthy that there are parameters such as gap voltage, or pulse-on time, that cause controversy: Some studies report reduction in MRR with increased gap voltage [64, 95], others argue that an increased gap voltage leads to higher MRR [74, 76, 96].

Further studies still report and increased MRR up to a point, before a decrease, sometimes without explanation [97]. The issue lies in the way that WEDM optimisation studies are very specialised to different setups, which use different dielectrics and machining parameters. This leads to largely individualist research that is hard to to compare. One study may only observe the range of gap voltages over which MRR increases with gap voltage, another may observe a higher range of gap voltages. In this example, at low gap voltages, with increased gap voltage pulse energy is increased. Larger, higher energy sparks are generated which remove more material per discharge. Once the gap voltage reaches a certain point, discharge gap between workpiece increases. This distance is dependant on machine design and setup. As the gap increases, the spark energy is dissipated across the gap, via the dielectric, and thus size of crater produced and chance of sparking is reduced.

To resolve this problem, a good scientific understanding of the the reasoning behind certain behaviours is required.

Table 2.2: Effect of altering different machining parameters in WEDM. Surface finish is typically measured using $R_a$values, where a smaller value denotes a better surface finish.

Parameter	**Effect on Surface Finish**	**Relevant Studies**
Pulse-on Time	Increase T_{on} leads to a higher pulse energy and thus surface finish is poorer.	[14, 70, 74, 98, 99] [17, 54, 72, 79, 100]
Pulse-off Time	T_{off} does not directly effect pulse energy, and thus machining time can be altered (sped up, or slowed down for difficult features) without affecting surface finish.	[67, 68, 72, 73, 75, 98]
Servo Speed	Increasing servo speed (or speed of advancing axis of wire) results in poorer surface finish.	[74]
Servo Reference Voltage	Increased servo referance voltage leads to increased gap voltage. This leads to a higher pulse energy and poorer surface finish, provided a minimum machining gap is maintained.	[14, 74, 75, 77, 101]
Machining Voltage (or Gap Voltage)	See "Servo Referance Voltage".	
Peak Current	Increased IP leads to increased pulse energy and increased surface roughness.	[7, 15, 72, 93, 98]

<table>
<tr><td>Wire Speed (or Wire Feed Rate)</td><td>Wire speed has a lesser effect that parameters directly affecting pulse energy, but low wire speeds result in higher discharge energy which degrades surface, and high wire speeds cause an increase in R_a.</td><td>Pasam et al. [74] found that when machining Ti6Al4V at the following wire speeds R_a values were:
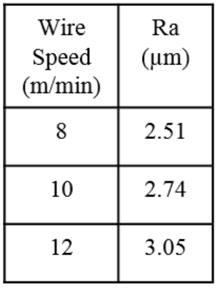<table><tr><th>Wire Speed (m/min)</th><th>Ra (µm)</th></tr><tr><td>8</td><td>2.51</td></tr><tr><td>10</td><td>2.74</td></tr><tr><td>12</td><td>3.05</td></tr></table></td></tr>
<tr><td>Wire Tension</td><td>Like WS, WT is relatively insignificant. At low tension, the wire vibrates excessively, causing poor surface finish while at high speeds the surface finish improves but the wire has a tendency to break.</td><td>Liao et al. [75] observed that a wire tension of 1 KgF R_a was 0.416 µm vs. 0.224 µm at 1.4 KgF [70–72, 99, 102–106]</td></tr>
<tr><td>Dielectric Flow Rate (or flushing pressure)</td><td>A minimal dielectric flow rate is required to flush molten debris, and increased LQ can improve surface finish by improving cooling and debris removal mechanisms.</td><td>[99]</td></tr>
<tr><td>Type of Dielectric</td><td>Typically, oil dielectrics are more likely to allow electrolysis which in turn results in a worse surface finish. In WEDM, water is often used, with de-ionising resins to reduce this effect.</td><td>[60, 67]</td></tr>
<tr><td>Machining History</td><td>Performing rough cuts followed by finishing cuts improves surface finish.</td><td>[103]</td></tr>
</table>

Type of pulse-generating circuit	Using a DC pulse-generating circuit can result in lower R_a than an AC one. Using an alternating polarity power source can yield a better finish than using a straight polarity power source.	Liao et al. [75] found that for a DC pulse generating circuit, an $\mathrm{R_a}$value of 0.22 µm could be achieved as compared to 0.34 µm with an AC one (material was not specified).
Capacitance of pulse-generating circuit	Using a higher capacitance can result in a higher R_a value.	This was verified by Liao et al.[75] but numerical values not given.
Polarity Effect	Reverse polarity can machined surface but results in increased wire erosion and wire material deposition on workpiece surface.	[107]
Wire Diameter	A smaller wire diameter can result in a better surface finish (lower R_a value).	Newton et al. [108] observed that at a spark energy of 5 mJ, a 100 µm diameter wire produced an $\mathrm{R_a}$value of 2.8 µm and a 250 µm diameter wire produced an $\mathrm{R_a}$value of 2.95 µm.[101]
Wire Offset	This alone has little effect on surface finish, but can be altered in trim cuts to significantly improve surface finish.	[18, 93]

2.2.2.2 *Improving Surface Finish using Multiple Passes*

While changing parameters on the WEDM provides a method of improving surface finish, another more traditional technique can be used: to carry out a rough cut and a series of trim cuts where the parameters have been altered. This is to achieve the best possible surface finish: the role of the first "rough" cut is to remove the bulk of the material while the second "trim" cut takes place at altered machining parameters (Figure 2.14) to produce a finer surface finish (often at a slower rate of machining [98] or lower discharge energy [18]). This is a technique used in conventional machining, for example during turning whereby the final cut has lower depth and takes place more slowly than the rough cuts.

From various studies it can be concluded that parameters used in finishing cuts can reduce the depth of the white layer [109]. The finish cut produces a much finer surface finish than the rough cut, but due to the lower MRR that can be achieved using finish cuts, a rough cut should be used to create the basic form. Furthermore, finishing passes enable residual stresses to be reduced due to smaller depths of melting with each spark [110]. Work by Huang et al. [17] suggests that a finishing pass with appropriate parameters can actually remove only white layer from the rough cut during the finishing pass, resulting in a smaller white layer than could be achieved by a finishing pass alone (see Figure 2.15).

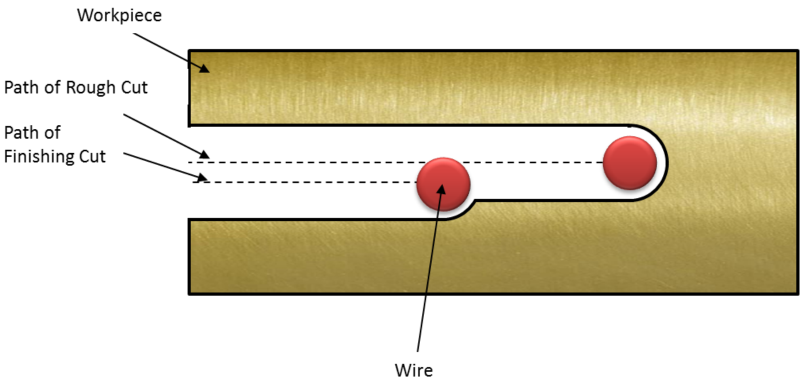
Workpiece
Path of Rough Cut
Path of Finishing Cut
Wire

Figure 2.14: Path followed by wire for finish cut.

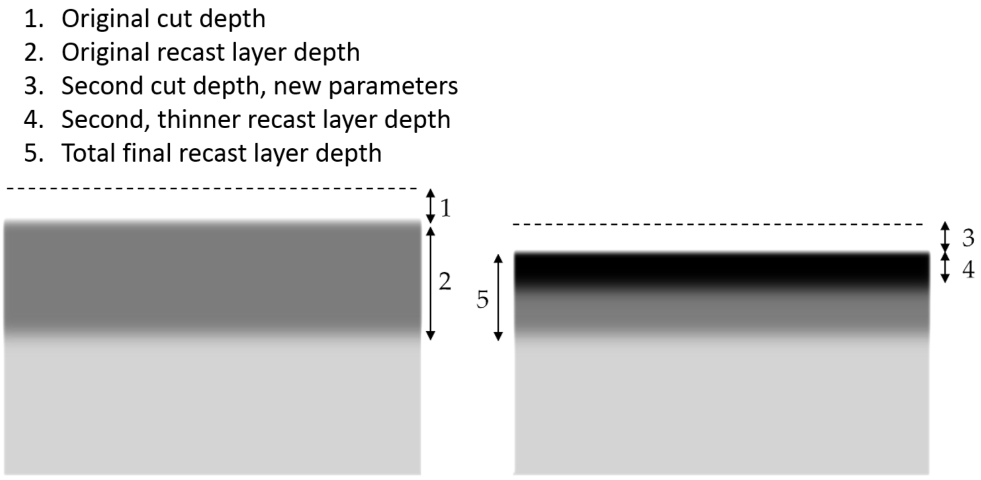
1. Original cut depth
2. Original recast layer depth
3. Second cut depth, new parameters
4. Second, thinner recast layer depth
5. Total final recast layer depth
1
2
5
3
4

Figure 2.15: The trim cut reduces the white layer depth without cutting into the bulk material.

It has been acknowledged that dimensional deviation depends on machining parameters, but since studies are typically conducted on straight cuts through materials, this is often ignored. Although Jangra et al., Sarkar et al. and Antar et al. [18, 98, 110] report improved surface roughness and white layer properties, these are all conducted on straight cuts. Inevitably, the geometry of a part affects sparking properties and thus there is a gap in research into the applicability of this method for complex geometries. Chalisgoankar et al. [109] machined only a simple square, measuring surface roughness only on the four sides. As a result, it is hypothesised here that the only conclusions that can be drawn geometrically are perhaps the differences in surface finish as the wire moves in the x-y direction, although this is not considered.

2.2.3 *White Layer*

The white layer is the layer of material that has been structurally modified by heat [94] and is influenced by pulse energy. This results in increased surface roughness and also alters the hardness of the material, reducing the fatigue strength and modifying the wear properties of the part. The thickness of the white layer can be reduced by altering various machining parameters, especially those influencing discharge energy [111].

The studies described have provided good insight into the properties and characteristics of white layer. However, they do not explain white layer variations over geometries for complex parts. Since depth of white layer depends on spark energy art the point at which the spark contacts the workpiece, it is reasonable to assume that a changing geometry (i.e. differences in spark gap) will impact white layer depth. Looking at white layer for straight cuts is useful when investigating the structural changes that take place and the conditions that lead to this, however. Thus, existing studies into the nature of the white layer produced by WEDM range from basic measurements of thickness of the layer and an investigation of the effect that changing parameters has on this to detailed studies of the metallic structure and characterisation of the white layer. This work is concerned with the former, and minimising the impact of the white layer.

White layer thickness is dominated by the parameters that affect discharge pulse energy Newton et al. [108], Spedding and Wang [112], Jose and Shunmugam [113] and Rao, Ramji and Satyanarayana [114], and the white layer thickness should be minimised to reduce the effects of altered material hardness [115, 116] or modulus of elasticity. Formation of oxides can also occur, which affect the material properties and should be minimised [70].

White layer is important in the context of micromachining as often micromechanical parts, such as gears, are dependant on surface integrity. Where the parts are small, the white layer can represent a significant proportion of the part size and can weaken the part, causing failure or inadequate performance.

2.2.4 *Miniature Gears*

Due to its capability to produce intricate, finely-machined parts [14, 16], WEDM has been considered for the machining of micro-gears in recent years. Traditionally, micro gears can be manufactured by one or more of:

1. Material removal processes such as hobbing [117],
2. Forming processes such as stamping, extrusion and injection moulding,
3. Additive processes such as die casting and powder metallurgy.

As WEDM technology has advanced, it has become approximately 20 times more accurate [118]: it has been found that for metals WEDM has better dimensional accuracy than technologies such as laser cutting [119], leading to its application in producing small gears.

There are a number of process outcomes, based on those discussed in Section 2.2.1, that can be considered important when producing miniature gears. These include depth of white layer, surface finish, and gear form (Figure 2.16). The white layer is important since it the white layer for brass has an increased hardness. Though this typically increases wear resistance, the white layer is also more brittle compared to the base material. The risk of this is that the surface of the gears is more susceptible to crack propagation when the gears are subjected to stresses. It is not known on this scale whether this crack propagation would slow as surface stresses were reduced and therefore in this study it is desirable to minimise structural changes to the brass.

Surface finish is important both from a tribological point of view and an aesthetic point of view: a rougher surface finish will result in more friction between the gears assuming no lubrication is used, and specific surface topologies can also lead to increased uptake of lubricant which can improve the lubrication of the gears [120, 121]. Gear form affects accuracy and efficiency of motion transmission [122–124].

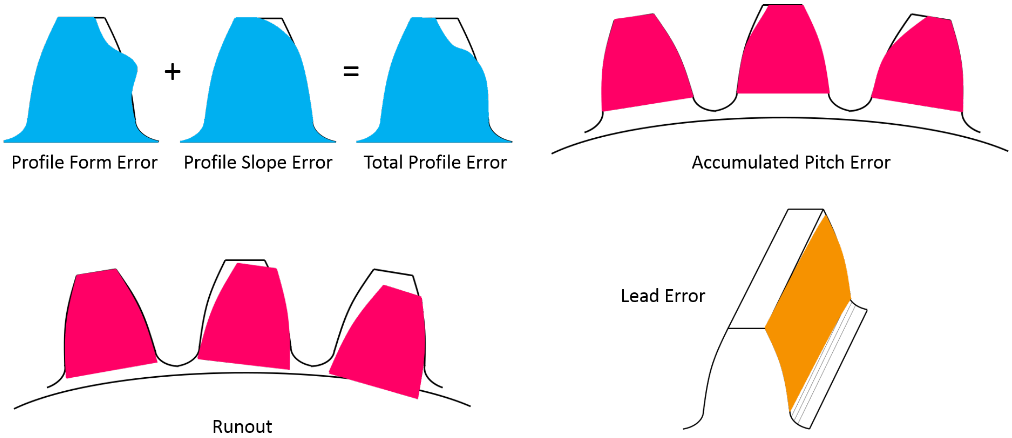

Figure 2.16: Gear Quality Measures: these include profile error, pitch error, lead error and runout.

Since hobbing and stamping are the traditional methods used for manufacturing small gears [56], the field of miniature gear production using WEDM is relatively small [66].

Some of the earliest work in this field was a capability study carried out by Hori and Murata [125] in 1994, who produced a micro spur gear of outside diameter 0.28 mm, using a tungsten wire of diameter 25 µm. This had involute profile and a profile error of less than 1 µm. The teeth of the gear were burr-free, and this study paved the way for further work on micro-gear production.

The research carried out has yielded a number of positive results [126–129]. By far the most limiting factor is wire diameter, since this limits the geometry of the gears [130]. As with any geometry, WEDM produces the white layer on the surface of the part which can have consequences for a part whose function is to transmit motion [131]. Similarly, deposition of the wire material can have this effect [132]. On the other hand, there are cases in which the surface geometry that the WEDM produces are actually favourable [133]compared with those hobbed or stamped [134], from a lubrication point of view. Gears produced using WEDM are typically burr-free, which saves further processing [135]. Gears with a very high aspect ratio (length, or thickness) to diameter) which can improve stability of WEDM machining [71] since there is more opportunity for sparks to form between wire and workpiece.

2.2.5 *Directions in the Field and Research Gaps*

Wire electrical discharge machining presents itself as an incredibly versatile machining process which can be used to accurately produce complex shapes using a single process. One of its major drawbacks is the speed at which parts can be machined: even when producing parts with a rougher surface finish machining is relatively slow, and if the aim is to produce a part where surface finish is critical, machining becomes slower still. On the other hand, if only a single part is being produced, such as a single specialised gear, WEDM becomes comparatively quick as opposed to producing dies, hobbing tools or grinding and then tumbling or otherwise finishing the part.

Extensive research into the parameters that affect the outcome of wire electrical discharge machining has revealed that there are several issues that create difficulty when researching the process: the first being the huge number of factors, and indeed levels, that can be changed (which often differ from machine to machine), the second being the optimisation problem that arises when most factors have the opposite effect on surface finish and MRR (and vice versa).

The most important machining parameters are those which affect the discharge energy, such as IP, T_{on} and VG. However, secondary factors have significant effects on surface finish, especially when combined. It is not possible, due to the sheer number of variables, to easily model the outcome of a given set of machining parameters. As a result, to achieve a good finish and decent MRR, an in-depth understanding of the effects of the various parameters is required, and often an iterative process of obtaining the best possible parameters.

WEDM has been successfully used to machine most metals and ceramics with sufficient levels of conductivity. In addition, a combination of research into minimising the white layer produced during machining, and production of miniature gears shows that there is significant potential to use WEDM in the production of miniature gears which are both highly accurate and possess appropriate tribological properties. Many miniature gears produced have had a high aspect ratio, which improves surface properties due to increased stability of machining [71].

Review of literature has identified that WEDM capability to produce very thin gears has not been studied in great detail. Only Benavides et al. [131] investigated optimum parameters for producing very thin miniature gears, and this was for an aspect ratio in the region of 0.1. Machining was successful but it was suggested that further investigation into white layer may be of interest. Furthermore, research is required into the relationship between white layer and geometry for complex parts, and how parameters can be optimised to improve this. In all studies considered, white layer is typically stated as a single depth value (without multiple measurements along the surface), as is R_a, and it is not clear how this varies and whether there is significance to this variation.

It is difficult to maintain stable machining in terms of reliable sparking opportunities under given conditions, and yet very thin gears have applications in space-saving micromechanical and micro-electrical systems. Production of gears with an aspect ratio of < 0.1 is likely to be more challenging due to the reduced area between workpiece and wire across which a spark can bridge the gap. However, the process has characteristics which make it a very attractive method for producing miniature gears such as high accuracy of machining and excellent surface finish. Further research should look at improving surface finish while maintaining stable machining as unstable machining can dramatically reduce MRR.

2.3 STATE-OF-THE-ART IN MICRO-MILLING

With increasing miniaturisation of engineered devices, micro-milling has emerged as one of the most popular processes for manufacturing small components because it is capable of rapidly producing high integrity parts [92]. It is widely used in the medical and aerospace sectors, and in fields where miniaturised machine elements are commonplace such as watchmaking; optics and electronics; and micro-mould manufacturing [4]. Some of these areas only require softer materials such as copper and brass alloys to be machined. However, the medical and aerospace industries make use of materials such as titanium and high-performance superalloys. These are typically difficult-to-machine using macro-scale tools, but present further complexity in micro-milling as burring and crystal irregularities lead to fracture of the tools. Wear studies of micro tools are essential since it is very important to achieve a high-quality surface finish in many of these industries, either for aesthetic purposes or because the function of the components is impaired where surface finish is poor (such as where components have moving parts). Furthermore, worn tools cause increased burring [136, 137] which causes dramatic increases in cutting forces [138]. It is also very difficult to remove burrs from micro components using conventional methods [90]. To understand the issues with size, tool wear measurement and burr formation with a view to characterising tool wear, existing studies into micro-milling and their applicability to this have been analysed.

2.3.1 *Tool Wear*

Based on the issues with machining on a micro-scale (subsection 2.1.4) especially regarding wear and fracture of tools, numerous studies have been carried out to investigate the effects of different parameters on micro tool wear.

Chip formation differs from the conventional case: for a small feed per tooth, a chip is not seen with each pass of the tooth [89, 139], and instead burnishing or rubbing occurs. This was seen by Kim et al. and Yuan et al. [89, 140], whereby a chip did not form for each pass. This differs from the conventional case and is attributed to the fact that when the uncut chip thickness is less than the edge radius of the tool, elastic deformation occurs rather than shearing (Figure 2.11).

Premature tool failure is a common problem in micro-machining and this presents difficulties when measuring wear: whereas in conventional machining the tool fails as cutting edges break, for micro-tools the entire shaft often fractures [91]. This is as a result of usage-related stresses, such as dulled, damaged or chipped cutting edges which cause excessive forces, or interrupted cutting. Cutting force variation patters observed by Tansel et al. [91] revealed that too failure was a result of chip clogging, fatigue and wear-related excessive stress. The effect that wear has on cutting forces is much more significant in micro-machining since a material loss of 0.095 x 0.127 mm at one cutting edge of a 12.7 mm end-mill will increase cutting forces a few percent, but on a micro-tool with 0.38 mm diameter half a cutting edge may be lost, and the cutting force on the other edge doubled.

Increased cutting velocity increases tool wear [141] which is similar to conventional machining [41]. Higher feed rates can reduce wear, but only provided that they are not high enough to cause fracture [142]. Interestingly, a study by Rahman et al. showed that a higher depth of cut resulted in a lower tool wear rate [139]. which contradicts the conventional machining results of Medicus et al. Medicus et al. [41] whereby a smaller radial depth of cut resulted in less tool wear. This suggests that the increased depth of cut resulted in reduced burnishing and plastic deformation of the workpiece which would reduce tool wear. It is also possible that a larger depth of cut resulted in increased tool stability thus reducing wear [139].

Since the edge radius of micro-tools is comparable with the grain size of materials that are being machined, microstructure is important and materials with a higher elasticity result in more ploughing (rather than shearing) [143]. This has been seen experimentally, although it should be noted that the focus was on different material properties of two grades of steel: SAE 01 high carbon and SAE 101 low carbon (the former having a perlite microstructure and the latter having a ferrite microstructure). Ferrite showed a higher rate of tool wear than pearlite in spite of the lower elasticity when compared with pearlite which causes less spring back and less burnishing. This was explained by the relatively higher toughness of ferrite which resulted in a build up of material on the tool which meant that ploughing was still a dominant mechanism for this crystal structure [143].

Temperatures in micro-milling are very low when compared with conventional milling operations (50-60°C for aluminium and 100-150°C for steel) due to small chip loads [144, 145]. However, in spite of the relatively low temperatures, the effects of temperature in micro-milling are important as feature sizes are small thus even small thermal expansion is significant, and tool life is generally short.

2.3.2 *Chip and Burr Formation*

The difference in behaviour of tools and materials when micro-machining results in differing mechanisms of chip and burr formation to the macro scale. Importantly, there is a minimum chip thickness below which a chip will not form [89, 145]: since the uncut chip thickness is similar to the tool edge radius (i.e. the tools appear relatively blunt) a chip is not generated if uncut chip thickness is less than a critical value [146]. This value can be increased with increased tool-workpiece friction [147, 148].

Burr formation is important in micro-machining since although burrs produced are typically smaller than those in macro-machining, they present the same assembly difficulties as larger burrs on macro-sized parts [149]. Lin et al. [150] found that for conventional face milling burr height increased with depth of cut. Work but Chern [151] agreed but found that this is only true up to a critical depth after which it suddenly decreases due to formation of another burr. It is essential to minimise burr formation, as burrs often cannot be removed easily from micro parts and contribute to tool fracture [152].

2.3.3 *Further Development of the Field*

Typically, tool wear studies in milling follow the protocols laid out in standards such as ISO8688-1 and ISO8688-2 [153, 154]. These determine what parameters, materials and sizes of cut should be used and are generally used as benchmarking tests for the quality of tools. However, for micro-milling the ISO standards are not appropriate and thus adapted tests must be carried out [155].

Furthermore, historically, studies on micro tool wear have plotted tool wear against cutting distance or cutting time. Measurement of cutting distance moved by the tool relative to the workpiece or cutting time (i.e. when the tool is engaged) does not consider the different feed rates and speeds used for different materials, and cannot be used to compare tool life of micro-tools between materials. Furthermore, micro tool wear studies are inconsistent across the literature reviewed since different metrics are used to measure the wear of the tool: edge radius, flank wear and tool radius reduction being the most popular. To better standardise micro tool wear studies and understand the wear of micro tools, a a novel protocol for measuring micro-milling tools should be established, with a view to unifying micro tool wear studies. This will overcome the issues of using existing methods that were primarily developed for macro-scale tools.

Part II

FUNDAMENTAL RESEARCH INTO PROCESSES

Following the motivations for work and the fundamental processes of interest identified in Part I, work has been carried out to improve these processes with a view to providing more efficient methods of producing micro-parts through optimised process parameters and increased tool life. This work looks at research on a more fundamental level (TRL 1 and TRL2) that can be applied to aerospace, medical and dentistry for producing miniature parts such as microchannels, dental implants and fuel injectors. Experimental methods for both WEDM and micro-milling are described, and then parameter optimisation for WEDM takes place. The majority of the research in this part is on micro-milling, ranging from development of a testing protocol for measuring and defining wear, to application of this protocol to tool life studies using different geometries and novel coatings.

3

EXPERIMENTAL METHODS

3.1 WEDM

3.1.1 *Machining Process*

Machining trials took place on a Mitsubishi Electric MV4800 Wire Electrical Discharge Machining (WEDM) centre. The machine consists of a submerged bed onto which the workpiece was mounted (Figure 3.1). The clamping system used is detailed in Figure 3.2. A wire of diameter 0.25 mm was used to cut in each instance. Machining parameters were altered according to the Mitsubishi Electric machining characteristics databook [156]. 1 mm holes were drilled prior to machining with WEDM to allow the wire to be threaded into the workpiece to be threaded using a water jet.

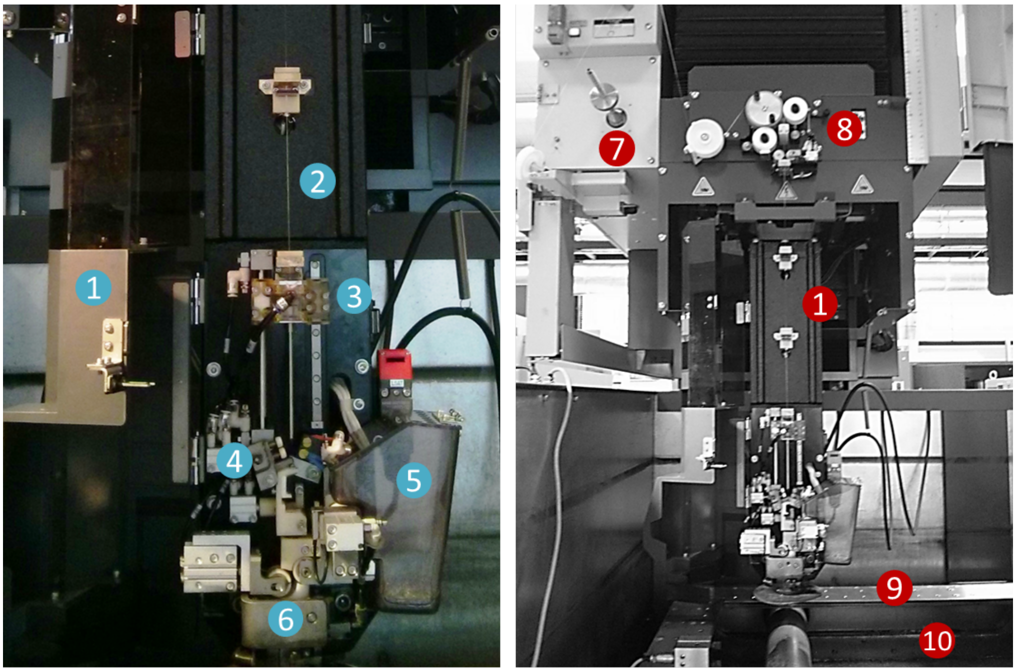

Figure 3.1: | 1. Guard | 2. Wire | 3. Tension control | 4. Wire cutter (spark) | 5. Wire collection | 6. Lower tension control | 7.Wire spool | 8. Guide rollers | 9. Machine bed | 10. Dielectric fluid tank |

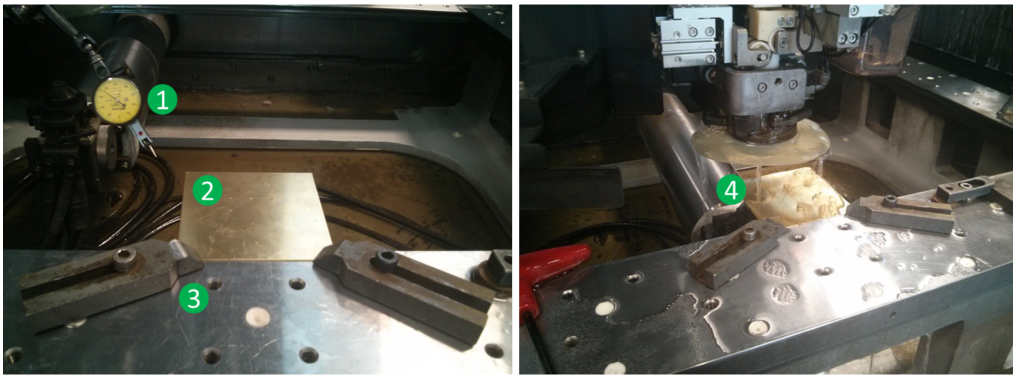

Figure 3.2: Clamping system for workpieces. | 1. Dial gauge for squaring workpiece | 2. Pre-drilled workpiece | 3. Clamps | 4. Water jet for threading |

All experiments were designed using a full-factorial 2-level Design of Experiments (DOE) which incorporated a number of machining parameters. In each instance, machined surfaces were tested for surface finish along the WEDMed edge, and depth of white layer was investigated. Where gears where produced, profile fidelity was also investigated.

3.1.2 *Analysis of Surface Finish*

In each experiment, surface finish of the machined edges were measured using an Alicona Infinite Focus microscope system. Two models of optical profilometer were used: the SL and G5. The SL is a three-axis imaging system which is capable of automatically scanning in the x, y and z axes with a single fixed magnification. The G5 system comprises a rotational axis in addition to the SL functionality and has multiple interchangable magnifying lenses. The SL was used with 10x magnification and automated movement of the testpiece x-y planes and the G5 used lenses with magnification between 10x and 50x and automated stage movement in the x, y and rotational axes about x and y.

The Infinite Forcus Microscope (IFM) rapidly produces 3D datasets using optical profilometry. A low depth of field of an optical microscope is combined with vertical scanning, and traverses the sample. This resuilts in topographical images which have both high resolution and high depth of field. At the same time field of view is large. The advantage of this is quick and simple measurement of information such as profile form, profile roughness, and surface texture. Measurement is quicker than using conventional tactile methods..

A 3D image is constructed from numerous of 2D images that have been captured between the lowest and highest focal plane (Figure 3.3). This data is then compiled to produce a numerical dataset which can be rendered in the Alicona software.

Where surface roughness is measured, the profile width and cut-off wavelength have been specified in experimental chapters. They have been controlled in order to conform with ISO4287.

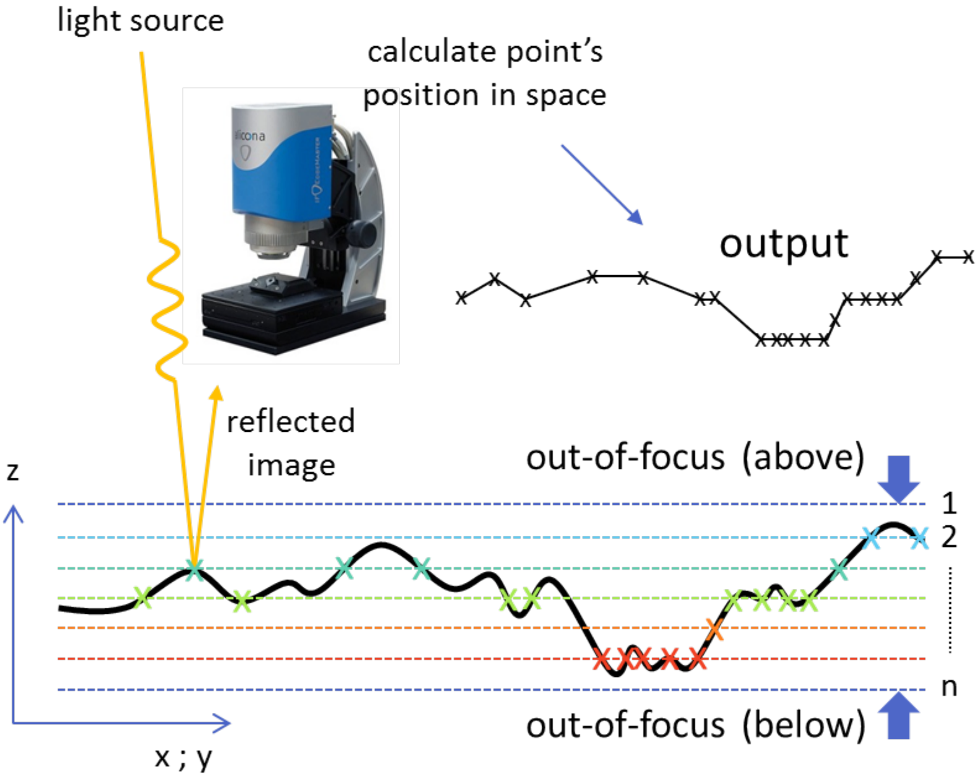

Figure 3.3: Working principles of Alicona optical profilometers.

3.1.3 *Analysis of White Layer*

Since white layer often represents significant changes in crystal structure of the outer layer of a WEDMed surface, it is typically undesirable and thus measurement is important. A Scanning Electron Microscope (SEM) can be used to examine the surface topography of WEDMed surface. Various methods of measuring the white layer are employed. Firstly, SEM imaging of the surface (Figure 3.4) was used to investigate morphology.

Following this a polishing and etching protocol was developed using testpieces from previous trials to maintain the integrity of the workpieces from the present trial. The testpieces were mounted in conductive mounting compound and polished using a diamond suspension until a scratch-free, mirror-like surface was achieved.

The mounted test pieces were then etched using a solution of water, hydrochloric acid (HCl) and iron nitrite ($Fe(NO_3)_3$)as follows:

- Hydrochloric acid – 25mL
- Iron (III) nitrate – 5g
- Water – 70mL

The solution was mixed in fume cupboard and then samples were submerged for 20 - 30 seconds and removed using tweezers. They were then dipped in water to terminate the etching process.

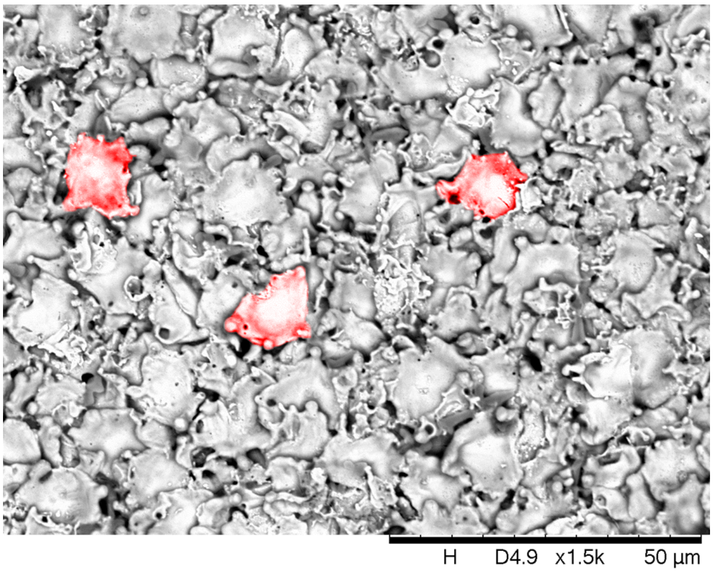

Figure 3.4: An example of the crater-like structure observed after a cut with a WEDM. Each crater (highlighted in red) represents an area melted by a single spark.

Following this, the testpieces were examined first using optical microscopes at 50x magnification, and then using an SEM . Figure 3.6a shows an optical image of straight line cuts. The images clearly show the grain structure throughout the brass. The edge of the testpiece reveals a dramatic structural change. A very fine-grained structure is seen, where the outer layer of the material has melted and been recast in a very short space of time (due to the cooling of the dielectric).

To quantify the depth of white layer, W_d, different points were measured on workpieces optically, as detailed in Figure 3.5. Sometimes this took place after etching.

SEM images (Figure 3.6b) were also taken, allowing a higher magnification which revealed the shape of the crystals. In the figure, not only are they much smaller, but a longer, thinner structure can be seen.

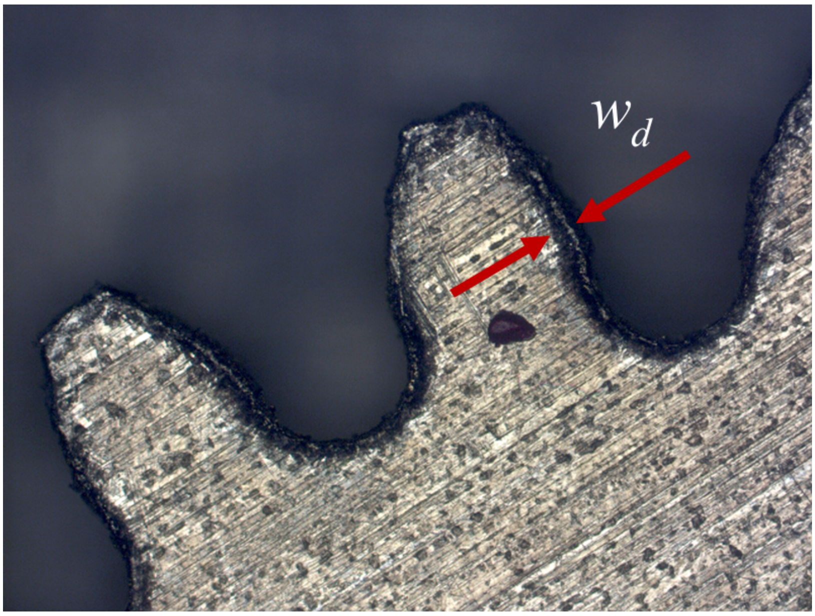

Figure 3.5: Optical measurement of white layer depth, w_d.

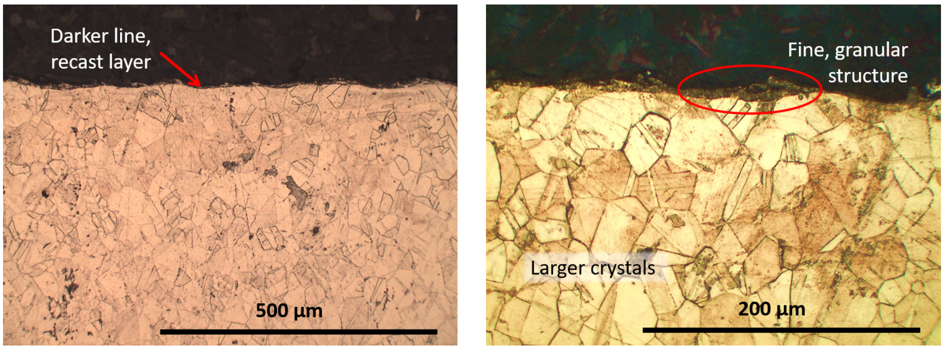
Darker line,
recast layer
500 µm
Fine, granular
structure
Larger crystals
200 µm

(a) Straight Cut testpiece magnified 200x (left) and 500x (right)

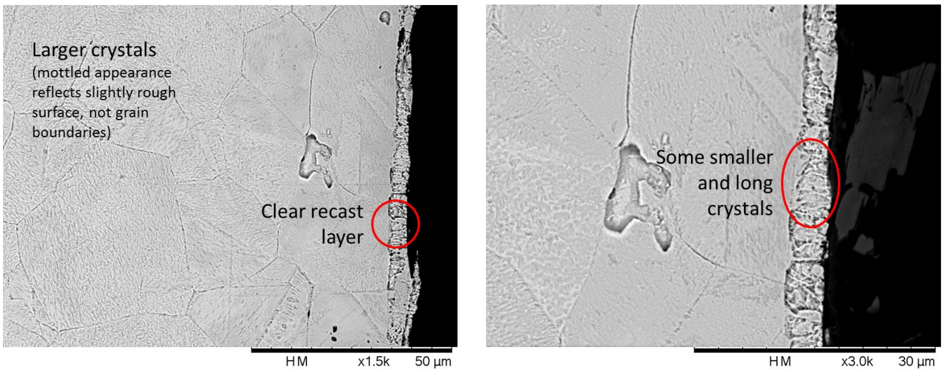
Larger crystals
(mottled appearance
reflects slightly rough
surface, not grain
boundaries)
Clear recast
layer
HM x1.5k 50 µm
Some smaller
and long
crystals
HM x3.0k 30 µm

(b) Straight Cut testpiece magnified 1500x (left) and 3000x (right)

Figure 3.6: Photos of a straight cut testpiece taken optically, and SEM micrographs of a straight-cut testpiece.

3.1.4 *Profile Fidelity*

A novel method of determining profile fidelity of gears was investigated (subsection 3.1.4). The purpose of this was to provide a low-cost method for basic gear measurement without the need for complex equipment. It also allows gears to be measured much more quickly than using more accurate methods.

There are a number of standard methods that companies use to assess the quality of gears [157]: these include pitch deviation f_p, pitch error f_u, radial runout F_r and pitch total deviation F_p. These values, amongst others, can be classified against various gear norms such as the American International Standards Institute ANSI/AGMA 2015-1-A01, the International Organisation for Standardisation ISO 53:1998 [122], the British Standards Institution BS 436-1:1967 and the Deutsches Institut für Normung (German Institute for Standardisation) DIN3961. DIN standards are widely used in the gear industry and at the AMRC.

The aim of the DIN standard is to ensure that the functional requirements of a gear are met by maintaining a high quality. To ensure this, certain parameters are constrained. The standards document DIN3961 covers gears from 1 to 70 mm [124], which is outside the scope of gears produced in this report (whose module ranged from 0.33 - 0.83). For small gears, the standard available is DIN58400:1984-06 which replaced DIN58400:1967-08. However, this was withdrawn without replacement in 2016-04.

When assessing the quality of WEDMed gears, both form errors and position errors are considered:

- Form errors describe a deviation form the nominal shape, and these include profile errors (depicted in Figure 3.7) and lead errors (Figure 3.8).
  - Profile error, which is a distortion in the involute profile, affects the noise of gears (gears with high profile error are noisier).
  - Lead error, which is a linear deviation along the tooth face, affects the load carrying capacity [158].
- Position errors describe the accuracy of the location of teeth, and include pitch error (Figure 3.9) and runout (Figure 3.10).
  - Pitch error is the difference between nominal angular locations and the actual measured location.
  - Runout is a maximum difference of radial position of teeth to designed position.
  - Both pitch error and runout affect the motion transfer of the gears.

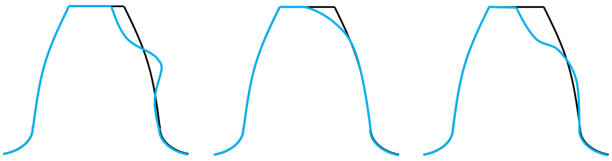

Figure 3.7: Profile errors, characterised by a deviation from the nominal profile. These increase noise.

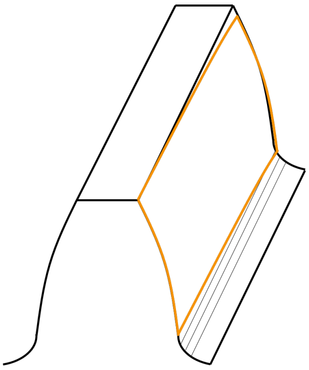

Figure 3.8: Lead errors, a linear deviation along the face of the tooth. This affects load-carrying capacity.

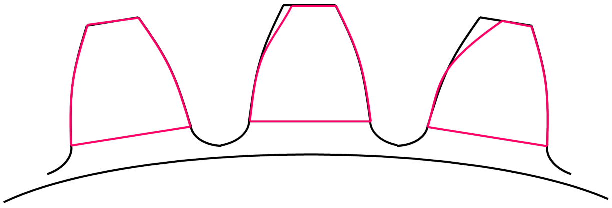

Figure 3.9: Pitch error, the difference between nominal angular location and actual measured location. This affects motion transfer.

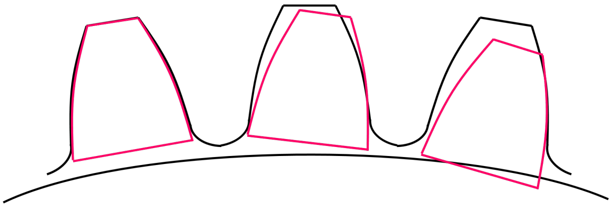

Figure 3.10: Runout, radial displacement of gear teeth which is cumulative across teeth. This affects motion transfer.

Profile error increases noise where gears are meshed, while lead error reduces the load-carrying capacity of the gears [158]. Form errors affect motion transfer. Thus, all of these errors must be correctly understood to assess the quality of a gear.

Assessing form errors and position errors usually involves measuring, amongst other things, the following: tooth thickness measurement (form), pitch (position), tooth alignment (position), lead (form), runout (position) and profile (form)[159]. Gear measurement can be either functional or analytical. Functional gear measurement involves placing the gear in a test rig and checking that the gear behaves in the manner expected when meshed with a known quality gear. The advantage of functional measurement is that it returns a 'real-world' result: this says how the gear will actually behave. However, functional measurement does not identify individual geometrical contributions to error. Usually a combination of both functional and analytical measurement are used [160].

Analytical gear measurement involves checking individual elements of a gear. The methods for checking the described form errors generally fall into one of three categories: tactile, optical and acoustic. Some of these are summarised in Tables 3.1 and 3.2.

3.1.4.1 *Tactile Techniques*

Traditionally, gear measurement has taken place using tactile or specialist optical measurement, with equipment such as Coordinate Measuring Machine (CMM)s, optical comparators, precision height gauge sets (all of which are expensive and specialist) or rotation through small angular increments and numerous measurements either optically or with callipers. Each of these require specialist equipment and are slow [160]. Tactile measurements include techniques such as double flank testing and probing using either a CMM or rolling test. Double flank gear roll testing, consisting of a master gear meshed with the test piece, which measures centredistance variation, which describes form errors. However, there has been difficulty in repeatability with this method due to part change, i.e. wear [161]. A further issue with this method is that slight sliding can occur, leading to unstable readings. Pueo et al. [162] also found fault in that there was no clarity or fixed guidelines for measuring or reporting in such inspection; necessary to allow comparison and repeatability of results between setups. An alternative to this method is a Double-Flank-Rack Probe (a rolling test using a probe rather than gear). This was found by Tang and Jia [163] to be faster and more repeatable than a gear-specific CMM although measurement time was not stated. Latterly, faster and more accurate methods have been developed using more sophisticated optical techniques such as triangulation and interferometry, and acoustic techniques, which allow on-line measurement.

3.1.4.2 *Optical Techniques*

There are various methods of optically measuring gears precisely. Laser-line triangulation can deliver uncertainties of only a few micrometers, and can be used on-line [164]. However, triangulation can be inaccurate, and deviates form tactile measurements due to reflection from the gear flanks and other systematic errors [165]. Laser interferometry presents a better method, allowing faster scanning speeds than can be achieved tactically [166]. As the beam has a small diameter, it is able to penetrate into small topologies. A major advantage of this method is that it can offer on-line inspection – however, initial calibration is required. Previously, calibration was difficult and nonstandardised although Seewig et al. [167] went some way improve this by developing a mathematical model. To further its applicability, this approach can also be carried out using a Light-emitting diode. In addition to laser interferometry, white-light interferometry-based sensors for the surface topography measurement of tooth flanks have also been developed [168], allowing enhanced speed of measurement over laser interferometry (although resolution is reduced). The method lacks the ability to measure steep geometries, requiring vertical observation and line-of-sight between measurement instrument and surface (thus eliminating gears with very small width of space [166]. As with tactile measurements, a difficulty with interferometry is that optimisation of parameters such as brightness and exposure is often carried out using trial-and-error, and would benefit standardisation [169].

3.1.4.3 *Acoustic Techniques*

When in operation, gear surface quality can be assessed by noise monitoring or acoustic emissions (AE). AE is less sensitive to background noise and resonance, although higher sampling rates are required. As a result of this lower susceptibility to environment, AE is considered much more reliable than vibration, which is not considered to consistently describe gear tooth damage [170]. Sophisticated modelling has been produced which allows AE to describe gear tooth topologies, profiles and asperity contacts. However, it requires gears to be meshed, i.e. at least tested in an operational environment, which is more time-consuming than measuring in the manufacturing environment [171]. All of the methods previously described represent the state-of the art in methods for high-quality gear measurements with improved timings as compared with traditional methods. A technique proposed here uses image-processing (described in Section 3.1.4.5) to give an indication of whether a gear has apparent geometrical errors. This can be used to determine whether the dimension or form of the gears lies outside the acceptable range. Surface topography and finish of teeth can be determined by methods such as stylus and optical profilometers, which is not possible optically. However, the information provided on geometry offers an initialstage elimination of gears which do not meet specification, reducing the number of more time-consuming measurements taken.

3.1.4.4 *Novel Optical Technique*

Based on the research into the tactile, optical and acoustic techniques described, a novel optical techniques for quickly measuring the gears is proposed. The method is design to overcome the high costs of traditional gear measurment and to provide a simple pre-inspection technique for measuring gears. The method uses image-process to compare a high-resolution microscope image of the gear cut-out with the Computer Aided Design (CAD) the file image output to determine the difference between designed profile and manufactured profile. This method is appropriate for use with a standard optical microscope and is thus both low cost and convenient for most laboratories.

The technique is used (described in Section 3.1.4.5) to give an indication of whether a gear has apparent geometrical errors. This can be used to determine whether the dimension or form of the gears lies outside the acceptable range. Surface topography and finish of teeth can be determined by methods such as stylus and optical profilometers, which is not possible optically. However, the information provided on geometry offers an initial stage elimination of gears which do not meet specification, reducing the number of more time-consuming measurements taken.

	Form Errors		
	Tooth Thickness	Lead Error	Profile Eerror
Method of Measurement	**Chordal thickness:** This uses a tooth calliper, which is referenced against the outside diameter of the gear. Thickness is measured at the pitch circle. As thickness varies, it is hard to take accurate chordal measurements. 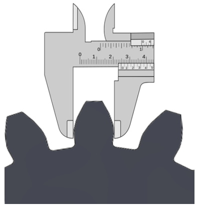 **Span measurement:** This uses the distance between numbers of teeth. A span measurement S_n is taken across a number of teeth Z_n using a special tooth thickness micrometer. The value measured is the sum of normal circular tooth thickness on the base circle, S_{bn}, and normal pitch $P_{en}(Z_n - 1)$. Measurement is not affected by runout or variations in outside diameter, but will be erroneous if profile is wrong. 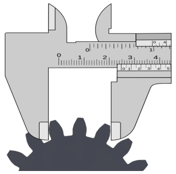 **Pin and ball method** Two or three cylindrical pins of specified diameter are place in diametrically opposite tooth spaces. If the number of teeth is odd, they are placed as close to opposite as possible. Accuracy depends on ball size. It is less accurate than angular indexing. 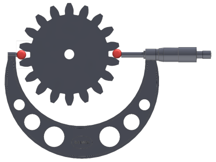	**Height Gauge[172]:** A spur gear has a theoretical lead angle of 90°. This is measured using a height gauge set for a fixed height H. The gear is then rotated to bring the tooth into contact with the indicator on the height gauge. This method can be automated for speed of measurement	**Indirect measurement:** Uses callipers with wires, rolls, pins or balls of varying diameters. Slow, but accurate. **Generative involute measurement:** This checks involute profiles of gears. A straight edge is rolled around a base without slipping, and the stylus of dial gauges attached to the straight edge will trace an involute. This can be automated, but only works for involute gears. **Optical methods:** An optical comparator and a profile projector are used to magnify the profile of the gear. This is then projected and compared to the master profile. Quick, and works well for small, thin gears but not larger gears, but less accurate than CMM. **Coordinate measuring machines (CMMs):** The tooth is probed at a series of discrete points, and the coordinates of each point are compared with the expected coordinate. Highly accurate but slow. Specialist CMMs are required. **Tooth displacement method:** The gear is rotated through small angular increments. Readings from height gauges touching the gear surface are compared with theoretical values. 5-10 measurements are taken along the tooth flank. Slow but highly accurate. Used for functional testing of precision components or master gears.

Table 3.1: Analytical methods for checking gears for form errors, and their relative uses, advantages and disadvantages.

	Position Errors	
	Pitch Measurement	Runout Measurement
Method of Measurement	**Pitch comparator** This is a two-probe device. The probes obtain positional data from adjacent tooth flanks. To obtain spacing values, this data must be subjected to mathematical operations. This only finds relative pitches around the gear. 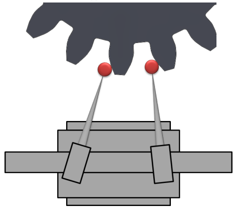	**Dial indicator and Ball** The primary method of measuring runout is using a dial indicator over a pin or ball placed in successive tooth spaces. 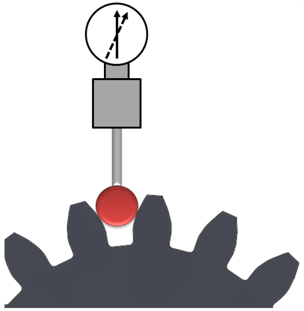
	Angular indexing This is a single probe which is used with an indexing system to determine actual position of gear teeth. Unlike the two-probe system, this can find exact locations of teeth[100]. 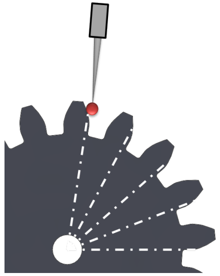	**Automated Measurement** The dial indicator and ball method can be carried out using CNC gear measuring machines. This means it can be fully automated, and quicker. It is also highly accurate.

Table 3.2: Analytical methods for checking gears for position errors, and their relative uses, advantages and disadvantages.

3.1.4.5 *Image processing method*

The gear is placed on a matt, red backdrop since a white background contained too much information in each plane for simple threshold calculations (Figure 3.11). An image processing method was used to compare a high-resolution microscope image of the gear to determine the difference between actual profile and ideal profile:

A. An image is taken using a a Zeiss Axio Imager optical microscope, with an objective lens of magnification 5x and 10x ocular lens in front of the camera. This has a resolution, calculated using a maximum of 700 nm for white light, of 2.69µm, while the camera has a resolution of 5MP (pixel size of 0.70µm).

B. The image is separated into red, green and blue planes. These are evaluated, visually, to determine the plane offering the most contrast between gear and background. The image is then converted to black and white, using a simple binary thresholding algorithm: pixel value is set to zero above a certain threshold (defined by the user) and set to 1 otherwise.

C. Using image dilation, the holes in the image are filled in. The value of the output pixel is the maximum value of all pixels in the neighbourhood. Thus in this case, a pixel is set to 1 if any of the neighbouring pixels have the value 1. A structuring element is defined, such that the neighbourhood of the pixel of interest was a square of dimensions 8x8 pixels. Thus, any pixel that was surrounded by a 1 in the neighbourhood was set to 1. The purpose of this was to remove noise.

D. An outline of the image is produced is produced by a pixel to 0 if its 4-connected neighbours are all 1's, thus leaving only boundary pixels. This allows subjective appraisal of form errors quickly to identify whether errors such as runout or burring have occurred.

E. Either the gear is filled, using image dilation or the image in (c) is inverted.

F. The image a, from the CAD file, and b, from the actual gear, are each subtracted from on another. This shows both areas where material outside the gear boundary is seen, and where material missing from the expected boundary is seen.

G. Green background returned the worst result, due to the difficulty discerning between gear and background. For a brass gear, the red plane is the most successful in thresholding. The overall volume of the measured gear is calculated in pixels. This is then compared to the number of pixels in the CAD image, to determine an area difference, in Pixels. The error factor (EF) describes the difference as a proportion of the expected tooth area.

An image processing method was used to compare a high-resolution microscope image of the gear cut-out with a CAD file image output to determine the difference between actual profile and ideal profile.

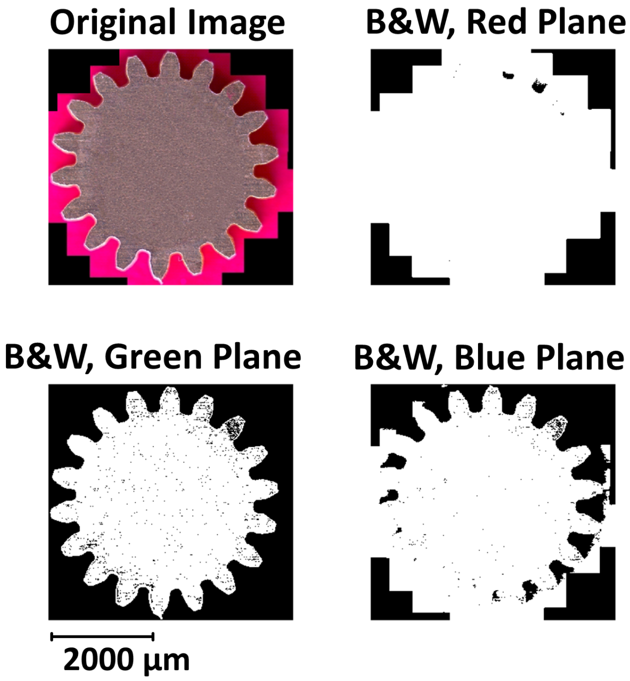
Original Image
B&W, Red Plane
B&W, Green Plane
B&W, Blue Plane
2000 µm

(a) Thresholding in RGB with red background.

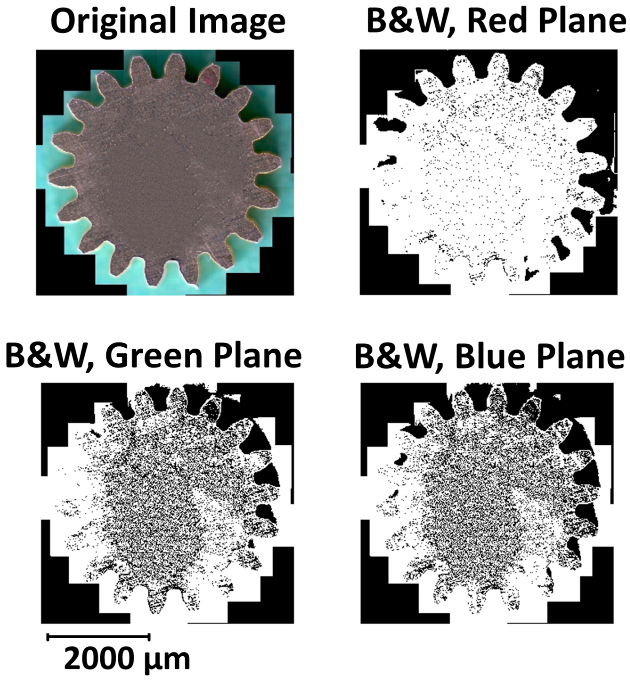
Original Image
B&W, Red Plane
B&W, Green Plane
B&W, Blue Plane
2000 µm

(b) Thresholding in RGB with green background.

Figure 3.11: Thresholding with a red and green background.

Following this, the absolute difference was calculated between the binary images, and the number of pixels counted N_D. This value was divided by the total number of pixels of the **teeth only** in the CAD file N_t. The analysis process used is depicted in Figure 3.12. The reason for using the teeth only is that the difference between the images returns almost no pixels from the centre of the gear since this is area is almost identical for both. Dividing N_D by total number of pixels in CAD file $N_T$would give an artificially low error. Thus the profile error of the gears can be calculated by

$$\text{Error Factor} = \frac{N_D}{N_t} \tag{3.1}$$

or

$$\text{Profile Error} = 100\left(\frac{N_D}{N_t}\right) \tag{3.2}$$

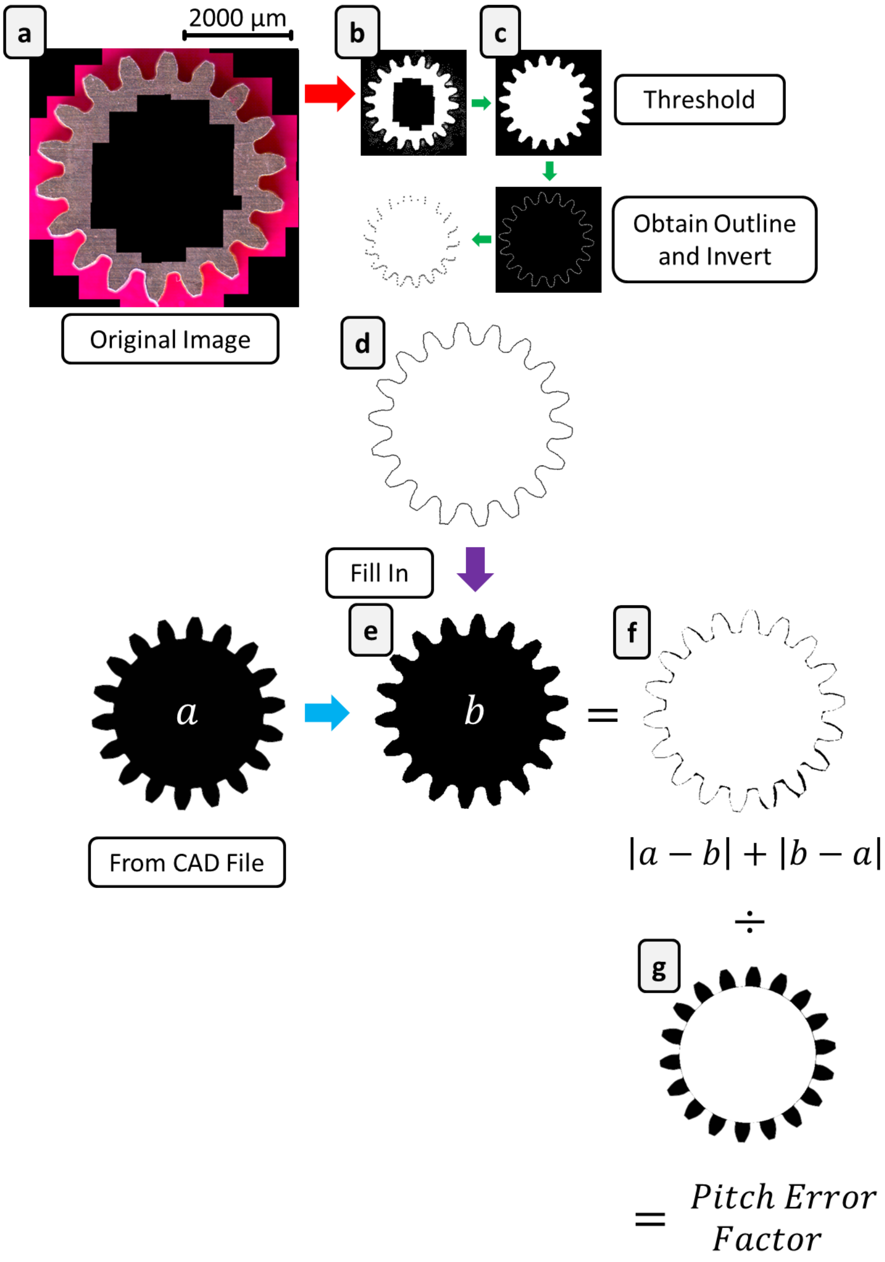
a
2000 µm
b
c
Threshold
Obtain Outline and Invert
Original Image
d
Fill In
e
a
b
=
f
From CAD File
$|a - b| + |b - a|$
÷
g
= Pitch Error Factor

Figure 3.12: Image analysis method for determining profile errors in gears.

3.1.4.6 *CMM Method*

Limited use of a CMM was provided by the Bremont Watch Company. The gear was mounted onto the machine bed and an optical vision system was used to locate the edges of the gear at various points. These points were then combined to produce a Drawing Exchange Format (DXF) file. This DXF file was registered with the originalCAD file used to produce the gears by aligning the centre points of the two gears, and then rotating the CAD image until corresponding burrs lined up.

3.2 MICRO-MILLING

3.2.1 *Machining Process*

All work was carried out using 500µmTungsten Carbide (WC) micro-end-mills. Where different coatings were applied, this is specified. Tools were obtained from multiple suppliers: Kyocera-SGS, OSG and SECO. The trials were designed with feeds and speeds as recommended by tool manufacturers. Exact values are quoted in experimental chapters. Wear of the tools was to be measured at specific points in the machining.

The trials took place on a KERN Evo micro-milling machine with a maximum spindle speed of 50,000 RPM. The recommended spindle speed 0.5 mm mills is in the order of 100,000 RPM. The KERN EVO had a maximum spindle speed of only 50,000 RPM, so the feed rate was reduced in accordance with Equation 3.3 to achieve a feed per tooth that matched manufacturer recommendations, where v_f is table feed rate, n is spindle speed and z_c is number of cutting teeth.. The workpiece and tool were flooded continuously thoughout the cutting process using synthetic Hocut 768.

$$v_f = f_z \times n \times z_c \tag{3.3}$$

Standard testpieces were used throughout all studies to allow for comparison. Four materials were investigated:

1. CZ108 Brass (CuZn38)
2. Titanium grade 2 (Table tab:Chemical-composition-ti)
3. Hastelloy C-276 (Table tab:Chemical-composition-of-hast)
4. Stainless steel 316 (Table tab:Chemical-composition-of-steel)

The standard test piece was 2mm thick, 35mm x 25mm, designed to fit on a Kistler force cell with a working area of 25 mm x 25 mm. The standard cuts were 25 mm slots to a depth of 0.2mm (Figure 7.5). A slot (or a number of slots as specified in individual chapters) was cut, then the tool was removed for wear measurement. This was repeated until 10 measurements had been carried out for each tool. Number of slots cut in between measurements were chosen based on preliminary trials.

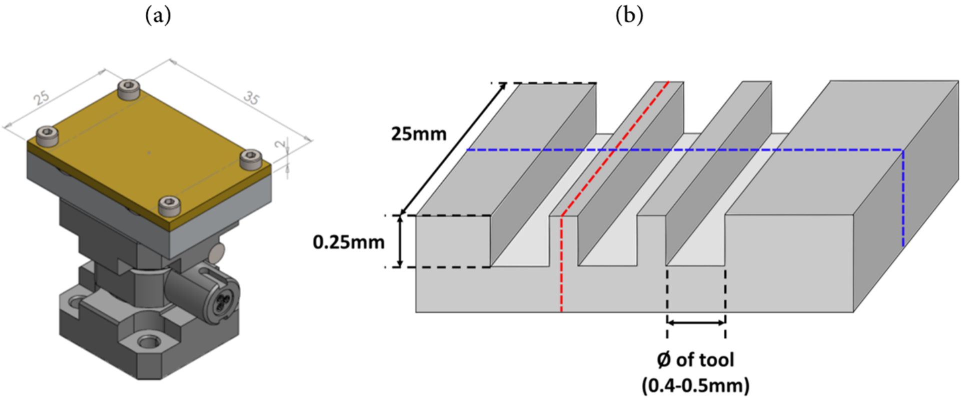
(a) (b)

Figure 3.13: (a) shows the workpiece mounted onto the load cell, (b) shows the slotting process that was carried out.

The testpiece used was brass (CuZn38) cut to a standard size of 25 × 35mm, and straight cuts of 25 mm (across the width of the testpiece) took place. During machining, the tools were then removed from the machine and collet at pre-determined intervals for measurement using an SEM using both secondary electrons (SE) and the back-scattered electrons (BSE) to allow optimal opportunity to recognise wear features. The tool was then re-installed as close to the original protrusion length and the process repeated until the tool fractured or 800 mm was reached. This allowed a picture of the wear to built up. The total length of the cutting edge (rake face) was measured, and this was subtracted from the inital length to give a wear percentage.

Four tools were tested, with two sets of parameters. The parameters used are detailed in Table 5.3.

C%	O%	N%	H%	Fe%	Ti%
0.10	0.25	0.03	0.0155	0.30	**rest/bal**

Table 3.3: Chemical composition of Titanium grade 2 (with major elements in **bold**). All alloying elements are an upper limit.

C%	Co%	Cr%	Mo%	V%	W%	Fe%	Ni%
0.02	2.5	**14.0 - 16.6**	**15.0 - 17.0**	0.35	3.0 - 4.5	4.0 - 7.0	**rest/bal**

Table 3.4: Chemical composition of Hastelloy C-276 (with major elements in **bold**).

Cr%	Ni%	Mo%	C%	Mn%	P%	S%	Si%	N%	FE%
16.0 - 18.0	**10.0 - 14.0**	2.0 - 3.0	0.08	2.0	0.045	0.03	0.75	0.1	**rest/bal**

Table 3.5: Chemical composition of Hastelloy C-276 (with major elements in **bold**).

3.2.2 *Measurement of Tool Wear*

It was determined that optical microscopy at a high enough magnification did not allow sufficient depth-of-field, and the infinite focus microscope (subsection 3.1.2) lacked sufficient magnification. The tools were therefore measured using an SEM, which was able to offer a much greater depth of field than optical microscopes [173]. This is due to the ability to create a small convergence angle of the beam, due to internal geometry of an SEM. Depth of field is given by

$$h = \frac{0.1}{M\alpha} mm \tag{3.4}$$

Where h = depth of field, M = magnification and α = convergence angle of the beam [174].

Furthermore, SEMs are able to provide higher resolution images than microscopes because the wavelength of the probing beam is orders of magnitude smaller.

Initially tools were measured end-on only, as in Figure 3.14. Rake face wear was the only parameter measured.

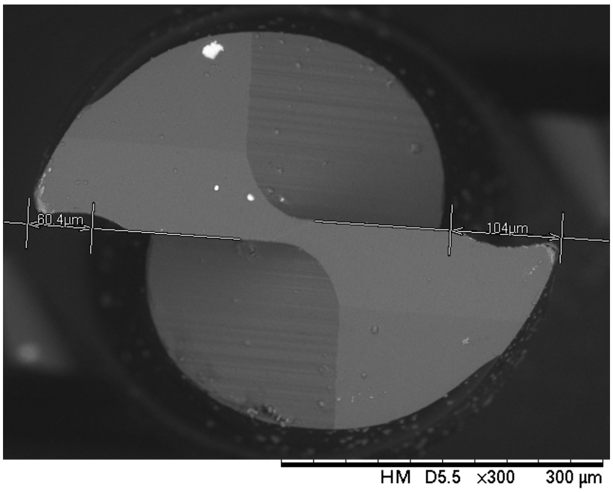

Figure 3.14: Measurement angle for tools in early studies.

Following the development of a formal wear measurement protocol, detailed in chapter 5, The tools were imaged in two orientations: side-on, and face on as shown in Figure 3.15) Three types of wear were measured: flank wear, denoted VB; rake face wear, denoted KT., and outside edge wear, denoted OE. The measurement process was as follows:

1. Tools were removed at pre-determined cutting distances
2. Tools were washed in acetone, and then air-dried to remove swarf and dust before:
   a) Imaging in an SEM using both scattered and back-scattered electrons, to enable;
   b) Analysis in image measurement software to determine the type and extent of wear seen

3. Tools were then replaced and steps 1-2 repeated
4. Catastrophic failure was recorded in the cases of the loss of one or both teeth (as seen in Figure 5).

All wear measurements throughout are expressed in terms of µm.

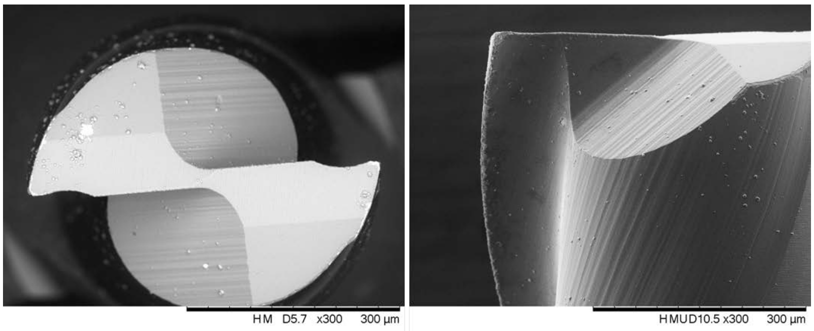
HM D5.7 x300 300 µm
HMUD10.5 x300 300 µm

Figure 3.15: Tools were measured face on (left) and side on (right) to determine wear.

3.2.3 *Measuring Cutting Forces*

Workpieces were mounted using a specialist fixture (Figure 7.5a) mounted onto a 3-component force link (Kistler 9317C) (Figure 3.16) capable of measuring cutting forces in three dimensions (x, y, z) aligned with the major axes of the cutting process. The cell is capable of measuring ±0.5 kN in the Fx anf Fy directions and ± 3 kN in the Fz direction with a sensetivity of 26 pC/N. This was connected to a National Instruments data acquisition system (DAQ) and cutting, feed and normal forces were post-processed to observe the relationship between tool wear and cutting forces where relevant.

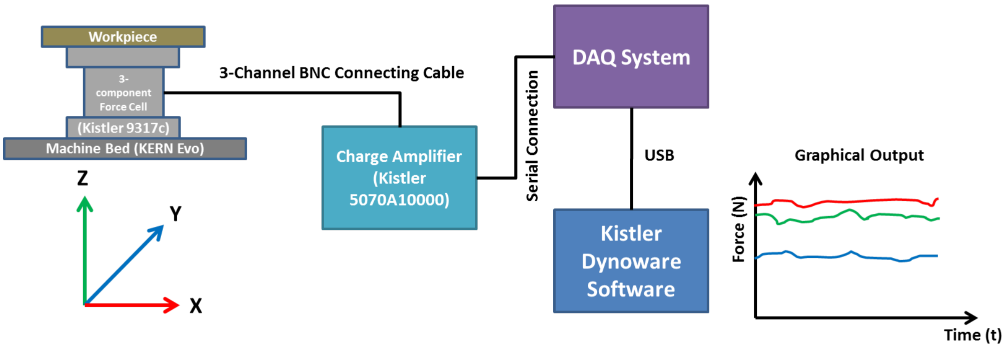
Workpiece
3-component Force Cell
(Kistler 9317c)
Machine Bed (KERN Evo)
Z
Y
X
3-Channel BNC Connecting Cable
Charge Amplifier (Kistler 5070A10000)
Serial Connection
DAQ System
USB
Kistler Dynoware Software
Graphical Output
Force (N)
Time (t)

Figure 3.16: Schematic of the force measurement setup

4

OPTIMISING MACHINING PARAMETERS IN WEDM

4.1 APPLICATION OF WEDM IN MICROMECHANICAL SYSTEMS

Electrical Discharge Machining (EDM) uses an electrode to initiate a spark which erodes the workpiece. Wire Electrical Discharge Machining (WEDM) is a special case of this, whereby the electrode is a wire that is continuously fed through the machine [16]. WEDM is capable of achieving excellent surface finish without the need for post-processing [14], and of producing intricate parts with high dimensional accuracy [16]. It is thus used in the dental, medical and jewellery industries, and to machine materials that are considered difficult-to-machine by conventional processes [15]. Parts produced by WEDM often require little or no finishing or polishing. Typically, on the micro-scale, WEDM is used to produce non-moving parts [82, 175]. However, increasingly it has been considered in the production of micromechanical parts designed to move, such as miniature gears.

An important consideration when machining with WEDM is the issue of the white layer; the layer of material affected by heat. The resulting surface can result in different tribological behaviour of machined parts when compared to polished or ground finishes, even where surface finish (R_a) is measured to be the same. This is especially case where lubrication is involved [175], and can be explained both by elastohydrodynamic lubrication theory (whereby elastic deformation of the machined surface changes alters the shape and thickness of the separating lubricant film [176]) and by the idea that surface topography influences the thickness and behaviour of the lubricant film [177]. This can have an impact on the functional behaviour of the gears and must therefore be taken into account. White layer can also alter the structural properties of the material, making it harder and more brittle, thus reducing fatigue strength and wear resistance.

A significant downside of WEDM is the length of time taken to complete macro-scale parts in comparison to conventional machining methods such as milling or turning. It is possible to produce gears more quickly using traditional processes such as hobbing or stamping [178]. On the other hand, hobbing has high set-up costs, and it requires specialist skills to design the tools. Furthermore, it is possible to produce the cutting tools used to stamp gears using a WEDM, which takes advantage of the high-fidelity geometry that WEDM can produce and indeed the surface finish which ultimately affects the accuracy of a stamped part. The applications of WEDMed gears that elicit further research fall into two distinct areas:

1. Research into surface finish and applicability of the process in producing small-run or prototype gears geometries.

2. Research into geometrical accuracy and validity of WEDM as a method for producing gear-cutting dies.

Although machining with WEDM is slow, it is possible to produce gears with fewer form errors than traditional machining processes such as hobbing [134]. WEDM also results in low residual stresses [16], so gears are much less likely to buckle due to machining-induced internal stresses, which results in more reliable meshing.

Micro-WEDM can be defined as a scaling down of the WEDM process. However, standard WEDM machines typically will not operate with wires below 0.1 mm in diameter, and it is thus that micro-WEDM is defined to machine with a wire smaller than 0.1 mm. As described in subsection 2.1.1, material removed from the centre of the wire is equal to $(1/2 \times D) + G$ where D is wire diameter and G is spark gap. As a result, machining geometry is limited by wire diameter. Various attempts in literature to produce gears using micro WEDM have resulted in a micro spur gear of outside diameter 0.29 mm with profile error of 1 µm [125]; gears of outside diameter 0.5 to 6 mm within 0.4% of original design [135], and a 6 mm gear with a profile error of 0.05% [131]. Using micro-WEDM setups it is possible to produce smaller geometries and fine surface finishes can be achieved. However, these machines are significantly less widely available than standard WEDM and it is desirable to optimise parameters for prototyping on a standard WEDM since the intention is to provide a method of prototyping gears which does not require specialist equipment or high set-up costs.

To this end, Ali et al.[126] used conventional WEDM to produce gears of outside diameter 3.5 mm, with 17 teeth. They achieved a dimensional accuracy of 0.09%, and a surface finish R_a of 1.8 µm. This was built upon by Gupta and Jain[134] who achieved a surface finish R_a of 1 µm. These results highlighted the potential to achieve good results in prototyping of novel gear geometries with WEDM and to produce the dies for stamping gears using a WEDM. The benefits of the former are that it allows quick changes to design with negligible setup, while the latter provides a viable alternative to milling or grinding.

4.2 ASSESSMENT OF CAPABILITY FOR PRODUCING SMALL GEARS

Based on the possible applications of WEDM for micromechanical systems, a need to investigate whether gears produced using WEDM were of sufficient quality to be used as a quick method of producing novel geometries in the design stage of gear profiles was identified. The capability of the WEDM process as an alternative method of producing small gears was thus first considered.

Process outcomes were determined based on required functionality and operation of gears. The first process outcome was identified as surface finish. This was measured using R_a as this is typically chosen as the measure of surface finish in literature on WEDM, and R_q which takes into account higher deviations from the mean. It was required that a good surface finish which negates the need to finish the parts be achieved. The definition of "good" was taken to be less than 1 µm, based on the work carried out by Gupta and Jain who hobbed small gears [134]. The effect of the white layer on tribological properties, fatigue strength and wear resistance of the part mean that white layer is also an important response factor to be measured. This work was concerned specifically with production of small gears with Aspect Ratio < 0.1 which is lower than those typically produced in literature but has applications in more compact mechanical systems such as watches and miniature gearboxes.

4.2.1 *Machining Process and Testing*

The gears were manufactured on a Mitsubishi Electric MV4800 WEDM machine. This machine is a macro-size WEDM, capable of machining parts up to 49.2 mm x 40.2 mm x 19.9 mm (L x W x H), with wire between 0.15 mm and 0.3 mm in diameter. Typically, these machines are used to machine parts such as large mould bases, and has capability for tapered parts up to 15 degrees . The machine consisted of a submerged bed onto which the workpiece (1 mm thick brass, CZ108 Half Hard) was mounted, as described in subsection 3.1.1. Gears were machined as described in Table 4.1.

Module	Pitch Diameter (mm)	Outside Diameter (mm)	Aspect Ratio (L/D)
0.33	6	6.67	0.15
0.56	10	11.11	0.09

Table 4.1: Sizes and modules of gears produced.

A wire of diameter 0.25 mm, chosen for its immediate availability, was fed from a spool through the workpiece, tensioned by a series of guides and pulleys. The wire was displaced according to the x-y coordinates specified in the Computer Aided Design (CAD) file, in order to cut the shape of the gear. The machined gap was calculated to be approximately 0.05 mm, thus each side from the centre of the wire $0.05 + {}^{0.25}/_{2}$ mm was cut, leaving a machined gap of approximately 0.6 mm. De-ionised water was used as a dielectric. The production plan for the gears was as follows:

1. 1 mm holes were drilled at intervals in a brass sheet.
2. The sheet was fixed to the bed of the wire machine, clamping in red highlighted positions (Figure 4.1).
3. The wire was fed through a given hole, using a water jet, and the hole centre was set as the datum.
4. The wire was then cut, and fed from outside the workpiece to cut the outside of the gear.

The gears produced were measured for errors in profile, surface finish along WEDMed edge (the outer edges of the teeth) and depth of white layer (heat affected layer). Profile was measured using the image processing method described in subsection 3.1.4 and a Coordinate Measuring Machine (CMM). Surface finish was measured using an Alicona optical profilometer (subsection 3.1.2). Surface finish of the machined parts of the gear (in this instance this refers to

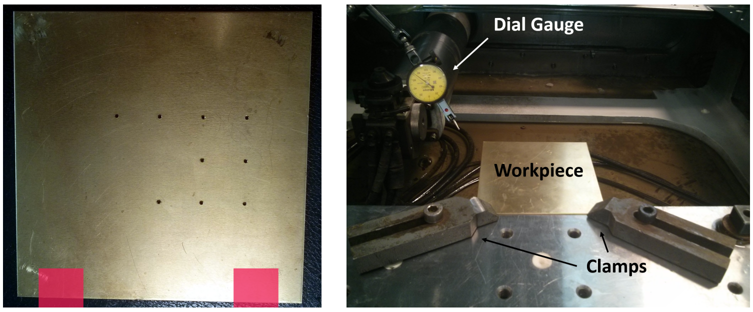

(a) Highlighted clamping locations for the workpiece.

(b) The Clamped Workpiece.

Figure 4.1: Clamping of the workpiece.

the faces and flanks of the gear, as seen in Figure 4.2) was measured using a 3D non-contact profilometer.

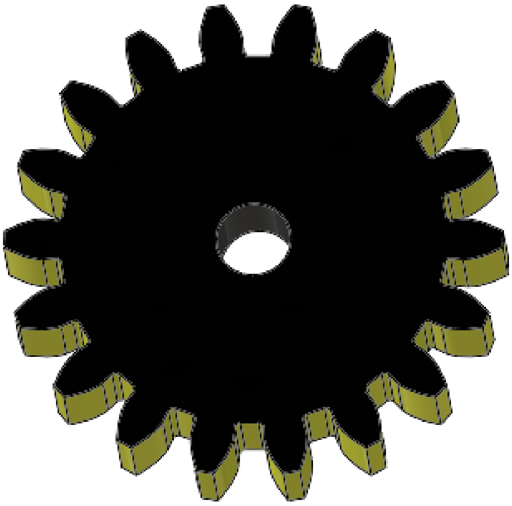

Figure 4.2: The yellow surface shows the machined part of the brass (the top and bottom faces of the gear are unmodified from the original gear blank).

Two profile roughness values and two surface texture values were measured. The profile roughness values measured were average roughness R_a and root-mean-square roughness R_q. The former is commonly used to measure WEDMed surfaces. Although R_a is directional, WEDMed surfaces are typically random [133, 179]. R_q adds to this data since R_a is not able to distinguish between larger spiky asperities and undulating surfaces: the squared term gives takes surface variations far from the mean into account. Since WEDM craters often vary in size and depth with differing machining parameters this is important.

An optical microscope was used to measure the white layer along a series of points across the tooth profile; and the depth of the white layer was plotted against position.

4.2.2 *Results and Discussion*

For comparison, a set of typical parameters have been used. These parameters are derived from tolerances drawings of a wheel and pinion used in a watch provided by the Bremont Watch Company. The wheel was produced by stamping, and the pinion by grinding thus the parts give a good idea of the output of competing technologies. However, in both cases the parts have been finished by tumbling with abrasive particles. A typical gear, produced by the ETA company and provided by the Bremont Watch Company was used for the reference gear since this represents a typical application of small brass gears. The tolerenced drawing depicts a gear of outside diameter of 4.45 mm with a manufacturer stated diameter tolerance of -8 µm or +10 µm, (0.2%). Measuring the surface roughness using an optical profilometry yielded an R_a value 0.4µm. Therefore, gears produced, which have a 10 mm outside diameter have been compared with this and a tolerance of 0.2% as with the ETA gear (±20 µm), aiming for an R_a value 0.4µm.

4.2.2.1 *Errors in Profile*

Values obtained using image processing for several different gears are given in Table 4.2. Error in profile appeared relatively high: for a gear with 12 teeth and pitch diameter 6, approximately 7.8% of the total tooth volume was either missing from the expected location (i.e. line of tooth lies inside the expected outline (Figure 4.3a) or was added to the expected location as in Figure 4.3b (i.e. line of tooth lies outside the expected outline). The profile errors measured for three other gears were higher still, ranging from 10.9-17.4%. Profile errors this high would at best result in poor efficiency of transmission, at at worst failure to transmit. Due to the simplicity of the method, it is likely that over-estimation of errors occurs since the size of the pitch error factor relates to overall tooth volume. Although it is appropriate to overestimate errors in terms of producing adequate quality, rejection of gears unnecessarily is problematic and thus a margin of error appropriate to the required application of the user should be used.

Number of Teeth	Pitch Diameter (mm)	Area of CAD File Teeth (Pixels)	Area of Absolute Tooth Difference (Pixels)	Error Factor	Error
12	6	18735	1466	0.078	7.8%
18	6	22004	3283	0.149	14.9%
18	8	23429	4069	0.174	17.4%
24	10	14061	1533	0.109	10.9%

Table 4.2: Profile Errors for Different Gears

There are three primary sources of uncertainty in calculating the "Error factor" (EF) used in this method. The first derives from the thresholding value chosen:

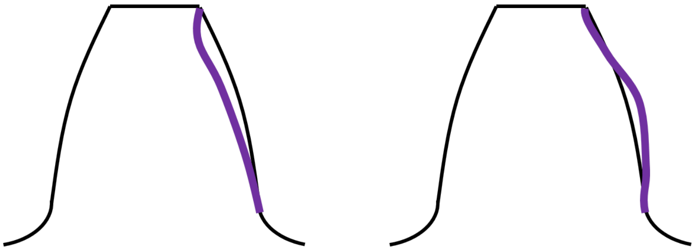

(a) The actual tooth is smaller than the CAD tooth.

(b) The actual tooth is larger than the CAD tooth.

Figure 4.3: The two possible errors in profile measured: missing material (a), and extra material (b).

this is determined based on the point at which the pixels of the gear (light grey) transition to the pixels of the background (dark grey). The gear is lighter due to the higher reflection of the brass as compared to the matt background. The second derives from the size of the gear, or number of teeth, which has significance since it is important to allow for the fact that different sized gears are measured. The third error of importance is the rotational accuracy of positioning of the gear when taking a measurement. If the gear is significantly rotated as compared with the CAD image, the result is that the error appears higher than it actually is, leading to unnecessary rejection. Thresholding error is calculated by evaluating the data with a number of thresholding values. The EF achieved is calculated in each case, both for different thresholding values and different sizes of gear. Similarly, size error was calculated by evaluating several different sizes of gear at a single threshold. Finally, the gear was rotated through 0.5, 1.0, 1.5 and 2.0 degrees to assess the change in EF over this range. The data produced was tested using the Anderson-Darling test for normality and found to meet assumption of normality, and thus the errors were calculated as follows:

$$E_T = \sqrt{\left(\frac{2\sigma N_T}{\bar{N}_T}\right)^2 + \left(\frac{2\sigma T}{\bar{T}}\right)^2 + \left(\frac{2\sigma R}{\bar{R}}\right)^2} \tag{4.1}$$

Where E_T is total error, N_T is standard deviation in result for different numbers of teeth,$\bar{N}_T$ is mean values for different numbers of teeth, T denotes a given thresholding value and R denotes angle of rotation (degrees). The method has been tested using three different sizes and numbers of teeth of gear, and 7 different thresholding values (from 0.05 to 0.35). This resulted in a nominal error of 0.12, which supports the proposal that the method should be used for preliminary assessment of gears only. The method is eminently reproducible since it requires only a small gear, the original dimensions in CAD file (such as DXF), an optical microscope (such as the Zeiss Axio Imager) and red card (in the region of R:255, G:0-50; B:0-50 when compared with the RGB colour scale).

A major advantage of the image processing method used is the output image which allows the user to instantly identify profile and form errors. Primarily, simple profile errors were seen (the shape of the gear often did not quite follow

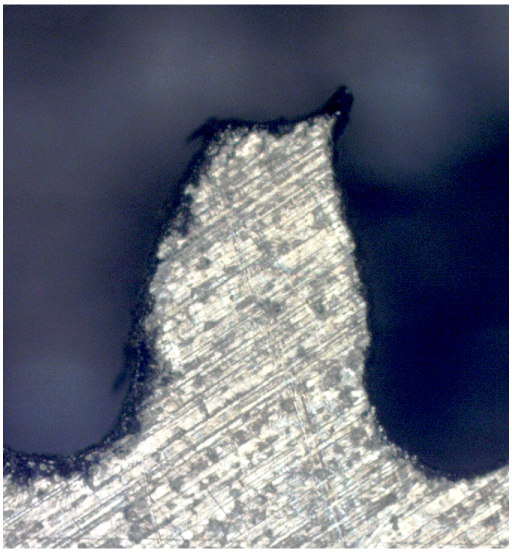

Figure 4.4: Error in profile that occurs as gear falls from workpiece.

the involute curve) and there was also a large burr seen where the tool path finished (Figure 4.4). For all gears there was evidence of tooth spacing error (the teeth are not all evenly spaced) as can be seen in Figure 4.5. In spite of high profile errors, there was little evidence of runout, but in some gears there was some suggestion of pitch error.

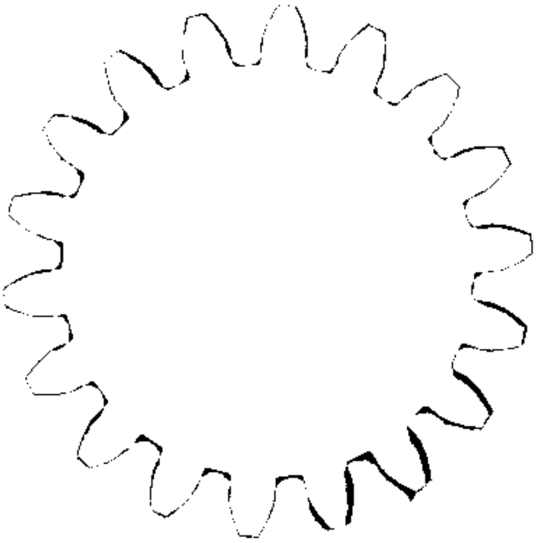

Figure 4.5: Graphical representation of the profile error for a gear with pitch diameter 6 mm and 18 teeth.

The DXF file and CAD file overlaid can be seen in Figure 4.5. The absolute difference between the two images was calculated in MATLAB. The profile error factor was calculated to be 0.115 giving a profile error of 11.5%. This is a smaller error than that recorded by the optical method, which measured 14.9%. There was, as with the optical method, mostly evidence of simple profile error.

There was also evidence of tooth spacing error but no evidence of runout or pitch error.

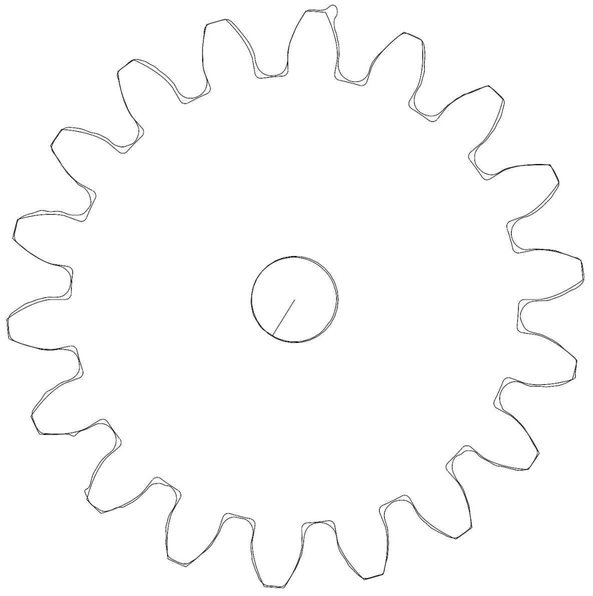

Figure 4.6: The CMM image and CAD file overlaid. The CMM image is be identified by the burr on one of the teeth.

Comparing the result from the CMM with the optical result (Figure 4.6) shows that the images are like but reveals some differences. The first is that the CMM (seen by a thinner image) is much smoother. The second is that the teeth in the optical image are slightly narrower than those of the CMM. This is probably partly due to the shadows in the optical image which make edge detection difficult. The total difference between the two images including the main body of the gear was found to be 3.2%, so based on the fact that the gear has an area of approximately $2 \times \pi \times r = 2 \times \pi \times 3.33 = 20.92$ mm^2, this represents 0.67 mm^2displaced area or 0.67mm^3 displaced volume (since the gear is 1 mm thick).

The method described here arose from a need to measure gears easily and quickly during machining, where no specialist equipment was available. As a result, it was not possible to provide data from machines such as CMMs, optical comparators and height gauges. Currently this method has two benefits:

A. To allow basic measurement of gear where access to more sophisticated equipment is unavailable.

B. To eliminate gears with severe (as defined by the specification) form or profile errors that cannot easily be seen by eye.

Surface Finish

The zigzag profile method is appropriate when the form has been removed and based on the fact that the surface roughness is random (rather than periodical).

For conformity with ISO4288, a measurement length of 1.25cm would have been required which was not possible due to size constraints. R_a values are given in Table 4.3. The values for R_a ranged from 3 µm to 6 µm, averaging at 4.0 ± 0.04 µm, where the error is derived from the measuring equipment [180]. Comparing this to previous studies, this value is is higher than those achieved by Ali et Al. [126] who achieved an R_a of 1.8µm and Gupta and Jain [129] who achieved a surface roughness of 1 µm, although the machining parameters used in this study were not closely controlled and thus this surface finish can be improved upon.

Tooth Measured	$R_a(\mu m)$	$R_q(\mu m)$	Measurement Length (mm)	Accuracy (μm)	R_a
Tooth 1	5.881	7.664	1.292	± 0.5	$5.8 \pm 0.5\mu m$
Tooth 2	4.302	5.451	0.279	± 0.5	$4.3 \pm 0.5\mu m$
Tooth 3	2.859	3.565	2.395	± 0.5	$2.9 \pm 0.5\mu m$
Tooth 4	3.071	3.768	2.200	± 0.5	$3.0 \pm 0.5\mu m$
Mean	4.028			± 0.5	$4.0 \pm 0.5\mu m$

Table 4.3: Profile roughness measurements across four different teeth.

4.2.2.2 *White Layer*

The white layer was measured for a number of teeth on two different gears: one with pitch diameter six and twelve teeth, the other with pitch diameter six and eighteen teeth. The white layer was measured along a series of points across the tooth profile and the depth of the white layer was plotted against position (Figure 4.7). The results from this are given in Figure 4.8 for the gear with 18 teeth and Figure 4.9 for the gear with 12 teeth. Comparing the position on the teeth with the thickness of white layer did not reveal any geometrical relationship between depth of the white layer (for example, the corners of the gear teeth had a similar depth of white layer to the sides of the teeth or tooth space), and the white layer was similar for the different gears: the average white layer for each tooth can be seen in Table 4.4. The white layer appeared to be influenced primarily by parameters such as pulse on-time and peak current: an increased pulse-on time reduces white layer [111] whereas increasing peak current increases white layer [181]. This is due to the energy of the pulse, which is proportional to both of these factors, being increased. Since the white layer was measured using visual observation at the surface of the gear, it was hard to make a precise measurement. It was thus hard to identify a relationship between gear geometry and white layer which is of interest. A more precise way to measure white layer would to etch the testpieces and image with an Scanning Electron Microscope (SEM), which is a method that has presented good results in previous literature [116].

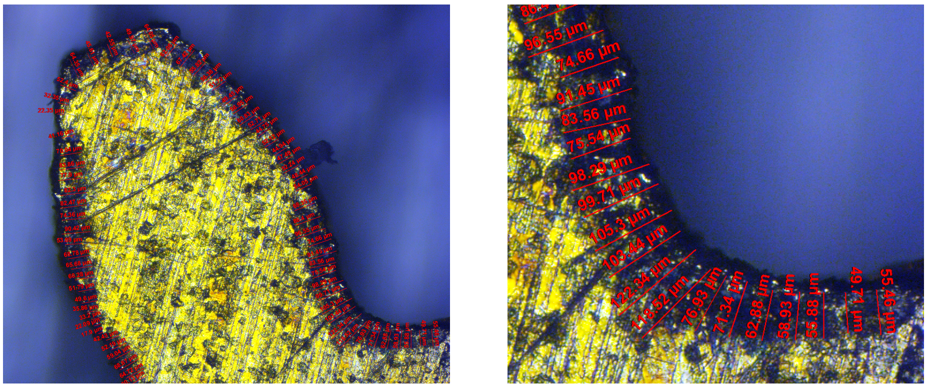
96.55 µm
74.66 µm
91.45 µm
83.56 µm
75.54 µm
98.29 µm
99.71 µm
105.3 µm
103.44 µm
122.34 µm
118.52 µm
76.93 µm
71.34 µm
62.88 µm
58.93 µm
55.88 µm
49.71 µm
55.46 µm

Figure 4.7: Measurement of white layer using optical measurement software for a microscope with 50x magnification.

Gear	White Layer Depth (mean) µm	Standard Deviation µm	Minimum µm	Maximum µm
Pitch Diameter 6, 18 teeth, tooth 1	63.7	16.4	34.4	112.3
Pitch Diameter 6, 18 teeth, tooth 2	52.0	8.6	36.3	71.9
Pitch Diameter 6, 18 teeth, tooth 3	58.3	17.0	22.4	91.0
Pitch Diameter 6, 12 teeth, tooth 1	39.2	19.5	7.8	84.5
Pitch Diameter 6, 12 teeth, tooth 2	61.3	21.3	10.5	122.4

Table 4.4: Mean white layers for the five teeth measured. The difference between minimum and maximum for each measurement indicates that white layer is highly variable for the set of parameters used.

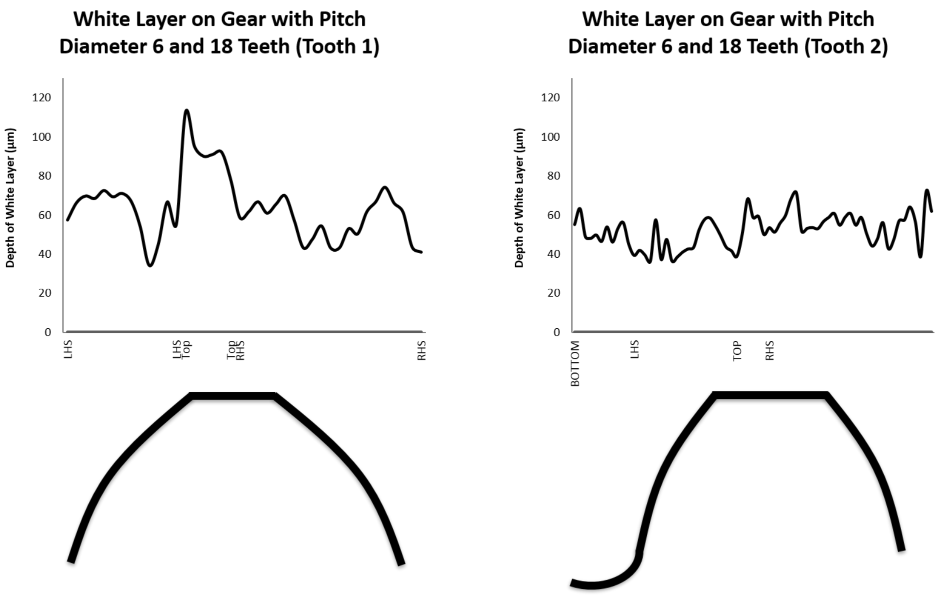

(a) White layer for gear with 18 teeth, pitch diameter 6. Tooth 1.

(b) White layer for gear with 18 teeth, pitch diameter 6. Tooth 2.

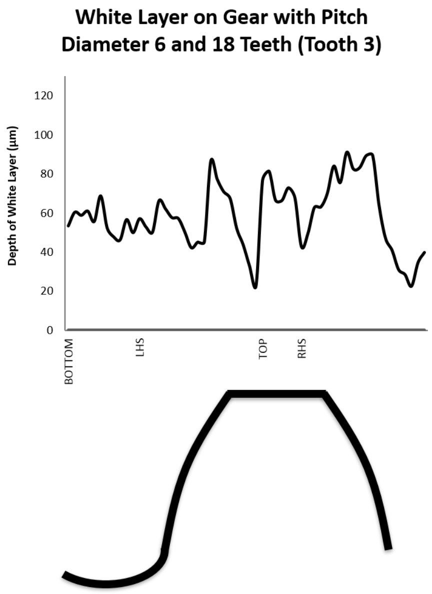

(c) White layer for gear with 18 teeth, pitch diameter 6. Tooth 3.

Figure 4.8: White layer plotted against position for three different gear teeth on 18 tooth gear.

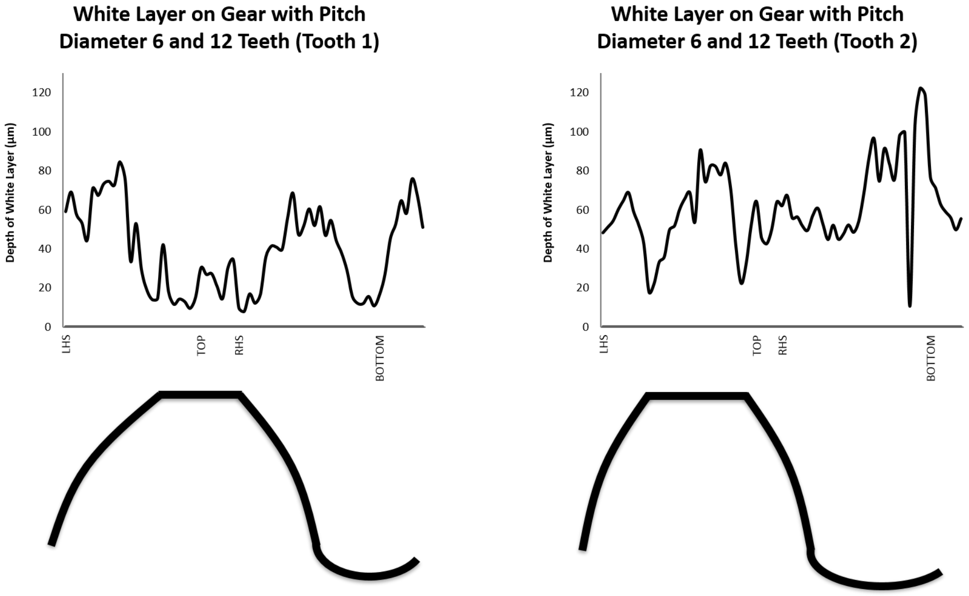

(a) White layer for gear with 12 teeth, pitch diameter 6. Tooth 1.

(b) White layer for gear with 12 teeth, pitch diameter 6. Tooth 2.

Figure 4.9: White layer plotted against position for two different gear teeth on 12 tooth gear.

4.2.3 *Conclusions and observations for further trial considerations*

Gears with module 0.33 to 0.56 and outside diameter 6.67 to 11.11 mm were manufactured from 1 mm thick brass sheet CZ108 using conventional WEDM with a wire diameter of 0.25 mm. The gears were examined for profile errors, surface finish and depth of white layer. Two methods were used to examine profile errors: optical microscopy and CMM. The optical method yielded errors ranging from 7.8% to 17.1%, while the CMM method yielded an error of 11.5% (compared with 14.9% for the same gear measured using the optical method).

It was proposed that an optical measurement method (subsection 3.1.2) presented a lower cost method of measuring gear form and profile available using standard laboratory equipment. This would negate the need for specialist equipment and training.

This was validated by comparing the result from the CMM with the optical result which yielded a total difference between the two images of 3.2%. Since CMM is an accepted method of measuring gears (subsection 3.1.4) it can be concluded the optical method provides good rough measures of profile, with the caveat that the image processing method requires a high quality image in terms of contrast and appropriate lighting: light levels should remain consistent for each image and therefore artificial light should be used in a windowless room. Ideally, light levels should be checked for consistency using a light meter.

Surface finishes achieved in the gear manufacture ranged from 3µm to 6µm which is relatively high. To investigate this further and determine the value of further work into WEDM prototyping of gears, an attempt to improve surface finish took place using two methods: changing the machining parameters (wire speed and discharge energy), and carrying out finishing passes. It was found that reducing the wire speed reduced the R_a values, thus for a lower wire speed surface finish was improved. It was also found that lowering gap voltage appeared to improve surface finish. Both of these agreed with literature [14, 126, 134]. Simply offsetting the wire by 100 µm and 150 µm without changing other parameters did not improve surface finish and in fact higher R_a values were seen. It is likely that this is due to re-melting and casting of existing white layer.

White layer measurements yielded mean values for different teeth ranging from 39.15 µm to 63.73 µm. Since white layer negatively affects surface finish, a white layer this thick is undesirable. An improvement in surface finishes could be achieved by carrying out finishing passes where the power is reduced (through reducing discharge current or gap voltage) as seen by others [18, 19, 110]. It was concluded that although further investigation was needed into machining parameters and finishing passes, there is value in further investigating WEDM as a method of prototyping gears. Due to the measurement method used, it was thus hard to identify a relationship between gear geometry and white layer which is of interest.

4.3 DEVELOPMENT OF OPTIMUM MACHINING PARAMETERS

Based on the work to establish WEDMs suitability in prototyping of small gears, work carried out to determine important parameters optimise surface finish (SF) and material removal rate (MRR) when designing skim cut parameters. Two experiments were carried out to investigate five factors: wire tension, dielectric flow rate, peak current, off time and machining voltage.

4.3.1 *Introduction*

Due to the physical processes involved in WEDM [67] discharge energy or pulse energy is the most important machining parameter affecting surface finish in WEDM, although this is not technically a parameter and is influenced by parameters such as discharge current, gap voltage [71], pulse duration, pulse-on time and peak current [72, 73].

Pulse energy, E, can be described as

$$E = \int_0^{t_0} u(t)i(t)dt \tag{4.2}$$

where t_0 is discharge duration, $u(t)$ is discharge voltage and $i(t)$ is discharge current [76].

In addition to discharge energy, WEDM machines have huge numbers of parameters to control their machining: and it is this that presents one of the major difficulties in machining using WEDM [16]. Aside from the need to optimise Surface Finish (SF) and Material Removal Rate (MRR), there is a need to identify important machining parameters and their relationships. The various possible machining parameters and the effect that these have on surface finish are described in subsection 2.1.2.

Typically, process outputs are chosen to be surface finish and MRR. Because these are contradictory (as one improves, the other degrades), optimisation must take place to achieve a compromise [71]. A higher discharge energy results in larger craters which causes a poorer SF [74–76] but a higher SF [72].

Based on review of literature, factors influencing micro-geometry (subsection 2.2.4 and section 4.1) such as surface finish and white layer were determined to have significance in micro and meso gear manufacture. This guided the following input parameter choices for preliminary investigation: Wire Tension (WT), Dielectric Flow Rate (LQ), Peak Current (IP), Off Time (T_{off}) and Machining Voltage (VG). Output parameters investigated for the preliminary trial were surface finish and white layer depth. This is because white layer is commonly investigated in WEDM machining [108, 113, 114] and therefore can easily be compared with other studies, and also affects the performance of a gear as described in Section 2.2. Meanwhile, surface finish (in particular $\mathrm{R_a}$value) is also commonly used in equivalent work [114] and therefore comparisons can be made with other literature. Furthermore, $\mathrm{R_a}$value can be quickly and easily measured using optical profilometry.

The purpose of the work was identify optimal parameters for achieving the best surface finish (lowest R_a value) and geometrical accuracy, while maintaining the thinnest possible white layer.

4.3.2 *Machining Process/Details of Experimentation*

Straight cuts of length 15 mm were made in 1 mm thick brass plate (CuZn38) to determine which of the chosen factors had the most significant effect on surface finish ($R_a$value) and MRR. Machining took place on a Mitsubishi Electric MV4800 WEDM machine using a wire of diameter 0.25 mm and de-ionised water as a dielectric. Length of cut was 15 mm. Cutting of complex geometries was not required for a basic study to compare importance of factors.

Two experiments were carried out: the first (Test 1) to investigate the individual and combined effects of WT, VG, IP and T_{off}. The experimental design method used each time was a full factorial method, since only four factors were used. This allowed a higher design resolution to be achieved. Full parameter sets used for are given in Table 4.5. In the case of wire tension and peak current, values used are preset levels specified by Mitsubishi and specific tension and current levels were not available. However, in each case a higher number indicates a higher current or tension value. Sixteen specimens were produced.

Run Order	Off Time	Machining Voltage (V)	Wire Tension	Peak Current
1	1	250	2	8
2	16	120	2	8
3	1	120	2	4
4	16	250	2	4
5	16	120	12	4
6	1	120	12	8
7	1	250	12	4
8	16	250	12	8
9	16	250	2	8
10	16	250	12	4
11	16	120	12	8
12	1	120	12	4
13	1	250	12	8
14	16	120	2	4
15	1	120	2	8
16	1	250	2	4

Table 4.5: Parameters used to investigate WT, LQ, IP and T_{off}. A full factorial design was used.

R_a values of the machined edges for the first trial were measured using an Alicona SL infinite focus microscope with a magnification of 5x. Profile roughness values were measured from images taken using a vertical resolution of 200nm (for the first experiment) and a lateral resolution of 2μm for a measurement length of 6 mm using a profile width of 500μm (for the first experiment) and 100μm (for the second experiment). A cut-off wavelength L_c of 2500μm was used, in order to conform with ISO4287 [180]. The $\mathrm{R_a}$ value was measured at three separate points along the machined surface, and a mean taken from this.

Material removal rate for the machined edges was calculated using Equation 4.3. The workpiece thickness for the first experiment was 1 mm, while the workpiece thickness for the second experiment was 0.2 mm. For each test piece, the distance cut was 15 mm. Cutting time was recorded, using the data from the machine console, while the width of the cut gap was calculated using the nominal spark gap stated in the machining characteristics table provided by Mitsubishi [182]: wire diameter $(0.25) + 2 \times$ spark gap $(0.05) = 0.35$ mm. Since the gap is dependent on compensation software which maintains the specified gap voltage, the nominal spark gap was assumed to have an error of 0.005.

$$MRR = \frac{V\,(\mathrm{m}m^3)}{t\,(\mathrm{s})} = \frac{\text{distance cut}}{\text{cutting time}} \times \text{width of cut} \times \text{thickness of workpiece} \tag{4.3}$$

4.3.3 *Results and Discussion*

Table 4.6 shows the mean $\mathrm{R_a}$ values and material removal rates for each gear, and their standard deviations respectively. The parameters used to machine the gears have been previously given in Table 4.8. In the case of $\mathrm{R_a}$, it can be seen that the value varies highly between machining runs, which immediately suggests that at least some parameters (or combinations of parameters) have an effect on the $\mathrm{R_a}$ value. Meanwhile, the standard deviation for $\mathrm{R_a}$ is relatively low compared with the $\mathrm{R_a}$value (in the order of 1%) - so the machining parameters seem to have an effect, which may become clear with statistical analysis.

For MRR, a large variation in material removal rates is seen across gears - for example, the gear produced in run 3 has an MRR of 0.7 m/min which is over three times that of the gear produced in run 1. These large differences indicate that statistical analysis is likely to show that at least some (parameters or combinations of) noticeably affect machining time.

Run Order	R_a (µm)	Standard Deviation (R_a)	MRR (m/min)
1	1.82	0.03	0.18
2	1.82	0.01	0.68
3	1.81	0.02	0.70
4	1.68	0.02	0.16
5	1.77	0.00	0.57
6	1.77	0.02	0.68
7	1.77	0.01	0.18
8	1.78	0.02	0.17
9	3.11	0.08	0.17
10	2.94	0.04	0.16
11	3.18	0.07	0.68
12	2.95	0.05	0.70
13	3.53	0.02	0.17
14	3.17	0.03	0.59
15	2.34	0.06	0.30
16	2.92	0.02	0.18

Table 4.6: Mean and standard deviations of R_a and white layer for each gear machined. The parameters used to machine each gear can be identified by the run order of each gear as seen in Table 4.8.

Based on the initial results, statistical analysis allows the effect of individual and interacting parameters to be evaluated.

4.3.3.1 *Test 1 - Effect of Wire Tension (WT), Machining Voltage (VG), Peak Current (IP) and Off Time (Toff)*

4.3.3.2 *Effects of Test 1 parameters on Ra*

The data was first tested for normality. A normal Q-Q plot of standardised residuals (Figure 4.10) confirms that the normality assumption can be met, and also indicates that there are no significant outliers. The Q-Q plot is produced by plotting the observed value against the expected value, and can be produced in statistical software such as SPSS from actual observed data. If the observed value and expected value come from a normal distribution, the points will sit along a straight line with a positive gradient at approximately 45° (as can be seen in Figure 4.10). This is essential for Analysis of Variables (ANOVA) to provide valid results.

Therefore, the Q-Q plot should show the points on this line for two reasons: firstly, to allow Standard Error of Measurement (EM) for R_a to be taken. Secondly, to determine whether the data obtained corresponded to a normal distribution so that ANOVA could be used to determine whether any of the machining parameters tested were significant.

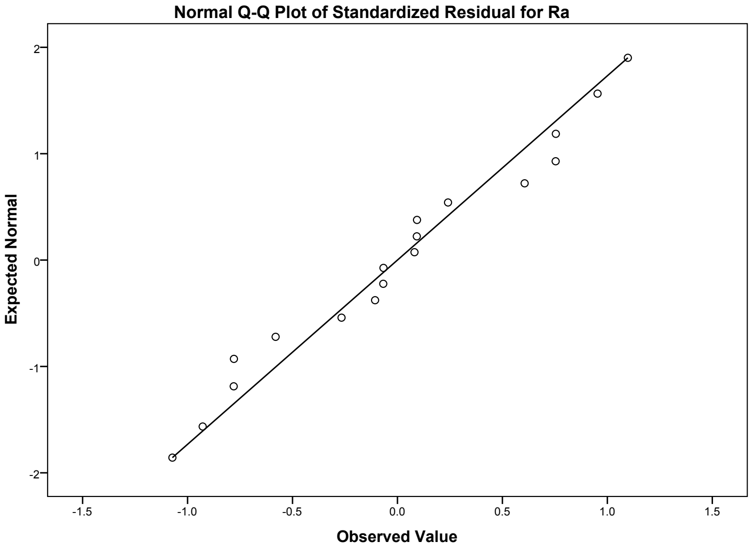

Figure 4.10: A normal Q-Q plot of standardised residuals shows that the data meets normality assumptions since the points fall along a straight line..

Following this, 4-way ANOVA was carried out to determine which input variables had a significant effect on R_a. Third and fourth-order interaction effects were ignored, since they were not found to be significant through ANOVA . To illustrate the significance of main interactions and second-order interactions, a Pareto plot of Main Effects was constructed (Figure 4.11). This type of chart is used to identify critical factors in a process by recording the frequency of defects [183]

The Pareto plot shows that IP had the most significant effect on R_a, followed by T_{off} and the interaction between IP and T_{off}.

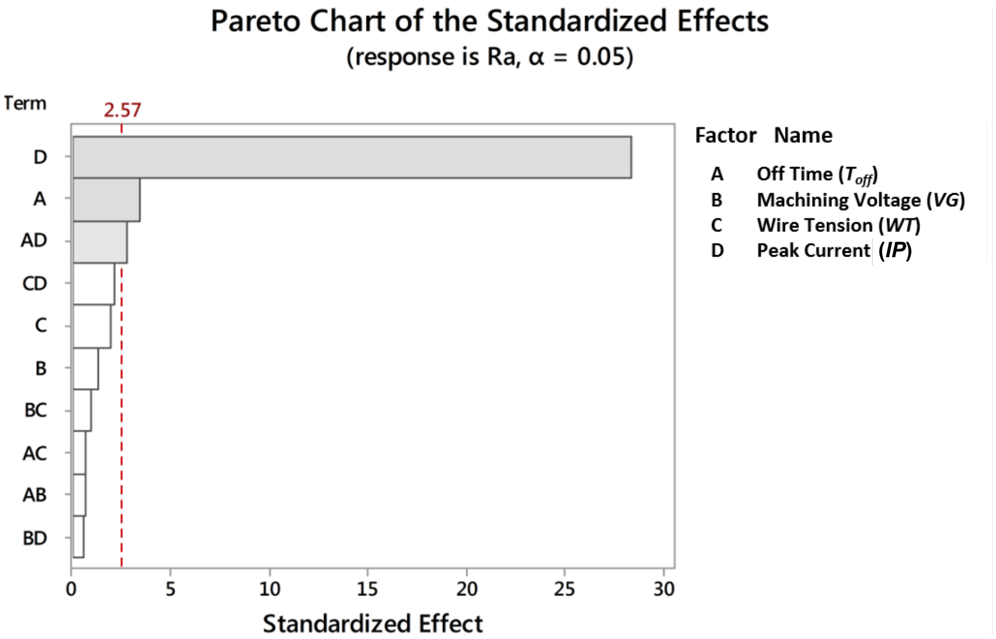

Figure 4.11: A Pareto Plot of Main Effects. Factors which extend beyond the significance line (dotted) have a significant effect on R_a.

Since factors other than IP and T_{off} were determined to be statistically insignificant, a plot of estimated marginal means was produced (Figure 4.14) . This showed that at a high IP (machine value of 8), the increased T_{off} resulted in a lower $R_a$value. However, at a low IP (machine value of 4) T_{off} had very little effect on R_a. This is because T_{off} describes the gap between machining pulses, whereas IP is directly related to crater size. Although no data on crater size is available, in physical terms for a classic homogeneous WEDM machined surface, a larger R_a typically results from larger craters. Simply plotting the $R_a$value with IP (Figure 4.13) very clearly shows that at higher values of IP the $R_a$value is always higher and so larger craters are to be expected. This is also seen in literature [75]. Thus, increased T_{off} resulted in larger distances between crater centres. At high IP, this resulted in crater overlap whereas at low IP craters did not overlap and surface was thus rougher, in spite of smaller craters.

Figure 4.12 shows profiles of two different WEDMed surfaces, the first of which (Figure 4.12a) has been machined with a lower peak current (and correspondingly pulse energy) and the second with a higher peak current (Figure 4.12b). Some examples of craters have been highlighted and it can be seen that in the case of the higher peak current, craters are significantly deeper and also wider. The two surfaces are combined onto a third graph for comparison (Figure 4.12c).

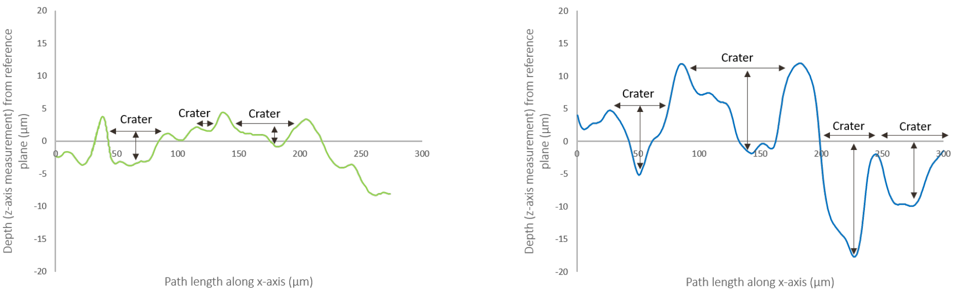

(a) A surface machined with a lower pulse energy.

(b) A surface machined with a higher pulse energy.

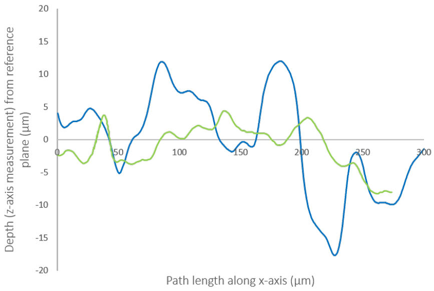

(c) Direct comparison between the two surfaces.

Figure 4.12: (a) shows a surface machined with a low *IP*, (b) shows a surface with a higher *IP* and (c) allows comparison between the two. It can be seen from the relative scales that craters machined with a higher *IP* are typically both deeper and wider.

When the $R_a$value is plotted against the two levels of current (4 and 8, as determined by pre-set parameters on the machine), it can be seen (Figure 4.13) that it appears that regardless of other parameters, a higher IP results in a worse surface finish (in agreement with Figure 4.11). This illustrates the idea that other parameters are much less significant.

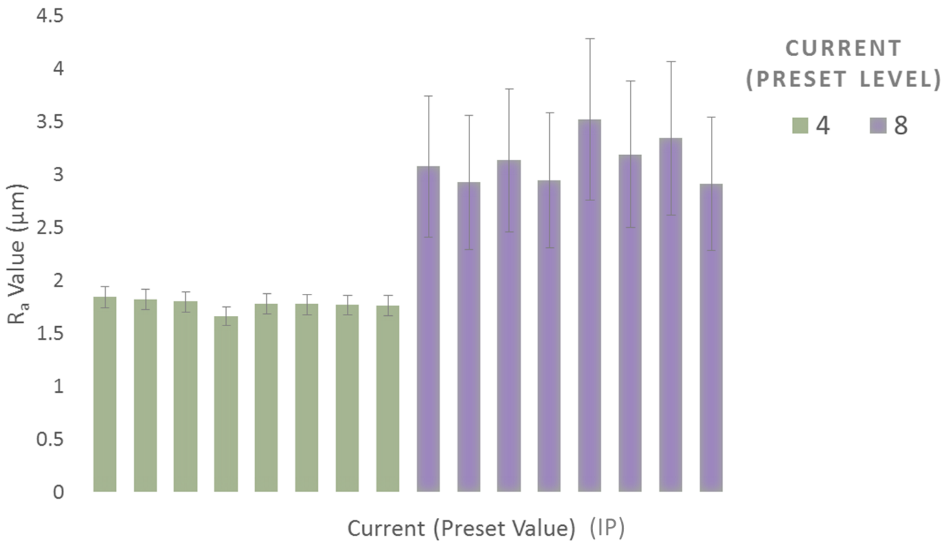

Figure 4.13: $R_a$value for each gear at the two different levels of current (8 gears are machined per level).

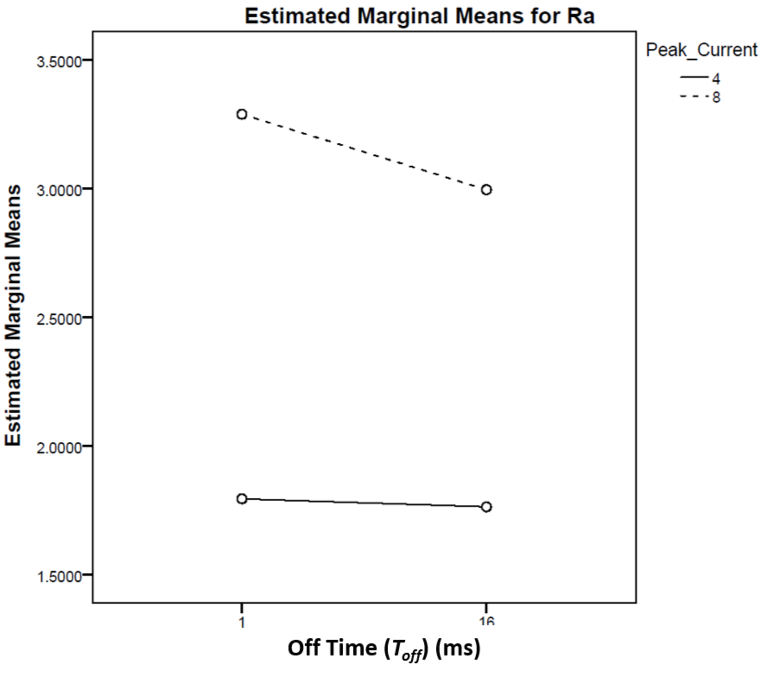

Figure 4.14: Estimated marginal means to show interaction between IP and T_{off}.

A main effects plot (Figure 4.15) was used to determine the effect of individual factors on R_a. This showed that optimal machining parameters tested for $R_a$were $T_{off} = High$, $VG = High$, $WT = Low$ and $IP = Low$, i.e. $T_{off} = 16$, $VG = 250$, $WT = 2$ and $IP = 4$. Thus increased T_{off} improves surface finish. There are mixed conclusions as to this result in literature [67, 68, 72, 73, 75, 98]. However, Lodhi et al. [73] found that surface roughness is improved for low values of R_a

(as in this case) with increased pulse-off time. This supports the work herein where R_a values are low. Furthermore, Goswami et al. [72] also determined that roughness decreases (improves) as pulse-off time increases.

It was also found that increased IP results in a rougher surface finish. This can be explained on a physical basis: the larger IP results in a higher discharge energy as defined by Equation 4.2, and thus a larger spark is generated which creates more localised heating, larger craters and a rougher machined surface. That high IP increases surface roughness is not contested [15, 72, 76, 93, 98]. Although VG and WT were deemed to be insignificant, the main effects plot shows that an increased VG results in a slightly smoother surface. Although typically, higher machining voltage is associated with a rougher surface since it directly affects the discharge energy [75, 101] it should be noted that the VG was not considered statistically significant. This is not the case for extremely low voltages (depending on the dielectric used), whereby a spark does not occur.

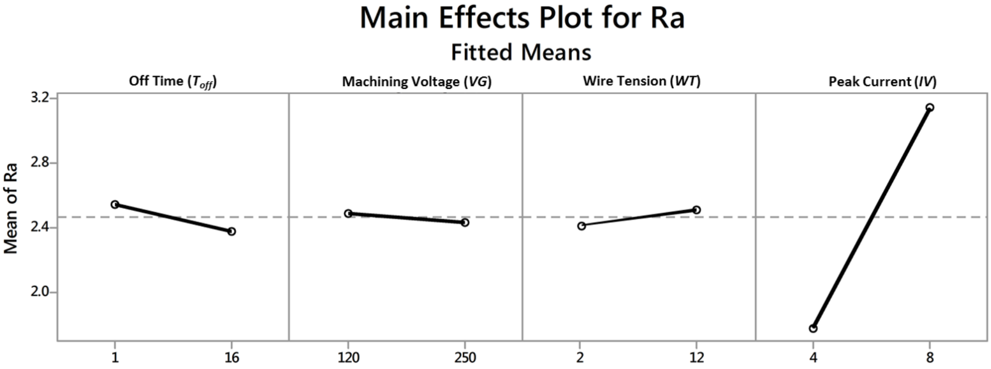

Figure 4.15: Main effects plot for R_a. A steep gradient indicates a relationship between parameter and output.

A minor issue with the statistical analysis is that the assumption of equality of variances is not met (using Levene's equality of variances, a p-value 0.057 is achieved, with a 95% confidence interval). This suggests that the sample size is too small, and as a result, p-values should be handled cautiously. However, the trends seen can still be interpreted in the same way. If a test with a lower confidence interval were carried out, only the effect of IP would appear significant: however, were the test repeated, it is likely that the equality of variances condition would be met.

ERRORS Errors in R_a were calculated using Standard Error of Measurement. This can be calculated (assuming a normal distribution of data) using Equation 4.4, where σ is the standard deviation, and R_{xx} is the reliability of estimate. Without knowing the reliability of the measurement, it was possible to estimate it using the Cronbach alpha reliability estimate [184] (which can be calculated using statistical software such as SPSS).

$$EM = \sigma\sqrt{1 - r_{xx}} \tag{4.4}$$

This yielded an EM value of 0.023. Measurement values for mean R_a could then be stated (using the properties of the normal distribution) with a 95% confidence interval as $score \pm (1.96 \times SEM)$, or $score \pm 0.045$.

Absolute error was also considered: the EM gave a measure of the size of the standard deviation of the data, which is relatively small. However, Alicona state that for a profile roughness of 500µm and error of ±40 µm can be expected [180]. As this is less than the EM value, the EM was used. Finally, the validity of the Alicona as a measurement instrument was considered by measuring the R_a value of a surface whose roughness was already known to be 0.8µm. Roughness values of 0.888 and 0.884 were measured at two different points, an error of roughly 10%.

Even with relatively low magnification (5x), assuming profile length and cut-off wavelength and scanning parameters (such as light levels) are kept constant, the optical profilometer provided reasonable comparison of the different surfaces.

4.3.3.3 *Effects of Test 2 parameters on MRR*

As with R_a , a normal Q-Q plot of standardised residuals confirmed that the normality assumption can be met. 4-way ANOVA was carried out to determine which input variables had a significant effect on R_a . The Pareto Chart (Figure 4.11) showed that VG was the most significant factor. It can be seen that IP, WT, and T_{off} did not have a significant effect on MRR. To further examine this, Main Effects Plot was constructed (Figure 4.17). These showed that a higher machining voltage resulted in a much lower MRR. This is supported by literature [64], and also supports the idea that at the lower machining voltage the pulse energy was lower and thus the volume of melted material being flushed was lower. Sparks can be heard due to expansion of heated air around the spark [185], and the machining at the higher voltage resulted in a continuous sound, measured using a microphone.

The results showed that the optimal parameters for a high MRR are are a high VG. IP was not found to be significant which is at odds with literature. It was concluded that this is due to the two levels for peak current being too close together, or the relatively small sample size.

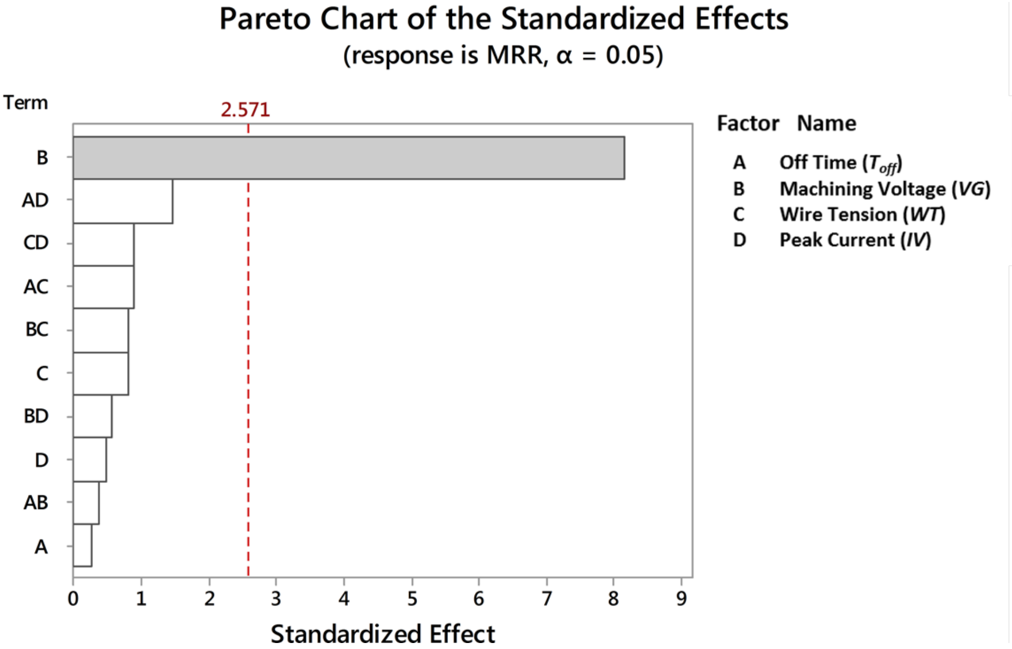

Figure 4.16: A Pareto Plot of Main Effects. Factors which extend beyond the significance line (dotted) have a significant effect on R_a.

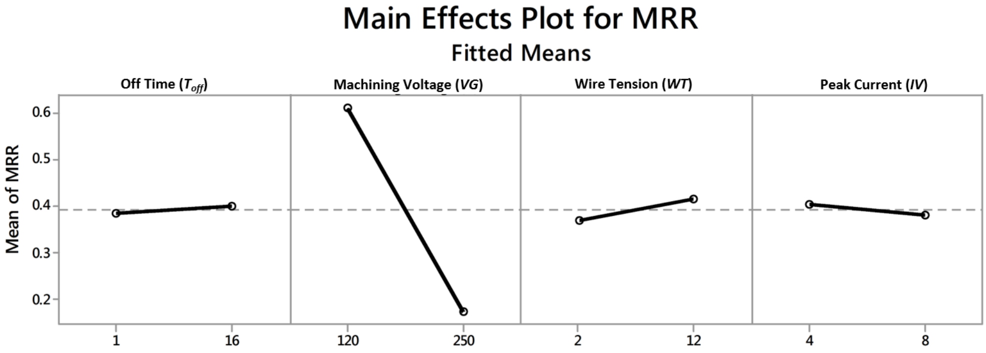

Figure 4.17: Main effects plot for R_a

ERRORS Distance was assumed to have an error of half the smallest unit used by the WEDM, i.e. 0.0005 m, while the cutting time as measured by the machine had an error of 0.005 minutes, calculated in the same way. Width of cut did not explicitly carry an error, since it is a theoretical value, and finally thickness of workpiece was supplied to a tolerance of ±5% or 0.05 mm. Total error was calculated using quadrature (Equation 4.5), where d is distance cut, T is thickness, w is width of cut and t is cutting time. Since only t is actually measured, this was be re-written as Equation 4.6.

$$\frac{\Delta MRR}{MRR} = \sqrt{\left(\frac{\Delta d}{d}\right)^2 + \left(\frac{\Delta T}{T}\right)^2 + \left(\frac{\Delta w}{w}\right)^2 - \left(\frac{\Delta t}{t}\right)^2} \tag{4.5}$$

$$\frac{\Delta MRR}{MRR} = \sqrt{0.0036\dot{1} - \left(\frac{\Delta t}{t}\right)^2} \tag{4.6}$$

Thus for an MRR of 0.7016m/min error is of 0.042m/min.

4.3.3.4 *Examination of surface using Scanning Electron Microscope (SEM)*

The machined surface of the testpieces were examined using an SEM. It was immediately easy to identify the classic "paint droplet" surface that is signature of WEDM (Figure 3.4).

On closer inspection (at a magnification of 10,000x) micro-cracking can be seen (Figure 4.18). This is a phenomenon that has been observed experimentally[186] and is due to the rapid localised heating and cooling. It has been suggested by Jangra et al. [18] that this can actually reduce stresses in the machined surface, which is advantageous as stresses can lead to warping which is especially problematic in small gears, where contact area can be sub-millimetre in width.

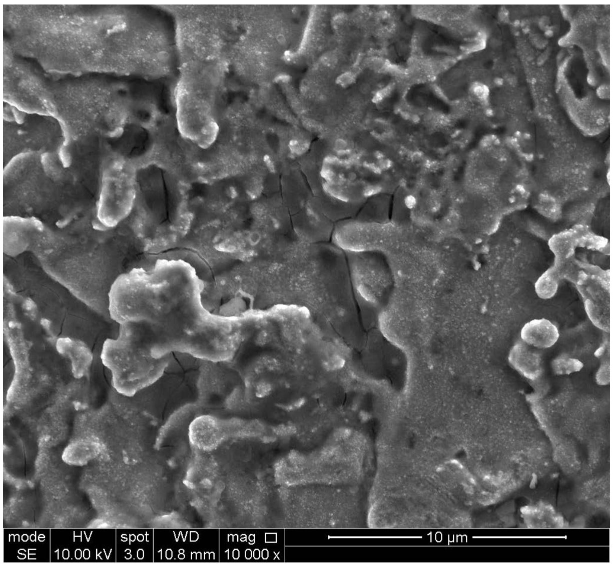

Figure 4.18: Micro-cracking of the machined surface can be seen.

4.3.4 *Conclusions*

The significance of the parameters IP, VG, T_{off}, WT and LQ had was investigated in optimising surface finish (measured by R_a value) and also for MRR, when cutting brass (CuZn38). It was found that the parameters had the following effects:

- IP resulted in an increased R_a value, i.e. a rougher surface finish. IP should thus be minimised to improve surface finish.
- At higher values of IP, a higher value of T_{off} resulted in an improved surface finish.

- VG below a certain voltage results in unstable machining and a rougher surface finish, so a relatively high value of VG should be used.
- VG was the most significant factor affecting MRR, while IP, T_{off} and the interaction $IP \times T_{off}$ were significant in determining R_a.

It is important to understand the effects of various machining parameters when trying to achieve a fine surface finish since machining time should also be sufficiently small that the process is viable. The purpose of this was to provide guidance in determining cutting parameters for rough and skim cuts to be used producing a number of involute spur gears from materials of a thickness of 0.3 mm or less. The application for this, as described in section 4.1 is in producing gear dies and small runs of miniature gears that have applications in micromechanical systems.

4.4 MULTI-PASS METHODS FOR PRODUCING A HIGH QUALITY SURFACE IN WEDM

Previously, gears of module 0.33, pitch diameter 6 mm and outside diameter 6.67 mm, and of module 0.56, pitch diameter 10 mm and outside diameter 11.11 mm were machined from a 1 mm thick brass workpiece (section 4.2).

The gears produced had *Ra* values ranging from 3 mm to 6 mm, with an average of 4.0 ± 0.04 µm. This is a relatively poor surface finish, the improvement of which was identified as essential before WEDM could be viable for producing prototype gears. It was found that simply making a second pass of smaller depth on the WEDM had an adverse effect (Figure 4.19). This is owing to the fact that the discharge current remained the same each time and thus depth of white layer actually increased.

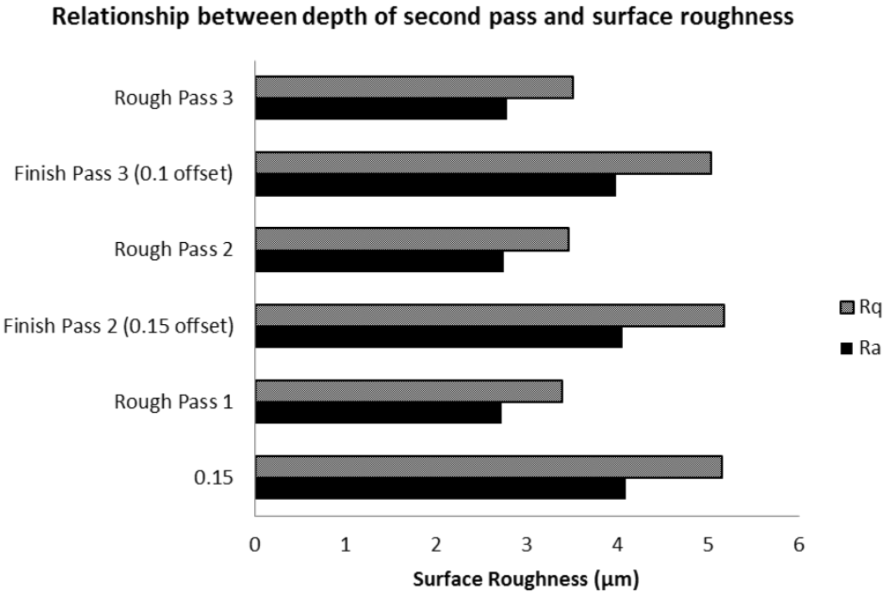

Figure 4.19: The effect of carrying out a second, sub-wire-width pass without changing other parameters. Errors can be propagated from quoted calibration errors to be .approximately 0.3 µm.

Based on the above requirements, trials took place to obtain an improved surface finish using WEDM. The effect of wire speed (WS) was first investigated, as theoretically an improved surface finish for a lower wire speed is expected (although a wire speed that is too low would result in erosion that is significant enough to fracture the wire before a section can be replaced). The effect of gap voltage (VG) was also considered by changing VG for a single cut to determine the effect of reduced gap voltage. It was expected that this would improve surface finish. Following this, a multi-pass method was employed whereby the second cut was offset from the first by 100 µm or by 150 µm for different rough and trim cuts. No other parameters were changed.

4.4.1 *Existing Work*

There have been a number of studies into improving the surface roughness of WEDMed parts using a method of multi-pass or trim cutting. This process involves taking a rough cut from the workpiece, then altering significant parameters (such as reducing discharge current) and taking a much smaller cut (see Figure 4.20). One such study by Antar et al. [110] carried out a series of trim passes during cutting of both nickel and titanium based alloys. Surface roughness was measured using 0.8 mm cut-off length and 4 mm evaluation length, and surface roughness was reduced with each pass (from 3.12 μm to 0.59 μm for the nickel alloy and from 3.39 μm to 0.43 μm for the titanium alloy) as parameters such as voltage and current were reduced to improve surface finish. Sarkar et al. [19] altered pulse-on time, peak current, wire offset and trim cutting speed when machining gamma titanium aluminide plate with the intention of improving surface finish. Their primary objective in second trim cuts was to achieve an improved surface finish and geometrical accuracy. It was found that the multi-pass method is more productive in achieving a fine surface finish. Jangra [18] carried out a study into multiple passes whereby the second passes used a lower discharge energy. Using this method, a much improved surface finish was achieved. Each of these studies supports the idea that trim cuts can be used to improve surface finish of parts while maintaining an acceptable MRR.

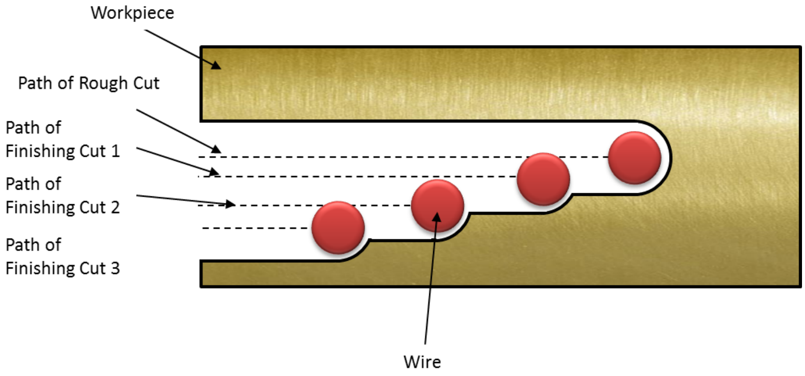

Figure 4.20: Path followed by EDM for finishing cuts.

4.4.2 *Machining Process*

A number of straight cuts using various different parameters were manufactured on a Mitsubishi Electric MV4800 WEDM machine. 1 mm thick brass sheet was used (CuZn37).

4.4.2.1 *Investigating WS and VG*

A wire of diameter 0.25 mm was used to machine firstly a cut of length 30 mm using an initial gap voltage and an initial wire speed. Following this, three more identical cuts were made at progressively lower speeds using the same voltage. A fifth cut was made using the original wire speed, and a lower gap voltage (Figure 4.21).

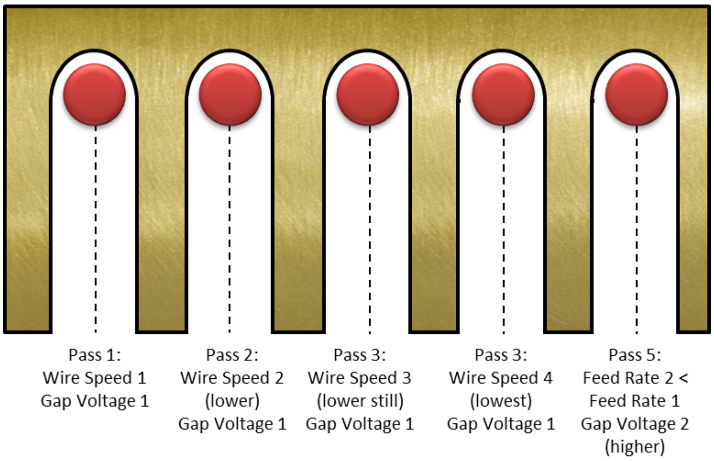
Pass 1:
Wire Speed 1
Gap Voltage 1
Pass 2:
Wire Speed 2
(lower)
Gap Voltage 1
Pass 3:
Wire Speed 3
(lower still)
Gap Voltage 1
Pass 3:
Wire Speed 4
(lowest)
Gap Voltage 1
Pass 5:
Feed Rate 2 <
Feed Rate 1
Gap Voltage 2
(higher)

Figure 4.21: Cuts made with changing machining parameters.

4.4.2.2 *Investigating Finishing Passes*

A set of rough cutting parameters was chosen for the initial rough cut, and a set of finishing parameters for all subsequent (finishing) cuts. These parameters are detailed in Table 4.7.

Parameter	Finish Cut	Rough Cut
E-Pack No.	400	401
Servo Speed	Slow	Normal
Power Set (discharge current)	Variable	6
Voltage (set level)	8	8
Pulse-off Time (ms)	1	3
Stability A	1	2
Stability B	1	15
Stability C	4	7
Stability E	1	4
Gap Voltage (V)	120	70
Fine Machining	ON	OFF
Wire Speed (m/min)	12	9

Table 4.7: Parameters used for rough and finishing cuts.

Three different sets of finishing passes were made: first, a 20 mm cut was made, and a finishing cut using an IP of 3 (where 3 is one of a range of values rather than a current value) was made with the wire offset by 150µm. This cut was made to a length of 10 mm, allowing both surfaces to be inspected. This was repeated for two more tests according to the parameters in Table 4.8.

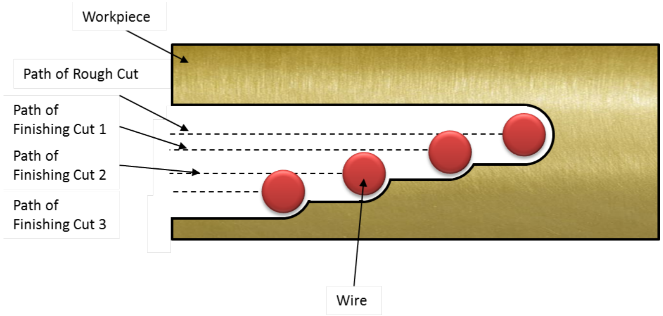

Figure 4.22: Four-pass cutting of the workpiece.

Test	Order	Rough/Finish	IP	Cut Length (mm)	Offset (μ)
1	1	R	6	20	0
	2	F	3	10	-150
2	1	R	6	20	0
	2	F	2	10	-150
3	1	R	6	30	0
	2	F	3	21	-150
	3	F	2	14	-150
	4	F	1	7	-150

Table 4.8: Parameters used to cut testpieces.

Thus in test 3, all four surface finishes were inspected. Figure 4.22 denotes a 4-pass cut.

Surface finish of the machined edges were measured using an Alicona Infinite Focus SL microscope system with a magnification of 10x .Two profile roughness values were measured:average roughness R_a and root-mean-square roughness R_a . Profile roughness values were measured from images taken using a vertical resolution of 1μm and a lateral resolution of 4μm for a measurement length of 3.5 mm using a profile width of 500μm, and a cut-off wavelength L_c of 800μm for the changing of parameters and 2500μm for the finishing passes, in order to conform with ISO4287 [180].

4.4.3 *Results and Discussion*

For the cuts where WS was reduced, it was seen (Figure 4.23a) R_a and R_q values were smaller. This is in agreement with the work of Tosun et al. [14]. For lower VG, an improved surface finish (manifested in smaller R_a values) was seen (Figure 4.23b), as in the study carried out by Ali et al. [126].

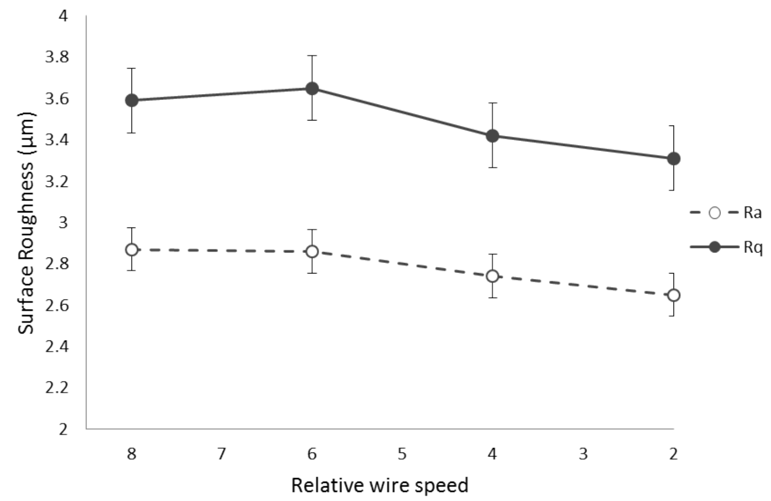

(a) The effect of wire speed on surface finish can be seen - for a higher speed, the R_a decreases.

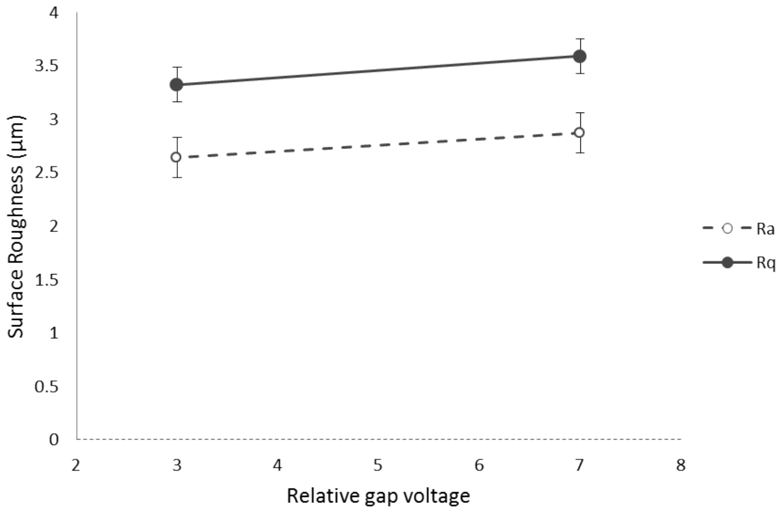

(b) The relationship between gap voltage and surface finish - as for a higher gap voltage, the surface is typically rougher - a higher $R_a$value is seen.

Figure 4.23: Effects of parameters on surface finish.

When machining parameters were changed as detailed in Table 4.7 for the finishing passes, a significant improvement in surface finish could be seen: both visibly and through measurement of R_a values with the optical profilometry. For both two-pass specimens the R_a was significantly lower after the finishing pass: for test 1 (Figure 4.24a), the rough cut gave an $R_a = 2.99 \pm 0.4$ µm while the finishing cut resulted in an $R_a = 4.27 \pm 40$ µm and for test 2 (Figure 4.24b), the rough cut gave an $R_a = 3.00 \pm 0.4$ µm while the finishing cut resulted in an $R_a = 3.86 \pm 40$ µm. This is approximately an order of magnitude in both cases, and clearly shows that the lower IP resulted in a lower R_a value.

For the four-pass specimen, the value of R_a decreased with each pass (Figure 4.25). This result is supported by the literature [18, 19, 110].

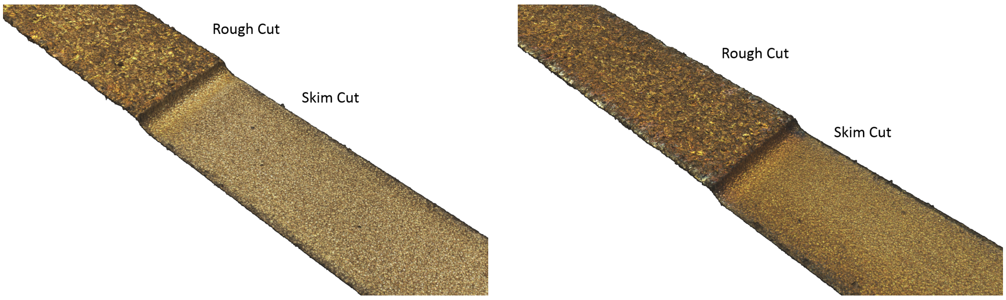

(a) Two-passes with an offset of 0.15 mm (b) Two-passes with an offset of 0.10 mm

Figure 4.24: Surface finishes with finishing passes.

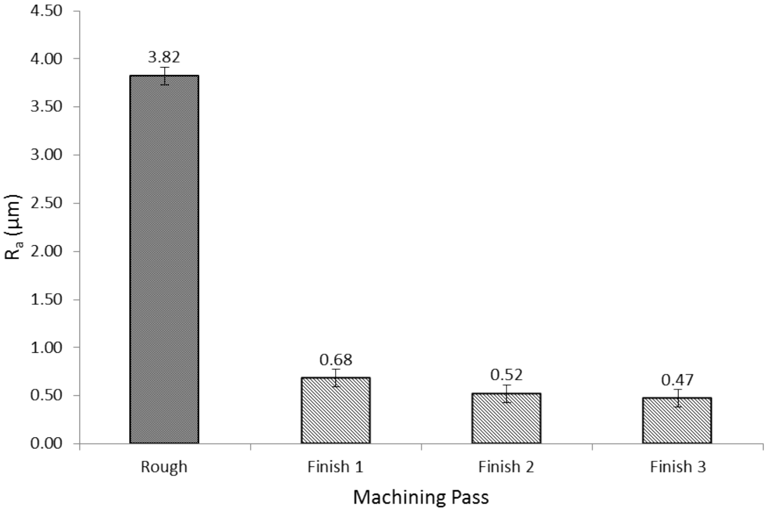

Figure 4.25: Surface finish with finishing passes. The bars show the four passes: rough cut on the left hand side and subsequent passes moving rightwards. A smoother finish (lower R_a) can be seen with each pass.

4.4.4 *Conclusions*

For the cuts where the wire speed was reduced, it was seen that as the wire speed is reduced, the R_a and R_q values fall, as can be seen in Figure 4.23a. A similar results was seen by Tosun et al. [14] and in other literature. Similarly, for lower gap voltage, an improved surface finish (manifested in smaller R_a values) was seen The same was seen when gap voltage was reduced (Figure 4.23b), as in the study carried out by Ali et al. [126].

Reducing VG resulted in an improved finish. This was not seen in earlier work but is supported by the results of Ali et al.[126]. A higher VG leads to higher spark energy, larger craters and thus a rougher machined surface. A lower WS also resulted in an improved surface finish and this was also in agreement with literature [14].

When carrying out multiple finishing passes, it was found that for two passes the second (finishing) pass yielded an R_a that was almost an order of magnitude smaller than the rough cut. In addition, reducing the IP from 3 to 2 for the finishing cut yielded further improvements to the R_a value. For four passes, where the *IP* was reduced to 3, 2 and 1 respectively for finishing passes 1, 2 and 3 an increasingly smooth surface was seen for each pass 4.25.

Machining with lower energy is typically slower than machining with higher energy pulses as smaller sparks result in a lower volume of molten material. The advantage, therefore, of skim cuts, is that the high surface finish is achieved while machining to less than the full depth of cut achieved in a rough cut. Thus, since material removal rate relates to depth of cut it is overall more efficient to carry out a faster rough cut followed by skim cuts.

4.5 VIABILITY OF THE WEDM FOR PROTOTYPING SMALL GEARS

The work undertaken has ranged from testing the capability the Mitsubishi MV400 to machine meso-gears (with outside diameter less than 10 mm and module less than 0.5) to testing of numerous input parameters and their relative significance using a Design of Experiments (DOE). Finally, this data was used to form design of a machining process that incorporated a series of skim cuts to improve machined surface finish.

The process has characteristics which make it a very attractive method for producing miniature gears such as high accuracy of machining and excellent surface finish. The complexity of the WEDM process is such that machining parts is typically iterative and subject to machine-specific constraints, such as range of parameter combinations. Furthermore, very thin parts are challenging to produce due to fixturing constraints. The idea of multiple cuts is interesting in the context of miniature gears since it would allow fine machining of the surfaces, but presents a practical challenge. The combined research into minimising the white layer produced during machining and production of miniature gears shows that there is significant potential to use WEDM in the production of miniature gears which are both highly accurate and possess appropriate tribological properties. This is supported by literature.

Many miniature gears produced have had a high aspect ratio and the capability of WEDM to produce very thin gears has not been studied in great detail. This has applications for precise motion control in limited spaces (for example in robotics, printers, medical devices and watches) and is likely to be more challenging due to the reduced area between workpiece and wire across which a spark can bridge the gap. There is also a need to relate the surface finish and depth of white layer to machining geometry for more complex parts since the premise in most parameter studies is that process outcomes are uniform, since the cuts are typically straight. However, in practise this is not the case.

5

DEVELOPMENT OF A PROTOCOL FOR MEASUREMENT OF MICRO-END-MILL TOOL WEAR

For ease of understanding, nomenclature used in this chapter is included in Table 5.1.

Nomenclature

x_{comp}	Total sliding distance
c_{inc}	Number of incomplete circles
c_{comp}	Number of complete circles
n_{rev}	Number of revolutions
D_{cap}	Engaged tool diameter
x_i	Sliding distance for incomplete circle
f_{cut}	Cutting frequency
n	Spindle speed
Z_c	Number of teeth
F_c	Cutting force
t	Cutting time
f_z	Feed rate
V_c	Cutting speed
F_c	Cutting Force
F_f	Feed Force
F_n	Normal Force

Table 5.1: Nomenclature used in this chapter.

5.1 INTRODUCTION

Micro-milling yields small accurate parts quickly for electromechanical, aerospace, and medical applications. Due to their small size, micro-tools wear quickly and unpredictably therefore tool wear is difficult to measure and is poorly understood, leading to excessive tool changes and reduced productivity. The development of tool wear curves for different micro-milling situations enables the prediction of tool life, thus allowing the tool to be used for the maximum possible length of time while maintaining a good surface finish. This maximises productivity and minimizes costs. The aim of the work presented here is therefore to propose a novel protocol for unifying measurement of wear of micro tools.

On the macro scale, tool wear studies follow the protocols laid out in standards such as ISO8688-1 and ISO8688-2 [153, 154]. These standards dictate cutting parameters and workpiece materials and can be used to benchmark or compare the quality of tools. It was noted by Bahrudin et al. that due to size and cutting mechanism differences, ISO standards are not appropriate for studying micro-mill wear [155], and thus adapted, micro-specific tests have been developed herein.

5.1.1 *Wear and wear measurement for micro-tools*

Some elements of ISO standards can be applied to measurement of micro-tools. One such is the terminology used to describe tool wear: this is useful as the wear of micro-tools can then be compared with that of macro tools. Another is identification of critical wear (i.e. the maximum acceptable wear of the tool). This is the point at which tool wear starts to increase rapidly towards the end of the tool life.

In literature, the wear of micro-tools is often much more poorly-described than that for macro-tools, and tool wear curves described using measurements of cutting edge radius and tool diameter do not typically yield traditional wear curves. Bahrudin et al. investigated flank wear behaviour of micro-milling tools of 0.5-1.5 mm for titanium and H13 tool steel using an Scanning Electron Microscope (SEM) against cutting time. Although they were able to produce wear curves for some of the tools investigated, this was not consistent across the entire range of tools and wear was only measured for one tooth of each tool. Since even a very small run-out has a very significant effect on tooth engagement for micro-tools, it is important to consider the wear on both teeth. They observed that surface finish was inconsistent over cutting time and inferred that this indicated an inconsistency in cutting forces. They did not, however, measure the cutting forces directly.

Based on the issues that arise when machining on a micro-scale especially regarding wear and fracture of tools, numerous studies have been carried out to investigate the effects of different parameters on micro tool wear. Increased cutting velocity increases tool wear [187] which is similar to conventional machining [41]. Moderate feed rates typically result in more stable forces which reduces tool wear (as opposed to very low or high feed rates), but only provided that they are not high enough to cause fracture [142]. Since the magnitude of the cutting edge radius of micro-tools is comparable with the grain size of materials that are being machined, micro structure is important and materials with a higher elasticity result in more ploughing (rather than shearing) [143].

To date, the most detailed curve produced using micro-tools used the surface finish of tools as a wear metric, citing that micro-tool wear is too difficult to measure [188]. The problem with this metric is that surface roughness is dependent on the sharpness of the tool, and whether rubbing or burnishing occurs. This means that if edge fractures occur at certain stages, or material builds up on the tool, the wear mechanisms taking place (e.g. degree of rubbing or shearing) can change. Thus, surface finish cannot be equated to tool wear.

Ucun et al. observed that the cutting edge radius does not give an adequate measure of tool wear, as over the lifetime of the micro-tool a new cutting edge is gradually formed, so that although cutting edge radius initially increases with tool radius decrease, it later decreases again [9]. They measured the diameter reduction for various tools under various cutting conditions but did not plot wear curves. The same method was used to measure tool wear on-line using a variety of sensors by Malekian et al. where similarly edge radius failed to describe the primary locations of wear for the tool, although it was a useful metric in terms of whether shearing or elastic deformation of the material occurs [189]. Measuring edge radius often shows increased wear with cutting distance but does not show similarities to conventional tool wear curves.

Flank wear, another possible metric for quantifying tool wear, was used by Aramcharoen et al. but as the primary aim of the study was to evaluate different coatings [10] , no wear curve was produced and thus the usefulness of this measure in producing wear curves could not be assessed. Flank wear was also used as a measure of wear by Ding et al., along with edge radius, for micro-mills of 0.1mm in diameter, but no defined wear curve was seen (although wear clearly increased with cutting time) [190, 191], perhaps due to the extremely small size of the tools and a limited number of measurements. Elkaseer et al. modelled the effects of steel microstructure on tool wear but did not investigate the evolution of wear for the tools [143].

A more efficient approach was investigated by Filiz et al. whereby a reduction of channel width as a measurement of cutting edge radius [142] was used to investigate machinability of copper, which did not require the tools to be removed for measurement during machining. This is similar to measuring tool radius and does not give information about individual teeth or uneven tooth wear. However, a similar process is applicable to micro-milling, in the sense that channel profile can give an indication of tool wear. Providing an appropriate level of data is held relating tool wear to channel profile, tools can effectively be measured without removal.

5.1.2 *A need for a common method*

Existing work and analysis verifies that, compared with macro-milling, no established protocol for measurement of tools. This leads to a lack of existing data to compare studies with which slows down the process of applying tools in an industrial context [192]. As previously described, flank wear and diameter are often used, but not always [193]. Wang et al. investigated cutting performance of cermet and coated Tungsten Carbide (WC) end-mills in the machining of TC4 alloy, with tool wear being one of the metrics to assess the process [12]. They stated that because "in micro-milling, there are no unified methods to appraise tool wear", width of micro-grooves was used as a measure of tool wear. This is clearly incomparable with measurement of the actual tool, and such a study could not be related to one that measures the flank and diameter of the tool. Clearly, the only way to achieve unification of these studies and compare them or combine them to benefit industry, is to define a standard protocol. The protocol developed is uniquely designed for micro-milling, which has not previously been attempted (subsection 2.3.3).

5.2 PRELIMINARY STUDY

Initial trials were carried out on Brass (CuZn37), based on its easy machinability and application in producing miniature gears which do not need lubrication [51]. In these trials, tool wear was plotted against cutting distance for AlTiN coated carbide tools. The results (Figure 5.1) showed that tool wear can be measured successfully using an SEM.

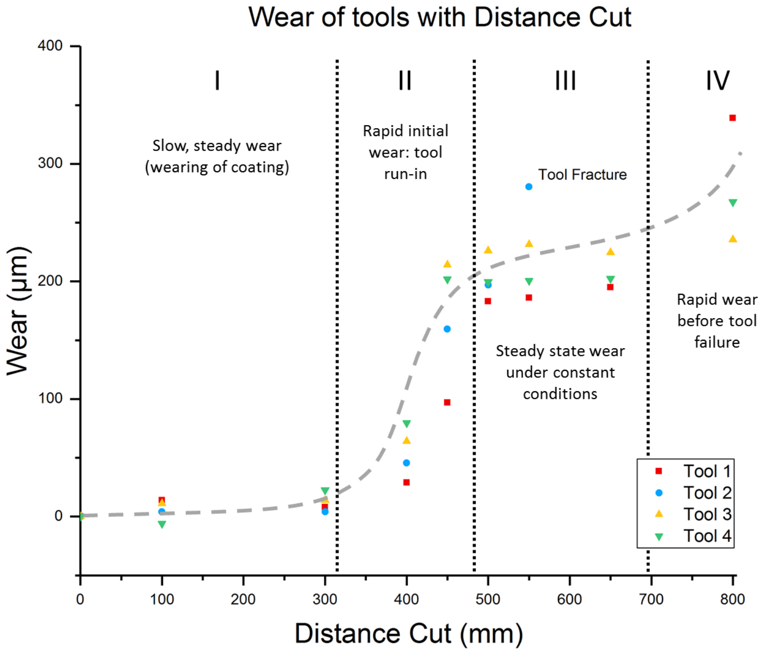

Figure 5.1: Wear of 0.5mm micro-end-mills cutting CuZn38. The wear is given in terms of total reduction in diameter.

The wear for the four tools can be examined in terms of zones. Initially, in Zone I (up to a cutting distance of 300 mm), very little wear was observed, and it is likely that this is the distance at which the AlTiN coating was removed. The coating, which is widely-used in high-performance applications such as micro-milling [194], and survived well before this point because brass is a very soft, easy-to-machine material [142] that is well-suited to AlTiN coatings [195]. After this point, the tool wear shows the characteristic wear curve typically seen for macro-tools [196]. This is not often seen in previous micro-mill wear studies due to under-sampling of the tool wear or inadequate measuring techniques.

In Zone II, rapid wear of the tools was seen as the cutting edge was initially blunted from a very sharp point. During Zone III a relatively slow, steady increase in wear was seen. Finally, Zone IV showed an increase in wear as the tools became severely worn. Fracture of tools occurred in this stage (with the exception of one tool, which broke in Zone III). Using an SEM with the tool in the two orientations shown in Figure 5.2, it is possible to measure the tool wear using the protocol detailed in subsection 2.3.3 (where the terminology used relates to the ISO standards). In reality, often more than one type of wear is seen (see Figure 5.3). These two angles are the minimum requirement to identify all the wear types described.

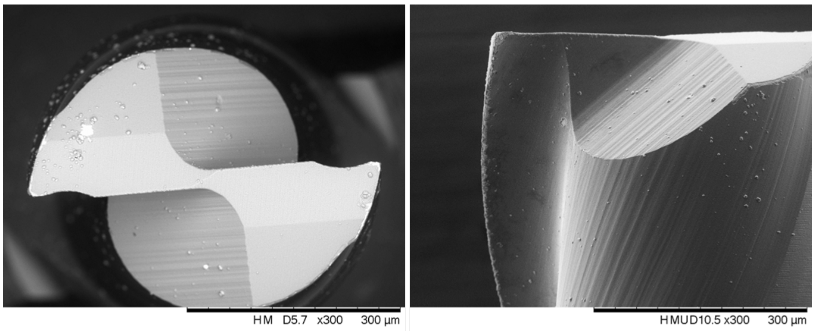

Figure 5.2: The two orientations in which tools were measured.

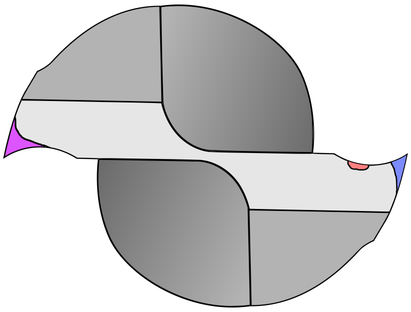

Figure 5.3: An example of multiple types of wear occurring - here, VB and KT2 can be seen in purple, while CH and KT1 are seen in red, and VB is seen in blue.

Type of Wear	Code	Description	Image - Side View
Flank Wear	VB1	Describes uniform flank wear	Figure 5.4a
Face Wear	KT1	Face wear occurring only on tool face	Figure 5.4c
	KT2	Face wear intersecting flank wear	Figure 5.4d
Outside Edge Wear	OE	Outside edge wear seen - no chipping	Figure 5.4b
Chipping	CH	Breaking away of parts of the cutting edge	Figure 5.4e
Catastrophic Failure	CF	Failure of cutting part - for example, loss of tooth	Figure 5.4f

Table 5.2: Types of wear: classification.

The preliminary study and the difficulties encountered when measuring micro tool wear using only outside diameter highlighted the need to achieve a standardised protocol that would provide more information than simply current tool radius.

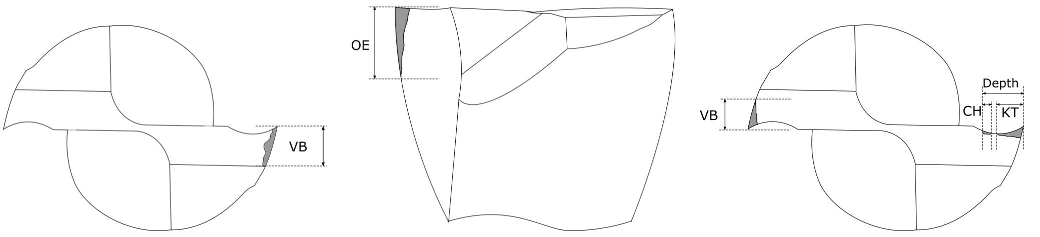

(a) Flank Wear. (b) Outside Edge Wear. (c) Face Wear, Flank Wear and Chipping.

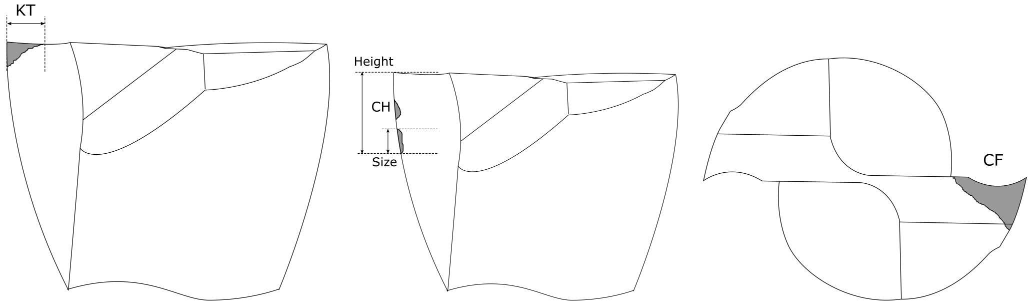

(d) Face Wear Intersecting Outside Edge Wear. (e) Chipping. (f) Catastrophic Failure.

Figure 5.4: Types of Wear - graphical representation.

5.3 DEVELOPMENT OF A PROTOCOL

5.3.1 *Purpose*

In the light of the lack of work on standardising tool wear studies for micromilling, a protocol for measuring tools has been developed to aid future studies of the wear progression and underlying mechanisms. This can be applied to both conventional engineering materials such as steel, and aerospace metals (such as titanium and nickel alloys) which are difficult-to-machine (subsection 1.2.2). It is clear both from preliminary experimentation in this work and a review of literature that the wear of micro tools can be directly observed using optical methods such as SEM to give a classical tool wear curve. However, aside from inconsistencies between studies and the need for standardisation if comparison between studies is to take place, there are some serious problems with methods such as measurement of tool radius. One such issue is the fact that it does not consider uneven wear of the teeth: for example, were catastrophic wear to take place on one tooth while the other tooth remained unworn, the measurement would be the same as if the two teeth were worn moderately (see Figure 3.4). As a result of the preliminary work described in

Section 5.2, it was established that a more precise measurement method for the wear of micro-tools is required to be developed and tested. The intention is that machining parameters and materials to cut should be flexible, but standard reporting methods should be used to allow comparison between studies.

5.3.2 *Definitions*

Certain parameters must be defined when measuring wear on micro-end mills; including cutting edge radius, tool radius, and surface finish of workpiece, and similarly a qualitative indication of the wear mechanism(s). Cutting edge radius is defined as the radius seen on the cutting edge of the tool rake face. The tool radius is defined as half of the working diameter of the tool (e.g. for a 0.5 mm end mill, this is 0.25 mm). The surface finish of the workpiece is defined as the measured $\mathrm{R_a}$ value and the surface texture as the measured $\mathrm{S_a}$ value. Types of tool wear are based on ISO8688 [154] and adapted for small tools. These are categorised (Table 5.2) as Flank Wear (VB), Face Wear (KT), Outside Edge Wear (OE) Chipping (CH) and Catastrophic Failure (CF). By measuring tools in relation to these types of wear, direct comparison between studies can be made.

5.3.3 *Materials: using sliding distance as a measure of distance cut*

In the literature reviewed in chapter 2 and subsection 5.1.1, tool wear for micro-tools has been expressed in literature in terms cutting distance or material removal rate. While this method is useful for describing the useful life of a tool in a given material, it is very hard to compare wear of tools between materials because the difference in cutting feed and speed results in dramatically different sliding distances for different materials. This was identified as an important gap in existing research (subsection 2.3.3). The sliding distance of the teeth was calculated using

$$x_{comp} = \pi D_{cap} c_{comp} + \sum_{1}^{C_{inc}} x_i \tag{5.1}$$

where c_{inc} is the number of incomplete circles, calculated by

$$c_{inc} = \left(\frac{D_{cap}}{s} - D_{cap} \mod 1 \right)$$

c_{comp} is the number of complete circles, calculated by $c_{comp} = n_{rev} - c_{inc}$, D_{cap} is engaged tool diameter, and $\sum_{1}^{C_{inc}} x_i$ is the sum of the sliding distances for all the incomplete circles (Figure 5.5). This method is more useful in a tribological sense, but also allows tool wear for different materials to be compared even in the face of different cutting conditions. The value of x_{comp} was calculated using a Matlab script which established $\sum_{1}^{C_{inc}} x_i$.

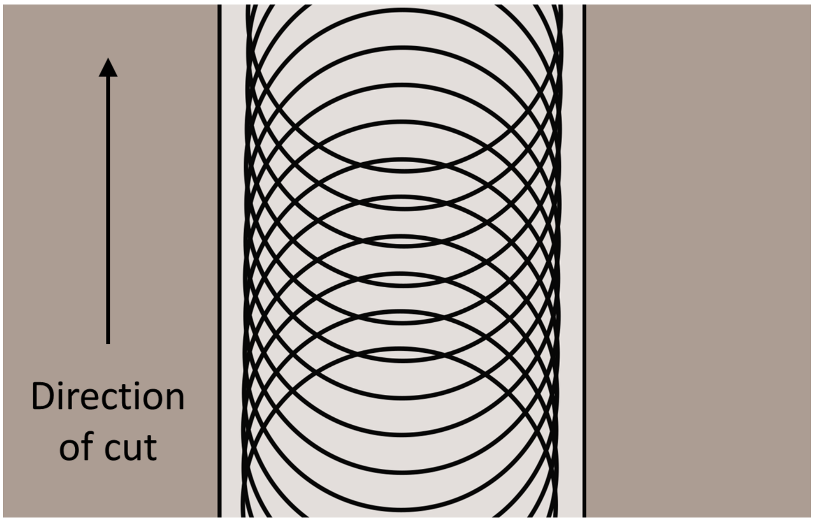

Figure 5.5: Path taken by milling cutter with tool starting and finishing clear of the work piece.

Use of sliding distance allows a more consistent metric to measure tool wear against than cutting distance or cutting time, as the amount of work carried out on the tool depends on spindle speed and feed rate. Conversion factors can be used to relate these sliding distances to either cutting distance or number of cuts given a known spindle speed and feed rate, allowing tool wear to be predicted under differing conditions.

5.4 WEAR MEASUREMENT PROTOCOL

5.4.1 *Tool and Workpiece Preparation*

Tools should be inspected before wear testing takes place to ensure minimum quality standards are met. For uncoated tools, Tests of kycera tools indicate that immediately post-grinding, the tools exhibit cutting edge radius of < 3 µm, while for coated tools this is increased by up to 0.2 µm. Grain size of the workpiece must be considered in terms of tool size, and these taken into account. No specification is given, but when comparing workpieces, the grain direction should be the same for each workpiece, and care should be taken where grain sizes are in the order of 0.1D, where D is tool diameter, to ensure that workpiece grain sizes do not differ by more than 0.02D. In addition, the following criteria regarding depth of cut [152] and unit removal [197] should be met. Unit Removal is defined by Taniguchi to be the amount of material removed per cut, having any of one, two or three dimensions [198]. These two criteria combine such that:

- edge radius < depth of cut and
- edge radius < unit removal × 10

All workpieces should be faced off to ensure flatness perpendicular to the tool and fixed to the machine bed such that the surface is normal to the z-axis. Typically, flood or mist lubricant should be used to control machining temperatures, where the pressure of this on the workpiece is monitored using a micro dynamometer or 3-component force link and taken into account when considering machining forces. Coolant method should be consistent across comparative studies.

5.4.2 *Measurement of Tool*

The micro tools should be measured both prior to testing and during testing. The basic equipment required for testing is as follows:

- Scanning electron microscope with both scattered and backscattered electron functionality.
- Optical profilometer (e.g. focus variation or white light interferometer).
- Ultrasound bath.
- Acetone or similar solvent based cleaner or machine tool cleaner such as castrol, which contains a mix of diluted alcohols. (as long as solven chosen is consistent).
- A compressed air source.
- A force cell for measuring lubricant pressure on workpiece.

During cutting, cutting forces should be measured to determine lubricant pressure as well as cutting forces. Tools should be removed at a pre-determined interval for measurement using an SEM. Before measuring using SEM, tools should be cleaned using acetone in an ultrasound bath and then dried using compressed air. Tools should be measured in two orientations, as shown in Figure 9.3 and it is possible to measure the tool wear using the protocol detailed in Table 5.2 (where the terminology used relates to the ISO standards). Often more than one type of wear is seen (see Figure 3.4). It is important to note that these two angles are the minimum requirement to identify all the wear types defined in the table. All wear measurements are expressed in terms of µm.

5.4.3 *Measurement of Slot Profiles*

The machined slots may be measured using one of two methods: either an image of the cross-section of the material should be taken, as in Figure 5.6; or a profilometer can be used to measure the slot profiles (Figure 5.7). If the latter is used, it is important to ensure that de-burring takes place as this will give inaccurate results. The de-burring must be carried out carefully and in such a way that there will be no further wear of the slots.

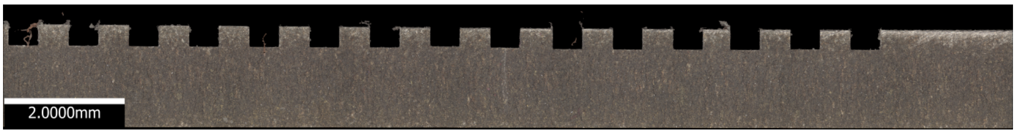

Figure 5.6: Image of the workpiece sectioned perpendicular to direction of cut. Cross section of the slots machined can be seen.

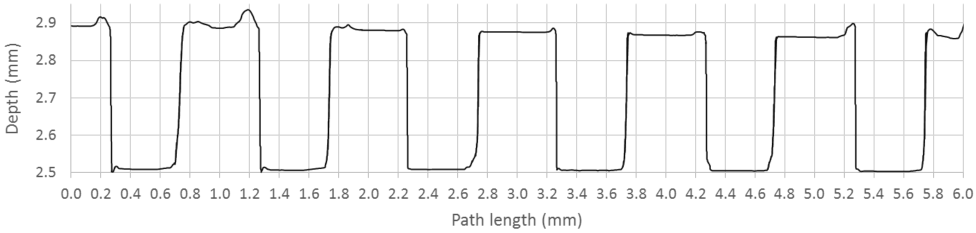

Figure 5.7: Cross-section of slots machined measured using profilometer.

Once measured, slot profiles can be described as seen in Figure 5.8, where W_{BT} and D_T are the theoretical width and depth of slot respectively, and W_B and D_A are the base width and actual depth. The depth of the slot may be a less reliable method of measuring flank wear than the width for measuring rake face wear, if the workpiece has not been faced off to a suitable flatness.

5.4.4 *Criteria for Tool Life*

Worn tools should be measured according to Section 3.5. Face wear (i.e. material removed from the face of the tool) should not exceed 0.2D as this is considered catastrophic failure of the tool. For the purpose of wear measurement, measurement of face wear up to 0.2D will provide data into Zone III of the tool which exceeds practical use and allows the tool life criterion to be established.

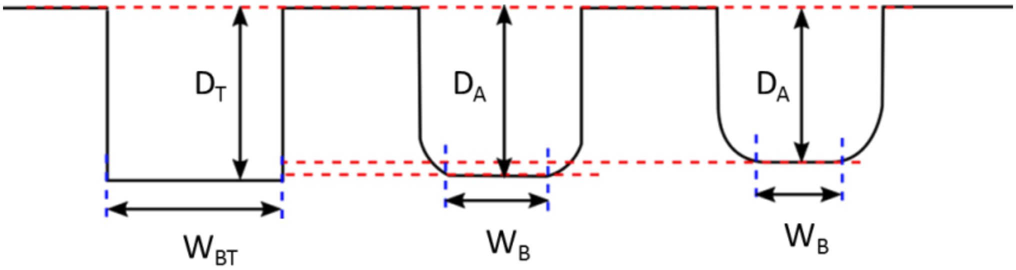

Figure 5.8: Slot profile measurement parameters. D_T represents total theoretical depth, D_A is actual measured depth. W_{BT} is the theoretical width of the base of the slot and W_B is the actual measurement.

5.4.5 *Test Procedure*

For wear testing, slots should be machined to a depth as recommended in the data provided by the tooling supplier or manufacturer. The slot should begin outside the workpiece and run in the y-direction of cut.

5.4.5.1 *Machine Tool Requirements*

The machine tool should be a specialist micro-machining centre capable of reaching spindle speeds of 50,000 rpm or higher. Lower speeds than this result in the need to use excessively low feed rates which cannot be used to simulate realistic milling operations.

5.4.5.2 *Measurement of Forces*

In micro-milling applications, very small run-out leads to significant errors in engagement of teeth and uneven tooth wear. It is therefore always useful to examine the force signature for each tooth engagement to establish whether tooth engagement is equal.

As the forces measured in micro-milling are very small, it is useful to analyse forces using two different methods: measurement of the average cutting force and measurement of the amplitude of cutting force. The former is used to give a general picture of the cutting forces in the feed direction (denoted by Y in Figure 5.9), and simply averages (mean) the value of the signal over the specified cutting time. The latter is slightly more complex because it considers the range of the cutting forces experienced over the specified time. To do this accurately, the difference in engagement of the teeth must be accounted for by plotting the second term of the Fourier Transform. First the second Fourier coefficient, a_2 must be calculated as shown in Equation 5.2, where f_{cut} is the cutting frequency which is found by $f_{cut} = \frac{n}{60} \times Z_c$ where n is the spindle speed in rev/min and Z_c is number of cutting teeth.

$$a_2 = \frac{2}{x} \sum_{m=1}^{x} \left[F_c e^{(-i \cdot 2\pi f_t \cdot t)} \right] \tag{5.2}$$

F_c is the cutting force, t is the cutting time and x is the number of data points. Using the second coefficient, the real part of the second Fourier term can then be plotted against time, using Equation 5.3.

$$f(x) = \mathrm{Re} \left[a_2 e^{(i \cdot 2\pi f_t \cdot t)} \right] \tag{5.3}$$

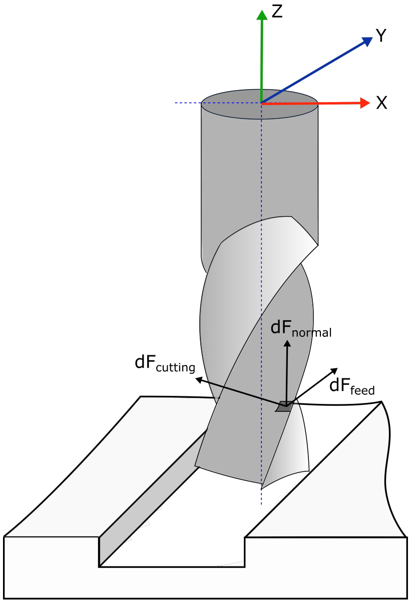

Figure 5.9: Forces exerted on the micro end mill.

5.4.6 *Reporting of Results*

Where tool wear evolution is plotted, wear should be reported in absolute terms relative to the original size of the tool (i.e. in µm). Sliding distance should be used for the x-axis, with a second axis being used as a conversion factor to cutting distance where required. An ideal case theoretical example of this is given in Figure 5.10. Tool wear should be identified as being in one of three zones:

I. Rapid initial wear
II. Steady state wear
III. Rapid wear before failure

The tool-life criterion can then be identified as the intersection between zones II and III.

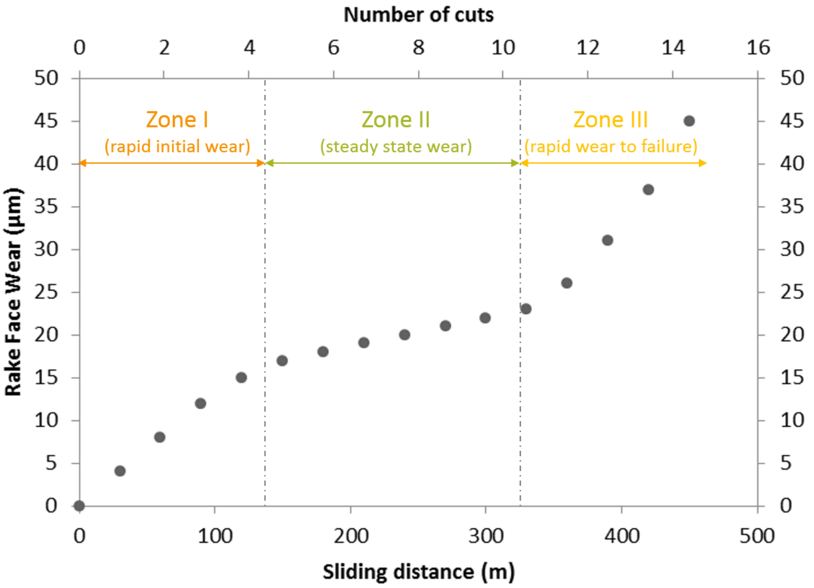

Figure 5.10: An example of the way in which results should be reported: the y-axis is represented both in terms of sliding distance and in terms of number of cuts.

5.5 VALIDATION TESTS

Once an acceptable wear testing protocol had been established, machining trials were designed to test the pertinence and consistency of the method.

5.5.1 *Materials and Method*

Three mechanically very different materials were used: brass (CuZn37), titanium grade 2 and Hastelloy (a nickel-molybdenum alloy containing zinc). Using three structurally disparate materials meant that a variety of wear mechanisms could be observed, representing a wide variety of industries. Tools were set up and measured as described in Sections 5.4.1-5.4.5. The trials took place on a KERN Evo micro-milling machine with a maximum spindle speed of 50,000 RPM. The tools used were commercially available 0.5 mm AlTiN coated tungsten carbide end mills (SGS SER M2SM 0.5 x 3 x 0.8 x 38). Straight slots of 25 mm in length were milled to a depth of 0.2 mm. The workpiece and tool were flooded continuously throughout the cutting process using synthetic Hocut 768. Machining parameters used were based on the manufacturer recommendations for the specific tools when cutting similar materials (Table 5.3).

	Titanium grade 2	Hastelloy C276
Spindle speed (rpm)	25205	6786
Feed (m/min)	69	11
F_z (mm)	0.00136	0.00080
Radial depth of cut (mm)	0.5	0.5
Axial depth of cut (mm)	0.2	0.2
Sliding distance per 25mm length	14.06	23.75

Table 5.3: Parameters used in machining. These were chosen based on manufacturer recommendations and titanium grade 2 was based on titanium alloys while Hastelloy was based on nickel alloys.

The different cutting speeds and feed rates used for each material can be accounted for through the use of sliding distance as the independent variable in reporting the results. The workpiece was mounted onto a 3-component force link (Kistler 9317C) (Figure 5.11) capable of measuring cutting forces in three dimensions (x, y, z) aligned with the major axes of the cutting process. This was connected to a National Instruments Data Acquisition (DAQ) system and Kistler manuware software was used to analyse the recorded data. After each cut was completed, the tools were imaged (by SEM) to measure the wear.

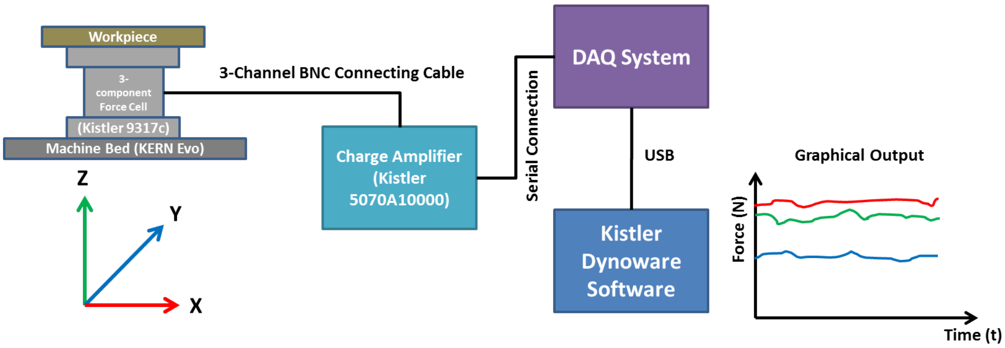
Workpiece
3-component Force Cell
(Kistler 9317c)
Machine Bed (KERN Evo)
Z
Y
X
3-Channel BNC Connecting Cable
Charge Amplifier (Kistler 5070A10000)
Serial Connection
DAQ System
USB
Kistler Dynoware Software
Graphical Output
Force (N)
Time (t)

Figure 5.11: Schematic of the force measurement setup.

Results of this work were then used both to investigate the wear of the tools with a view to extending their useful life, and to confirm the testing protocol described.

5.5.2 *Results*

S-curves were produced for Hastelloy, titanium and brass.

5.5.2.1 *Hastelloy*

Figure 5.12 shows a tool wear curve for rake face wear due to cutting of Hastelloy C-276. Unfortunately, sampling rate in terms of measuring wear is less than desirable (wear measurement took place every 21.84m) and future studies were designed to measure the wear after a shorter sliding distance. For one of the teeth (where tooth number has no physical meaning), the following stages of wear can be seen:

1. An initial rapid wear as the tool is run-in (this is shown in the yellow portion of the graph).
2. Steady state wear (green).
3. Rapid wear before tool failure (red).

Occasionally, a region with apparently zero gradient is seen at the end of tool life, where wear has exceeded the length of the cutting edge: that is to say, the tool is no longer cutting effectively. At this point, rubbing and shaft failure occurs. The other tooth shows no apparent adherence to these stages, due to the initial state of the tool: this tooth was already rounded. This reinforces the need to initial inspection of tools to ensure they have met a minimum standard.

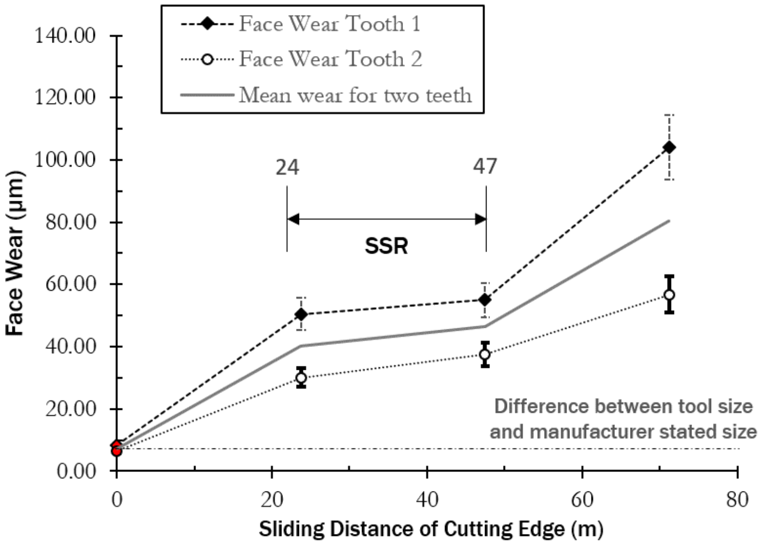

Figure 5.12: Tool wear curve measured for face wear of tool used to machine Hastelloy C-276. Red points indicate how much smaller new tool is compared to manufacturer stated size 500 µm. Starting size is shown with dotted line.

The tool wear for one tooth was higher than that for the other. To understand this, the force signature of the tool was examined as seen in Figure 5.13. It can clearly be seen that one tooth has experienced more engagement than the other, and thus the cutting forces experienced are higher. There are two possible reasons for this: the first is that the initial wear on the second tooth is greater (and indeed this was verified by looking at images of the tool before cutting took place), and the second is that tool run-out causes uneven engagement of teeth. It is known that the machine spindle has some run out from existing service data. This has been reported as being highly significant in micro-machining, in general, where the tools are smaller [152, 199] and this type of behaviour is typically seen in micro-milling, to the extent that sometimes only one tooth is engaged [200].

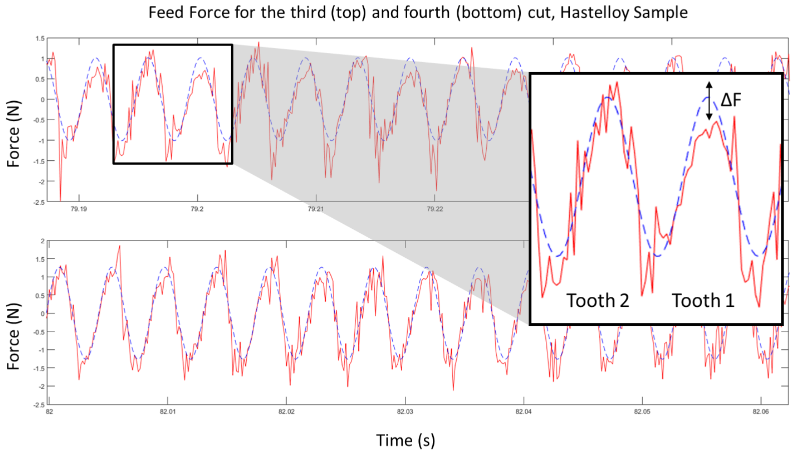

Figure 5.13: The force signature for the tool used to machine Hastelloy C-276.

The outside cutting edge data (Figure 5.14) showed little, if any, closeness to a traditional wear curve, resulting from the combined effects of too few measurement points for this tool, and the inherent challenges in measuring very small tools.

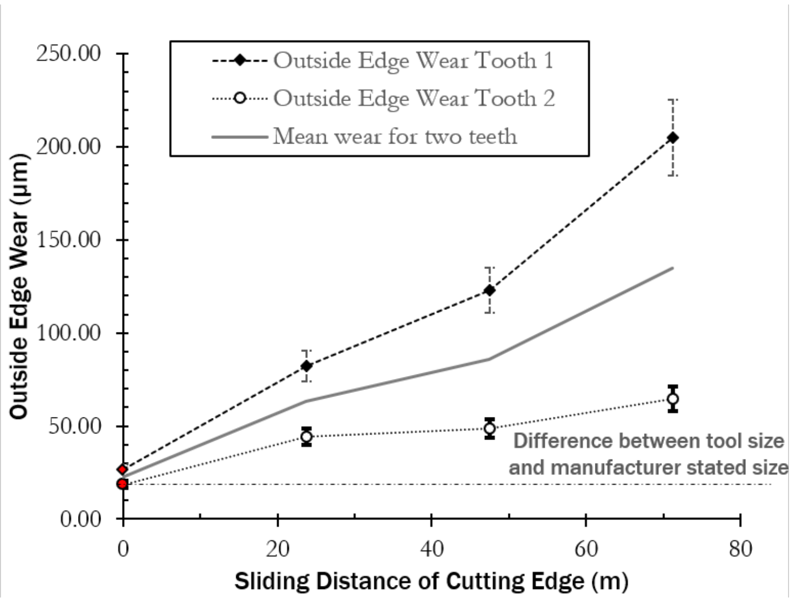

Figure 5.14: Tool wear curve measured for outside edge wear of tool used to machine Hastelloy C-276. The dotted horizontal line represents a baseline - tools were measured and discrepancy between actual size and manufacturer stated measurement. These points are differentiated as red.

Flank wear (Figure 5.15) reveals a much more consistent result than face or outside edge wear and the onset of wear appears to lag behind face wear in terms of the wear stage. Here, initial quality of the tool is less significant since the flank face is set back from the leading edge of the tool, and both teeth show the first two stages of the classic wear curve.

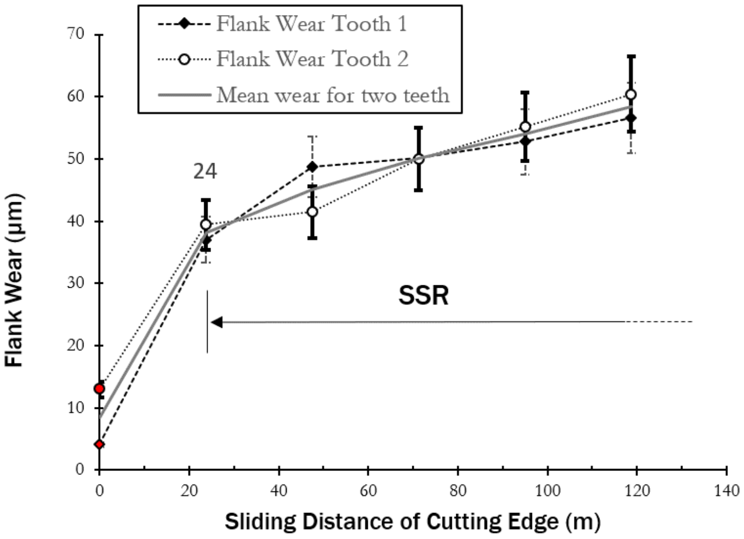

Figure 5.15: Tool wear curve measured for outside edge wear of tool used to machine Hastelloy C-276. Red points indicate how much smaller new tool is compared to manufacturer stated size of 500 µm.

5.5.2.2 *Titanium*

For the tools used to cut titanium, the rake face wear curve (Figure 5.16) shows a typical s-curve up to approximately 130 µm. Wear is steady between approximately 35 µm and 90 µm, after which it accelerates rapidly - thus the tool life criterion, defined as the point at which the tool begins to wear rapidly[155], is identified to be 90 µm or 8% of the tool radius.

After 100 µm of wear has occurred, the entire cutting edge has been worn off and the tool can be considered to have failed. Tool shaft fracture may or may not occur at this point, depending on whether the centre of the tool remains engaged with the workpiece to an extent that a cut could be attempted.

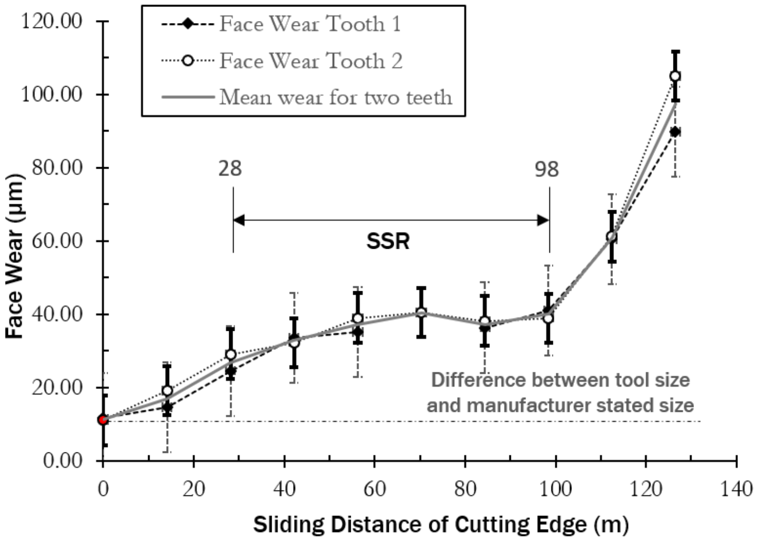

Figure 5.16: Tool wear curve measured for face wear of tool used to machine Ti grade 2. Red points indicate how much smaller new tool is compared to manufacturer stated size 500 µm. Starting size is shown with dotted line.

As with the Hastelloy tools, outside edge wear (Figure 5.17) does not show a well-defined traditional wear curve. Abrasive wear continues to take beyond the depth of cut, because of swarf from the workpiece acting as a third body. This is evacuated by the lubricant (coolant) but rubs past the tool in this process. Wear appears to reach a steady state above a depth of 300 µm, at which point the swarf is no longer travelling up the shaft and little contact between the tool and material takes place. Although outside edge wear is unable to provide a defined tool wear curve, chipping on the outside edge of the tool may affect the tool's ability to produce a good surface finish, or indeed the tool's ability to remove swarf. Thus, outside edge wear does provide some indication of impending tool failure.

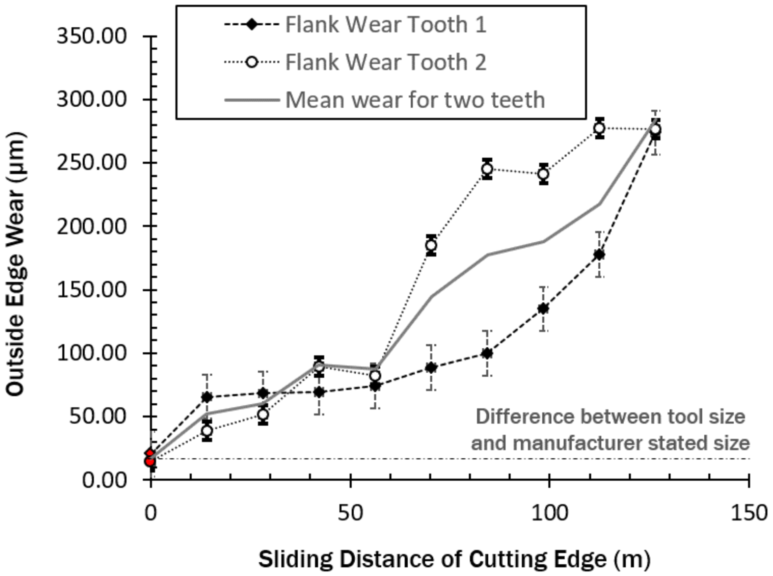

Figure 5.17: Tool wear curve measured for outside edge wear of tool used to machine Ti grade 2. Red points indicate how much smaller new tool is compared to manufacturer stated size 500 µm. Starting size is shown with dotted line.

Flank wear, on the other hand, shows an s-curve as seen with face wear (Figure 5.18), with the only obvious difference being the point at which each wear stage is reached.

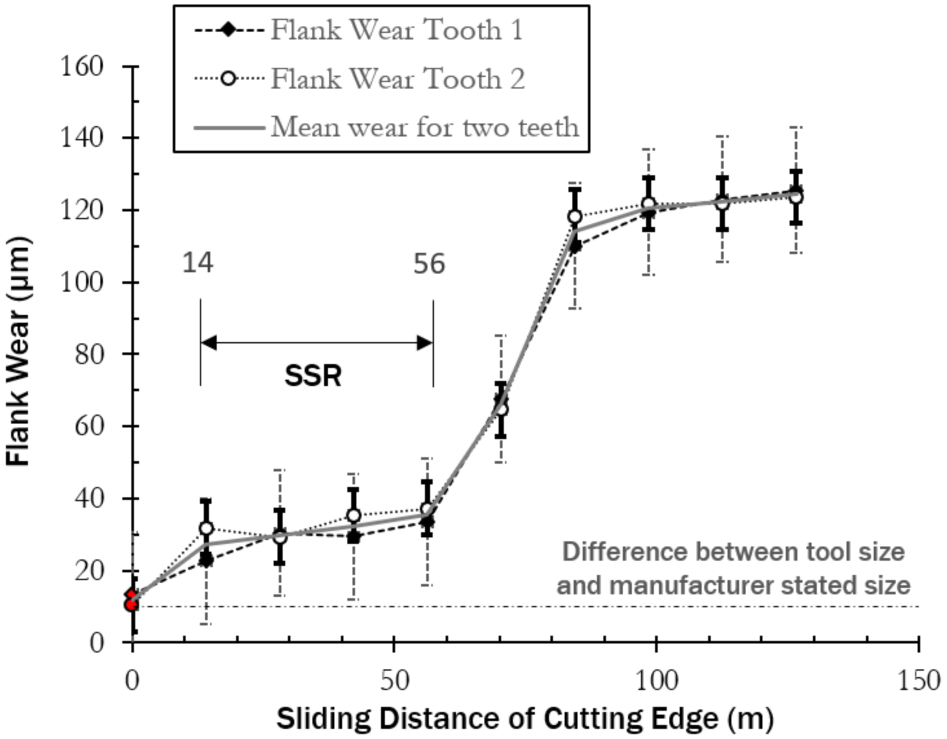

Figure 5.18: Tool wear curve measured for flank wear of tool used to machine Ti grade 2. Red points indicate how much smaller new tool is compared to manufacturer stated size 500 µm. Starting size is shown with dotted line.

The shapes of the tool wear curves achieved are strikingly similar to conventional tool wear curves [82] - as previously noted by Bahrudin et al. [155] - in each case, a traditional s-curve is seen. This allows the critical wear point or tool life criterion to be identified as the point after which tool wear becomes intolerable. Depending on the required workpiece dimension tolerance, the actual tool wear volume that is acceptable may be less than this.

5.5.2.3 *Brass*

Two different types of tool were used to machine brass: those with no coating, and those with an AlTiN coating. The initial tools used were TiB_2, chosen based on the tooling manufacturer recommendation for brass. As for titanium and Hastelloy, as shape approximating an s-curve can be seen, although machining time was so short for the uncoated tools that data is limited. Comparison between the TiB_2 tools used to machine brass, and the tools which were coated with AlTiN clearly shows that the steady state portion of the graph is over twice the length for AlTiN coated tools than TiB_2 tools. Furthermore, the steady state region for the TiB_2 tools occurred at a higher level of wear. One of the TiB_2 tools fractured before rapid wear could be seen (Figure 5.19). Rake face wear is seen in the Figure, as the tool wear curve see for coated brass tools is taken from the preliminary study described in Section 5.2, during which only rake face wear was seen, and thus this is the only wear measurement that can be compared.

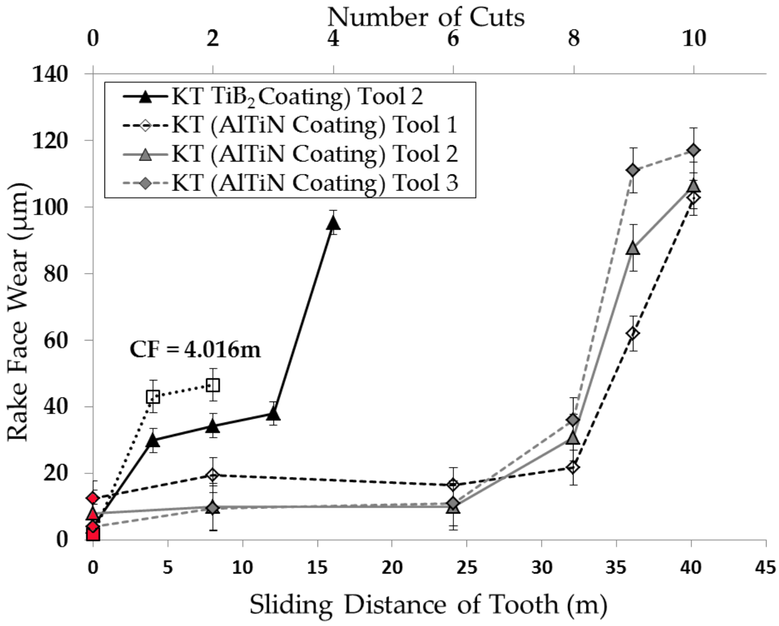

Figure 5.19: Rake face wear for uncoated and coated tools used to machine brass. CF indicates catastrophic tool failure. Red points indicate how much smaller new tool is compared to manufacturer stated size 500 µm.

5.6 REFLECTION ON PROTOCOL

Section 5.5.2 describes the results obtained using the protocol described in Section 5.4. Well-defined wear curves were seen using the imaging methods described for both rake face and flank wear. Other metrics, such as slot profile, were not able to provide as much information. This section considers each part of the protocol and its relative success, in order to determine which parts of the protocol can be concluded to be optimal when measuring tools.

5.6.1 *Improvement of new method over tool diameter*

As discussed in both in chapter 2 and subsection 5.1.1, it is possible to describe the tool wear in terms of diameter reduction. However, in an addition to the fact that this does not take into account features such as tool geometry and uneven tooth wear, it can be seen from the tool wear curves in Section 5.5.2 that flank wear and face wear result in different points at which extreme wear begins to take place, and even outside edge wear, while not producing a curve, can provide information about tool chipping and imminent failure. The useful life of the tool should be identified as the point at which either flank or face wear reaches III, which in the case of the titanium workpiece was the flank wear. This is not reflected in a simple diameter measurement. Although measurement of diameter may be sufficient once tool life criterion is known, it cannot be used to determine it. The data arising from the use of the protocol described here allows the wear for each tooth to be measured for both tool flank and face such that a much clearer understanding of how the tools are wearing can be achieved, in a more consistent fashion, than has been previously carried out.

5.6.2 *Efficacy of measuring slot profiles as a post-machining tool wear measurement technique*

Figure 5.20 shows the tool wear observed for a titanium sample using the method described in Section 5.4. Both wear to the flank and wear to the rake face can be seen.

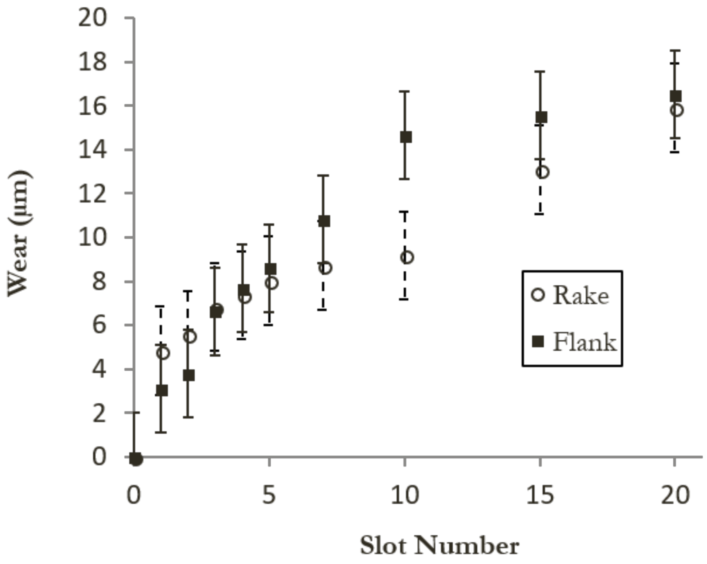

Figure 5.20: Tool wear curve measured using slot dimensions for Ti grade 2.

One issue with this method was the fact that if the workpiece was removed after the initial levelling stage; its orientation in the fixture was such that its surface was not completely perpendicular with respect to the tool. This led to an error in W_f and W_r, as can be seen in the Figure. The result of this is that absolute wear of the tools cannot be determined using this method. However, it is still possible to identify the steady state sections of the wear, which suggests that with refinement this method could be used as a quick method of analysing tool wear. Typically, an error in angle of workpiece would be small enough that W_f are W_r are not significantly changed relative to the quoted cutting edge radius.

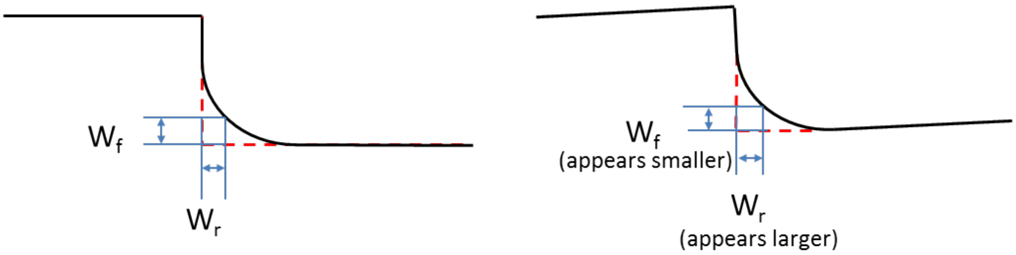

Figure 5.21: Possible sources of error when measuring slots.

This method cannot be used where tools have been removed for measurement since relocation of the tool and workpiece causes the systematic error to become large and random, and the results become unreliable.

5.6.3 *Sliding distance vs. Cutting distance*

As described in Section 5.3.3, sliding distance is more appropriate for plotting tool wear against than cutting distance or cutting time, as the amount of work carried out on the tool depends on spindle rotational speed (RPM) and feed rate.

When the tool wear for titanium and Hastelloy are compared as in Figure 5.22 using cutting distance, the tools used to cut Hastelloy enter the third wear stage at approximately the same cutting distance that the tools used to cut titanium enter steady state wear. This comparison is misleading since the tools used to cut Hastelloy use lower feed rates and speeds due to Hastelloy's comparative resistance to cutting, and thus the graph plotted using sliding distance is more representative. Using sliding distance, it can be seen that even considering the higher sliding distance per cutting length for the tools used to cut Hastelloy, these tools wear much faster than those used for titanium.

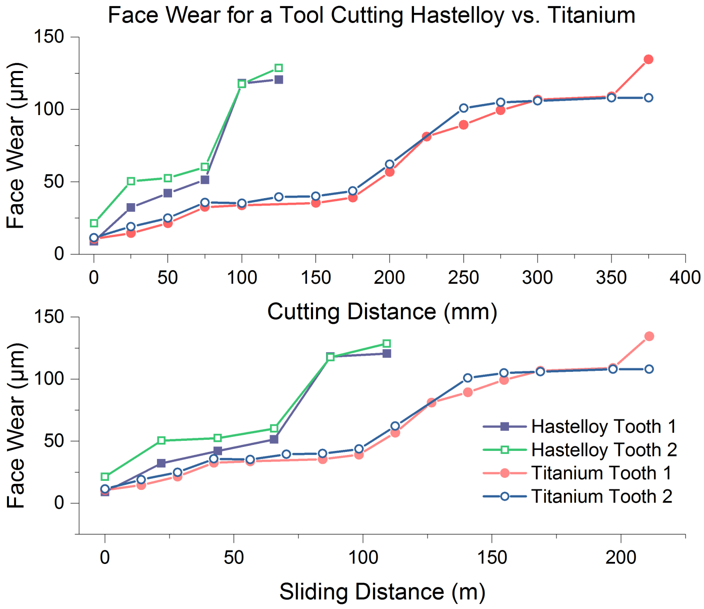

Figure 5.22: Comparison between using sliding distance and cutting distance.

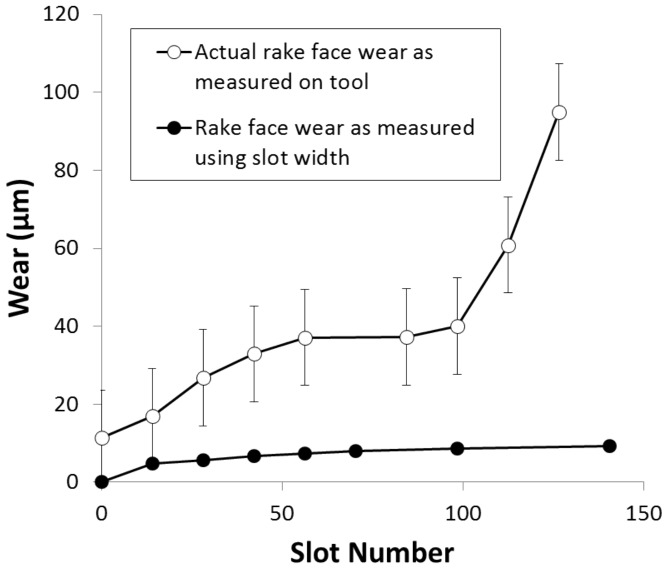

Figure 5.23: Relationship between tool and slot measurement.

5.6.4 *Direct tool measurement vs. Slot measurement*

Figure 5.23 shows the comparison between measurement of the slot profile for a tool used to cut titanium and the actual measurement of the tool. It can be seen that the slot measurement of rake face does not accurately describe the tool wear curve for the tool, and therefore fails to produce the correct wear curve. This highlights the fact that although slot profile can be used as a fast method of identifying where wear has taken place, to obtain detailed information on tool wear direct measurement is needed.

5.6.5 *Rake face wear vs. Cutting Forces*

Rake face wear is compared with the feed component of cutting forces to the relationship between the two. This comparison for Hastelloy is seen in Figure 5.24: Both teeth experienced similar wear for the rake face, with the transition between zone I and II (as described in Section 5) occurring at 22m of sliding distance, and the tool life criterion occurring at a sliding distance of 65m.

It can be seen for both sets of force data that both the average feed force and the range of feed forces (tool vibrations) initially increase with tool wear but that the rate of this increase plateaus with tool wear - this is consistent with the hypothesis that if the tool is sufficiently worn that there is little engagement between tool and workpiece.

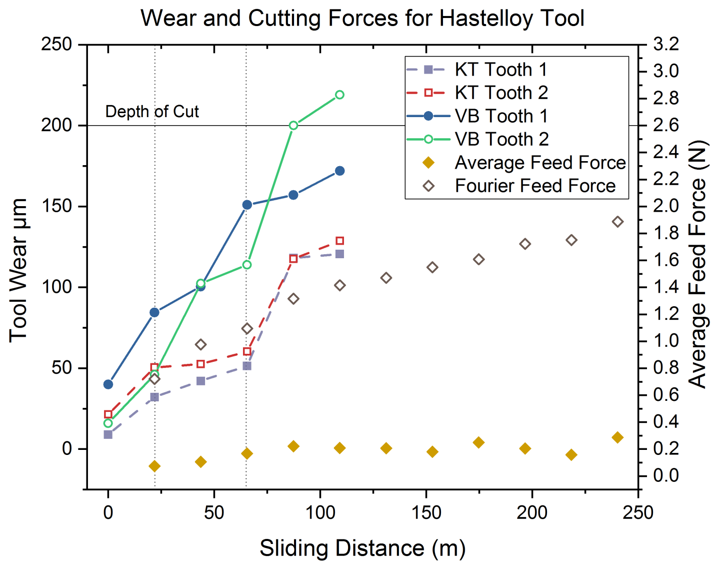

Figure 5.24: Wear in relation to cutting forces for a tool used to cut Hastelloy C-276.

Compared with the data for Hastelloy, the tool used to cut the first titanium sample has significantly more data points. A defined s-curve is initially seen for face wear (Figure 5.25), with steady state wear occurring at a sliding distance of 42m and the tool life criterion occurring at a sliding distance of 99 m. The curve then flattens out with reduced engagement and a dramatic wear increase is seen when tooth 1 fractures. Average feed force increases consistently, and continues to do so linearly with sliding distance even when the gradient of tool wear is at its lowest (i.e. in stage 2). The average feed force only plateaus when tool wear plateaus at the end of cutting due to lack of engagement. The Fourier transform of the force also starts by increasing linearly, but plateaus after the steady state region, likely because of reduced tool-workpiece contact.

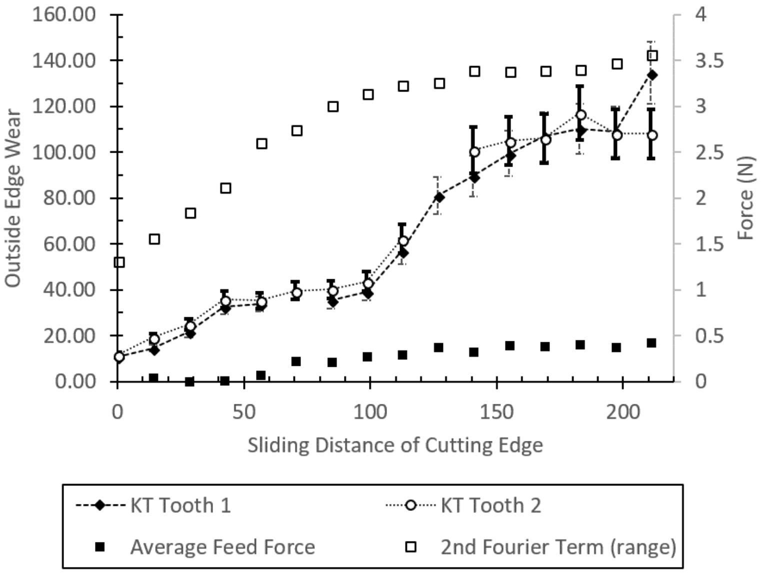

Figure 5.25: Wear in relation to cutting forces for a tool used to cut Ti grade 2.

As well as initial edge rounding having much more significance for smaller tools, the coating thickness can be much more significant: both because it comprises more of the diameter of the tool (a thickness of 2 µm represents 0.4% of the tool diameter as compared with 0.04% for a 5 mm end mill) and because it increases the initial edge radius [201]. The issues with consistency in results discussed here indicate again the importance of ensuring that the tools are closely inspected before cutting takes place in future studies and reinforce the need for a standard protocol for micro tool wear measurement.

5.6.6 *Force Signature - uneven engagement of teeth*

The force signature was investigated for each of the cuts made. The difference in force signal between teeth was seen to vary between tools, with an example for one of the Hastelloy cuts given in Figure 5.26.

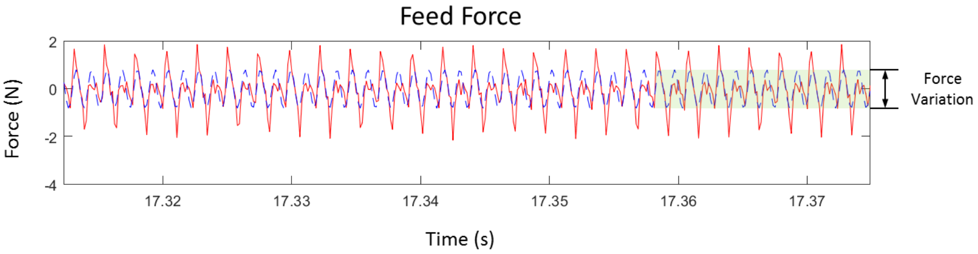

Figure 5.26: The fit made using the second term of the Fourier series.

The raw force signature for the tools indicates that tooth wear engagement is often much more uneven than that seen for macro-milling tools. This has been observed previously by Mativenga and Hon [202], who reported an engagement difference of no more than 30%. However, this amounted to a force difference of approximately 20N. Similarly, Kim and Jeon observed a force difference of approximately 10N over a 50N range (<20% difference) for 8, 12 and 14 mm end mills cutting Al6061-T6 aluminium alloy [203] but the magnitude of the forces is much lower in micro machining. Furthermore, tool run-out has much more significance for a smaller tool [152], as demonstrated by Figure 5.27. Uneven engagement of teeth caused by runout causes different levels of wear to each tooth than that experienced by micro-milling. This results in a force signature that can be dramatically different for both teeth. Where the wear curve for each tooth is very similar, it should be expected that the force signature for each tooth is also similar since cutting forces have a positive relationship.

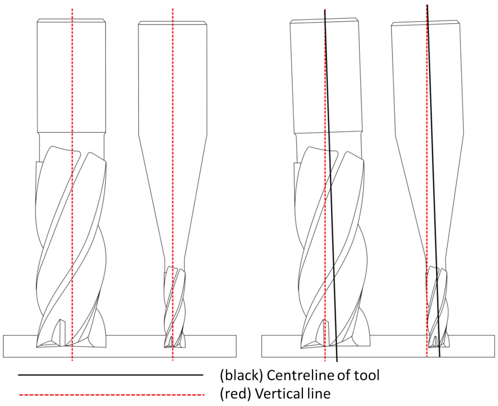

Figure 5.27: Effect of runout is magnified for a smaller tools.

5.6.7 *Mechanism of tool breakage*

One major consideration in micro-milling is the relative size of the workpiece grains in relation to the tools. Figure 5.28 shows (to approximate scale) the size of the grains for Hastelloy. Many of the grains are in the order of 10 µm, which is 2% of the tool's diameter. The structure appears inhomogeneous to the tool and thus the cutting forces can vary significantly from pass to pass. This causes sudden fracture to the teeth from time to time, rather than the smooth, even wear that would be expected in macro milling. To further understand the mechanism of tool breakage, it is useful to look at the chips produced during the tool wear process.

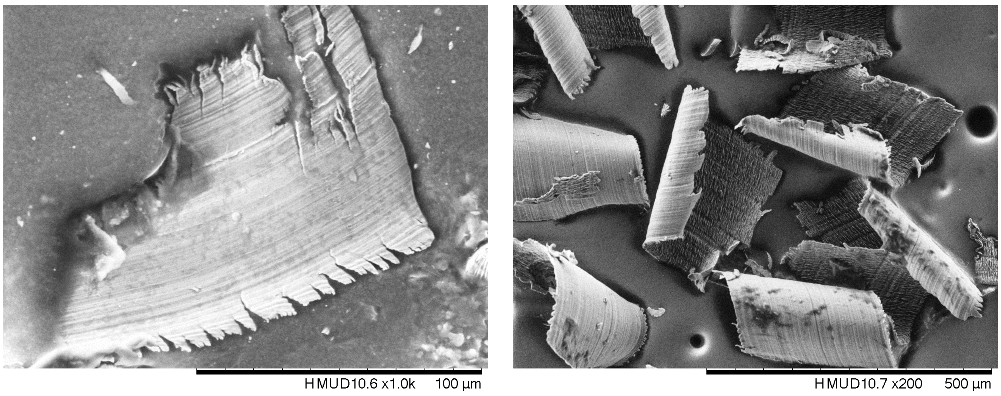

(a) Chip produced from machining of Hastelloy. (b) Chip produced from machining of titanium.

Figure 5.29: Chips produced in machining.

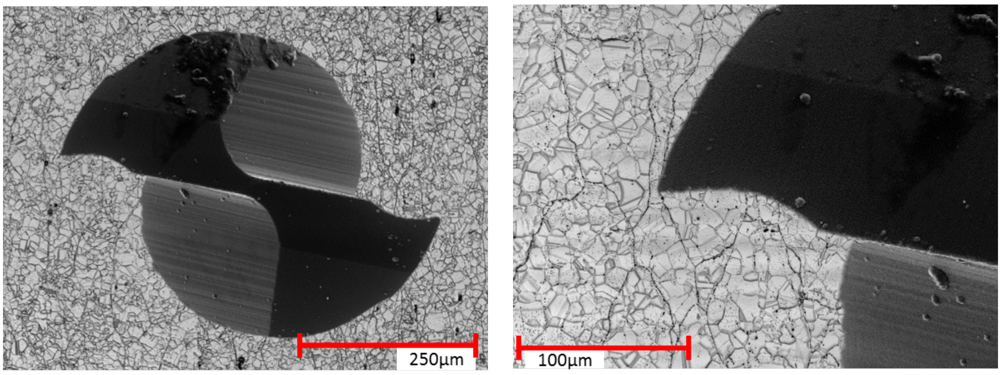

(a) Workpiece grain size is relatively large compared to the cutting edge. (b) Grain boundaries make the material appear inhomogeneous.

Figure 5.28: Grain sizes relative to tool size.

Due to the very small size of the chips (typically the chips are no more than 200 µm in length and width) it is very difficult to collect and study them. However, some examples of chips for each material were collected directly from the work pieces. For both the titanium and the Hastelloy, serrated type chips were seen, of the type shown in Figure 22. Examples of both chips are given in Figure 21. The chip formation is an indicator of regions of intense shear followed by regions which are relatively undeformed. This results from high machining temperatures which are not dissipated quickly, as is common when cutting titanium and nickel alloys [204]. This can cause cutting edge attrition due to irregular flow of material as well as thermal fatiguing which results in chipping and fracture of the tools. The result of this can be the eventual catastrophic failure of the tools.

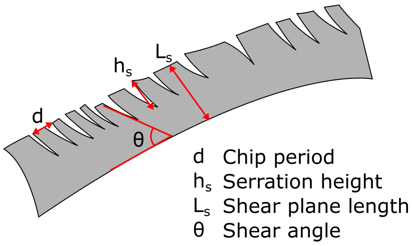

Figure 5.30: A serrated-type or discontinuous chip.

Tribological phenomena in micro-tool wear and the relationship between these and micro tools is discussed further in chapter 6 .

5.6.8 *Considering alternative coatings: an early investigation into extending tool life through tool coatings*

Coating tools used to machine brass with AlTiN (Figure5.19) showed a dramatic lengthening of the steady state region of the tool wear curve for AlTiN coated tools. Additionally, the steady state occurred at a lower wear level for these tools. The latter result has previously been reported [15] but the lengthening of the curve is significant as it indicates a longer tool life. The early fracture of one of the TiB_2 tools is likely to have been caused by imperfections in the carbide material or excessive cutting forces generated by burring or larger crystals in the brass and serves as a reminder of the difficulty of measuring tools on the micro-scale and the importance of pre-inspection. This result suggests that even for softer metals such as brass, coating tools can significantly improve tool life. To a certain extent, this relates to cutting edge radius - the applied coating increases the cutting edge radius of the tools, and this cutting edge radius reduces stresses on the tools [6, 7].

Based on literature reviewed in chapter 2 and subsection 5.1.1, there is scope for significant further investigation of coatings for micro-end-mills, since many tooling companies offer only standard coated or uncoated micro-end-mills. Compared with macro-tools, the research into coatings for micro end mills is significantly less extensive.

Despite the disadvantages that coatings have (for example, increased cutting edge radius) there is opportunity for significantly extending tool life. This protocol offers a method for testing tools comparatively, and can be used to investigate the effects of different coatings on tool life. To extend upon this, future research should consider applicability of this protocol to more complex machined geometries, with a view to applying the results to engineering environments.

5.7 CONCLUSIONS

Considering the difficulties encountered when comparing studies on tool wear in micro-end-milling, a protocol for measuring, characterising and reporting wear on sub-millimetre end mills is proposed. The purpose is to provide a method such that studies between different tool geometries and materials can reasonably be compared. Standardisation will make building on existing studies possible, while the characterisation of wear curves for different tools has direct applications in manufacturing for maximising process efficiency.

The results obtained in the validation wear tests have indicated that the novel wear measurement protocol proposed allows the wear curve of sub-millimetre micro end mills to be plotted, with the following points of note:

1. Using the suggested protocol, stages of wear can be identified as with macro end mills, such that the wear of the tool is not allowed to go beyond the steady state region.
2. Outside edge wear provides little information when studying the wear of micro end mills. A combination of face wear and flank wear provides much more consistent data.
3. It is common for the teeth of the tools to wear unevenly due to spindle run-out, which can lead to single tooth failure even relatively early in the tool wear curve.
4. In allowing for different speeds and feed rates, slliding distance presents a much more appropriate measure of reporting micro end mill wear than cutting distance or cutting time.
5. This method is only able to provide information about the tools after the event and requires very strict machining to be of use.

6

INVESTIGATING TOOL COATINGS AS A MEANS OF EXTENDING MICRO-END-MILL LIFE

6.1 INTRODUCTION

With increased miniaturisation of systems and components, micro milling has emerged as a popular process for manufacturing small components. It is used in industries such as aerospace, medical and dentistry for producing miniature parts such as dental implants and fuel injectors. Furthermore, due to its capability to produce high integrity parts relatively quickly, it has uses in optics and electronics. Although not directly applicable to mass production (due to low productivity), micro milling provides a pathway to mass-production through micro-mould manufacturing [4]. Both the medical and aerospace industries make use of materials such as titanium and high-performance superalloys. These are typically difficult-to-machine even on the macro-scale tools, but present further complexity in micro milling as burring and crystal irregularities lead to regular catastrophic fracture of the tools. These high tool fracture rates lead to poor machining efficiency, increased costs and difficulties predicting machining times.

6.1.1 *Definitions*

The typical tool-life wear curve for macro-scale cutting tools is well documented, and a distinct curve can be expected [82, 205] as seen in Figure 6.1. Tool wear should be identified as being in one of three zones:

I Rapid initial wear

II Steady state wear

III Rapid wear before failure.

The axis labelled 'distance cut' could equally be replaced with time, number of cuts or sliding distance, depending on whichever is the most useful for the end user.

As described in (subsection 5.4.6), in Zone I, rapid wear of the tools is seen as the cutting edge is initially blunted from a very sharp point. During Zone II a relatively slow, steady increase in wear is seen, referred to as the steady state. Finally, Zone III shows an increase in wear as the tools become severely worn. Fracture of tools occurs in this stage. This work focusses on the identification of this curve for micro-sized tools. Micro-machining is defined as the use of mechanical tools which have dimensions in the order of micrometers [10].

The tool life criterion is defined as the point at which the tool begins to wear rapidly [91], at the intersection between zones II and III. Monitoring the wear of micro milling tools allows processes to be characterised: a wear curve indicates the point at which the tool can no longer cut to the required standard [91]. A longer wear curve in terms of sliding distance is meaningless because it may be that the tool is achieving poor cutting for much of its life. Figures 6.1 to 6.3 illustrate this: in 6.1a, two tool wear curves of the same overall length are seen, where (b) has a longer Steady-state Region (SSR) . Figure 6.2b shows these two curves and a binary value (medium or high) describing the reliability with which wear can be predicted (in terms of reduced diameter) of the tool. Tool (a) shown in grey, is predictable for a much shorter time. Finally, Figure 6.3c shows the surface quality for both tools: the tool with the longer steady state results in an overall higher quality part.

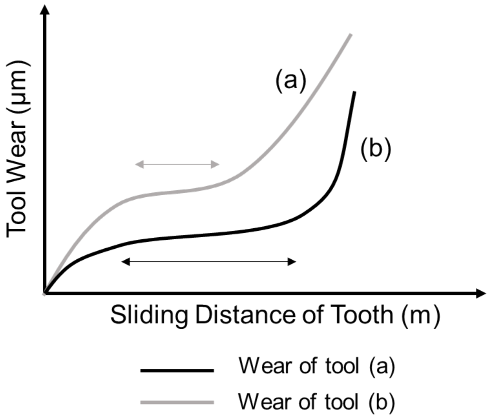

Figure 6.1: Wear curves of two different tools.

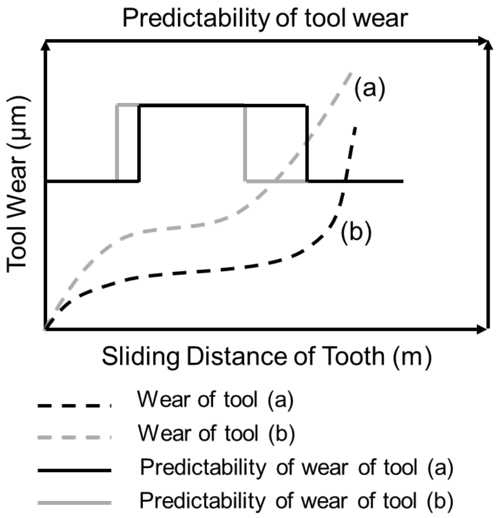

Figure 6.2: A schematic to show the relationship between position on tool wear curve and predictability of the tool's wear. The step function shows that predictability is either high or low, and occurs in the steady state region. It is longer for the tool with the black wear curve.

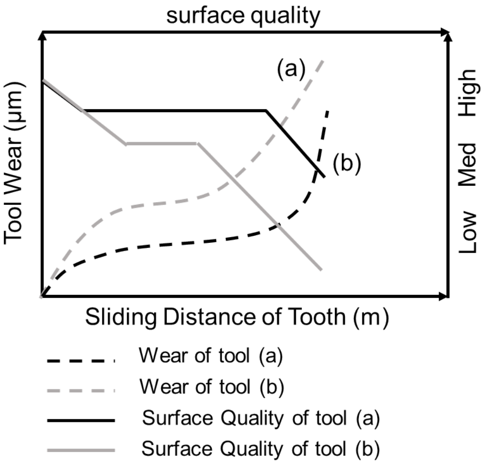

Figure 6.3: A schematic to show the relationship between position on tool wear curve and surface finish quality of machined part. The tool with the longer steady state region produces a good surface finish for much longer, as shown by the larger area under the curve.

6.1.2 *Existing Studies into Tool Wear of Micro-milling*

As described in subsection 2.1.4, approximation of micro milling as a scaled-down version of conventional milling is flawed: micro milling exhibits different wear and dynamic characteristics [88]. There are a number of reasons for this: the first being that in micro milling, feed per tooth and depth of cut are often smaller than or comparable to the cutting edge radius, resulting in failure to shear material [206]. Due to their small size, micro milling cutters generally have poor resistance to fracture [90], which in itself makes study of micro-tool wear challenging [91]. Furthermore, although on a macro-scale a polycrystalline structure appears homogeneous, at the micro-scale grain sizes are relatively large when compared to the size of the tool which causes dramatic force fluctuation [92]. These effects combine to create an effect known as the size effect [88].

In addition to machining difficulties, there are measurement challenges for very small tools. They cannot easily be measured on-line using a hand-held/machine mounted optical microscope due to insufficient magnification or depth-of-field. Thus, tools must be removed from the machine and subsequently measured offline using methods such as scanning electron microscopy Scanning Electron Microscope (SEM). This influences the measurement itself, and can affect run-out. On a practical level, micro-mills experience chip clogging, fatigue-related material removal (as occurs with macro tools) and excessive stress-related fracture. The latter may occur due to irregular grains in the workpiece or indeed due to weaknesses in the carbides used to produce the tools. Here, small irregularities in tool construction can have catastrophic effects [91].

Despite these issues, a significant body of research into micro tool wear exists [206]. As with macro milling, tool wear is influence by parameters such as cutting velocity and spindle speed [207], feed rate and axial depth of cut [208]. Similarly, there is a consistently positive result between flank wear and cutting forces in end milling (on both macro and micro scales) [209]. It follows that reducing cutting forces can reduce the rate of tool wear. One of the methods for this is to apply coatings to tools, where the mechanism for reduced wear includes altered toughness or reduced frictional forces and therefore reduced heating and wear of tools.

Unlike macro-milling, tool wear measurement for micro tools has traditionally been poorly-defined. There are no unified methods to appraise tool wear [12] and ISO standards cannot be applied to this scale [155]. Thus, wear of micro-tools is often much more poorly-described than that for macro-tools, and well-resolved tool wear curves are not necessarily seen.

This has hampered fundamental understanding of the wear processes and makes tool optimisation difficult. Rake face or flank wear has typically been used to provide the best-quality tool wear curves in the context of micro end mills, although often measurement resolution is insufficient [193, 210]. One of the best examples of the use of flank wear as a method for producing wear curves is Rajabi et al. [211] who observed a lower overall wear of end mills for TiC based tools with different binders. The practical outcome was improved geometrical accuracy rather than increased tool life (since the tool life criterion occurred at the same point for both tools).

Although geometrical accuracy is essential, the authors focus in this work on extending the working life of the tools, not just absolute wear. Where flank wear is used as a measure of tool wear, it is important to consider the wear on both teeth since even a very small runout has a very significant effect on tooth engagement for micro-tools. Often this is overlooked, and a single tooth is measured to save time [155]. Premature fracture means this type of measurement is inadequate if high fidelity tool wear curves are to be achieved.

As well as flank wear, reduction in diameter is a common metric for measuring micro end mill wear. For full characterisation, this should be considered inadequate as it provides no data on individual teeth and only an overall approximation. Indeed, Oliaei and Karpat investigated the influence of tool wear on machining forces and used both diameter reduction and flank wear as measures of tool wear[212]. The diameter reduction did not allude to a tool wear curve (in fact, it appeared to reduce linearly) whereas the flank wear showed tool wear similar to the traditional tool-life curve described in Figure 5.1.

For coarser measurements, reduction in diameter can be measured - for example on-line measurement systems such as light gates, which can provide quick feedback that is useful in measuring geometrical accuracy. Due to the difficulties with measuring micro tools, width of machined slot has been proposed as an indication of tool wear [142]. This did not successfully produce a wear curve and is unreliable as it is highly dependent on run-out of the micro-tool [92]. This was also seen in a previous study by the authors [13]. Outside edge wear is not used to measure wear curves for micro-tools due to significant irregular wear from chips.

Due to the difficulties with measuring micro tools, width of machined slot is sometimes used to indicate tool wear. However, this method has certain pitfalls, not least the fact that it is highly dependent on run-out of the micro tool if an even depth and width slot is to be produced. Wang et al. used this method to measure tool wear, although this did not yield any apparent tool wear curve. An attempt to use slot width, prior to this experiment, by the authors was also not successful in producing a tool wear curve due to the issues in micro milling with even a very small run-out. Finally, outside edge wear has not been found to be particularly useful in producing wear curves for micro-milling because the difficulties in removing chips on the small-scale leads to significant irregular wear from chips [13].

6.1.3 *The use of Coatings in Macro- and Micro-milling*

The application of different coatings to cutting tools is an established method of increasing tool life on both the macro and micro-scale. Lin et al. investigated the effect of a PVD applied AlCrN coating for tool inserts in turning [213]. It was clear that tool life is a critical variable when estimating productivity levels in manufacturing, and that predictable tool wear is desirable since unpredictable tool wear makes prediction of future wear and adjustment of tool paths for improved accuracy impossible. A dramatic increase in performance was seen upon coating the inserts, due not only to increased strength but also due to reduced chemical inertness (important at high temperatures where diffusion wear becomes more likely) and, importantly, reducing friction during machining. This is important since high friction results in high cutting forces, faster tool wear rates, energy losses and high temperatures.

Zareena et al. were able to successfully reduce friction at the tool-workpiece interface when machining titanium to a high precision by coating macro tools with Perfluoropolyether which in turn resulted in longer tool life and improved surface finish of the tools [214]. They noted that this reduced friction goes some way to reducing the Built-up Edge (BUE) which is responsible for material pull-out and poor surface finish.

It can be challenging to coat tools in a manner that is appropriate for machining on the micro milling scale. Texturing is difficult, and it is important that coatings applied are thin to minimise edge radius. A coating applied to a micro milling tool will naturally increase the edge radius of the tool which is important when depth of cut is small [10].

Increasingly, coatings have been used with varying success at extending micro-tool life [10]. Although coatings can improve tool life, the small scale can lead to a trade-off whereby surface finish is better for uncoated tools due to a smoother tool surface. Often, this is outweighed by the reduced tool-workpiece friction and corresponding lengthening of tool life and reduced burr size seen.

Lower wear rates for coated micro-tools has been attributed to lower friction and hardness of coatings, and the fact that certain coatings suppressed BUE [9], as is seen on the macro-scale [215].

In some studies single-toothed mills are designed to measure wear, for example the effect of PCD coatings on micro end milling of ceramics [216]. Though tool wear curves were seen, in practice single toothed tools are less appropriate for precision or finish micro-machining since it affects both productivity 6.1 and surface finish [217]. It also results in increased burr height [149], which is important since burrs are more difficult to remove on micro-parts and should thus be avoided or suppressed where possible [90].

$$Q = \frac{a_p a_e v_f}{1000} = \frac{a_p a_e f_z n z}{1000} \rightarrow Q \propto z \tag{6.1}$$

As the body of research has increased, the use of coatings on micro mills has focused on specific types of coating, minimising coating thickness and cutting-edge coating technologies. Typically, micro-tools studied have been coated using Physical Vapour Deposition (PVD). This is popular with tooling companies due to the lower complexity temperatures required, fine surface finish and low thicknesses achievable which is essential for micro tools [218]. Coating of tools works to lengthen tool life can be extended beyond simply reducing friction at the tool-workpiece interface: Neves et al. looked at texturing tools prior to coating to increase coating adhesion and found that the textured tools retained their coating for longer [219], which in turn improved the life of the tools.

It is important to note that improved tool wear is situational. Biermann et al. found that AlCrN and TiAlN, showed improved tool wear but other coatings such as TiN and CrN wore dramatically due to high reactivity between the tools and the workpieces [220]. Due to limited availability of micro-mill coatings, some studies have conducted only very limited comparisons, such as two coatings [12]. This work aims to improve upon this with the use of custom coatings based on those use to cut similar materials on the macro scale. Typically, lower cutting forces are attributed to lower tool-WP friction [25].

In coating research, AlTiN has seen significant interest. Fox-Rabinovich et al. machined titanium and nickel alloys on the macro scale, and observed that AlTiN coatings combine high plasticity with high impact fatigue fracture resistance, especially important for interrupted cutting, resulting in reduced likelihood of cracks forming compared with TiAlCrN. This significantly improved length of cut over TiAlCrN [221]. Also on the macro-scale, Faga et al. observed that the high Coefficient of Friction (COF) for AlSiTiN results in a high interface temperature and reduced wear resistance as compared with AlCrN, noting that AlTiN particles removed from the tool contribute to 3rd body abrasion [222].

Multi-layer coatings have also been employed extensively on the macro-tooling scale in milling and turning. Sui et al. developed performed turning tests using a TiAlN/TiAlSiN multilayer coating [223]. Adhesion between the TiAlN and titanium was reported, resulting in BUE, and attributed to a higher wear rate than that seen for TiAlN/TiSiN. It was also seen that the multi-layer reduced spalling over TiSiN alone, due to the protective TiAlN layer.

TiB_2 coatings were compared with CBN and PCD inserts by Corduan et al. and less notch wear was observed for the TiB_2 tools. Instead, flank wear and crater on the rake face dominated, due to two-stage wear: coating delamination, and substrate damage. They noted that this is exacerbated where coating-tool adhesion is lower, as in the case of TiB_2 .

A limitation with existing research is the focus on overall improvement of cutting tools: surface finish and tool wear at a given time are considered [12], but in spite of conclusions that tool performance is improved, overall tool life is often not investigated and the length of the steady state wear region, a critical factor in tool performance, does not get considered. It is proposed here that to properly develop improved tool design, the length of the steady state wear region should be well characterised and understood, and this has not been adequately carried out in existing research.

In addition, in spite of investigations into coatings on both the micro- and macro- scale, there is little investigation into the relationship between the two. Comparisons between deposition types on inserts give some insight into the expected deposition behaviour of a micro-tool [224] and a number of decent studies into the sliding behaviour of different tool coatings have taken place: Hedenqvist and Olsson comprehensively studied wear mechanisms for TiC-coated carbide and TiN-coated steel [225].

However, this fundamental study provides no insight into the different behaviour of these materials under workshop conditions. Furthermore, the use of a different substrate presents an extra variable. A study that compared PVD ZrN coated carbide in both sliding tests did observe wear mechanisms in both turning and in a sliding wear test, but links between the two physical environments were made and the dominant wear mechanisms not explained [226]. Similarly, the work took place using turning, on the macro scale, which tells us little about micro-milling [227]. This work relates the wear behaviours seen on pin-on disc tests for coatings used on micro-tools, to those seen during machining.

As a result, comparisons can be made between wear mechanisms on the macro and micro-milling scales. This is novel on two counts:

1. It is acknowledged that wear behaviour differs on the micro-scale, but this often poorly explained. There is also much more limited research onto micro-mill coatings.

2. Similarities seen between the micro-and macro-scale allow technologies from macro-milling to be adapted to a smaller scale.

6.1.4 *Expected Wear*

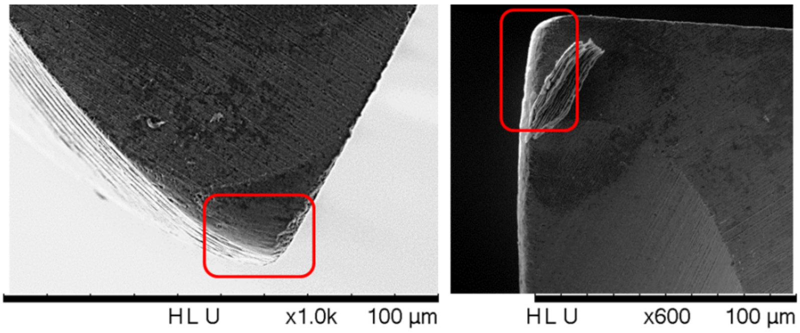

Figure 6.4: Micro mill measured using an SEM in two orientations. Where tools were uncoated, abrasive wear dominated.

The difficulty in predicting the wear of micro-milling tools is that they often do not wear as expected: due to their mechanical properties and their relatively small size in relation to workpiece grain size (subsection 2.1.3), and the large size of tool grains in relation to tool diameter.

Typically abrasive wear often dominates the wear of macro-tools, resulting in a defined tool wear curve (Figure 6.1) [228]. Adhesive wear, resulting in a BUE is also common. High temperatures at the tool-chip interface can lead to plastic deformation and cracking, while crater wear and edge chipping are also seen.

Some uncoated 0.5mm tools were used to machine Hastelloy, brass and titanium, and qualitative observations of this revealed that abrasive wear was the dominant method of failure for the tools (Figure fig:Where-tools-were-uncoated). For these tools, wear rate was more constant and relatively more predictable than for the other micro-milling tools.

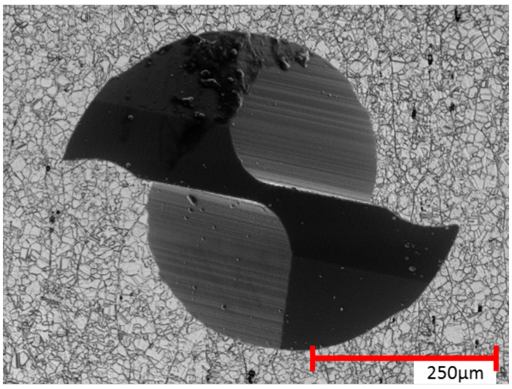

Figure 6.5: Example of the relatively large grain size in relation to tooth size end edge radius.

In observing the performance of different coatings and the effect that these have on wear predictability of tools, some of the wear mechanisms that take place and lead to failure have been investigated in the discussion henceforth.

6.1.5 *Motivations for Current Work*

The fundamental aim of the current work was to increase the life of the tools being used. In doing so, it is intended that machining processes will be more efficient due to fewer tool changes, and that accuracy for micro milling operations can be more tightly controlled. To achieve the latter, the time (or machining distance) that the tool spends in steady state wear (identified as zone II in Figure 5.1) must be maximised.

The novelty of this work is derives from the following aims:

AIM 1 To extend the length of the SSR using coatings not previously applied to micro-mills, since this region represents the operating region where tool wear is predictable (and hence can be adjusted for),

AIM 2 To reduce the length of the tool run-in time, allowing the SSR to be reached more quickly and so reducing the nonlinear region of wear.

Three materials were chosen for this work: brass, for its easy machinability and application in producing miniature gears which do not need lubrication [51], titanium grade 2 for its applicability in the medical and dental industries [229–231] and Hastelloy (a nickel-molybdenum superalloy), as it is difficult-to-cut due to high temperatures, adhesive and diffusion wear, and the formation of BUE [36]. Nickel-molybdenum is difficult-to-cut due to high temperatures, adhesive and diffusion wear, and the formation of a BUE [36], leading to its application in chemical waste processing, marine pumps and similarly corrosive environments for producing heat exchangers or pollution control – such as flue desulfurization systems or fans/fan housings.

6.2 METHODOLOGY

To evaluate the length of SSR of the tools the relative performance of generic AlTiN coatings with custom coatings was examined. Experiments were designed to observe tool wear regularly across the life of the tool. Two possible outcomes were expected:

1. Observation of the improvement in this region over the original coating would take place (thus validating the assertion that tool design can be used to extend this region and fulfilling the first aim of this work). Alternatively, this region would remain the same and tribological observations could be used to inform further design.

2. Reduction of length of run-in. The coatings were designed with the intention to achieve this.

It should be noted that there is some degree of trial-and-error regarding this. It is intended that the understanding of wear mechanisms developed over time will reduce this run-in time.

Tools of 0.5 mm diameter consisting of fine-grained tungsten carbide coated with Kyocera proprietary coatings were used to machine three materials: brass

Coating	AlTiN	TiB_2	TiAlN/TiSiN	AlTiCrN
Microhardness (GPa)	38	39	37	34
Friction Coefficient (Fretting, steel ball)	0.7	0.9	0.6 - 0.9	0.24
Typical Thickness (µm)	2-4	2	1.5-3	3
Typical Working Temperature (°C)	900	900	1100	1100

Table 6.2: Coating material properties datasheet as provided by the tooling manufacturer,

(CuZn37); titanium (Grade II); and Hastelloy (C-276). The materials were machined using tool coatings depicted in Table 6.1. Cutting parameters (Table 6.3), chosen based on tool manufacturer recommendations, remained the same for each material.

Workpiece	Coating	Parameter set (Table 6.3)	Sliding distance between observation
Brass	AlTiN	1	8
Brass	TiB_2	1	8
Titanium	AlTiN	2	56
Titanium	TiAlN/TiSiN	2	28
Hastelloy	AlTiN	3	26
Hastelloy	AlTiCrN	3	26

Table 6.1: Coatings used for each material and measurement intervals.

All tools were coated using HiPIMS (High Power Impulse Magnetron Sputter) which results in a smooth finish, to minimise the effect that varied coating geometries have on the micro-scale. The material properties are given in Table 6.2. The machining parameters based on those provided by Kyocera-SGS used for each material were the same for both coatings for each material. These are given in Table 6.1.

Parameter	Brass (1)	Titanium (2)	Hastelloy (3)
Spindle speed (rpm)	50000	25205	6786
Feed (m/min)	479	69	11
Feed/tooth F_z (mm)	0.00479	0.00136	0.00080
Radial depth of cut (mm)	0.5	0.5	0.5
Axial depth of cut (mm)	0.2	0.2	0.2
Sliding distance per 25mm length (m)	4.016	14.06	23.75

Table 6.3: Machining parameters used to machine the three materials tested. These were consistent across different coatings.

The trials took place on a KERN Evo micro milling machine with a maximum spindle speed of 50,000 RPM. Straight slots of 25 mm in length were milled to a depth of 0.2 mm. The workpiece and tool were flooded continuously throughout the cutting process using synthetic Hocut 768, a general-purpose synthetic lubricant.

The tools were measured both prior to testing and during testing using a standardised methodology [13] as described in (section 5.4. During machining, the tools were then removed at pre-determined intervals for measurement using an SEM using both Secondary Electron (SE) and Backscattered Electron (BSE) imaging to allow optimal opportunity to recognise wear features. The tools are imaged in two orientations: side-on, and face on as shown in Figure 6.6. Three types of wear were measured: flank wear, denoted VB; rake face wear, denoted KT, and outside edge wear, denoted OE (Figure 6.7). The measurement process was as follows:

1. Tools were removed at pre-determined cutting distances (Table 6.1).
2. Tools were washed in acetone, and then air-dried to remove swarf and dust before:
   a) Imaging in an SEM using both scattered and backscattered electrons, to enable;
   b) Analysis in image measurement software to determine the type and extent of wear observed.
3. Tools were then replaced and steps 1-2 repeated.

Catastrophic failure was recorded in the cases of the loss of one or both teeth (Figure 6.8). All wear measurements are expressed in terms of ¯m.

Sliding distance was used as the measure for "length" or "time" of cut, since the different cutting speeds and feed rates used for each material can be accounted for through the use of sliding distance. This was calculated computationally (sliding distance per 25mm is given in Table 6.1).

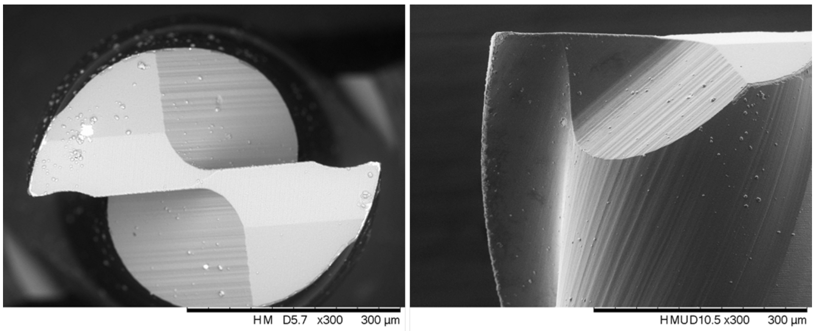

Figure 6.6: The tools were measured in the two orientations shown, with rake face and flank wear considered from the end-on perspective, and chipping considered from the side-on perspective.

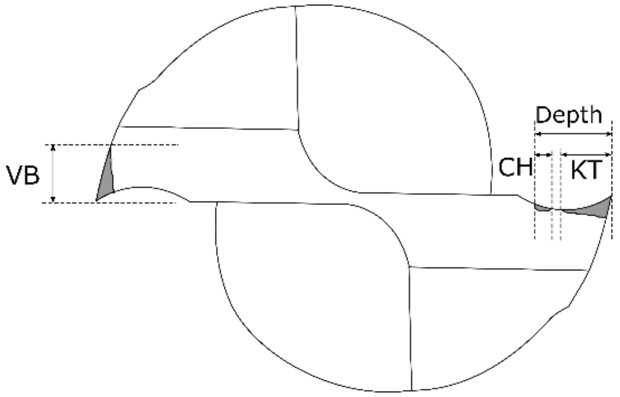

Figure 6.7: Flank wear is denoted VB, while rake face wear is denoted KT.

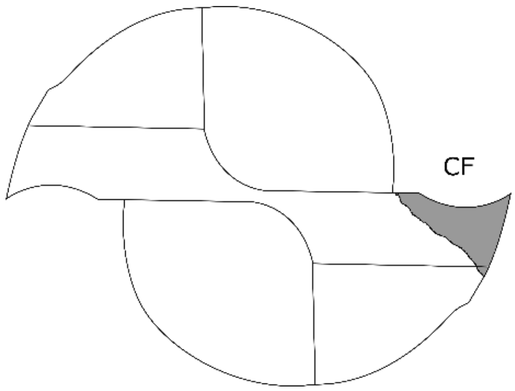

Figure 6.8: If one or both teeth were lost, catastrophic failure (CF) was indicated.

To further investigate wear mechanisms, coated discs were tested using a pin on disc machine (Bruker UMT). Coatings of the same thickness as those applied to the micro-tools tested using reciprocating-sliding pin-on-flat tests (Figure 8). A vertical load applied to the surface acting along the axis of the pin simulated the wear mechanisms experienced by the tools. An 8 mm diameter AISI 52100 steel ball was used to apply contact pressures to simulate those experienced by the tools during machining. A reciprocating motion with a speed of 40 mm/s was used.

6.3 RESULTS

In micro-milling, challenges in measuring tools result in relatively large measurement errors. This is due to the difficulties in identifying exactly where wear has taken place, even using high-quality images. Wear of micro-milling is measured using similar metrics as those used for macro-milling, but here the wear is much greater relative to the overall size of the tool (for 20 ¯m of wear constitutes 4% of an 0.5 mm tool, compared to only 0.2% of a 10 mm tool). Since a very small error in macro milling (and thus have few consequences for workpiece geometrical accuracy) can be large in the context if micro milling, errors are considered in subsection 6.3.1. These are displayed as error bars on the graphs.

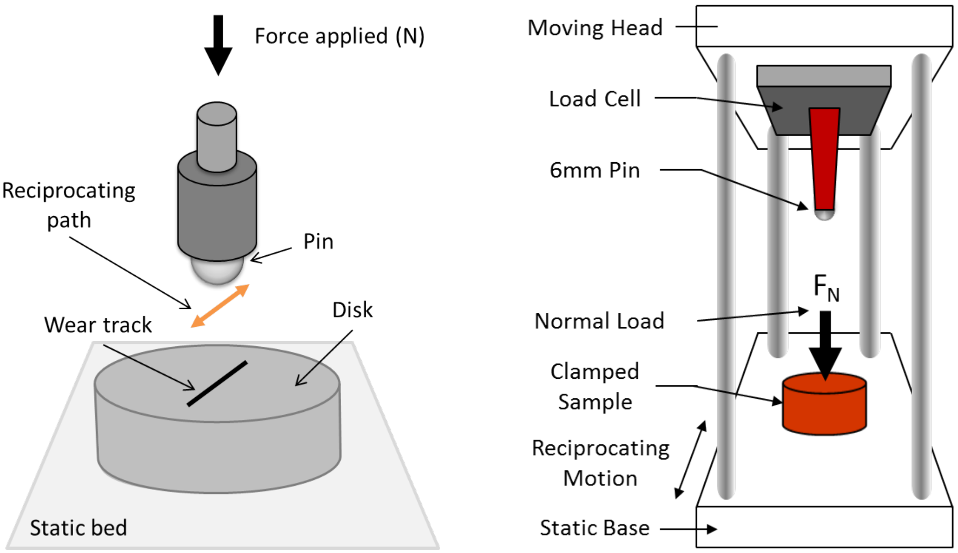
Force applied (N)
Reciprocating path
Pin
Wear track
Disk
Static bed
Moving Head
Load Cell
6mm Pin
F_N
Normal Load
Clamped Sample
Reciprocating Motion
Static Base

Figure 6.9: Schematic of the UMT used to carry out pin-on-disc testing of the samples.

In this study, information is only taken for teeth which did not experience catastrophic failure to circumnavigate this issue. Tool wear for both flank and rake face are provided for Hastelloy and titanium. Experiments on brass took place earlier, alongside the development of a standardised tool wear measurement protocol.

6.3.1 *Sources of Error*

Both teeth for each tool were marked separately, and wear measured for each tooth. For each tooth, two images were taken, one using secondary electrons (SE) and the other using BSE. The wear measured for both teeth was then averaged to give a mean tooth wear for the tool (Equation 6.2), and errors were calculated to be standard deviation for all images, and then propagated (Equation 6.3).

$$T_\mu = \frac{T_{1,SE} + T_{1,BSE} + T_{2,SE} + T_{2,BSE}}{4} \tag{6.2}$$

Where T_μ is the mean tooth wear for one tool, and $T_{n,xE}$denotes tooth number, n, and image type xE. This gives errors of

$$\Delta T_1 = \frac{|T_{1,SE} - T_{1,BSE}|}{2}$$

$$\Delta T_2 = \frac{|T_{2,SE} - T_{2,BSE}|}{2}$$

and

$$\Delta T_{\mu} = T_{\mu}\sqrt{(\Delta T_1)^2 + (\Delta T_2)^2)} \tag{6.3}$$

6.3.2 *Comparison between TiB_2 tools and an AlTiN coating for CuZn38 brass*

Figure 6.10 shows a comparison between the TiB_2 tools used to machine brass, and the tools which were coated with AlTiN. The steady state portion of the graph is over twice the length for AlTiN. The uncoated tool used for comparison fractured early in the machining, confirming its unsuitability.

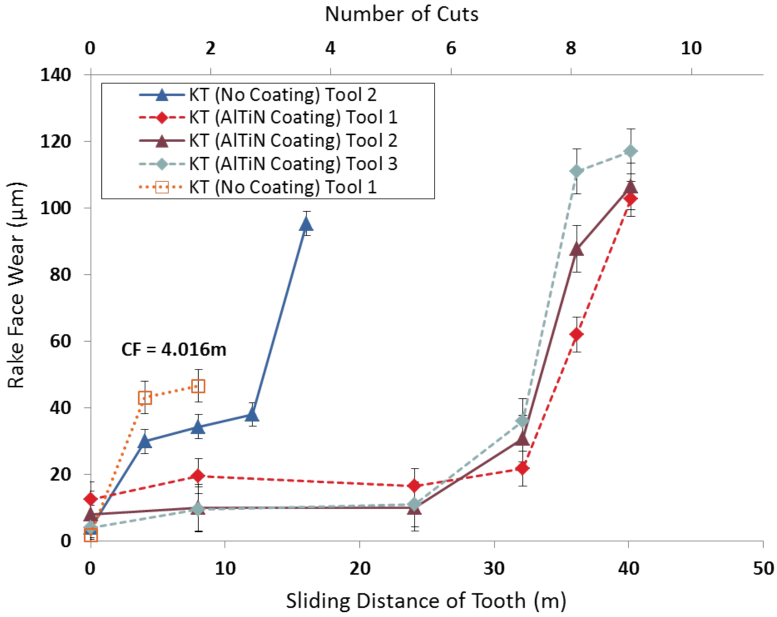

Figure 6.10: Tool wear plotted for tools used to machine brass with different coatings (TiB_2 and AlTiN). CF indicates catastrophic failure of the tool.

6.3.3 *Comparison between AlTiN coated tools and TiAlN/TiSiN for cutting titanium grade 2*

For face wear, the tool wear curves for the AlTiN and TiAlN/TiSiN coatings used to machine titanium grade 2 have a similar length SSR for both types of coating (Figure 6.11). This occurs at a lower wear level for the TiAlN/TiSiN coating. For flank wear, on the other hand, the TiAlN/TiSiN coating does not enter stage III of wear during the measurement period, and a long SSR is seen. This region also takes place at a slightly lower degree of wear than for the AlTiN coating (Figure 6.12).

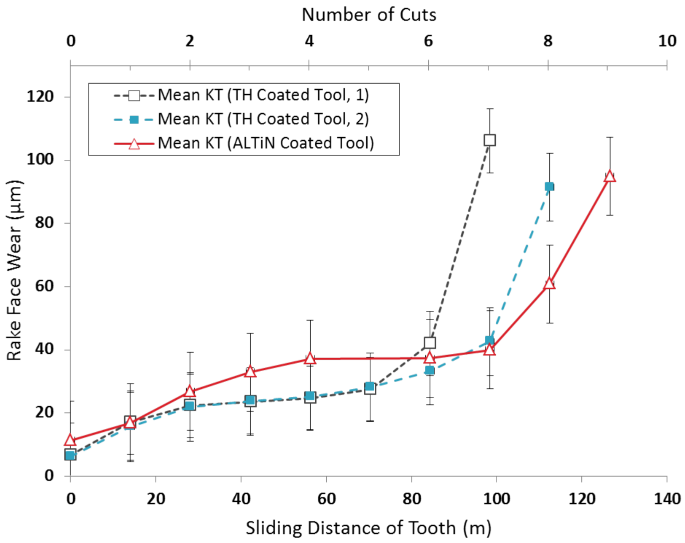

Figure 6.11: Rake face wear for tools used to machine titanium grade 2. TH coating is TiAlN/TiSiN.

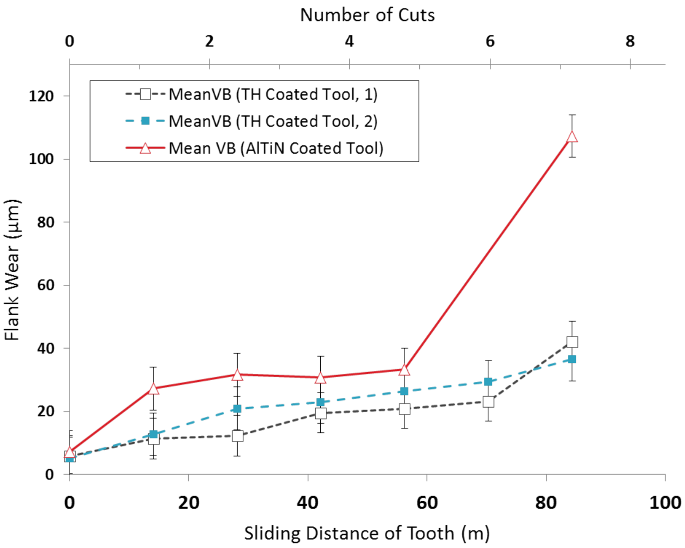

Figure 6.12: Flank wear for tools used to machine titanium grade 2. TH coating is TiAlN/TiSiN.

6.3.4 *Comparison between AlTiN coated tools and AlTiCrN for cutting Hastelloy*

The AlTiCrN coated tools showed a decreased length of steady state wear and stage III wear for the rake face of the tools (Figure 6.13), and indeed for the flank of the tools (Figure 6.14). The original AlTiN coated tools had both a longer and more clearly-defined SSR .

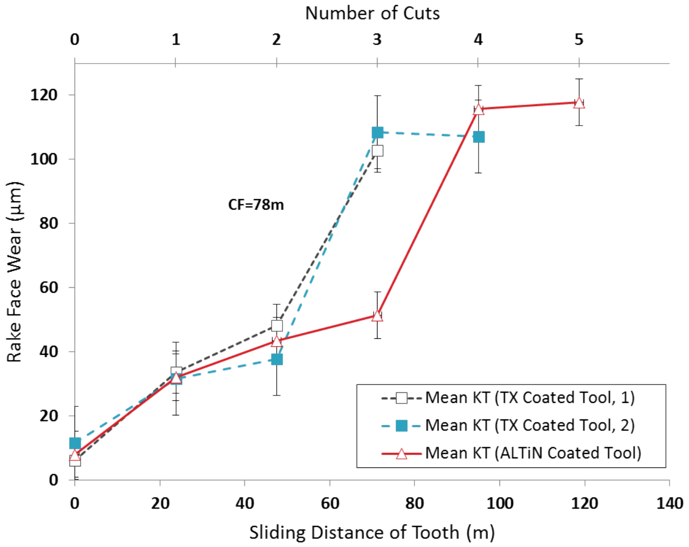

Figure 6.13: Rake face wear for tools used to machine Hastelloy. TX coating is AlTiCrN.

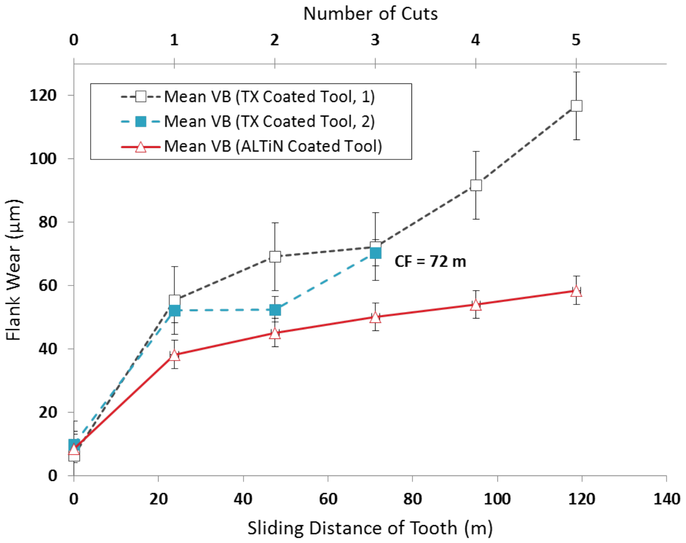

Figure 6.14: Flank wear for tools used to machine Hastelloy. TX coating is AlTiCrN.

6.3.5 *Relative wear of AlTiN coated tools across materials*

A comparison was made between the wear on the rake face for AlTiN coated materials to determine the relative rates of wear across materials (Figure 6.15). Wear occurred most rapidly for brass, and similarly that the SSR was shortest for brass. The steady state wear region for cutting titanium was shorter than that achieved for Hastelloy.

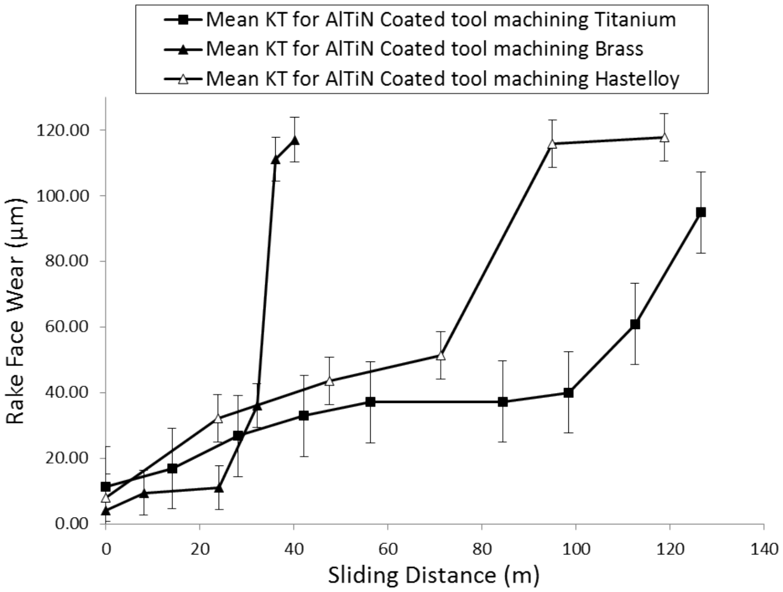

Figure 6.15: Relative rates of rake face wear for the three materials tested, with the original AlTiN coating.

6.4 DISCUSSION

6.4.1 *Relationship between SSR and running in period as a measure of tool performance*

The relative performance of coatings can be compared by comparing the length of the Run-in Period (RIP) of the tools to their SSR.RIP is used since it represents an period of machining where tool wear is unpredictable. Rake face wear was used as complete datasets were available for all three types of material. The criterion for higher tool performance is to have a proportionally higher SSR when compared with other areas of the wear curve. For the tools used to cut brass, the SSR:RIP ratio was much higher for AlTiN, and thus AlTiN performed better. Coating performance for each material is discussed with respect to wear mechanisms seen. For each material, the SSR was longer where overall tool life and performance was better, verifying that length of steady state region is indeed a useful measure of tool life and indicator of performance. This was especially clear in the cases of brass and Hastelloy, where AlTiN and TiAlN/TiSiN increased the SSR by factors of 4.3 and 2.6 respectively. For titanium and Hastelloy, when the tools performed better the SSR was longer and occurred at a lower level of absolute wear (Section 3.2). Comparisons between the AlTiN coating used to machine all three materials and the relative rake face wear verify that where tool performance was better, SSRwas longer relative to the whole length of the curve. Thus, in each case, SSR proves to be a good metric for predicting tool life.

Coating	Workpiece	Face of Tool	Mean RIP (m)	Mean SRR (m)	SSR:RIP
AlTiN	Brass	Rake	2	26	**13**
TiB_2	Brass	Rake	4	6	0.5
AlTiN	Titanium	Rake	56	42	0.75
TiAlN/TiSiN	Titanium	Rake	28	49	**1.75**
AlTiN	Hastelloy	Rake	26	52	**2**
AlTiCrN	Hastelloy	Rake	24	24	1

Table 6.4: Calculated ratio of SSR to RIP for milling tools.

6.4.2 *Coating Performance and Wear for Brass*

Table 6.4 and the graph in Figure 6.10 revealed:

1. A dramatic lengthening of the steady state region of the tool wear curve for AlTiN coated tools.
2. That the steady state region of wear for the TiB_2 tools occurred at a higher level of wear than that for the coated tools.

Observation (2) is noted in literature [211], but a longer SSR presents a significant result as it indicates a longer tool life. For best performance, the SSR should ideally occur when the tool is less worn. Over their life, the AlTiN tools exhibit some adhesion to workpiece but primarily abrasion to the outside edges of the teeth (Figure 6.17), with exposure of tool material underneath. The workpiece adheres more to the TiB_2 tools (Figure), and more plastic deformation is seen. Brass exhibits high adhesion in machining [232], which contributes to the adhesive wear observed. On a macro-scale, TiB_2 adheres to the workpiece during machining, resulting in failure as it is a brittle material [233]. This may explain why, in comparison to the AlTiN, large parts of the coating have fractured earlier in the wear. Abrasion occurs later in the tool wear, after parts of the coating have been removed. This is seen in both macro and micro-tools [226], but the issue is exacerbated on the micro-scale due to difficulty in flushing abrasive particles from the smaller gaps between tool and workpiece on a smaller scale [234], and smaller edge radii which expedite mechanical failure.

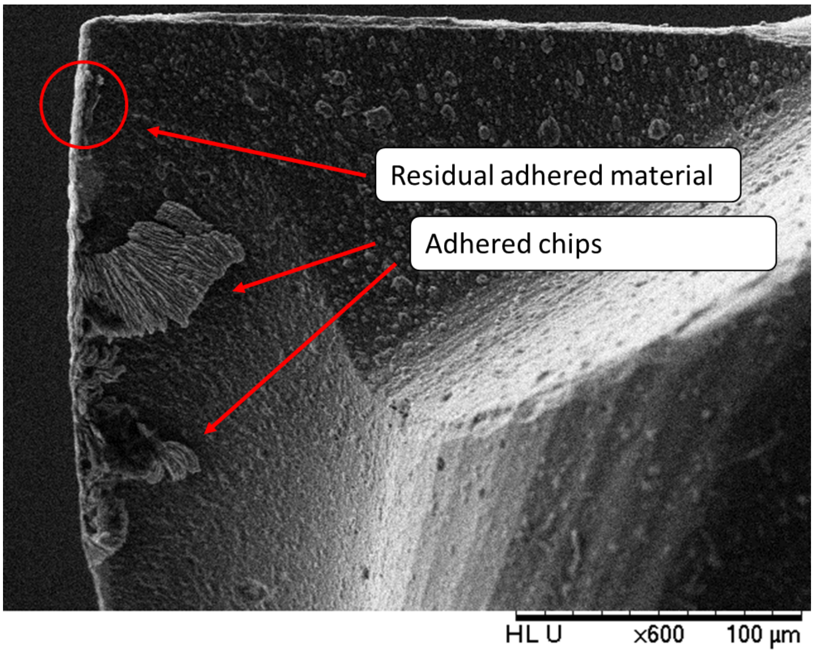

Figure 6.16: Adhesion can be seen on the tool, especially in the form of adhered chips. There is also some sign of residual adhered material.

6.4.3 *Coating Performance and Wear for Titanium*

The TiAlN/TiSiN demonstrated a better SSR to run in ratio than the AlTiN (Table 6.4) and a lower overall level of wear (Figure 6.10) for the TiAlN/TiSiN coating. SEM images of both AlTiN and TiAlN/TiSiN coated tools (Figure 6.17) taken show removal of coating. Some chip adhesion and chipping of the rake face of the TiAlN/TiSiN tool is seen (Figure 6.17a). Comparatively, wear of the rake face for the AlTiN tool was less severe (Figure 6.17c). This suggests that there is some interaction between the TiAlN/TiSiN coating [214] and the titanium, which is known to be chemically active [214, 235]. This results in increased wear rates on the rake face, and exposure of the rake face to excess forces as a BUE forms. Thus, even if the TiAlN/TiSiN coating is theoretically more resistant to wear than the AlTiN coating, it wears quickly. Furthermore, material has not built up on the flank, which possibly explains the longer SSR for the TiAlN/TiSiN tools. Figure 6.17b shows the side-on view of the TiAlN/TiSiN tool, where material has adhered to the rake face. Such interaction is often seen between carbide and coated carbide tools; and workpiece materials, in both macro- and micro milling: for example, Nouri and Ginting observed both adhesion wear and diffusion wear when machining Ti-6242S, observing that both the rake face and flank experienced diffusion wear, common when machining titanium [236]. Similar wear mechanisms are seen for macro-tool coatings containing Ti, Al and Si to those observed here [25]. The higher rate of wear for smaller tools is influenced by a very small tool-chip interface which results in higher stresses for micro-tools [91], and the poor heat conductivity of titanium [25]. Chipping is seen on both scales due to a high chemical reactivity with titanium which leads to welding. For the TiAlN/TiSiN more adhesion was seen due to the addition of silicon, which has been seen on both the macro and micro-scale for milling and turning [237]. However, the silicon increases wear resistance by hardening the material and homogenising grain structure, which results in better tool performance in spite of increased adhesion [238].

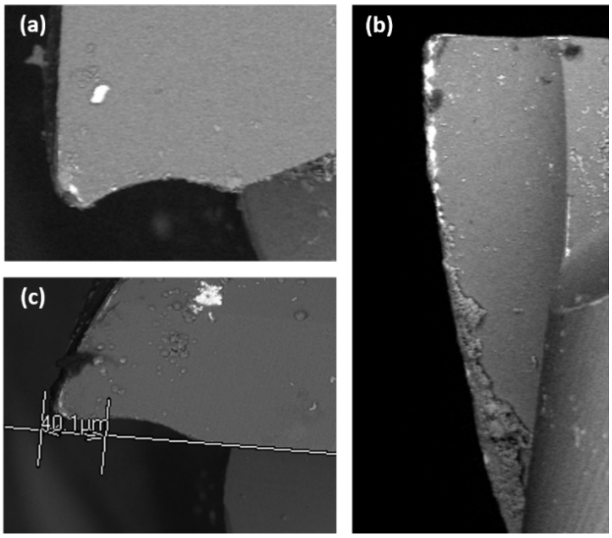

Figure 6.17: Three images of teeth: (a) and (b) are the front-on and side-on views for TH-coated tool, while (c) is the front-on view for an AlTiN coated tool.

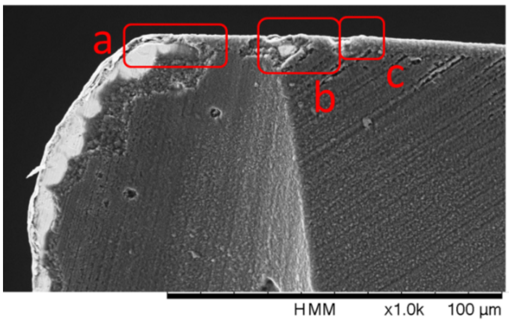

Figure 6.18: Examples of micro-chipping to the coating, exposing the tool underneath (a).

6.4.4 *Coating Performance and Wear for Hastelloy*

The AlTiN actually performed better than the AlTiCrN coating (Table 6.4) in terms of SSR:RIP and the absolute wear of both coatings during the SSR for each tool was similar (Figure 6.13).. The length (and consistency of gradient) of the SSR of the tool wear curves is greater for both rake face and flank wear for the AlTiCrN tool.

Thus the rate of wear can be much better predicted for AlTiN, and end workpiece geometry more easily controlled. For macro tools this was similarly noted by Fox-Rabinovich et al. This was attributed to the high plasticity and impact fatigue resistance which reduces tool fracture [221]. A significant BUE and some removal of chips or areas of coating is seen for the AlTiN. However, the AlTiCrN coating exhibits primarily removed areas of coating - fatigue due to adhesion - which appears to result in rapid abrasive wear. Abrasive wear is likely to be caused by areas of removed coating, trapped between the tool and workpiece, acting as abrasive particles. .

A similar run-in gradient was seen for both the AlTiCrN and the AlTiN coated tools. Both of these tools have a low COF; however, the adhesive properties of Hastelloy result in significant wear during run-in compared to other materials. Carbide particles in Hastelloy can contribute to abrasive wear for macro-scale cutting tools [51], and indeed this was seen to some extent during machining. Work carried out by Ucun et al. on 4 mm end mills supports this result [239]. Ucun used Inconel; compositionally similar to Hastelloy thus comparison is reasonable. The macro-tools also showed significantly more built-up material for the CrN-containing coating, due to an affinity between the coating material and workpiece. More corner-chipping and chipping was seen for the CrN tools, while the AlTiN demonstrated peeling of coating. SEM micrographs of the micro-tools revealed very similar wear mechanisms to the discs, suggesting that the tribological behaviour of the tools is dictated primarily by the coating and workpiece, while the increased wear on micro-tools over macro tools reflects the geometrical issues faced. Interestingly, the AlTiN tools exhibited increased wear on the macro-scale, this is because the affinity between the AlTiCrN coating and Hastelloy results in increased adhesion leading to chipping by fatigue. Whereas on the macro-scale this contributes to wear over time, on the micro scale area of coating removed is very large compared to the overall size of the tool, after which catastrophic failure occurs (Figure 6.19) through severe abrasion and chemical wear.

Similarly, micro-tools suffer from catastrophic failure due to edge chipping [212] earlier than macro tools, grain removal represents a significantly larger area of the tool. Thus, tribologically, there are significant similarities, but mechanically wear mechanisms are influenced by size. These effects, and the impact from interrupted cutting, are exacerbated by the irregularity of the boundaries between grains which are large compare with the cutting tooth. Overall, there is overlap between wear mechanisms seen on both macro-and micro scales, but relatively larger chunks of coating material on the micro-scale contribute to more irregular wear.

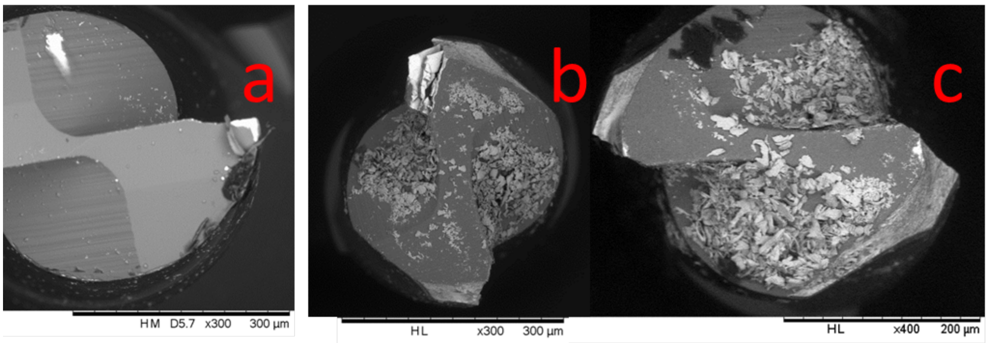

(a) Peeling of the coating, (b) shows severe cracking to one of the teeth after a cut. 100mm later, the entire tooth has fractured (c), thus the failure mode here was cracking.

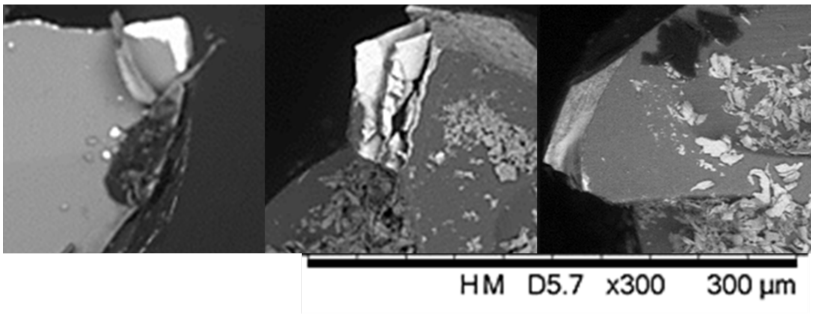

(b) Each feature shown on a larger scale.

Figure 6.19: (a) shows three different tools with interesting wear mechanisms. These can be seen zoomed in, in (b).

6.4.5 *Differences between wear mechanisms seen in micro and macro*

It has been seen in this work (subsection 6.1.2) and elsewhere (subsection 6.1.2) that micro-milling does not always yield the expected wear curves; and in some cases coatings which improve wear on the macro scale do not on the micro scale. For each coating tested the results for the micro-tools have been compared to macro tests with good agreement, seeing evidence of abrasion, adhesion, BUE and plastic deformation. However, in many cases the nature of the tool geometry on the micro scale appears to have modified or accelerated wear mechanisms, therefore, to further explore these points, pin-on-disc testing was undertaken,

The coatings tested using a reciprocating-sliding pin-on-flat tests represented the actual thicknesses of coatings applied to the micro-tools. A vertical load applied to the surface acting along the axis of the pin simulated the wear mechanisms experienced by the tools. An 8 mm diameter AISI 52100 steel ball was used to apply contact pressures in the order of 4 GPa (similar to those seen in the machining to flat coated discs), with a reciprocating motion at a speed of 40 mm/s.

However, the disk removed the geometrical effects of the tools. This allowed a comparison between the micro-and macro behaviour of the coatings to be considered, literature presenting studies of coating performance typically present findings limited to a single workpiece /material combination.

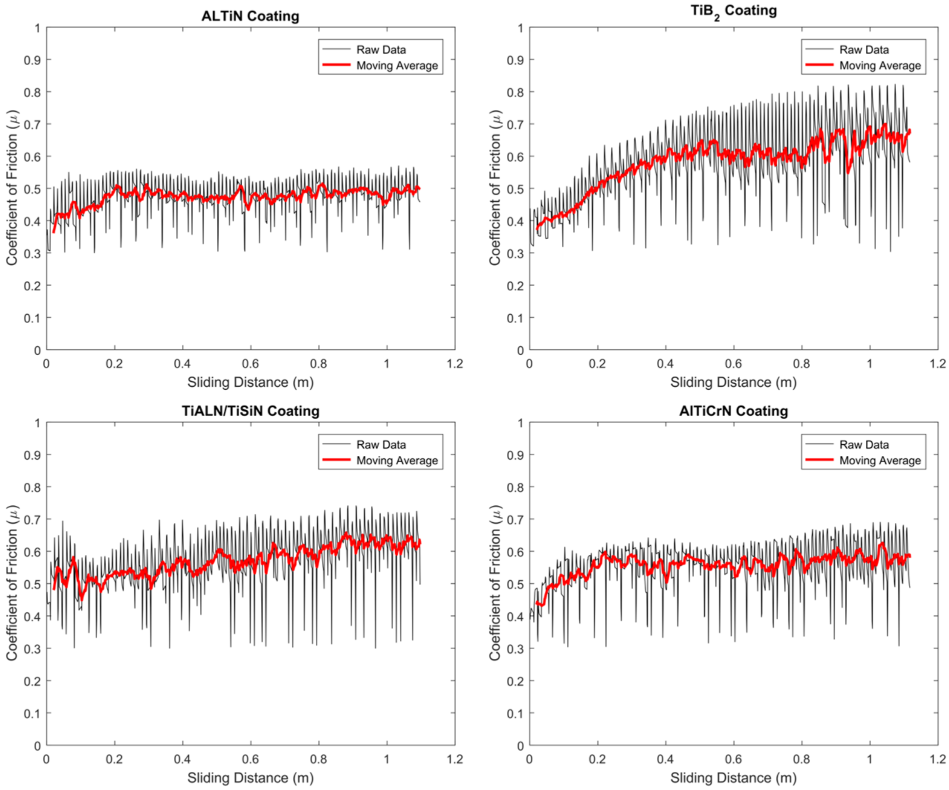

Figure 6.20: Friction coefficient for the four coatings over 1m of sliding distance.

Significant conclusions have been drawn from sliding tests which support mechanisms seen on the micro-scale and highlight relationships between the micro and macro scale. Friction data for each material can be seen in Figure fig:Friction-coefficient-for.

6.4.5.1 *Observations for AlTiN Mechanisms*

For AlTiN, observation of the COF (Figure 6.20) in sliding tests showed that over the first 0.2 metres the COF has increased by approximately 0.1. This indicates that some adhesion is taking place, rather than simply abrasion, supporting the data seen in the machining trial. Optical images of the disc revealed mostly adhesive wear (Figure 6.21), where coating removal takes place by surface fatigue due to adhesion. As in machining tests, abrasion was seen later when a third body – flakes of the coating – was introduced (Figure 6.21). Delamination and detachment of AlTiN coating by brittle failure, which lead to third body abrasion was also observed by Aihuia et al during pin-on-disc tests [227]. This is exacerbated by the sharp tool geometries which cause stresses on the coating at the cutting edge [232].

Comparing this to the micro-milling trial, SEM images of the tools show first adhesive wear, and later abrasive wear. Faga et al. also saw abrasive wear from 3rd body abrasion, and here some grain detachment is seen after 10 test runs which contributes to this [240]. AlTiN tools showed abrasive wear after a much shorter time than the discs, reflecting the geometrical weaknesses of the sharp teeth, and impact wear was also seen based on the interrupted cuts.

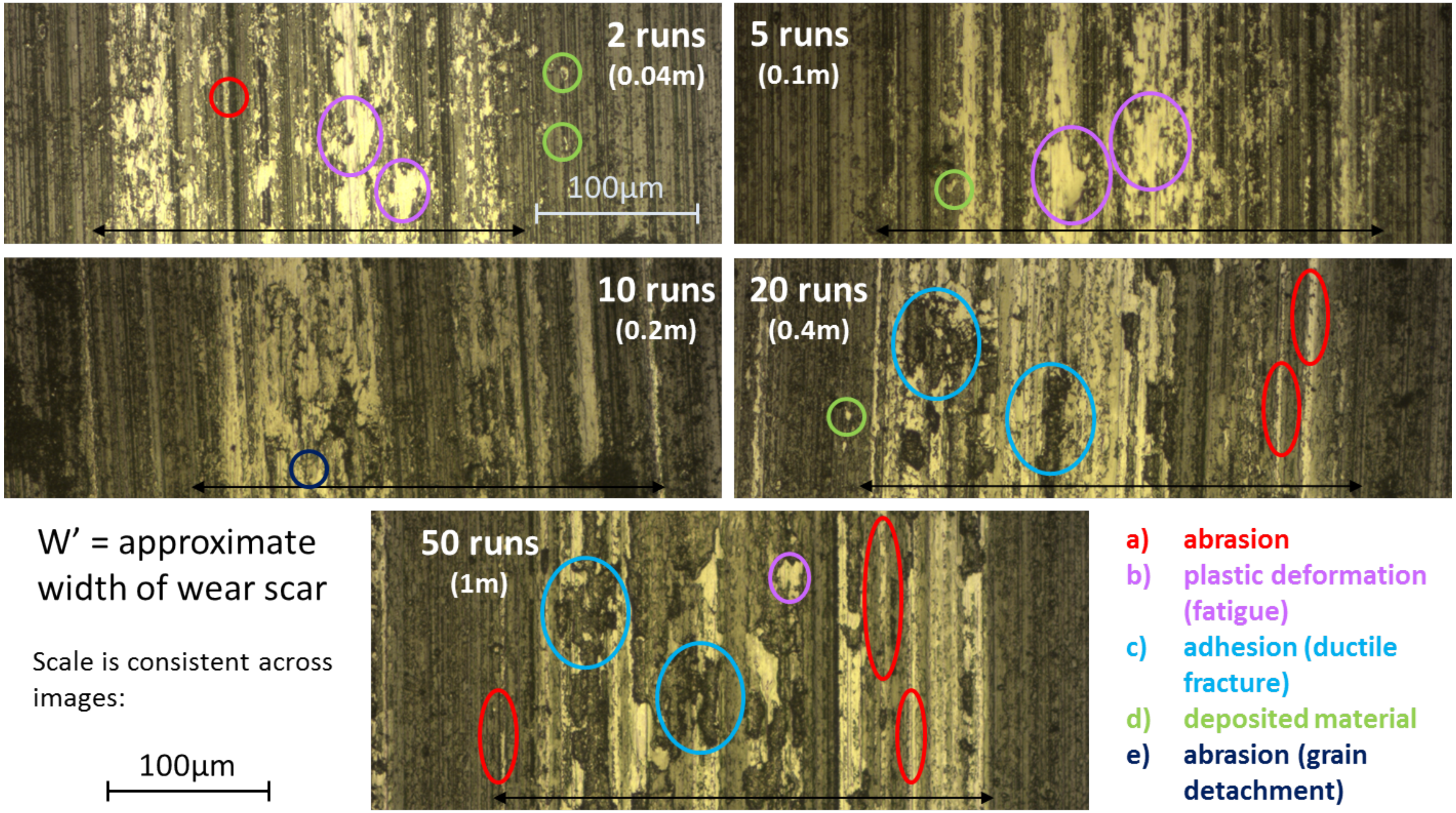
2 runs
(0.04m)
100µm
5 runs
(0.1m)
10 runs
(0.2m)
20 runs
(0.4m)
W' = approximate width of wear scar
Scale is consistent across images:
100µm
50 runs
(1m)
a) abrasion
b) plastic deformation (fatigue)
c) adhesion (ductile fracture)
d) deposited material
e) abrasion (grain detachment)

Figure 6.21: Wear of AlTiN coated discs when rubbed in a reciprocating sliding motion. Observed optically after 2, 5, 10, 20 and 50 runs. Some types of wear are highlighted.

6.4.5.2 *Observations for TiB_2 Mechanisms*

For TiB_2 , the COF is increased from 0.4 to 0.65 over 1 m, as adhesive contact area increased. Intense adhesion explains occurrence of the SSR for the TiB_2 tools at a higher absolute level of wear. This has also been seen in macro-milling operations Paiva et al. 2017. As with the AlTiN, TiB_2 tools used to machine brass exhibited, during sliding tests, both plastic deformation and a BUE early in the wear and later abrasion and removal of coating (Figure 6.23). There was also adhesion of chips to the tool which contributed to abrasive wear. In a machining context, TiB_2 has both a higher working temperature and a higher coefficient of friction with steel to AlTiN, which results in comparatively higher temperatures and plastic deformation. Coating was removed early for the TiB_2 tools. After only two measurements significant loss can be seen (Figure 6.22a). This suggests relatively poor adhesion of coating to tool, as suggested by Corduan et al. Craters and notching are then seen (Figure 6.22b), with substrate exposed to chemical and adhesive wear, and tools fail quickly [241].

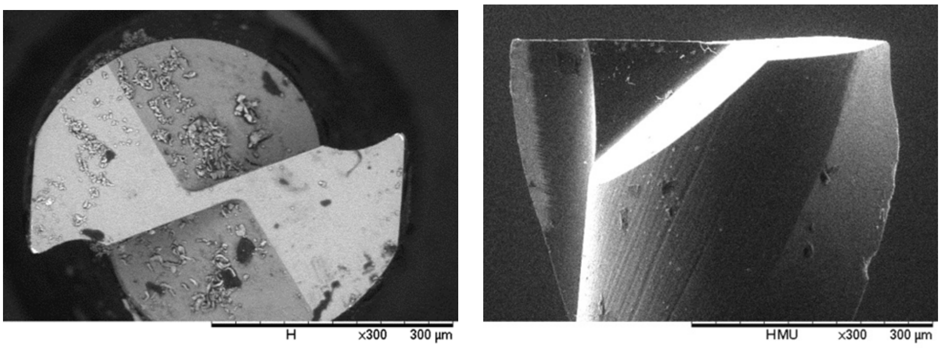

(a) Tool wear after only two cuts.

(b) Loss of coating has resulted in notching.

Figure 6.22: Wear to TiB_2 tools in the form of abrasion and chipping/notching.

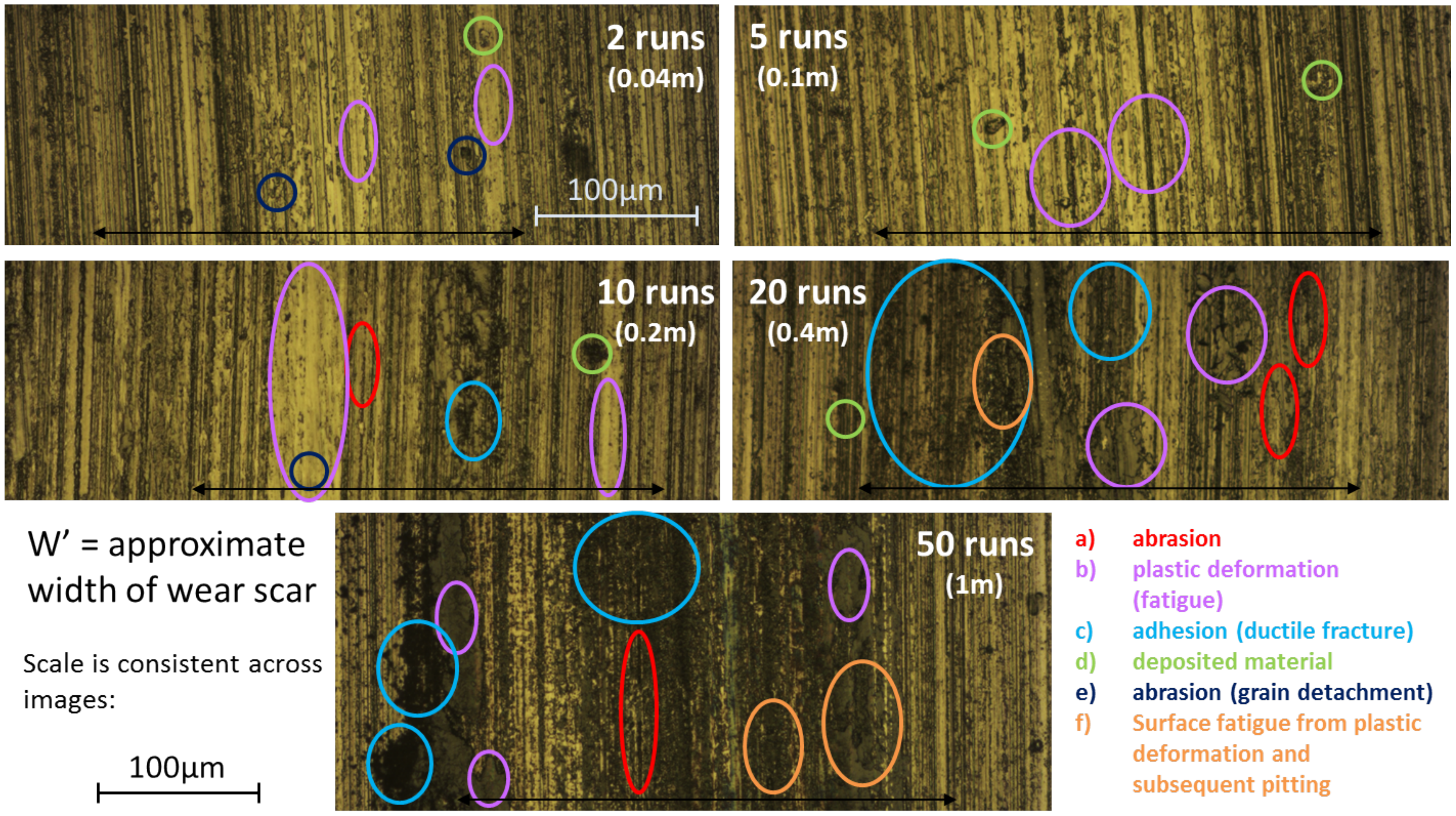
2 runs
(0.04m)
100µm
5 runs
(0.1m)
10 runs
(0.2m)
20 runs
(0.4m)
W’ = approximate width of wear scar
Scale is consistent across images:
100µm
50 runs
(1m)
a) abrasion
b) plastic deformation (fatigue)
c) adhesion (ductile fracture)
d) deposited material
e) abrasion (grain detachment)
f) Surface fatigue from plastic deformation and subsequent pitting

Figure 6.23: Wear of discs coated with TiB_2 when rubbed in a reciprocating sliding motion. Observed optically after 2, 5, 10, 20 and 50 runs. Some types of wear observed are highlighted here.

6.4.5.3 *Observations for TiAlN/TiSiN Mechanisms*

COF between TiAlN/TiSiN and disc was initially higher than for AlTiN, at 0.5. However, it increased less over the wear distance. For TiAlN/TiSiN coating abrasive and adhesive wear were seen, leading to coating fatigue and then pitting towards the later stages of coating wear (Figure 6.18). A cross-section of the coating layer was visible. After coating removal, the carbide is then vulnerable to rapid abrasive and chemical wear due to chemical affinity between the tools, exacerbated by high temperatures. This is supported by the conclusions of Faga et al. [240], who attributed these high temperatures to a high COF. It is reasonable to compare in spite of the fact that Faga et al. investigated macro tools since the disc test pieces do not have micro geometry and the coatings are of similar thickness. Coating removal for the disc was influenced only by fatigue due to adhesion; with abrasion occurring later as for AlTiN. Sui et al. saw this and also spalling, which can be seen in the figure and contributes to abrasive wear [223].

COF between TiAlN/TiSiN and disc was initially higher than for AlTiN, at 0.5. However, it increased less over the wear distance. For TiAlN/TiSiN coating abrasive and adhesive wear were seen, leading to coating fatigue and then pitting towards the later stages of coating wear (Figure 6.18). A cross-section of the coating layer was visible. After coating removal, the carbide is then vulnerable to rapid abrasive and chemical wear due to chemical affinity between the tools, exacerbated by high temperatures. Coating removal for the disc was influenced only by fatigue due to adhesion; with abrasion occurring later as for AlTiN.

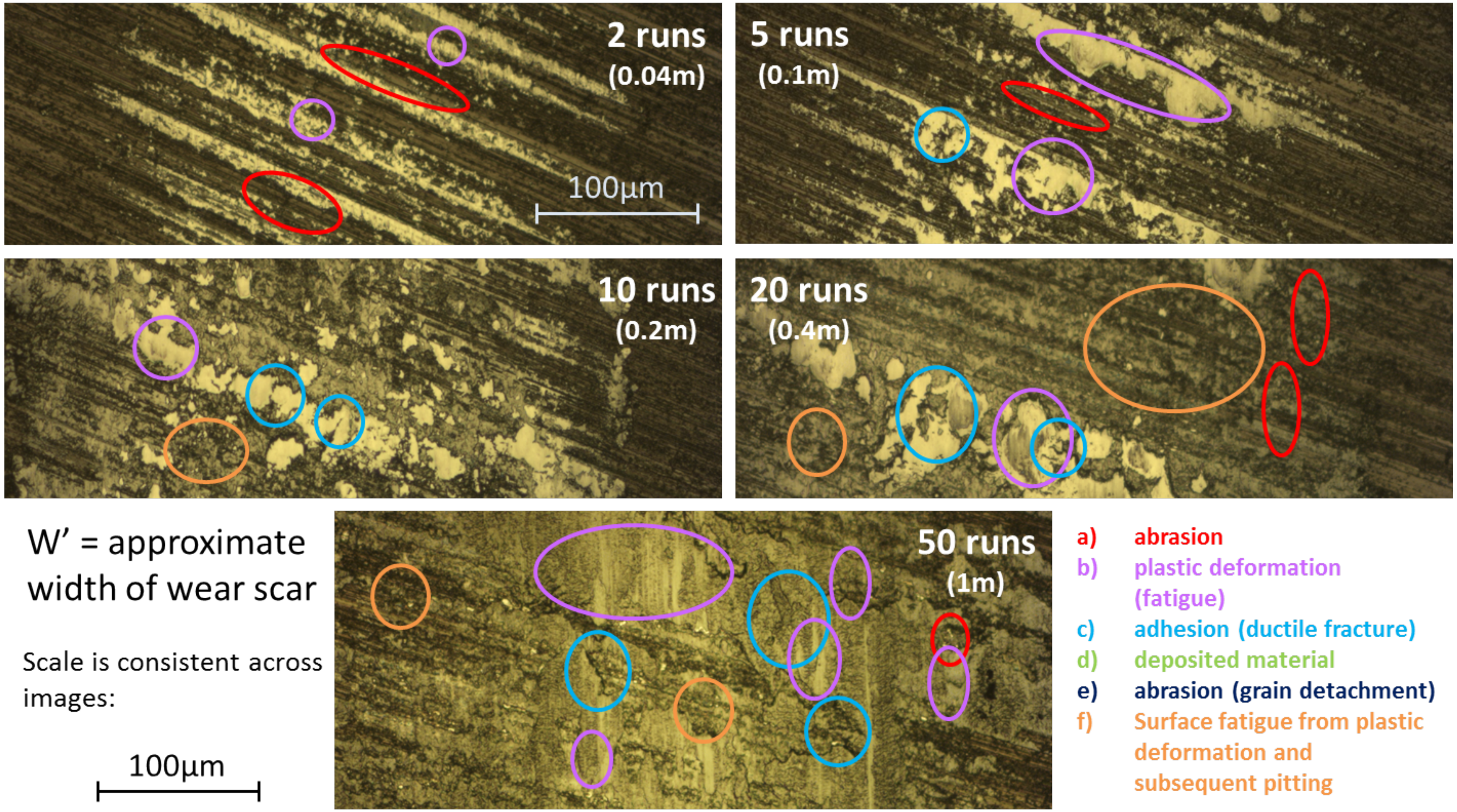
2 runs
(0.04m)
100µm
5 runs
(0.1m)
10 runs
(0.2m)
20 runs
(0.4m)
W' = approximate width of wear scar
Scale is consistent across images:
100µm
50 runs
(1m)
a) abrasion
b) plastic deformation (fatigue)
c) adhesion (ductile fracture)
d) deposited material
e) abrasion (grain detachment)
f) Surface fatigue from plastic deformation and subsequent pitting

Figure 6.24: Wear of discs coated with TiAlN/TiSiN when rubbed in a reciprocating sliding motion. Observed optically after 2, 5, 10, 20 and 50 runs. Some types of wear observed are highlighted here.

6.4.5.4 *Observations for AlTiCrN Mechanisms*

Less ductile fracture was seen than for AlTiCrN than the AlTiN coatings, in spite of higher plastic deformation: thus the tools wore less dramatically. A smoother surface caused by mild abrasion would likely reduce the COF which suggests that some adhesion is taking place, verified by optical images taken. This supports the data seen in the machining trial.

Finally, COF for AlTiCrN increased linearly for the first 0.2 m, before plateauing. Wear evolved primarily by adhesive mechanisms. Early on, the primary effect seen was some plastic deformation which increased linearly. After 0.2m, the addition of both ductile fracture and surface fatigue were seen, increasing over sliding distance (Figure 6.25).

Deep pitting, corresponding to tool chipping in a machining context, was later seen and more plastic deformation than for AlTiN coating. When tools were used to machine, the primary issue with adhesion was the formation of a BUE which, due to the geometry of the tool, can easily cause catastrophic material removal from the tool. This leads to notching which has been observed experimentally both in this and other studies [239].

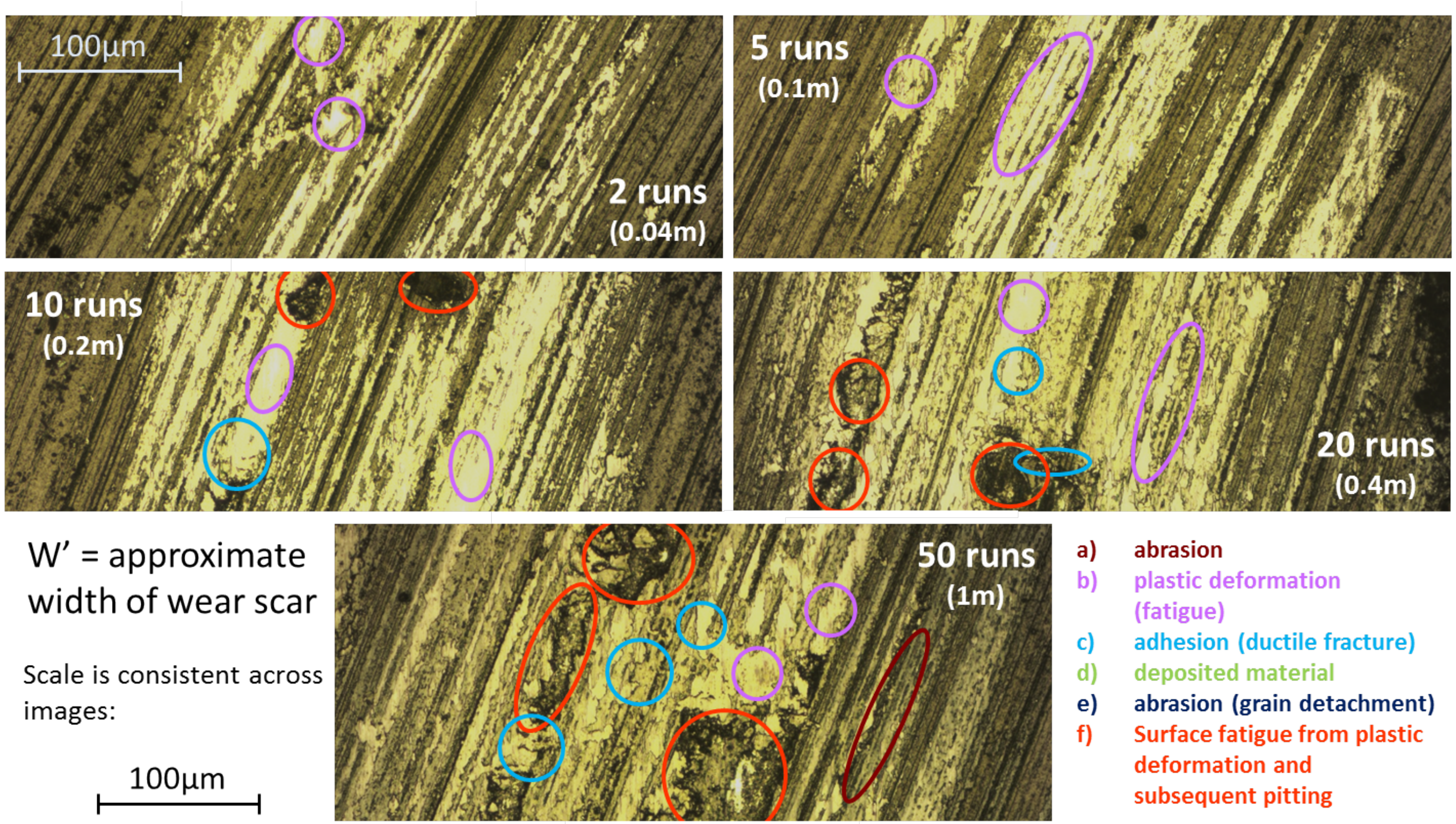
100µm
2 runs
(0.04m)
5 runs
(0.1m)
10 runs
(0.2m)
20 runs
(0.4m)
W' = approximate width of wear scar
Scale is consistent across images:
100µm
50 runs
(1m)
a) abrasion
b) plastic deformation (fatigue)
c) adhesion (ductile fracture)
d) deposited material
e) abrasion (grain detachment)
f) Surface fatigue from plastic deformation and subsequent pitting

Figure 6.25: Wear of discs coated with AlTiCrN when rubbed in a reciprocating sliding motion. Observed optically after 2, 5, 10, 20 and 50 runs. Some types of wear observed are highlighted here

The disparities in wear rates and failure mechanisms for micro and macro tools then lie not in differences in primary wear mechanisms, but in the geometrical properties of the tools and altered machining conditions. The addition on this scale of factors such as high machining stresses, impact due to interrupted cutting and small tool grains result in two outcomes:

1 Speeding up of the effect (and onset of failure) of primary wear mechanisms (for example, material removal having relatively higher significance).

2 Addition of volatile mechanical failure mechanisms such as chipping, cracking, and flaking of coatings.

As the process is scaled down, these mechanisms become more dominant and wear of tools becomes less predictable. Explanations for this include the mechanical stresses described due to tool geometries, and thermal cycling which is extreme due to the very small tool-workpiece interface area and the limitations of cooling systems at the smaller scale. The combination of thermal cycling and high mechanical stresses caused by tool geometries means that, relatively speaking, the types of wear that cause catastrophic failure such as chipping, attrition, and cracking occur more. Abrasion, which generally dominates the macro tool wear, has less of an effect.

6.4.5.5 *1.4.6 Use of wear curves and pin-on disc as tools to evaluate coatings*

Due to commonalities in wear mechanisms and friction behaviours between the micro-and macro scale for coatings, pin-on-disc represents a simple method of comparing some of the behaviours of different coatings seen, even in a micromilling environment. Meanwhile, production of wear curves using testing in a real-world environment allows a comparison between coatings in a real-life environment, and provides an insight into wear mechanisms seen, highlighting behavioural differences between micro and macro. However, direct testing of tools is time-consuming and expensive. Results from both pin-on-disc testing and micromachining tests showed that for both brass and Hastelloy, it was possible to extend the SSR:RIP of the wear curves. In both cases SSR was proportionally longer for the coating which performed better. This extending of the steady state has two functions:

1 It extends the overall life of the tool.

2 Crucially, it extends the working life of the tool, during which wear can be predicted from the gradient found in zone II of wear.

Simply extending overall length of tool life does not improve wear predictability and is thus not a useful result. The method presented here of evaluating the effect coatings have on tool life is significantly more useful than simply comparing absolute wear of the tools since absolute wear does not necessarily indicate tool life.

The method presented here of evaluating the effect coatings have on tool life is significantly more useful than simply comparing absolute wear of the tools since absolute wear does not necessarily indicate tool life. This work verifies the feasibility using well-resolved tool wear curves combined with pin-on-disc testing to improve micro-tool coatings. Pin-on-disc supports micromachining trials since results it is hard to produce well-resolved curves in micro-milling due to the tendency of tools to fracture, and also allows direct comparisons to macro-scale milling to be made quickly. There is value in further investigating both the novel application of coatings that have previously only be used in a macro-milling and in modifying the design of these coatings to increase the SSR of the tools.

6.5 CONCLUSIONS

Important results have been presented here that demonstrate a decrease in tool wear and thus improvements to machining accuracy and reduced production costs. In doing so, this work has considered the elongation of the SSR of the tool wear curve for micro-milling as a means to improve the prediction of the evolution of tool wear. This allows cutting processes to be modified to maximise geometrical accuracy as the tool wears and to measure the efficacy of applying different coatings to micro tools. The following conclusions can be drawn:

1. For each material investigated, one of the coatings yielded a longer SSR. It can therefore be concluded that coating design can be used to extend the length of the steady state wear region and not simply reduce overall tool wear.

2. RIP:SSR ratio is a novel metric and associated methodology of assessing the performance of tools. The relatively shorter run-in periods for some coating/material combinations indicate that different coatings result in different RIP:SSR ratios. It is important that appropriate coatings are selected to reduce the length of tool run-in, thus allowing the SSR to be reached more quickly.

3. Despite the difficulty measuring micro-tool wear and differences in wear mechanisms that dominate for macro-tools and micro-tools, it is possible to combine tool wear curves for micro-end-mills with pin-on-disc testing to evaluate coatings, highlighting similarities seen between micro and macro-tool wear. This can be harnessed when predicting tool wear.

4. Observation of wear and COF using pin-on-disc tests, combined with wear observed in a machining scenario, allows the differences in wear at the macro and micro-scale to be better understood: the small sizes of micro-milling tools, small cutting-edge radius, corresponding high temperatures and stresses result in additional wear mechanisms that are seen less on the macro scale.

5. While abrasive and adhesive mechanisms dominate in macro-milling, at the micro-scale the effects of impact wear and cracking are exacerbated due to relatively large workpiece grain size and very high stresses where tool-workpiece contact is small.

6 There is value in further investigating both the novel application of coatings that have previously only be used in a macro-milling and in modifying the design of these coatings to increase the SSR of the tools.

7

INVESTIGATING MODIFIED GEOMETRIES AS A MEANS OF EXTENDING MICRO-END-MILL LIFE

Micro-milling is a viable method for producing high-precision parts. Tool wear presents a problem as this process is highly susceptible to abrupt tool failure. In macro-milling, producing a honed edge radius can increase the life of the tool. This is now something that is being applied to to micro-scale which is more difficult due to the size effect.

Slot testing showed the tool wear of tools with both a straight edge and a cutting edge radius using commonly used engineering materials. Results show that for the materials tested, using a tool with a cutting edge radius resulted in more linear wear curves and extended the lengths of the tool lives.

7.1 EDGE RADIUS IN MACRO- AND MICRO-MILLING

The use of edge radius as a method of reducing tool wear has been used as a method of protecting the tool edge from chipping [6, 7]. It is important to clearly define different cutting edges here:

CORNER RADIUS Describes the radius between the leading edge and the minor edge of the tooth (Figure 7.1a).

EDGE RADIUS Describes the radius between the rake and flank faces: it is here that work material is sheared and the tool comes into contact with the machined surface (Figure 7.1b).

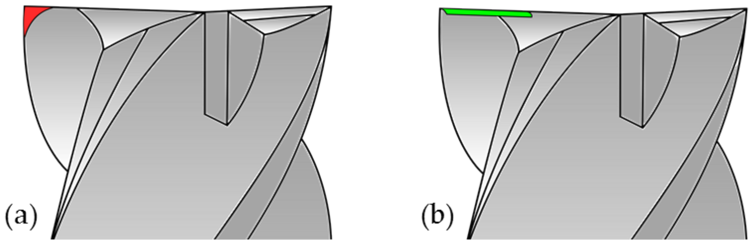

Figure 7.1: The two types of radii discussed herein are identified as (a) Corner Radius and (b) Edge Radius.

There is little work on the effects of varying the cutting edge radius of tools used for micro-milling: indeed, edge radius has been used as a measure of wear in micro-milling studies [189] and it is extremely difficult to accurately measure the wear of a radiused tool on the micro-scale. The process is somewhat complicated by the issues of scaling that are associated with micro-milling, since two factors are crucial:

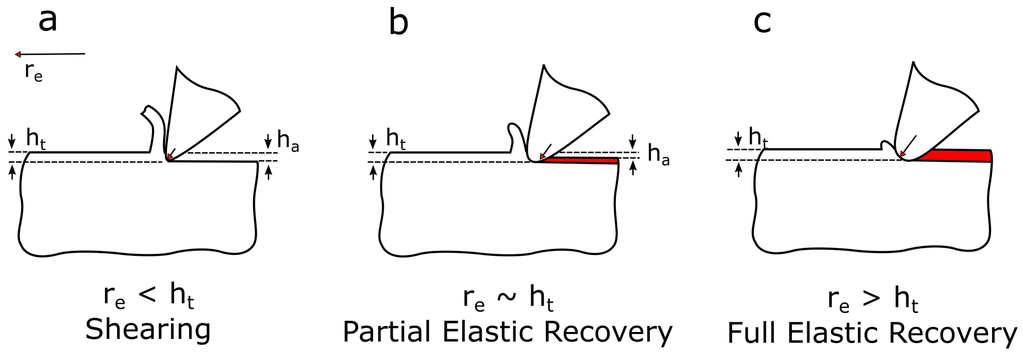

Figure 7.2: Types of cutting seen with tools with cutting edge radius for tools in the region where cutting edge radius is similar to cutting depth.

1 Cutting edge radius is limited by chip thickness in the sense that uncut chip thickness cannot be less than the radius of the cutting edge of the tool [242]

2 Geometrical features which are dependent on very precise tolerances may not tolerate an edge radius that is large compared with the overall size of the tool.

Of these two factors, (1) is the most significant. In the macro-milling case, $r_e \ll h_t$, where r_e is cutting edge radius of tool and h_t is cutting depth (and theoretical chip thickness). For micro-milling, due to limitations in tool grinding and coating technologies, it is common to see the difference between $h_t$and $r_e$to be much less. This results in three different phenomena (Figure 7.2): $r_e < h_t$ in this case, shearing occurs as the cutting edge radius is smaller than the depth of cut: material is removed as expected (Figure 7.2a).

$r_e \sim h_t$ in this case, shearing does not occur properly, chip thickness is unpredictable since some elastic recovery of the workpiece is seen, and rubbing or burnishing occurs (Figure 7.2b).

$r_e > h_t$ in the third case, significant elastic recovery of the workpiece occurs as the tool passes over it, and the tool simply polishes the workpiece (Figure 7.2c). On the other hand, it has been seen in macro-milling that cutting edge radius reduces stresses on the outside of the cutting tools [243–245]). The sharp edges of the tool lead to stress concentrations, and by applying a radius to these tools, the stresses are reduced (Figure 7.3) [246]. Since these stresses then lead to increased wear, due to thermal loading, reduced contact area with workpiece and faster crack propagation.

Yang et al. used simulation to examine the effects of cutting edge radius on cutting temperature in the micro-milling. Although it does not directly investigate wear, it is known that temperature has a significant effect on the wear of both macro- and micro-cutting tools [8]. Tools with a smaller cutting edge radius inherently have a smaller contact area with the workpiece [247], and typically modelling considers contact zone as a predictor of temperature increases in cutting tools [248].

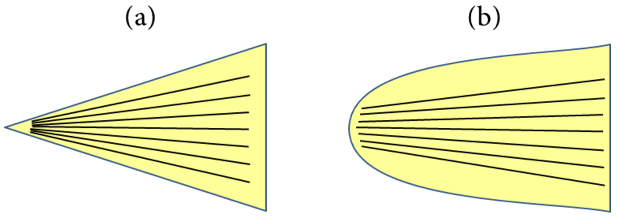

Figure 7.3: Depiction of stress distribution for (a) a sharp tool and (b) a tool with cutting edge radius introduced.

7.2 JUSTIFICATION FOR TRIAL

Compared with tools on the macro-scale, micro-milling tools can wear unpredictably, making it difficult to design efficient machining processes. Fracture of micro-tools is frequent and results in damaged workpieces and delays to machining time. Worn tools result in lower feature accuracy, worse surface finish and higher cutting forces. To reduce this problem, it is useful to characterise tool wear for micro-mills, understanding the wear patterns and wear mechanisms seen and how these differ from the macro-scale. Characterising wear leads to:

- Increased productivity of micro-milling cutting process
- Reduced tool wear
- Simplification of tool measurement techniques such that tool changes can be minimised.

Surface integrity is also improved by using less worn tools.

7.2.1 *Trial Design*

As contact stresses are influenced by cutting too geometry, two different cutting geometries were used; one with nominally zero edge radius (the deviation from which is determined by manufacturing process) and one with an edge radius. The effect that these geometries, i.e. cutting edge radius, have on the wear and the lifetime of the tools was investigated for three different materials commonly used in the chemical, medical and Aerospace industries: Stainless 316, Hastelloy and Titanium (grade 2). Two sets of tools were used: 905005-MEGA-T with Diameter 0.5mm, edge radius 0.05mm and 905004-MEGA-T: Diameter 0.4mm, no corner radius. These are shown in Figure 7.4

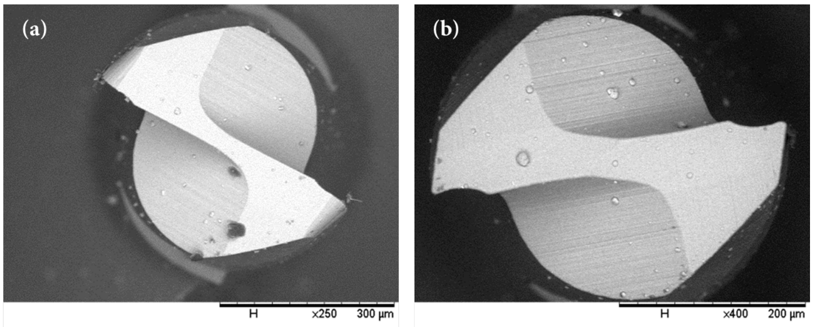

Figure 7.4: The two tools used in the investigation .

7.3 EXPERIMENTAL SET-UP

The standard test piece is 2 mm thick, 35 mm x 25 mm, designed to fit on a Kistler force cell with a working area of 25 mm x 25 mm. The standard cuts are 25 mm slots to a depth of 0.2 mm (Figure 7.5). Machining took place on a KERN Evo machining centre using Hocut 318 synthetic lubricant. A slot (or a number of slots to achieve a longer sliding distance) was cut, then the tool was removed for wear measurement. This was repeated until 10 measurements had been carried out for each tool. Number of slots cut in between measurements for each material is given in Table 7.1.

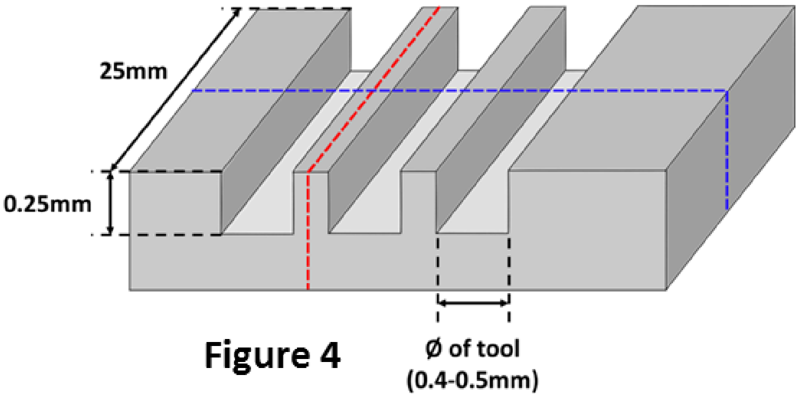

Figure 7.5: (a) shows the workpiece mounted onto the load cell, (b) shows the slotting process that was carried out.

Material	Number of slots cut before each measurement
Titanium	2
Steel	3
Hastelloy	0.5

Table 7.1: Number of slots cut before measurement for each material.

7.3.1 *Measurements Taken*

Before machining, all tools were thoroughly cleaned using acetone in an ultrasound bath, dried using compressed air and examined for defects using a scanning electron microscope (SEM). The tools were imaged in two orientations: side-on, and face on (Figure 7.6). Cutting forces were measured for each cut, so that the evolution of cutting forces as tool wears could be examined. This uses the Kistler setup previously described.

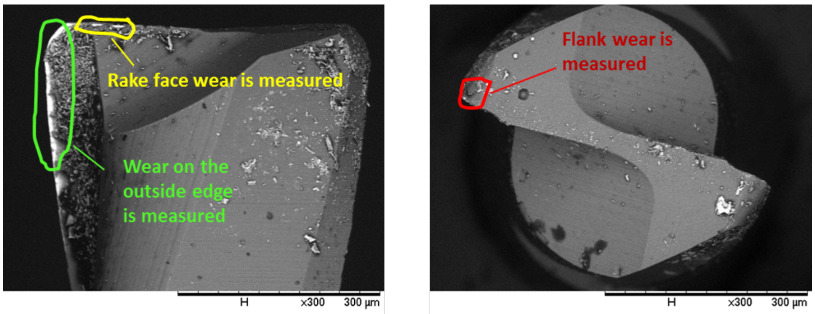
Rake face wear is measured
Wear on the outside edge is measured
H x300 300 µm
Flank wear is measured
H x300 300 µm

Figure 7.6: Orientations in which tools were measured.

7.3.2 *Analysis*

Images taken of the tool were analysed using image measurement software and the extent of and type of wear for each tool was considered. This was then plotted against sliding distance of the teeth so that the performance of the tools could be compared in spite of differing cutting speeds and feed rates across materials.

7.4 RESULTS

Results are presented herein in the form of graphs which show the rate at which the tools wore over sliding distance.

7.4.1 *Titanium - Edge Radius Vs Sharp*

For the flanks of the tools, steadily increasing wear is seen for the tools with a cutting edge radius (Figure 7.7a). Sharp tools show rapid initial wear followed by a much slower rate of wear, but greater overall wear volume (Figure 7.7b). For the rake faces of the tools, the radiused tools once again show steadily increasing wear (Figure 7.8a). The sharp tools show rapid initial wear followed by much slower rate of wear (Figure 7.8b). Wear volume is similar for both types of tool.

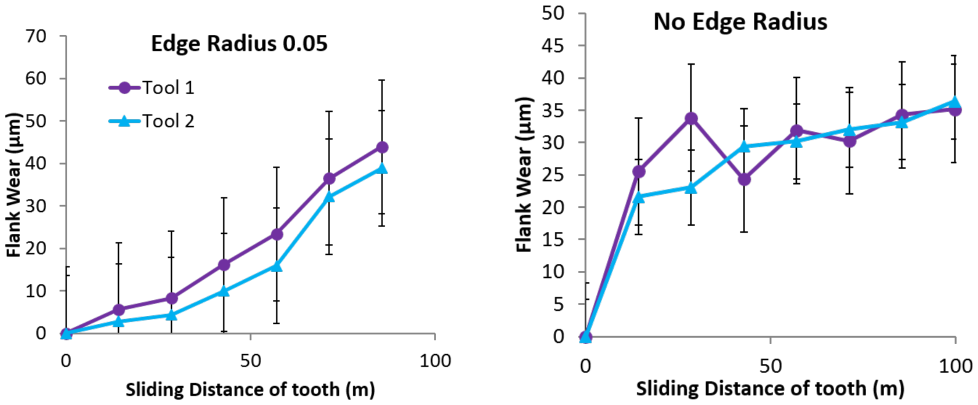

(a) Edge radiused tool.

(b) Tool with no edge radius.

Figure 7.7: Wear with sliding distance on the flank of the tools used to machine titanium. In both cases a long steady state region is seen and catastrophic failure is not reached.

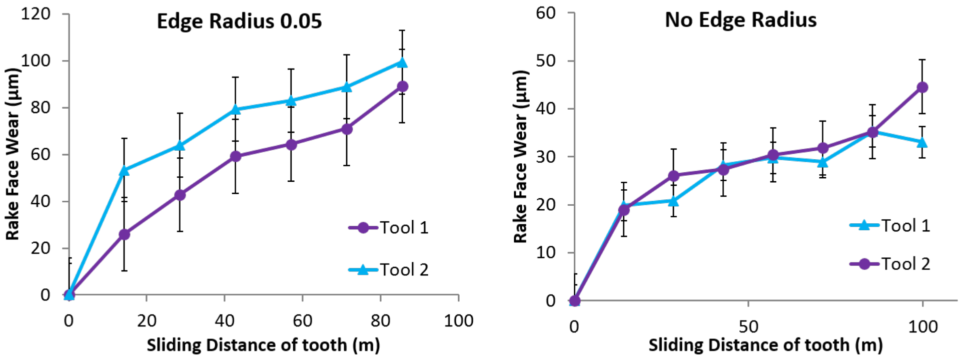

(a) Edge radiused tool.

(b) Tool with no edge radius.

Figure 7.8: Wear with sliding distance on the rake face of the tools.

7.4.2 *Steel - Edge Radius Vs Sharp*

For the flank wear, radiused tools show significantly longer life, with steady state wear before rapid wear (Figure 7.9a). Sharp tools almost immediately fracture (Figure 7.9b). For the rake face, wear is initially rapid then reaches steady state (Figure 7.10a). Once again, sharp tools almost immediately fracture.

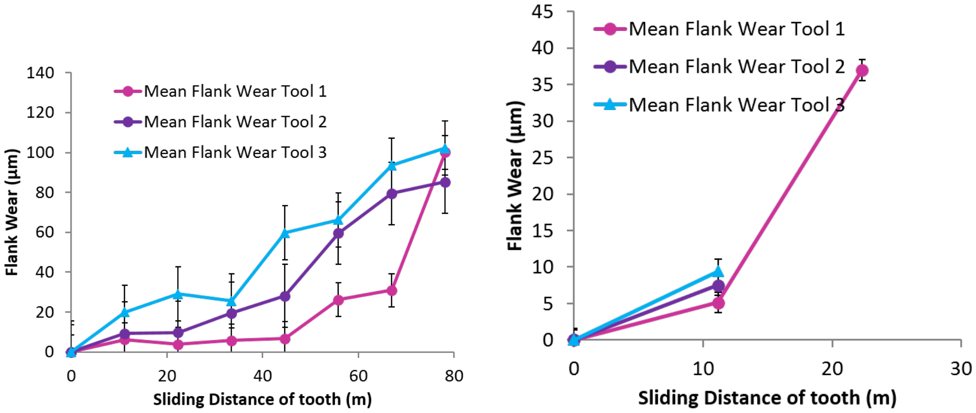

(a) Edge radiused tool. (b) Tool with no edge radius.

Figure 7.9: Wear with sliding distance on the flank of the tools used to machine steel. The tool which does not have a designed edge radius wears much faster and fails catastropcially at less than 20 m of cutting in each case.

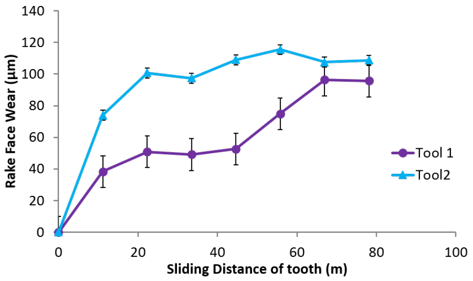

(a) Edge radiused tool.

Figure 7.10: Wear with sliding distance on the rake face of the tools.

7.4.3 *Hastelloy - Edge Radius Vs Sharp*

Flank wear for for the 0.05 edge radius tool was initially rapid, before steady state and finally rapid wear (Figure 7.11a). The result of this was the plotting of a traditional tool wear curve. Rake face wear was initially rapid and reached steady state quickly (Figure 7.11b). Sharp tools fractured after only two cuts, indicating their lack of suitability for cutting Hastelloy.

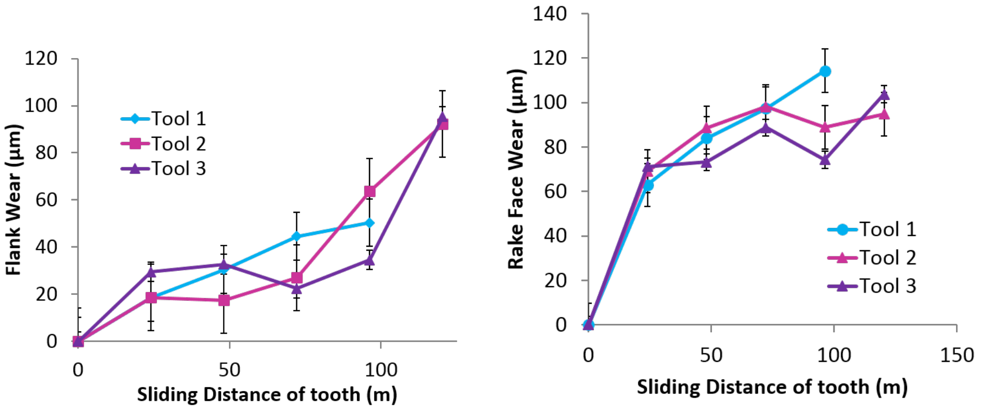

(a) Flank wear for edge radiused tool.

(b) Rake face wear for edge radiused tool.

Figure 7.11: Wear with sliding distance for the radiused tools.

7.4.4 *Cutting Forces - Feed Force*

The feed force for the three materials was plotted against the sliding distance for each tool (Figure 7.12). There was no apparent relationship between cutting force and sliding distance for steel or titanium, the cutting force and tool wear do not appear linked. Cutting forces increase steadily for tools with edge radius for Hastelloy, while for the sharp tool, the cutting forces increased up to a sliding distance of 120 then decreased.

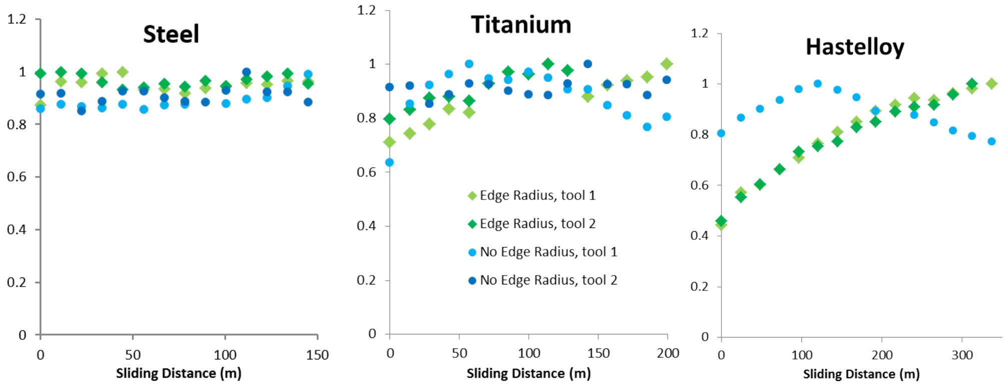

(a) Stainless 316

(b) Titanium Grade 2

(c) Hastelloy

Figure 7.12: Cutting forces plotted against sliding distance for three materials. In the case of steel and titanium, the cutting forces remain similar throughout tool life, while they increase linearly and plateau for two of the Hastelloy tools.

7.5 DISCUSSION

It was quite clear for all three materials that the tools with a cutting edge radius wore less rapidly in the early stages of machining than the sharper tools. The steady state or slower wear rate of the sharp tools (no edge radius) reflects the face that the tools were blunted during the run-in stage and thus the tools then had a cutting edge radius which reduced the stresses on them.

For titanium, the overall volume of wear by the final measurement was similar for sharp and edge radiused tools. However, the wear was linear and thus predictable for the radiused tool whereas the sharp tool reached a steady state at a higher degree of wear, making the round tool a better candidate for machining. The rake face showed more similar wear curves for both types of tools, and the performance of the tool on the rake face is similar. Overall, due to better flank wear characteristics, the rounded edge tool would be more appropriate. However, if precise machining of difficult features was required, the wear characteristics of the sharp tool are suitably close to those of the rounded tool that it would be a good tooling solution.

For steel, the flank and rake face of the sharp tools was such that they fractured after only two cuts. This is likely due to a feed rate or cutting speed that was too high given the maximum spindle speed of the machine. It is typically recommended that these tools machine at a spindle speed in the region of 100,000 RPM. This was not possible on a machining centre with a maximum spindle speed of 50,000. However, the rounded edge tools clearly presented a significant improvement on machining distances in spite of high stresses and temperatures, due to better stress and temperature distribution, as has been seen in other experimental studies [243–245].

A similar result was seen with Hastelloy, with only the cutting tools with an edge radius demonstrating acceptable performance. Unfortunately, once again the cutting parameters were too aggressive to see a pattern for the sharper tools, but nevertheless, since the same parameters were used for both types of tool it is reasonable to conclude that the tools with a cutting edge radius performed significantly better.

7.5.1 *Note on Quality of Results*

As previously discussed, the machining parameters used for some tools were not ideal. Furthermore, the measurement resolution (i.e. frequency of measurement was insufficient. Both of these issues reflect the difficulties of measuring wear of micro-milling tools: machining parameters must be chosen to be finely optimised. This then benefits manufacturing applications where the same issues are experienced.

Another of the issues seen in measuring micro-tools is the need to remove them from the machining centre: the tools can not easily be measured on-line using a handheld microscope, as either the magnification will be too low, or the depth of field is not sufficient. Each time the tool is removed, accuracy is lost. Although the machining centre measures tool length using a laser, minor differences in tool position can be significant on the scale of the tools used, and runout has a much greater effect.

These effects combine to demonstrate the importance of using a carefully constructed standard of measurement when conducting wear studies on micro-milling tools, both to minimise these issues and to ensure that the difficulties that cannot be controlled are consistent across studies.

7.5.2 *Future Work*

It would be beneficial to analyse workpieces to plot surface finish with tool wear in order to determine whether SF deteriorates less rapidly for tools with cutting edge radius. Tools could be etched and then imaged at high magnification with SEM to investigate wear mechanisms more closely. There is also an interesting relationship between surface finish and number of teeth that has significance in micro-machining.

7.6 CONCLUSIONS

This work investigated the effects of applying a cutting edge radius to micro-milling tools, where the edge radius is significant as compared to the size of the tool (10% of diameter). Based on the work carried out, the following conclusions can be drawn:

In general:

- Tools with cutting edge radius typically show lower wear rates, particularly at running-in.
- Cutting force does not appear to be linked to tool wear for steel and titanium, although some relationship was seen for hastelloy.

For specific materials:

- Both sharp tools and those with an edge radius are appropriate to machine titanium grade 2; wear is steadier and easier to predict for the radiused tools, but if geometrical precision requires sharp tools, they are suitable.
- For steel, the sharp tools are not appropriate for machining due to their rapid initial wear and subsequent failure. Radiused tools show a typical wear curve.
- A similar results was seen for Hastelloy as for steel.

Part III

RE-APPLICATION OF FUNDAMENTAL RESEARCH TO INDUSTRY

The following two chapters describe two research projects that re-apply the work carried out in Part I to an industrial context. The first describes the Wire Electrical Discharge Machining (WEDM) of miniature gears, while the second is a study of the application of the wear study techniques used to investigate micro-mills to more complex parts that reflect industrial applications. This leads to a reflection of the project aims and a conclusion of the thesis.

8

WEDM OF GEARS FOR MICROMECHANICAL WATCHES

8.1 INTRODUCTION

As discussed in chapter 4, Wire Electrical Discharge Machining (WEDM) is capable of producing intricate parts with high dimensional accuracy and excellent surface finish that do not require significant post-processing. It can therefore be used to produce parts that require little or no finishing or polishing. This results in its application to medical, microelectronic, dental ,and jewellery industries amongst others, and to machine materials that are considered difficult-to-machine by conventional processes [15]. Furthermore, minimal set-up times make it a very attractive method for prototyping complex geometries such as modified gear geometries [16]. There is extensive literature focused on optimising the Surface Finish (SF) and Material Removal Rate (MRR) in WEDM. As material is removed by melting small regions of the workpiece, pulse energy is the most important factor affecting SF in WEDM. This is influenced by machining parameters such as discharge current, gap voltage, pulse duration, pulse-on time and peak current.

Pulse energy, E, can be described as

$$E = \int_{0}^{t_0} u(t)i(t)dt \tag{8.1}$$

where t_0 is discharge duration, $u(t)$ is discharge voltage and $i(t)$ is discharge current. E is pulse energy.

To produce prototype gear forms or gear dies using WEDM, it is necessary to achieve an excellent SF and high profile accuracy. One of the critical factors influencing SF in WEDM is an area referred to as the white layer. This layer of material has been structurally modified by heat and is often harder and more brittle than the base material [108], reducing the fatigue strength and altering the wear properties of the part [111]. Since fatigue strength and wear are both significant for gears, and indeed for dies used for cutting gears, white layer is also an important response factor to be measured.

The use of rough cuts followed by skim cuts is frequently employed to achieve a fine SF [110]. The rough cut will employ a higher pulse energy to cut the rough geometry, and skim cuts with a reduced pulse energy yield the desired SF. It has been suggested that with the appropriate machining parameters, the skim cut can be used to remove solely recast material and not base material [17]. This could enable a rough cut with a relatively short machining time to be used, thus maximising productivity.

Hobbing and stamping are the traditional methods used for manufacturing small gears, and the field of miniature gear production using WEDM is relatively small [66]. Research into miniature gear production has yielded successful production of miniature gears. Typically, gears produced have had a high aspect ratio (thickness as compared with diameter). This can improve surface properties due to increased stability of machining [71], i.e. the reliable bridging of the gap with appropriate spark energy [249, 250] . The capability of WEDM to produce very thin parts has been explored less thoroughly, and is likely to be more challenging due to the reduced cross sectional area between workpiece and wire across which a spark can bridge the gap [71].

8.1.1 *Aims*

This work identifies the optimal parameters for achieving a high rate of rough cut machining, while maintaining a good SF and the thinnest possible white layer. Initial trials were carried out before designing the experiment, to select desirable parameters for both the rough and skim cuts.

8.2 EXPERIMENTAL PROCEDURES

A commercial macro (not cabable of holding wires less than 0.15 mm) WEDM (Mitsubishi MV400) was used to machine the parts, using de-ionised water as a dielectric. Due to the capability of the machine used, the smallest wire diameter that could be used was 0.25 mm. This limited the minimum size of gear that could be produced and thus gears of 10mm outside Outside Diameter (OD) with 18 teeth were produced, with a module of 0.5.

The gears had an involute profile in line with similar studies referred to in chapter 2, such as that of Hori and Murata, [125] and were cut from 0.3 mm thick CuZn38 brass. A thickness of 0.3 mm was used as it is similar to the thickness of a gear used in a micromehcanical system such as a mechanical watch. Brass was used in line with previous studies in this thesis for consistency. A full factorial experiment was designed with mid points (Table 8.1), with the factors being rough cut parameters and offset for skim cut parameters. Three rough cut parameter sets were used, which had peak currents of the order typically seen when rough cutting (making initial cuts). These were designed to machine fast, without consideration of output quality. These are detailed in Table 8.2. Two offset values were then used for the finer, skim cut, 100 µm and 140 µm, as well as two mid-point measurements at an offset of 120 µmt. Following machining, the gears were cleaned using a standardised procedure before observation with a 3D non-contact profilometer (Alicona G5) microscope to determine surface roughness, and then mounted, polished and etched so that the white layer could be analysed using an Scanning Electron Microscope (SEM).

Gear Number	Run Order	Rough Cut Parameter Set	Finish Cut Offset
GM1	7	Set 1	100
GM2	10	Set 1	140
GM3	5	Set 3	100
GM4	3	Set 3	140
GM5	1	Set 1	100
GM6	6	Set 1	140
GM7	2	Set 3	100
GM8	4	Set 3	140
GM9	8	Set 1	120
GM10	9	Set 3	120

Table 8.1: The full factorial experimental parameters.

Rough Cut Parameter Set	Peak Current Value	Offset (μm)	Feed Rate (mm/s)
Set 1	7	175	0.2
Set 2	10	190	0.2
Set 3	13	205	0.2

Table 8.2: The three rough cut parameter sets used.

Two-way (Analysis of Variables (ANOVA)) was then used to determine how the rough cut parameters could be modified in conjunction with skim cut offset to achieve a high material removal rate and good SF. ANOVA is a method of analysis commonly used when machining with WEDM [14, 251]. This is because the nature of the machining; a high number of possible input parameters and multiple process outcomes lend it to Design of Experiments (DOE) that uses factorial design. Commonly used designs in WEDM machining are full factorial, fractional-factorial [252] and Taguchi [73, 74, 79, 99, 253]. These, and their relative functionality for investigating WEDM are detailed in Table 8.3.

Factorial design allows the effects of several factors can have on a response [254]. When conducting an experiment, varying the levels of all factors at the same time allows interactions between factors to be studied [255]. A simple example of factorial design is 2-level factorial design. Each experimental factor has only two levels. Every possible combination of factor levels is tested. This is depicted in Figure 8.1, where three variables with two levels are measured. For a 2-level full factorial design, 2^k runs are required, where k is the number of factors. Fractional factorial designs reduce the number of runs that is required carrying out only a few of the runs (fraction). This is shown in Figure 8.2. Only a selected subset or "fraction" of the runs in the full factorial design. This has advantages and disadvantages, as described in the table. 2-level factorial designs have disadvantages in the sense that they are not able to provide a complete picture of parameter effect: for example, they do not necessarily provide information between the points that are tested and it is assumed that this is linear. However, they provide information in only a small number of runs.

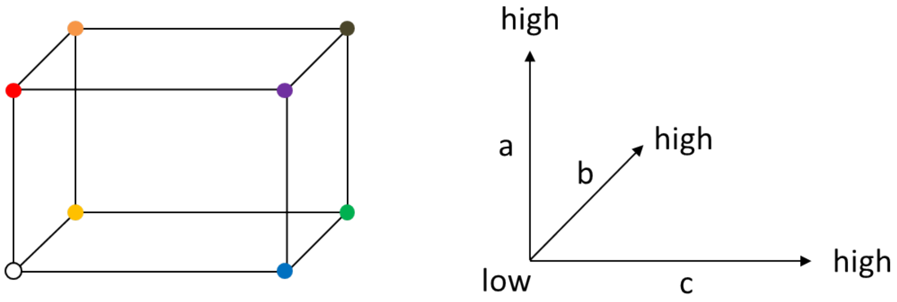

Figure 8.1: A two-level factorial design.

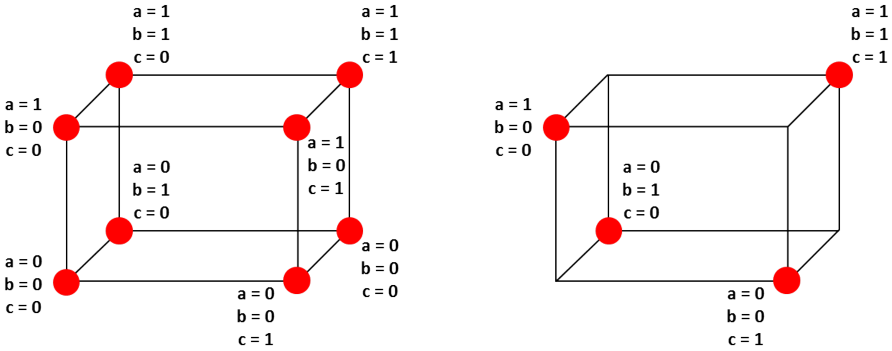

Figure 8.2: Full factorial vs. half-factorial design. Measurements are made at the red circled points.

Taguchi designs are typically based on factorial design. An example of this is Taguchi's L8 design which is a standard $k = 3$ 8-run design. Often Taguchi designs are based on factorial designs but are fractional designs and are thus simple to implement [256]. Due to using fractional design, it is necessary to identify a-priori the factors that will be significant and those that will not to avoid confounding, an inability to the experimental controls do not allow the experimenter to reasonably determine which variable(s) have caused a result, as they cannot be resolved. A comparison between typical and Taguchi DOE when investigating factors affecting machined surface during turning of AISI 2030 steel. They found that, provided number of variables was low and there were few confounding factors, the two could produce similar results with 88% time savings from the Taguchi method [255]. Based on the fact that it is common to experience confounding factors in ANOVA and it was not known a-priori which factors would be confounded, full-factorial design was used for this trial.

The benefits of the use of ANOVA are that it allows significance (both statistically, and relatively) of different factors (such as VG and IP) to be compared, but also allows interactions between factors to be investigated. It does so by checking whether the means of two or more groups are significantly different from each other. Figure 8.3 denotes examples of normally distributed means and their overlap. By comparing the means, the impact of factors is investigated by comparing the means (in terms of process outcome) of the different samples (machining parameters) different samples. An example of this, is mean R_a value for VG and IP.

Experimental Design	Relative Advantages and disadvantages
Full Factorial	• Identifies links between variables. • Allows multi-level analysis - allows variables to be analysed in isolation. • Allows interactions on multiple levels to be explored, e,g: $A \times B$, $B \times C$, $A \times B \times C$
Fractional Factorial	• Requires fewer runs than the full factorial designs. • Some of the main effects and 2-way interactions are confounded, so indistinguishable from the higher-order interactions.
Taguchi	• separates factors into control factors and noise factors [257]. Control factors are controllable process variables and noise factors are uncontrollable factors that vary the response [258]. • Defines a loss function to account for these noise factors. • Fractional design reduces costs and time needed for a designed experiment. • Some interactions may be confounded. • Confounding interations must be determined in advance.

Table 8.3: Experimental design techniques used to investigate WEDM parameters.

In this instance, the null hypothesis (Equation 8.2) is valid when all the sample means are equal, or they have no significant difference. The alternate hypothesis (Equation 8.3) is valid when at least one of the sample means is different.

$$H_0 : \mu_1 = \mu_2 = \cdots = \mu_L \tag{8.2}$$

$$H_1 : \mu_1 \neq \mu_m \tag{8.3}$$

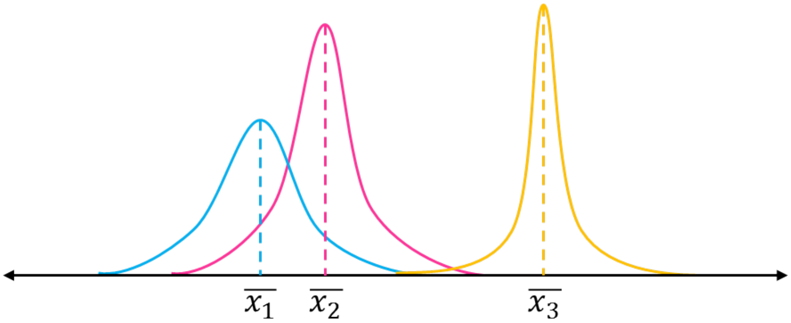

Figure 8.3: $\bar{x}_1$overlaps with $\bar{x}_2$, but $\bar{x}_3$overlaps with neither.

8.2.1 *Fixturing*

A fixture was designed (Figure 8.4) to clamp the 0.3mm thick brass in place. This aimed to minimise workpiece vibrations, since their size and effect cannot easily be determined, as the gears were being cut.

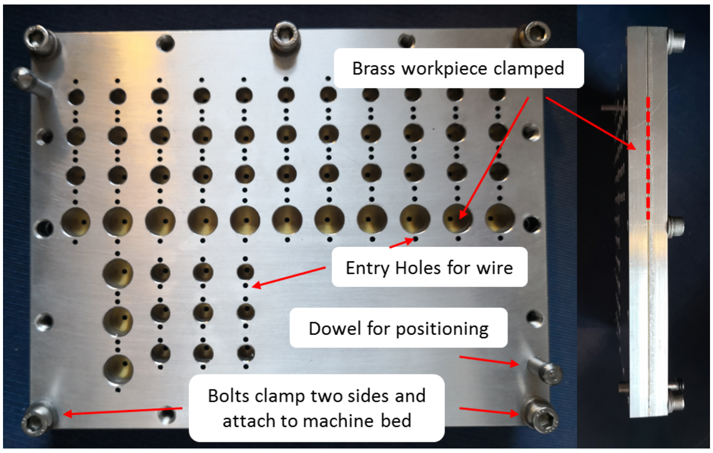
Brass workpiece clamped
Entry Holes for wire
Dowel for positioning
Bolts clamp two sides and attach to machine bed

Figure 8.4: Fixture used to machine gears.

8.2.2 *Evaluation*

Following machining, the gears were cleaned using a standardised procedure before observation with a 3D non-contact profilometer (Alicona G5) microscope to determine surface roughness, and then mounted in conductive bakelite, polished using a diamond suspension and then etched using a solution of water, hydrochloric acid (HCl) and iron nitrite ($Fe(NO_3)_3$) so that the white layer could be analysed by SEM.

8.3 RESULTS AND DISCUSSION

8.3.1 *Effects of Parameters on White Layer*

The white layer has a finer micro structure compared to the base material, as can be seen in Figure 8.5. This easily-identified layer was measured for thickness. It was measured in three places on the tooth - tip, flank and root (see Figure 8.6). For the roots of the teeth, it was found that neither offset or rough cut parameter set yielded a statistically significant difference. Mean white layer depth for this part of the tooth ranged from 1.77 µm to 3.37 µm, which is very low and compares favourably with thicker gears [126] with which it is easier to produce a smooth finish because spark contact between wire and workpiece is more stable.

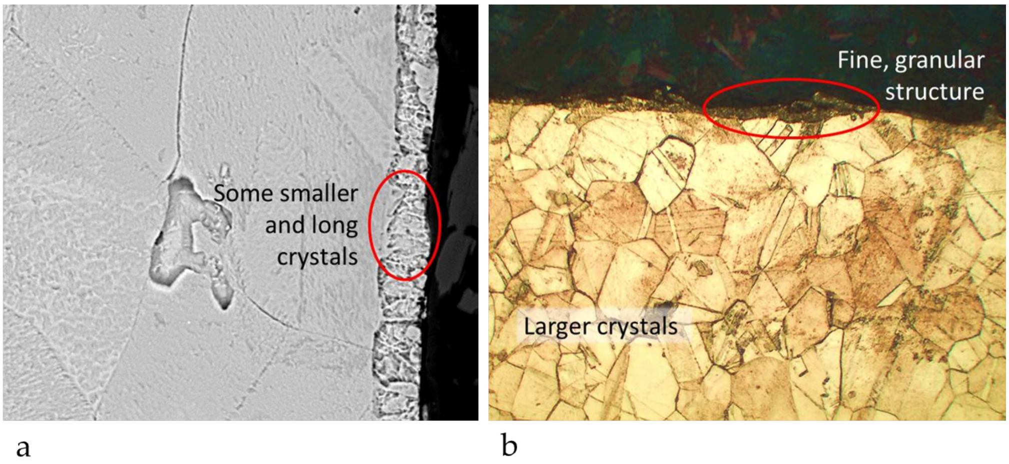

Figure 8.5: (a) an SEM image of the smaller grains in the white layer; (b) and optical image of the same.

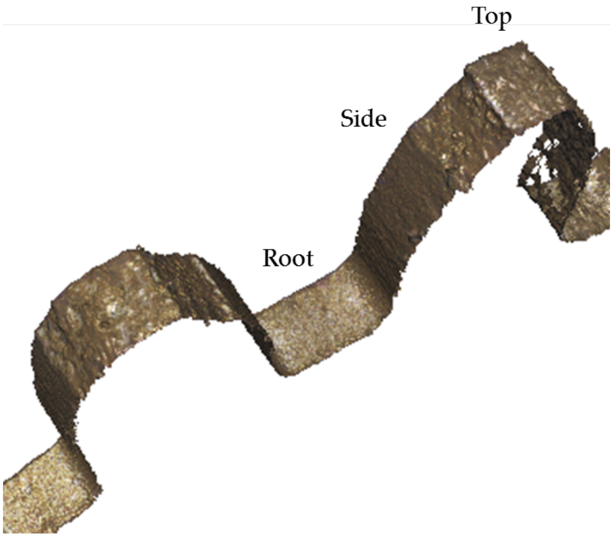

Figure 8.6: Varying SF across tooth profile can be seen. Below the label 'Root' can be seen an apparently smoother surface than below either 'side' or 'top'.

The null hypothesis was proposed to be that rough cut set is insignificant. The resultant p-value (i.e. level of marginal significance of the results) of 0.399 validated this and conclluded that rough cut set is insignificant in terms of SF. In this case, the threshold for the null hypothesis to be rejected was set at 0.05 based on the Fisher limit for statistical significance [259]. Figure 8.7a shows a Main Effects plot for the white layer depth at the root of the gears. It can be seen that for a higher offset a thicker white layer is seen, while for a more aggressive rough cut set (primarily characterised by higher current for faster MRR), a thinner white layer is seen after a finish cut. The red point indicates the mid-point: the experiment is run at paramerters that lie between thet two extremes. This is helpful because it helps to reinforce the idea that there is actually a relationship.

The thicker white layer occurs because at a lower offset, the wire cuts through the white layer from the previous cut, leaving a thinner final white layer, while for a large offset the in-affected material beneath is machined, resulting in a new white layer. The result that a more aggressive rough cut reduces final white layer is both interesting and useful. While typically aggressive parameters result in a thicker white layer, a low offset and fine finish parameters have resulted in removal of some of the recast material which suggests that it is possible to carry out a fast rough cut without compromising final SF.

However, the interaction plot (Figure 8.7b) shows that the effect of changing the offset depends on the rough cut settings: at a less aggressive rough cut setting, a large offset makes more difference (i.e. more of the original white layer is removed). For an interaction plot, where lines for each parameter are parallel there is no suggestion of interaction, while different gradients of the two slopes suggest a possible interaction. Where the two lines cross, an interaction is suggested. In the case of white layer at the root of the gear, it appears that there is an interaction between these parameters.

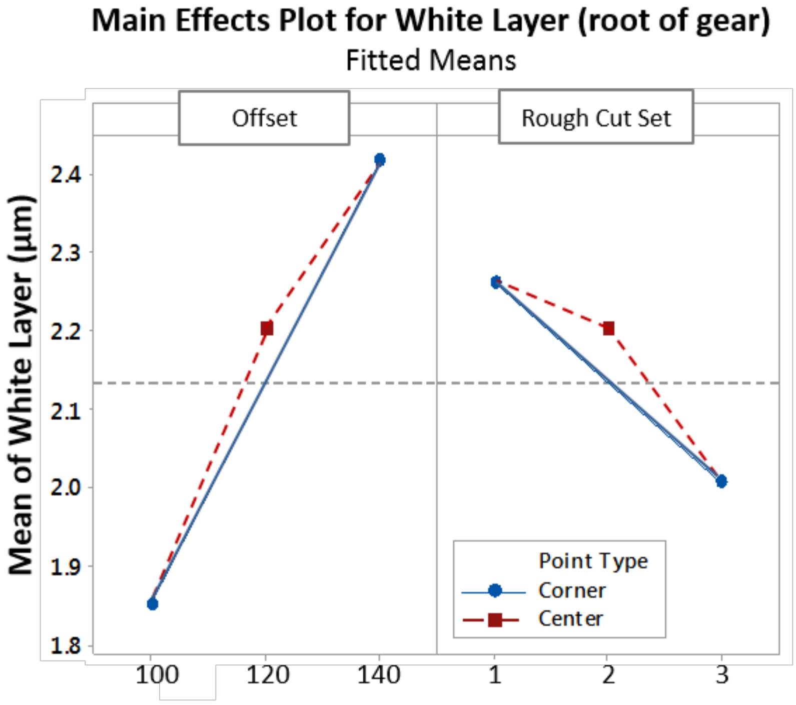

(a) Main effects plot for white layer at the root of the gear. The red points indicate mid-points and validate the blue linear relationships shown.

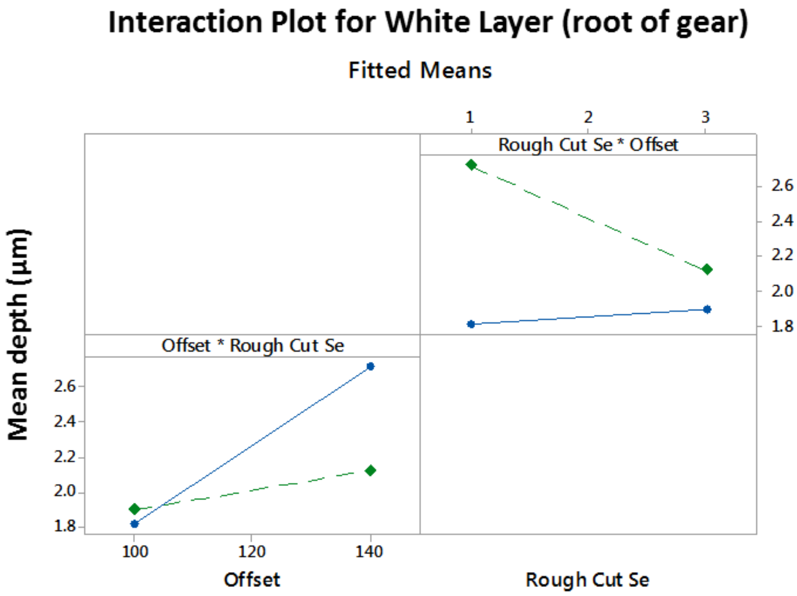

(b) Interactions plot for white layer at the root of the gear. The crossed line in the bottom left-hand corner and the opposite direction of gradient in the upper right suggest that the two parameters interact.

Figure 8.7: Main effects and interactions plots for white layer depth at the root of the gear.

For the flanks of the teeth, a similar result was seen. It was found that the rough cut parameter set is significant, and suggested that the smallest white layer depth could be achieved using the most aggressive parameter set (set 3) and the smallest offset - indeed, a larger offset was not desirable. A p-value of

0.015 indicated that the rough cut parameter set was the most significant factor which can also be seen on the Pareto Plot of Standardised Effects (Figure 8.8).

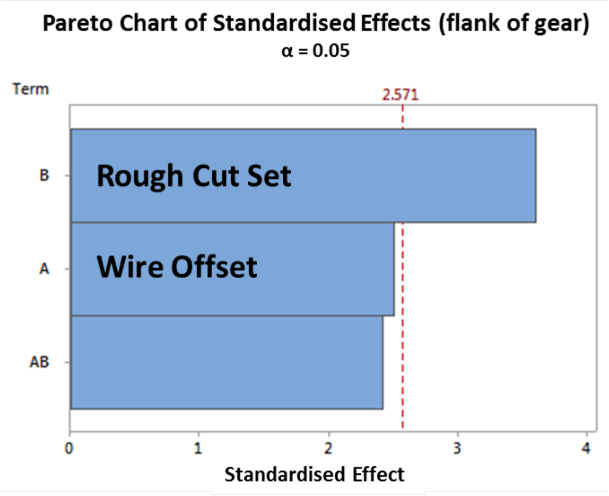

Figure 8.8: Pareto plot for significant parameters afecting white layer depth.

For the tip of the teeth, there was once again no statistically significant change in white layer thickness. However, this time the ANOVA suggested that both a higher offset and faster rough cut set improved the white layer thickness. This is explored further in Section 8.3.4. When white layer from the finish cut was compared with that of the rough cut, it was noted that for a more aggressive rough cut, a greater proportion of the white layer produced was removed by the skim cut, while a lower offset was optimal. It is likely that a increasing the 'offset' parameter resulted in cutting of base material rather than just recast material, as depicted in Figure 8.12. The variation of white layer thickness across all gears was evaluated. To maintain the most constant white layer depth and lowest standard deviation, parameter Set 1 and a small offset should be used.

8.3.2 *Effects of Parameters on Surface Finish*

R_a, R_q and R_z values were used to assess SF as these are easily comparable with other literature in the field. While R_a provides an average roughness, R_q uses root-mean-square to take extremes into account further while R_z averages highest and lowest peaks. Thus the combination of these is useful. The surface topography of the parts was of the classic cratered texture that is typical of WEDM parts [260] (Figure 8.9). The best SF (lower $R_{a,q,z}$ values) was seen at the base of the teeth (see Figure 8.9), and since an excellent SF is desirable, this is where measurements were taken. A minimum R_a of 0.37 µm was achieved, and 0.46 µm and 1.30 µm for R_q and R_z respectively. These are comparable to that achieved using multi-stage finishing processes [133] and compare favourably to gears produced only using WEDM [261], although it is a slightly rougher surface than can be achieved by hobbing [134].

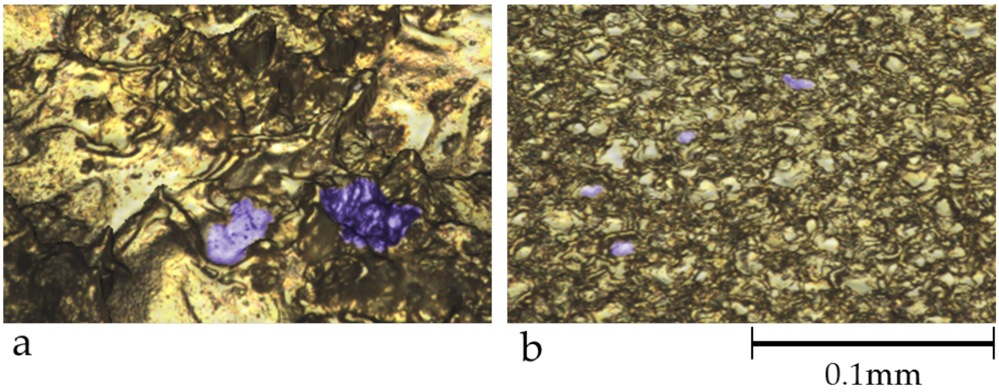

Figure 8.9: Highlighted in dark purple are (a) an example of the large irregular crater-like SF seen at the base of the teeth after the initial rough cut; (b) smaller and more regular craters visible after the finish cut.

Whereas rough cut parameter set is significant in determining white layer, the skim cut offset had the most significance in minimising surface roughness (Figure 8.10a). This was an interesting result as higher rough cut parameters are faster and thus their relative insignificance can allow faster rough cuts to take place wihtout comromising part quality. For R_a, offset was the most important parameter, and increased offset resulted in a higher $R_a$value. This is similar to the result seen for recast layer thickness in that increased offset resulted in increased recast layer thickness. It is desirable to reduce offset such that only the white layer from the rough cut is removed, and not base material. Therefore, using this result, prototype parts can be produced to build up an understanding of the way in which the part geometry responds to machining parameters and optimise cutting parameters for an individual part geometry.

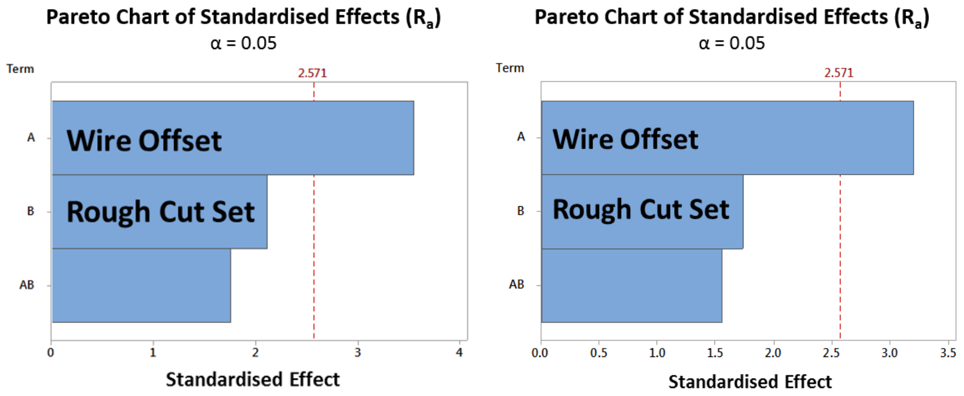

(a) Pareto plot showing significant factors for R_a. Wire offset is significant because it extends beyond the dotted line.

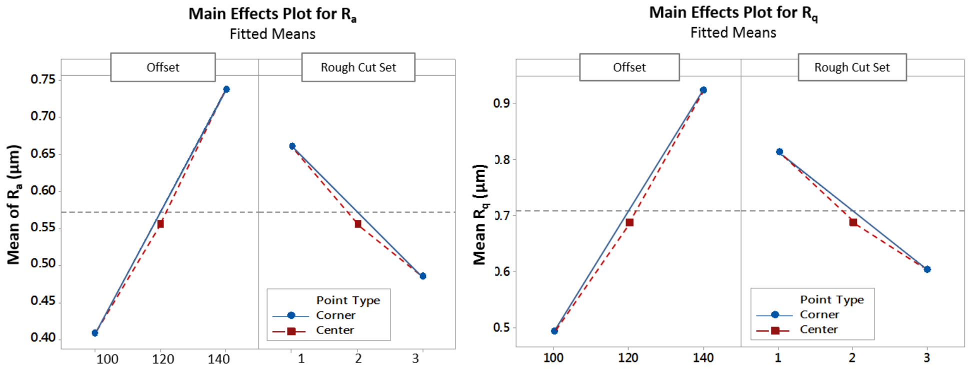

(b) Main effects plot for R_a at the root of the gear. Once again, the mid points (red) are in agreement with the gradient of the blue line.

Figure 8.10: Pareto plot and main effects plots for R_a and R_q.

For R_q, once again, offset was the most significant of the factors influencing SF. The Pareto and main effects plots seen were extremely similar (shown together in Figure 8.10) As offset was increased, the surface became rougher; however a more aggressive rough cut set did not seem to cause a higher R_a value. Furthermore, rough cut parameters were not significant in influencing R_q, because the finish cut largely determines SF of the final part. This is a useful result, as it enables more aggressive (and hence faster) rough cut sets to be used with no detriment to R_q.

As with the other R-values, R_z was only significantly affected by the offset used for the finish cut. Both the Pareto and main effects plots can be seen in Figure 8.11. Increased offset resulted in a rougher surface, as seen in Figure 8.11b. This is because for offset values which are similar to spark gap size, the finish cut surface and rough cut surface constructively interfere to give a smoother finish. A larger offset instead generates a new surface. Rough cut Set 3 (the most aggressive) resulted in the best SF (although this was not significant). Interstingly, the mid-point in the right hand plot of Figure 8.11b actually suggests that the relationship between the blue points should be reconsidered since the red lines linking it to the end points have very different gradients; one is positive, one negative.

The optimal parameter sets were parameter set 3 and an offset of 100. In order to look at the consistency in the roughness across the entire gear, the variance of R_z was evaluated. Increased offset resulted in a less consistent value, and more aggressive rough cut sets appeared to have no negative effect. Since the lubrication and tribological behaviour of small gears depends heavily on the SF, it is very important that this is consistent and so variation should be minimised. As with R_a, R_q and R_z, the optimum result (i.e. least variation) was achieved with an aggressive (fast, high pulse energy) rough cut and low offset.

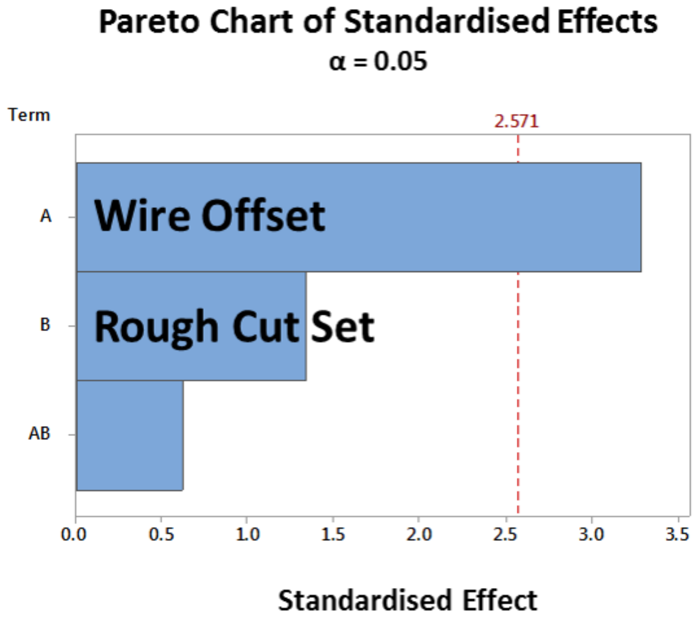

(a) Pareto plot showing significant factors for R_Z. Once again, only rough cut set is statistically significant.

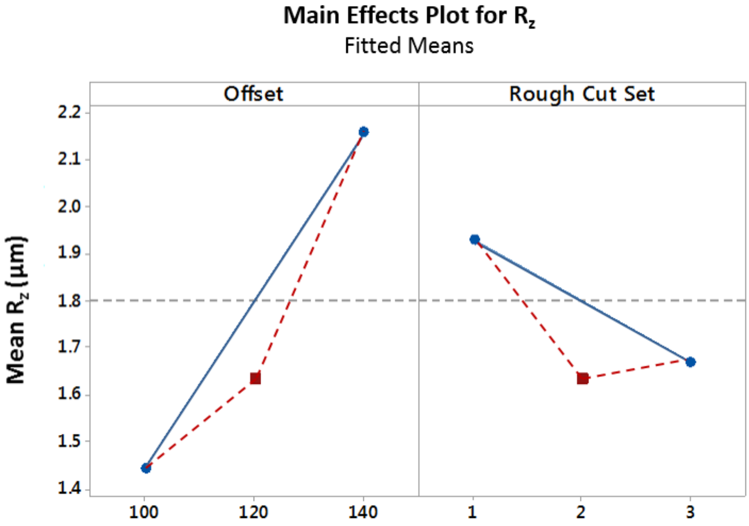

(b) Main effects plot for R_Z at the root of the gear. The mid-point in the right hand plot actually suggestions that the relationship between the blue points should be reconsidered.

Figure 8.11: Pareto plot and main effects plots for R_Z.

In terms of overall improvement in SF finish between rough and finish cuts, the offset was seen to be most significant. A smaller offset lead to a smoother surface compared to the original. In general, results showed that the finish cut offset can indeed be optimised such that white layer only is removed, and this will allow the white layer depth to be reduced while still maintaining a high machining rate during the rough cut, as has been alluded to in previous work [17].

8.3.3 *Relationship between White Layer Depth and Surface Finish*

As explained in subsection 2.2.4, both the white layer depth and surface topography are important in the production of very small gears to achieve appropriate material and lubrication properties. It is therefore important to understand how machining parameters affect both of these, and indeed how they are related. The ratio of white layer depth (D_r) to SF (R_a, R_z etc) for the base of the teeth is given in Table 8.4. Generally speaking for the rougher surfaces the white layer was not only thicker in absolute terms, but thicker relative to SF. It is clear that for a white layer thickness, a higher surface roughness in terms of crater size and depth is also seen, i.e. parameters that increase one also increase the other.

By setting cutting parameters such that the second white layer only cuts into the original white layer, total depth of white layer can be reduced without needing specific rough cut parameters (Figure 8.12).

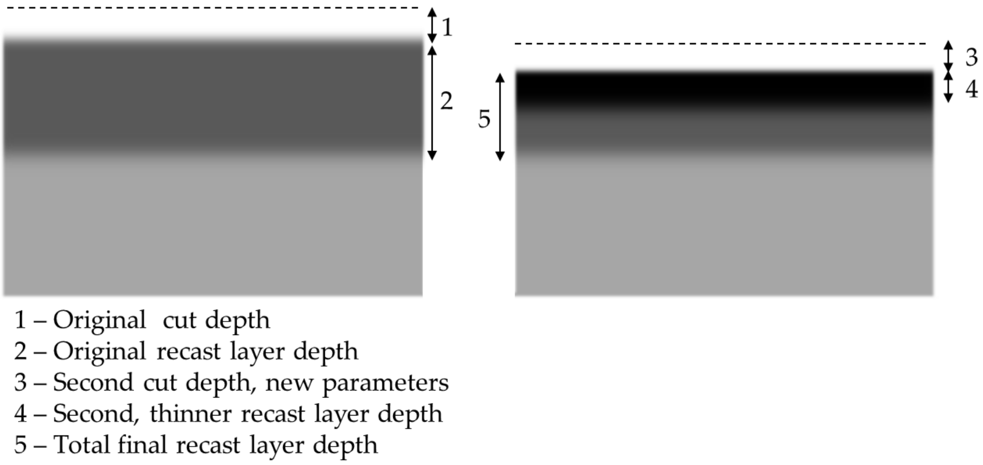
1
2
5
3
4
1 – Original cut depth
2 – Original recast layer depth
3 – Second cut depth, new parameters
4 – Second, thinner recast layer depth
5 – Total final recast layer depth

Figure 8.12: Removal of only white layer using a skim cut.

Area	Ratio of D_r to R_a	Ratio of D_r to R_z
Base of teeth	$D_r/R_a = 3.94 \pm 1.27$	$D_r/R_z = 3.21 \pm 1.08$
Tip of teeth	$D_r/R_a = 2.00 \pm 0.56$	$D_r/R_z = 1.64 \pm 0.51$

Table 8.4: The ratio of white layer to surface roughness parameters R_a and R_z was used to indicate relative thickness of white layer to surface roughness.

8.3.4 *Notes on White Layer Depth and Surface Finish across Tooth Geometry*

It was observed that the SF achieved (and indeed white layer depth) was inconsistent across the entire tooth profile. This can be seen in Figure 8.13. This phenomenon was seen for all gears, and has two physical explanations. The

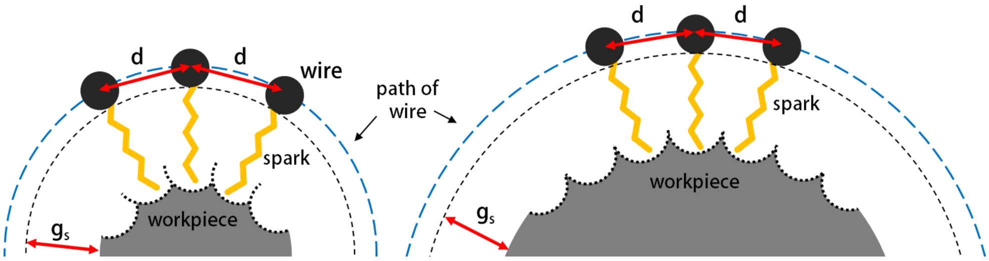

Figure 8.14: For a smaller radius of cut (left), the craters overlap in such a way as to reduce overall surface roughness as compared to a larger radius (right).

first relates to radius of the wire path. It can be assumed that spark energy is constant and thus each spark produces an identical sized crater, perpendicular to the workpiece surface. For a greater path radius (i.e. flatter path) with the same feed rate, the craters overlap less which results in a higher peak between craters (Figure 8.14).

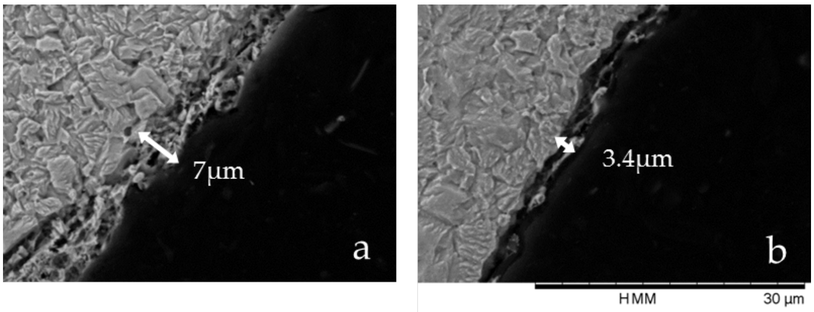

Figure 8.13: (a) white layer depth for the top of a tooth (seen as smaller crystals in a slightly darker shade of grey); (b) white layer depth for the root of a tooth.

The second explanation relates to the smoothness seen at the root inner radii (between the root and flank). Here, the wire is surrounded by material and there is much more opportunity for sparking and thus machining is more stable. On outer corners such as the tip of the teeth, there is very little opportunity for sparking which leads to unstable machining and a rougher surface as well as more random crater geometries. The result is that wire feed rate should be slower for the tips of gears and external corners, which is significant for MRR. This solution can be easily implimented even on basic systems by the operator or indeed automatically.

8.4 CONCLUSIONS

This work focussed on the investigation of the use of multiple rough cut parameter sets used with different offsets, with a view to producing the minimum white layer depth and best possible surface finish while maintaining a high rate of machining for the rough cut. Key findings were that:

- In terms of white layer, the rough cut parameter set is significant, but an aggressive rough cut combined with a smaller offset achieves a desirable thickness.
- Regarding surface finish, rough cut parameters set is insignificant within the bounds investigated, which allows a fast (or more aggressive) rough cut parameter set to be used and speeds up machining time.
- The tool path radius of the wire had an effect on the surface finish, thus parameter control is required such that pulse energy is reduced in these areas.
- Using the premise that wire offset and finish cut parameters have the most significance when determining surface roughness and white layer thickness, it is possible to have a fast rough cut while minimising these so that machining rate is higher and quality is adequate.

The outcome of this work and its application in industry lies in the capability to use the theory behind surface quality in WEDM to speed up the machining process for miniature gears while maintaining required SF. This speeds up efficiency of processes and reduces wire material used.

9

APPLYING STRAIGHT CUT MEASUREMENTS TO INDUSTRIAL ENVIRONMENTS

9.1 INTRODUCTION

Thus far, work has taken place to characterise the wear of micro-end mills cutting straight slots. This information has been used to inform coating choices for industrial applications of micro-end-mills. It is therefore interesting to investigate the relationship between wear curves produced for straight slots and those produced in realistic, industrial applications.

9.1.1 *Fundamental Studies and Transfer to Industry*

While there have been many successful studies into the micro-milling process in literature, they and the studies that have taken place in this work typically focus on straight slot cuts [5, 9, 10, 155, 262], shoulder milling [263] or the type of cut is simply not described [139, 189], with the view to characterising the process. On the other hand, in industry it is typical to develop processes iteratively using trial-and-error [264–266]. The crucial requirement for fundamental research in machining is that it should be used in industry to improve process efficiency. However, The concept of TRLs has been discussed in Section). TRLs relate to the maturity of the process in terms of applying it to industry. These are as follows:

TRL 1 Basic principles observed and reported.

TRL 2 Technology concept and/or application formulated.

TRL 3 Analytical and experimental critical function and/or characteristic proof-of-concept.

TRL 4 Component or process validation in laboratory environment.

TRL 5 Component or process validation in realistic environment.

TRL 6 System/subsystem model or prototype demonstration in a realistic environment.

TRL 7 System prototype demonstration in end environment.

TRL 8 System completed and verified through test and demonstration in end environment.

TRL 9 System successfully implemented.

It is typical in an academic environment to carry out research up to TRL 3 or 4. Meanwhile, TRLs 8 and 9 are most common in industry, with TRL 7 where industrial R&D takes place. Commonly, it is difficult to implement low-level research in the realistic environments, while many industrial set-ups have limited R&D. The result is that often, the middle levels are not fulfilled and the academic research does not get implemented in industry [267]. This is commonly referred to as a research gap (Figure 9.1).

The first step to bridging this gap is to validate whether the most fundamental research (for example, straight slots or single shoulder cuts) and the results from this apply to more complex situations.

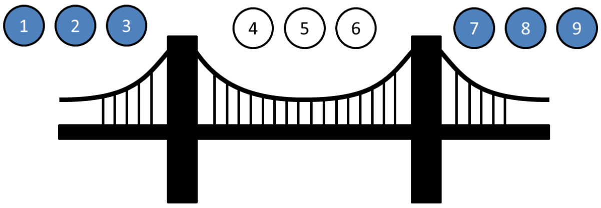

Figure 9.1: Commonly the mid-level TRLs are missing. Catapult centres help to bridge this gap.

The higher the TRL level, the more certainty as to the applicability and success of the process there is. Therefore, in study which aims to increase tool life and reduce machining costs in industry, higher-level research validates the processes and provides the customer, in this instance tooling companies, with usable data. The work carried out herein represents **TRL 4**: the process has moved towards industrial levels of complexity but is not being used for production. In the context of this work, this means the measurement of tool wear and determination of coatings performance has been applied to semi-realistic situations. In this case, that is useful since Kyocera are not looking to produce the parts themselves, and so representative features give a broad overview of what their customers, the end users, will use the tools for. The purpose of initial tests, which included longer machining times, is to simulate the industrial machining environment more realistically since tools of this size are typically used to machine for minutes rather than seconds.

9.1.2 *Tool Wear Measurement On- and Off-line*

On-line and continuous tool wear techniques measure significant parameters throughout the cutting process. Off-line methods measure these parameters during intervals, often by removing the tools from the system [268]. Tool wear measurement both on and off-line have different benefits. On-line tool wear measurement allows tool-change policies to be determined, adaptive machining control and removes the errors caused by tool removal [269]. Off-line measurement, on the other hand, allows more complex imaging techniques such as scanning electron microscopy to be used. On-line measurement uses techniques such as optical methods [270], force measurement [271] and acoustic measurements[272].

On the micro scale, optical imaging is much more challenging due to the small scale. Force measurement is used, but this lacks the resolution in terms of wear over tool life that optical imaging offers. Acoustic emissions has also been used successfully to identify tool breakage, and the ability to map force and acoustic signals is desirable but has not yet taken place. As a result, optical measurement of micro-milling tools takes place off-line. Typically, the methods used and the orientations measured are hugely variable. This has lead to the development of a tool wear measurement protocol [13]. The aim of this was to standardise the way micro milling tools are measured, in the way that they are on a larger scale. Since micro-milling standards are not appropriate for micro-machining [155], this was required before significant research could take place and provides the field with an opportunity to make comparisons between results, tools and across materials.

9.1.3 *Tool Wear Measurement Protocol*

The tool wear measurement protocol is described in brief in this section, although more detail can be found in protocol for tool wear measurement in micro-milling [13].

9.1.3.1 *Definitions*

The surface finish of the workpiece is is measured using R_a value and surface texture measured using S_a. Types of tool wear are based on ISO8688 [154] and adapted for small tools. These are categorised (Table 9.2) as Flank Wear (VB), Face Wear (KT), Outside Edge Wear (OE) Chipping (CH) and Catastrophic Failure (CF). By measuring tools in relation to these types of wear, direct comparison between studies can be made.

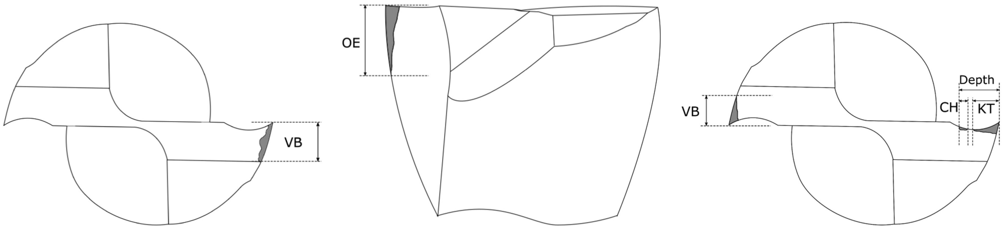

(a) Flank Wear (b) Outside Edge Wear (c) Face Wear, Flank Wear and Chipping

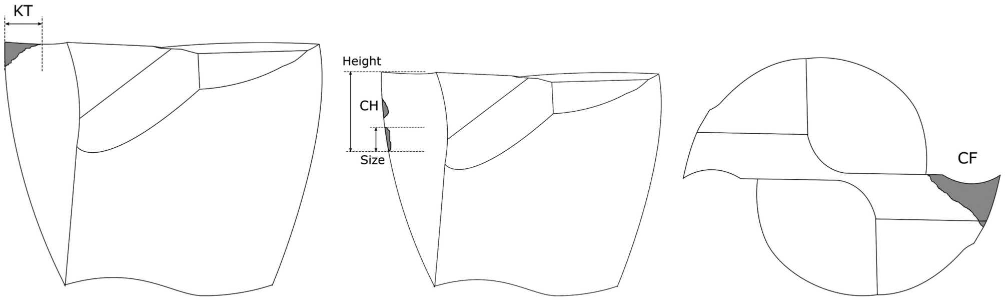

(d) Face Wear Intersecting Outside Edge Wear (e) Chipping (f) Catastrophic Failure

Figure 9.2: Types of wear seen.

9.1.3.2 *Measure of Distance Cut*

Distance cut is measured using the sliding distance of the cutting edge (chapter 5). This is calculated using:

$$x_{comp} = \pi D_{cap} c_{comp} + \sum_{1}^{c_{inc}} x_i \tag{9.1}$$

where c_{inc} is the number of incomplete circles, c_{comp} is the number of complete circles, D_{cap} is engaged tool diameter, and x_i is the sliding distance for the i^{th}circle. x_{comp} can be calculated wither analytically or computationally. This allows a more consistent metric to measure tool wear against than cutting distance or cutting time, as the amount of work carried out on the tool depends on spindle speed and feed rate.

9.1.3.3 *Tool and Workpiece Preparation*

Tools are inspected prior to machining to ensure a minimum quality standard. Workpiece grain direction should be the same for each workpiece. Depth of cut [152] and unit removal [197] should meet the following requirements:

- edge radius < depth of cut and
- edge radius < unit removal × 10

All workpieces should be faced off to ensure flatness perpendicular to the tool and fixed to the machine bed such that the surface is normal to the z-axis. Coolant method should be consistent across comparative studies.

9.1.3.4 *Measurement of Tool*

Tools should be measured both prior to testing and during testing. The basic equipment required for testing is as follows:

- Scanning electron microscope with both secondary and backscattered electron functionality.
- Optical profilometer (e.g. focus variation or white light interferometer).
- Ultrasound bath.
- Acetone.
- A compressed air source.
- A force cell for measuring lubricant pressure on workpiece.

Where measured, lubricant pressure should be established before a cutting force is applied. Tools should be removed and cleaned at a pre-determined interval for measurement using an Scanning Electron Microscope (SEM). Measurement orientations are shown in Figure 9.3.

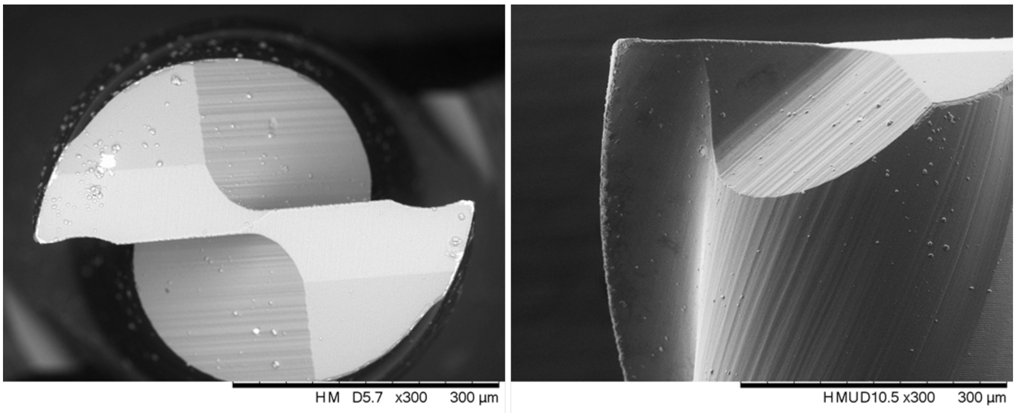

Figure 9.3: The two orientations in which tools were measured.

9.1.3.5 *Criteria for Tool Life*

Face wear of 0.2D should not be exceeded as this is considered catastrophic failure of the tool.

9.1.3.6 *Test Procedures*

For wear testing, slots should be machined to a chosen depth. The slot should begin outside the workpiece and run in the y-direction of cut.

9.1.3.7 *Measurement of Forces*

Optionally, force measurement can be measured for mapping to optical wear measurements.

9.1.3.8 *Reporting of Results*

Wear should be reported in absolute terms relative to the original size of the tool (in µm). Sliding distance forms the x-axis, with a second axis being used as a conversion factor to cutting distance where required. An example of this is given in Figure 9.4. Tool wear is identified as being in one of three zones:

I. Rapid initial wear

II. Steady state wear

III. Rapid wear before failure

The tool-life criterion can then be identified as the intersection between phases II and III.

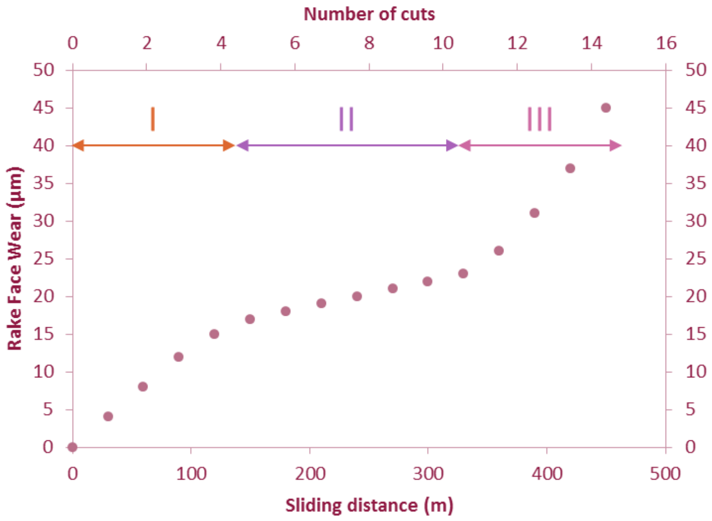

Figure 9.4: An example of the way in which results should be reported.

9.1.4 *Purpose of Work*

To establish the applicability to an industrial context of tool wear curves that are produced during straight slots in micromachining, testpieces with characteristic features seen in micromachining were used. The work took place collaboratively between the University of Sheffield and Kyocera-SGS. The outcome of this work, and the tool wear investigations carried out previously, is extended tool life and provision of a basis on which Kyocera-SGS is able to select choose the optimum coatings to apply to micro-tools. This has reduced machining costs and advanced Kyocera-SGS in the micro-tool market.

9.2 EXPERIMENTAL METHODS

The trials took place on a KERN Evo micro-milling machine with a maximum spindle speed of 50,000 RPM. The tools used were 0.5 mm tungsten carbide end-mills provided by Kyocera-SGS. The recommended spindle speed for these mills is 100,000 RPM, and since the machine used has a maximum spindle speed of half this, the feed rate was reduced in accordance with Equation 9.2 to achieve an appropriate feed per tooth, where v_f is table feed rate, n is spindle speed and z_c is number of cutting teeth.. The workpiece and tool were flooded continuously throughout the cutting process using synthetic Hocut 768 lubricant.

$$v_f = f_z \times n \times z_c \tag{9.2}$$

Hastelloy and brass (CuZn38) were each machined with a different coating (Table 9.1). A standard test part designed to mimic features commonly encountered in the micro-mechanical, medical and chemical industries. This is detailed in Figure 9.6. Multiple depths of cuts used were used, as defined in

Figure 9.5. Cutting speeds and feeds for used for each material are given in Table 9.2.

Materials	Coating 1	Coating 2	Coating 3
Brass	Uncoated	AlTiN	TiB_2
Hastelloy	AlTiN	TiAlCrN	///////////

Table 9.1: Materials used, and coating used to machine each of these.

Parameter	Brass	Hastelloy
Spindle speed (rpm)	50,000	6,786
Feed (m/min)	479	11
F_z (mm)	0.00479	0.00080
Radial depth of cut (mm)	0.50	0.50
Axial depth of cut (mm)	0.20	0.20
Sliding distance (of tool) per 1m of cut	16.064	95

Table 9.2: Speeds and feeds used for machining each material.

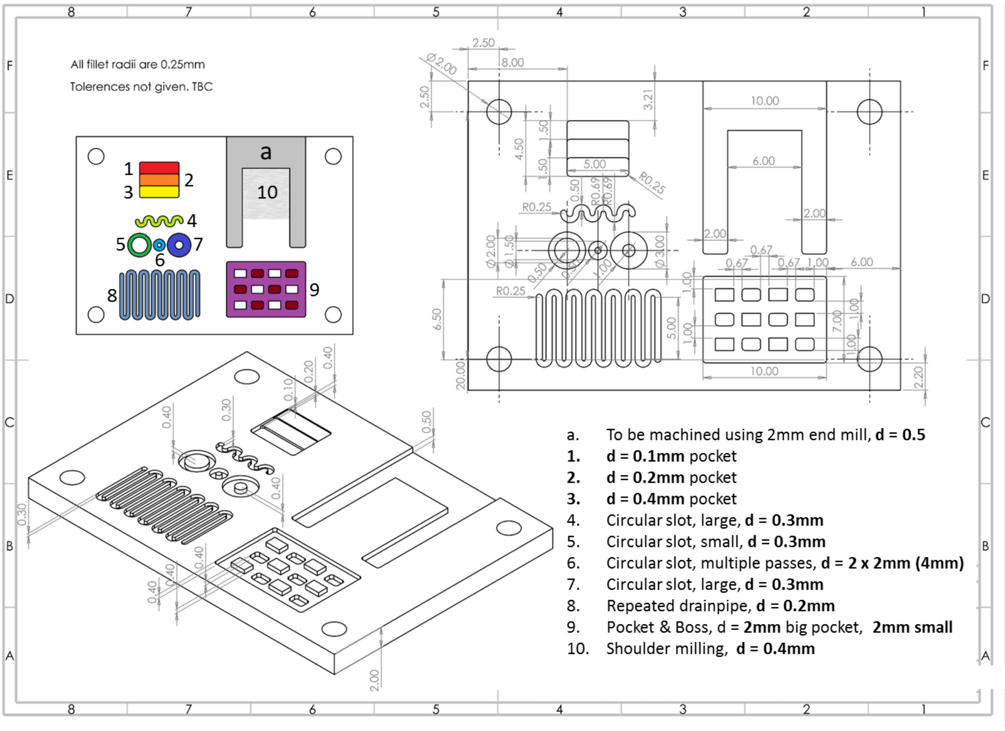
a
1
2
3
4
5
6
7
8
9
10
2.50
8.00
Ø2.00
2.50
3.21
10.00
6.00
4.50
1.50
5.00
R0.25
R0.69
2.00
Ø3.00
0.67
1.00
6.00
6.50
20.00
7.00
10.00
2.20
0.40
0.30
0.20
0.10
0.50
2.00

All fillet radii are 0.25mm

Tolerences not given. TBC

a. To be machined using 2mm end mill, **d = 0.5**
1. **d = 0.1mm** pocket
2. **d = 0.2mm** pocket
3. **d = 0.4mm** pocket
4. Circular slot, large, **d = 0.3mm**
5. Circular slot, small, **d = 0.3mm**
6. Circular slot, multiple passes, **d = 2 x 2mm (4mm)**
7. Circular slot, large, **d = 0.3mm**
8. Repeated drainpipe, **d = 0.2mm**
9. Pocket & Boss, d = **2mm** big pocket, **2mm small**
10. Shoulder milling, **d = 0.4mm**

Figure 9.5: Depths to be cut for each feature.

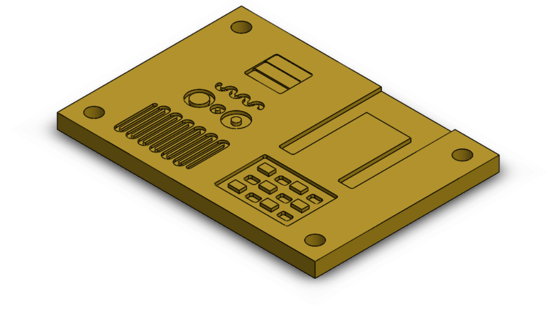

Figure 9.6: Testpiece to be machined.

9.2.1 *Testing Process*

Initially, three brass (CuZn38) testpieces were machined. A single tool of each coating type was used for each, and machined to failure to give an idea of surface finish over entire, uninterrupted tool life and overall tool life. This allowed machining intervals for the measured tools to be determined. Ongoing force testing took place for each of the testpieces.

Following this, two uncoated, two AlTiN and two TiB$_2$tools were used to machine. They were removed at set intervals according to Figure 9.5 and measured according to subsection 9.1.3.

Forces were measured using a Kistler 9317c force cell, in the setup seen in Figure 9.7. The workpiece was attached to the force cell such that workpieces could be replaced easily and to maximise available machining area (Figure 9.8).

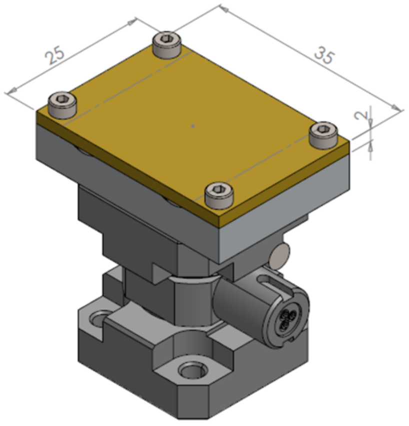

Figure 9.7: Workpiece mounted on force cell.

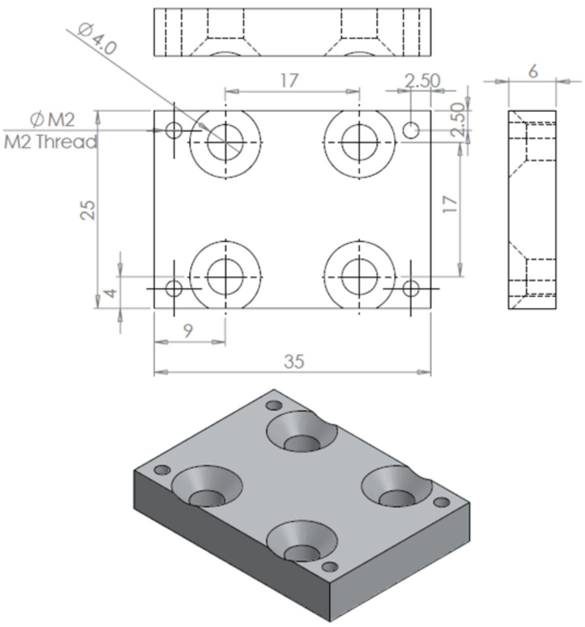

Figure 9.8: Mounting for force cell.

9.3 RESULTS AND DISCUSSIONS

9.3.1 *Cutting Forces*

To illustrate the variation in cutting forces across the cuts, and therefore validate the variability in cutting forces (as would be seen in industrial applications), cutting forces are illustrated. A full set of force measurements was made for TiB_2, while some data was lost for the AlTiN coated and uncoated tools. The cuts made shown in Figures 9.5, 9.6 are as follows:

I. 0.1mm deep pocket, square [labelled 1 in Figure 9.5]
II. 0.2mm deep pocket, square [labelled 2 in Figure 9.5]
III. Waved slot, full width of tool, depth 0.3mm, 3 repeats [labelled 4 in Figure 9.5]
IV. Circular slot, full width of tool, depth 0.3mm, inner radius 0.75 [labelled 5 in Figure 9.5]
V. Circular slot, full width of tool, depth 0.3mm, inner radius 0.25 [labelled 6 in Figure 9.5]
VI. Circular slot, 1mm width, depth 0.4mm carried out in 2 0.2mm passes [labelled 7 in Figure 9.5]
VII. Drainpipe slot, full width of tool, depth 0.3mm, 6 repeats [labelled 8 in Figure 9.5]

Figures 9.9 and 9.10 show cutting forces for tools coated with TiB_2. It can be seen clearly that the different types of cuts represented in Figure 9.5 result in very different force signatures, which is something that needs to be considered further when designing cutting paths - peak forces are typically seen where the cut is interrupted.

Meanwhile, Figure 9.11 shows that the uncoated tool experiences the highest cutting forces, followed by the TiB_2 tool. $TiB_2$is known to have a higher coefficient of friction (0.9 as compared with 0.7 for AlTiN) which explains the higher cutting and feed forces since the friction is proportional to the normal force and coefficient of friction value.

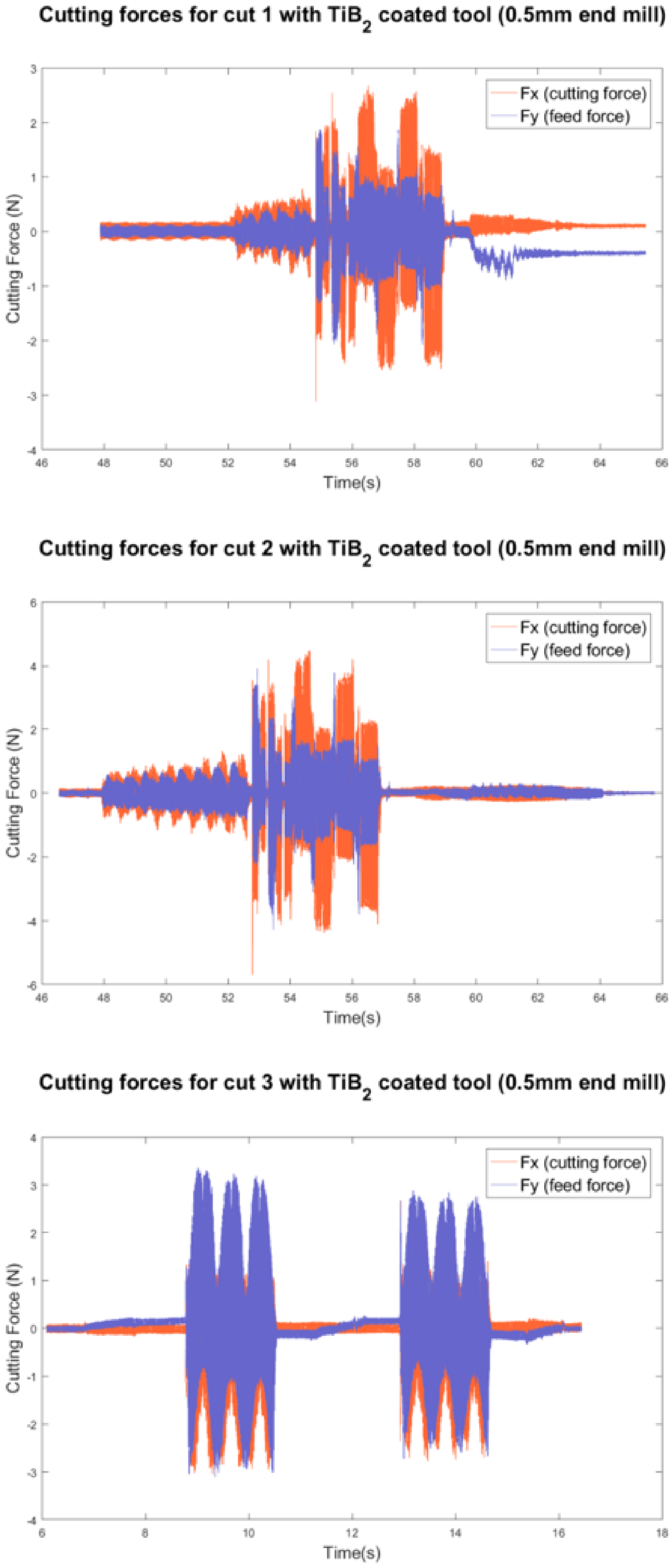

Figure 9.9: Cutting forces signatures for cuts 1 - 3 (see Figure 9.5) made with tools coated with TiB_2.

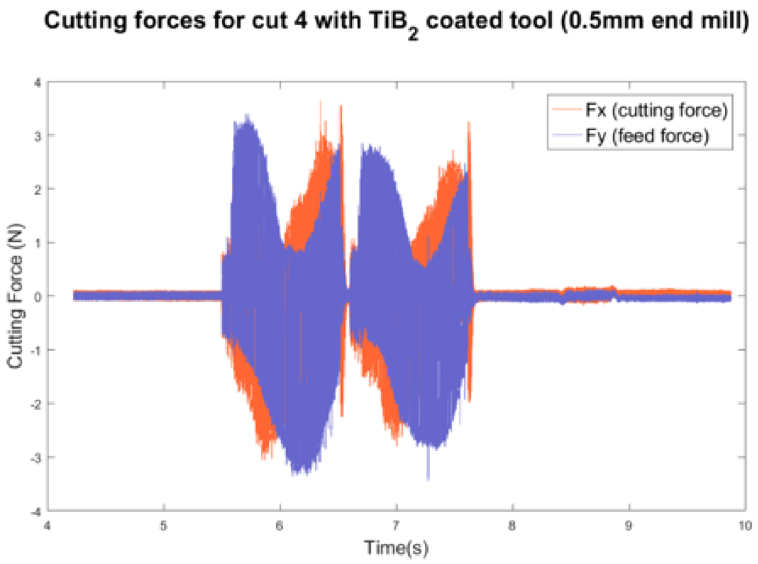

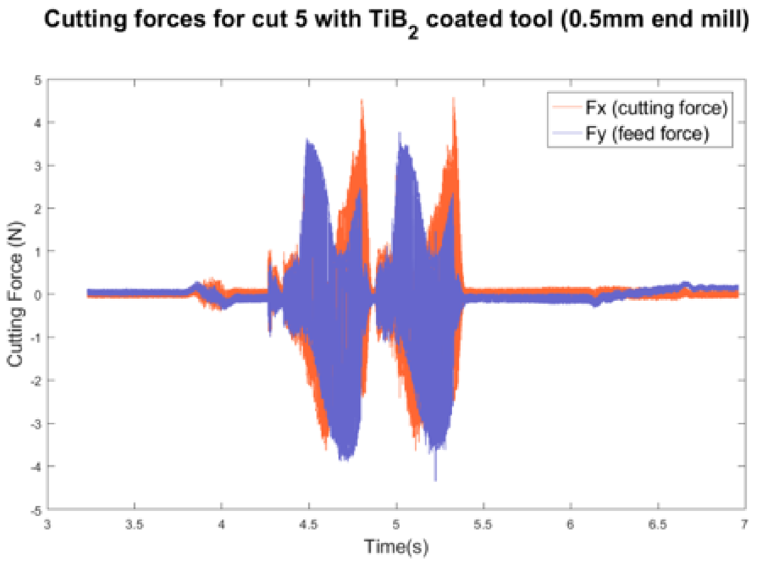

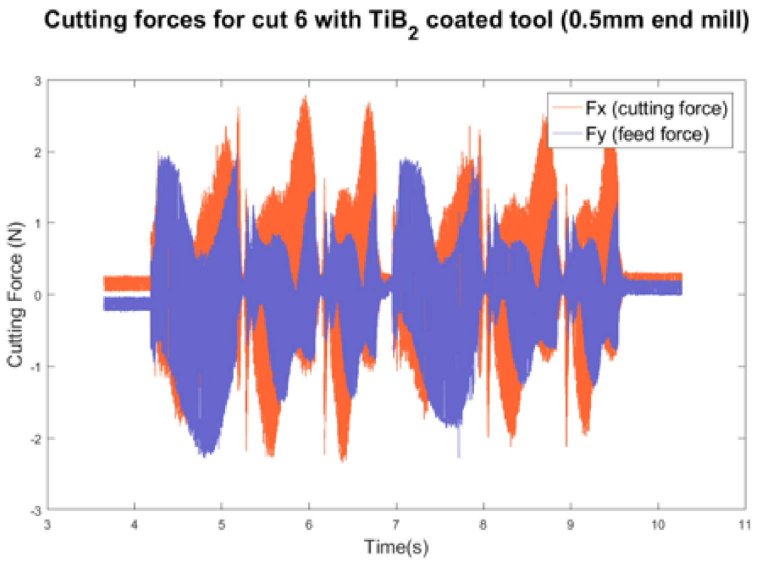

Figure 9.10: Cutting forces signatures for cuts 4 - 6 (see Figure 9.5) made with tools coated with TiB_2.

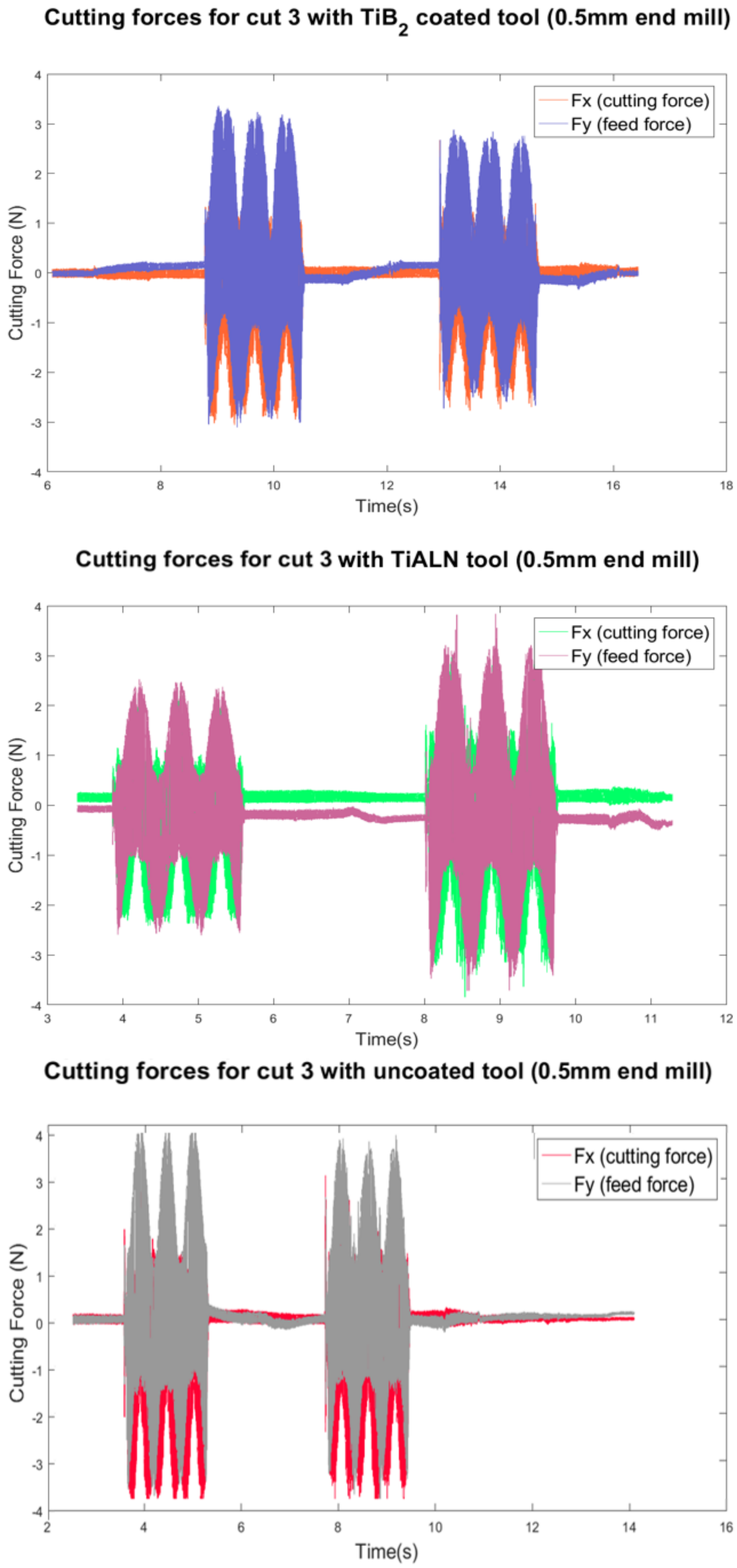

Figure 9.11: When the same cut (cut 3) is compared, differences in magnitudes of force can be seen.

The similar force signatures across tool coating indicates that each tool experiences similar forces throughout its life.

9.3.2 *Tool Wear*

For each of the sets of tools, tool wear curves were constructed. This fulfils two purposes:

I. To verify that the construction of a tool wear curve for micro-end-mills results in the classic tool wear curve as for straight cuts. This simply requires the observation of tool wear curves.

II. To compare the length of tool life between straight line cuts and geometrically more complex cuts for the two coatings: AlTiN and Uncoated.

9.3.2.1 *Wear Curve Behaviour of Micro-milling Tools in Practical Applications as compared with Straight Cuts*

Face and flank wear curves for the two tools measured for uncoated and TiB2 coated tools are provided in Figures and respectively. The wear is given as the average of the measurements from Backscattered Electron (BSE) and Secondary Electron (SE) images for each tooth. Due to dramatically different measurements between BSE and SE images for the teeth of the AlTiN coated tools, it was determined that uncertainty in the data was such that no useful conclusions could be drawn although there was suggestion of a wear curve for individual teeth (Figure 9.12).

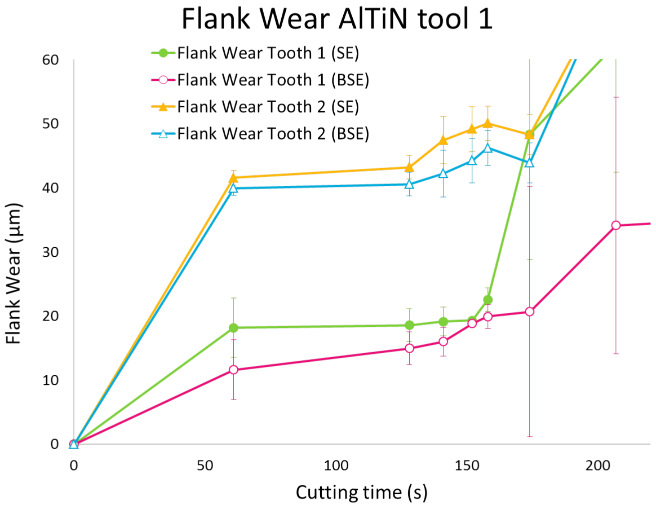

Figure 9.12: Although there is suggestion of a wear curve in the raw data, the averaged data is not conclusive due to high uncertainty.

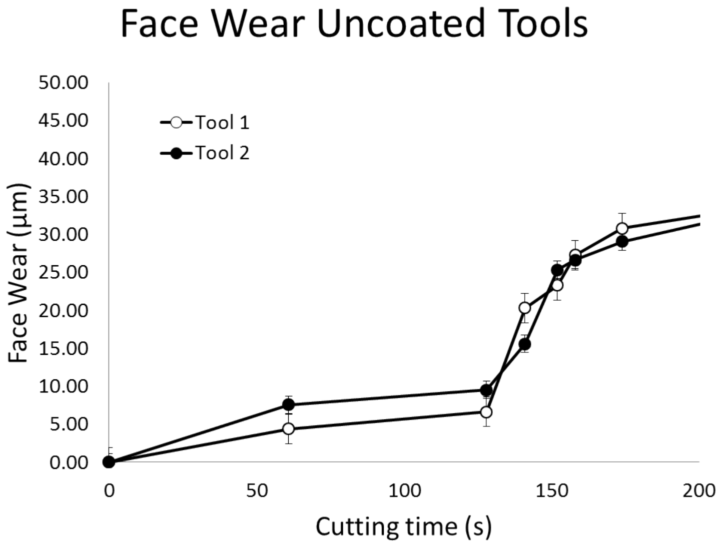

(a) Face wear for uncoated tools used to machine realistic features.

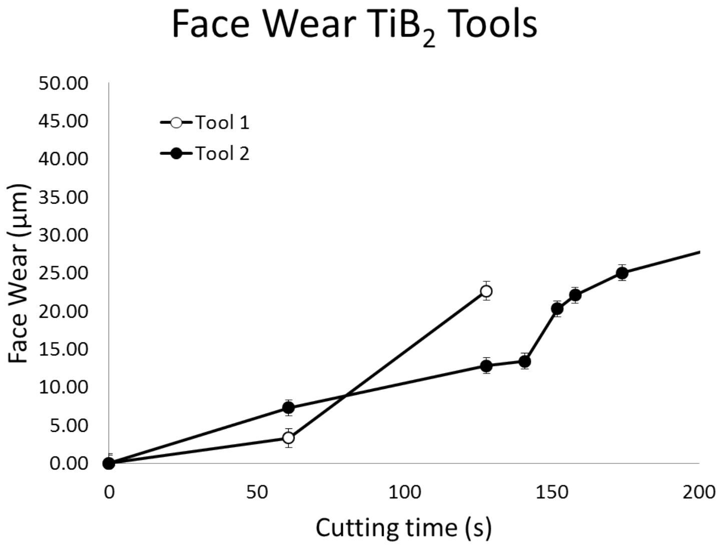

(b) Face wear for TiB2 coated tools used to machine realistic features..

Figure 9.13: Comparison of face wear for uncoated and TiB2 coated tools.

The face wear for both uncoated and TiB_2 coated tools, the former especially, follows the same wear curves seen in the straight-slot machining tests, verifying that wear curves can be identified in more realistic environments as well as the type of strict straight slot testing that has occurred thus far. This is important because previously it had not been verified that the micro-tools behave as predicted from simplistic cutting trials in a real-world environment. This moves the level of research from TRL3 to TRL5. The flank wear curves show a similar result, with both tools producing wear curves.

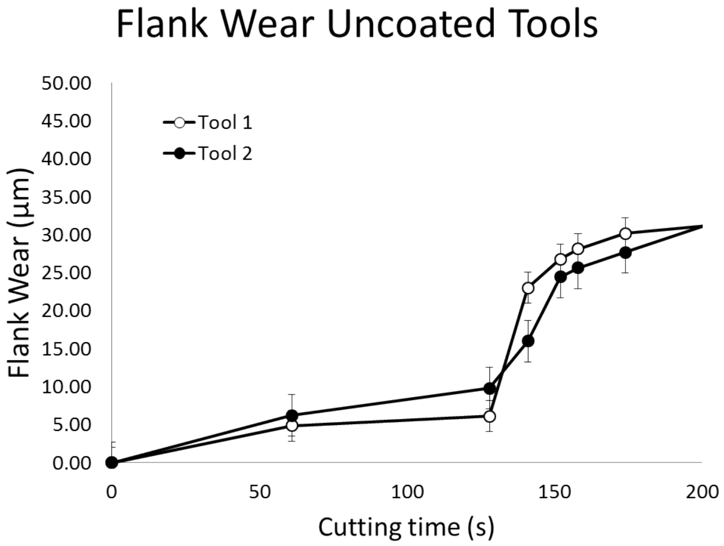

(a) Flank wear for uncoated tools used to machine realistic features.

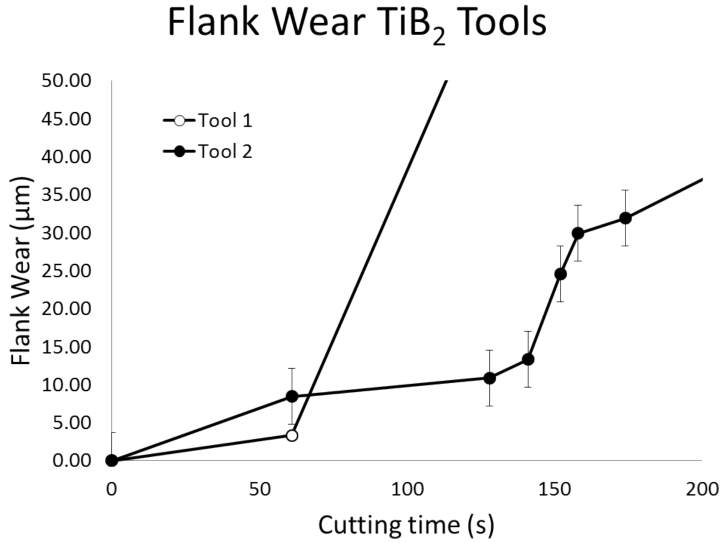

(b) Flank wear for TiB2 coated tools used to machine realistic features..

Figure 9.14: Comparison of flank wear for uncoated and TiB2 coated tools.

9.3.2.2 *Comparison of tool life coatings between straight line cuts and realistic geometries*

Comparisons could not reasonably be made between straight line and geometrically more complex cuts due to significant differences in tool life. The overall tool lives measured for tools used to machine straight slots were much shorter. This raises an important issue when measuring micro-milling: the small size of the tools means that measurement has significance for tool wear. Because the tools are so small, run-out has a large impact on cutting forces on the teeth.There is also an experimental issue: abrupt, interrupted cuts such as straight lines exert extreme forces at the start of the slot which wears the tools faster than a longer, continuous tool path would [273]. This is due to mechanical shock applied to the teeth at the start of cuts.

It is also important to note that since only two tools for each coating was measured, it is not possible to draw statistically significant conclusions between the two studies, and between different coatings in this study. Difficult measuring conditions results in high uncertainty, especially for the AlTiN tools. However, it can be seen from the results in both studies that some information can be drawn from the results. Figure 9.15a shows the face wear for three different types of tool: one uncoated, one TiB2 coated and one AlTiN coated. Although uncertainty is high, it appears that the steady state wear region for the AlTiN lasts longer for the AlTiN tool. Similarly, the life of the TiB2 coated tool is shorter. This is also seen in Figure 9.15b.

It should be noted that scales for the two graphs are different, since it was not possible to estimate sliding distance easily. In reality, the tools used to machine more complex geometries actually lasted longer due to the shocks to the tools applied at the start of each slot when milling straight slots.

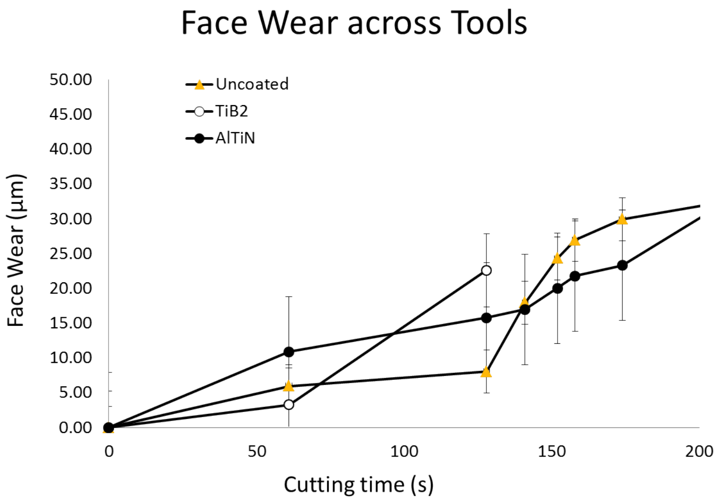

(a) Face wear for different coatings; tools used to machine realistic features.

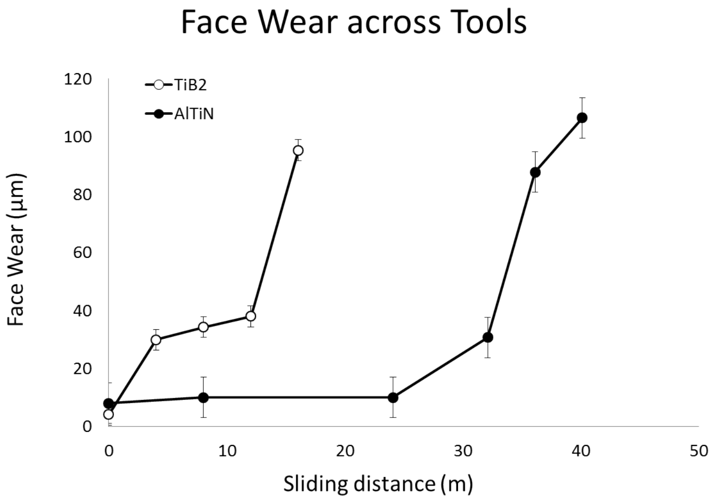

(b) Face wear for different coatings; tools used to machine straight slots.

Figure 9.15: Comparison of face wear for realistic cuts and straight slots.

A second perspective can be seen in Figure 9.16b. This time, the face wear within error bounds is shown. This highlights the fact that it is difficult to determine with certainty over large distances which tool performs better. However, at the extremes of the curve (beginning and end) errors overlap less and it is likely that the uncoated tool is performing better (slower run-in and later rapid failure 9.16a) than the AlTiN tool. The TiB2 fractures early, as in the case of the straight cut tests (Figure 9.16b).

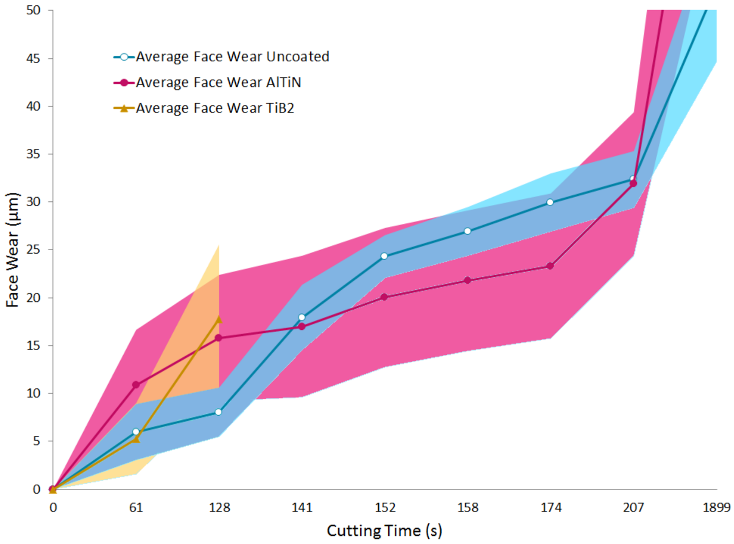

(a) Face wear for different coatings; tools used to machine realistic features. Data shown in darker lines is surrounded by a lighter shaded area which represents the error region for each tool.

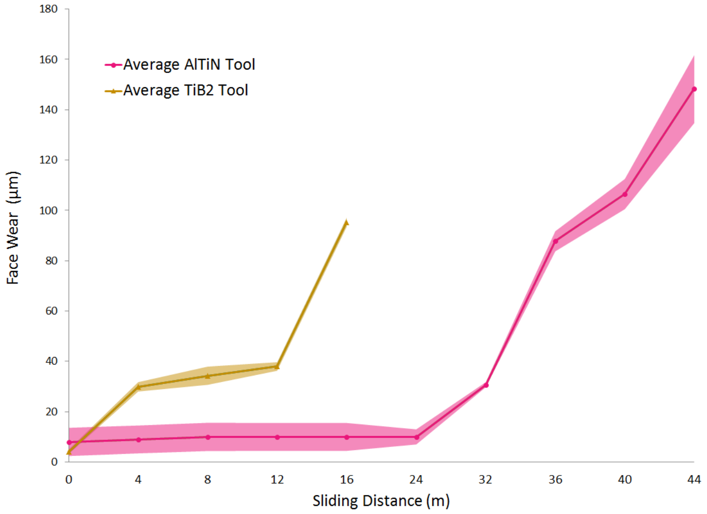

(b) Face wear for different coatings; tools used to machine straight slots.

Figure 9.16: Comparison of face wear for realistic cuts and straight slots, with error bounds shaded for clarity.

Therefore, the tool lives exhibited for straight line cuts bear some relation to the tool lives seen for more realistic cutting scenarios. In spite of the much higher wear rates seen for slot cutting, comparisons can be made between tools in this laboratory environment and then used to inform tool choices in a more realistic environment.

9.3.3 *Industrial Outcomes*

This work has applications for Kyocera-SGS, providing an insight into the way their tools wear which can be used to inform tool design. It builds upon the straight slot work and verifies that the micro-milling tools behave similarly in a realistic machining environment.

9.4 CONCLUSIONS

The conclusion that can be drawn from this validation experiment is that although the methodology described in chapter 5 is valid and useful for characterising the wear of micro-milling tools, measurement of the tools regularly influences the final result. The process of removing the tools subjects them to minor damage and wear, although this does not to be significant. More importantly, the tools cannot be returned to the exact condition - run out and length of tool not clamped - that they held initially, in spite of efforts to do so.

An issue with the data analysed is the high error bounds - this arises from limited data collection due to time constraints, and the more volatile wear of the micro tools as compared with macro tools - for example, susceptibility to fracture. Some points of interest were noted:

I. The face wear and flank wear for both uncoated and TiB2 coated tools used to machine complex geometries follow the traditional wear curve as seen in the straight-slot machining tests.

II. This verifies that wear curves can be identified in more realistic environments as well as straight slot testing.

III. Abrupt, interrupted cuts as carried out in previous straight slot milling exert extreme forces at the start of the slot which wears the tools faster than a longer, continuous tool path would.

IV. Tool lives exhibited for straight line cuts can be related to tool lives seen for more realistic cutting scenarios.

V. This can be used to inform tool choices in a more realistic environment.

This data provides an interesting insight into the applicability of straight cut testing to a realistic environment, with the caveat that more measurements would be required to further validate this theory.

CONCLUSIONS

10

10.1 INTRODUCTION

To conclude the work presented in this thesis the outcomes are considered in terms of the objectives identified in chapter 1. For clarity, the conclusion is split into two parts: Wire Electrical Discharge Machining (WEDM) and micro-milling. The section is closed with a formal statement of novelty.

As described in section 1.4, the aim of this work is to develop advanced manufacturing operations and improve process outcomes for small static and micro-mechanical parts in terms of material removal rate and surface finish and quality, and tool wear reduction. The purpose of this was to provide concrete research findings to contribute to both research and industrial environments. It is described how each of the objectives has been met in order to fulfill this aim.

10.2 WIRE ELECTRICAL DISCHARGE MACHINING - KEY OUTCOMES AND CONCLUSIONS

10.2.1 *Outcomes*

Outcomes for WEDM are described herein in terms of the objectives identified in chapter 1. Currently, primary outcomes are academic in the sense that even application to parts represents a theoretical possibility rather than actual implementation in industry. However, transfer to small-scale industry would be relatively easy to implement as described in Section 10.2.3.

10.2.1.1 *Objective 1: Review into important parameters in WEDM*

Literature review revealed that parameters affecting discharge energy had high significance for Material Removal Rate (MRR) and Surface Finish (SF). It showed capability for machining small micromechanical parts as described in chapter 1 but it was clear that there were difficulties in solving the optimisation problem between MRR and SF. It was clear that WEDM of ultra-thin gears had seen little investigation and thin parts presented difficulties in machining stable sparking and consistent surface finish. This also resulted in low MRR. The literature review informed Objectives 1 and 2, by identifying research gaps and allowing efficient Design of Experiments (DOE).

10.2.1.2 *Objective 2: Testing machining parameters of WEDM to speed up production times while maintaining part quality, increasing employment of WEDM in industry*

It was possible to produce a significant improvement in surface finish by optimising the machining parameters used. The R_a value was improved by almost an order of magnitude. This conclusion is significant both in terms of agreement with literature, which warranted further study using the setup available, and in terms of allowing the design of further experiments to allow furthering of the field by producing parts that have not currently been studied in detail. Investigation of multi-pass methods of improving machining rate and surface finish yielded a research opportunity for developing micromechanical parts efficiently, which lead to Objective 3.

10.2.1.3 *Objective 3: Application and validation of Parameter testing in WEDM to production of micromechanical parts.*

Ultra-thin (0.3 mm) gears were successfully produced using a macro WEDM and techniques for speeding up their production were identified. The work preceding this was based on optimisation of parameters in a pure sense: using straight cuts. This work was able to validate that the techniques investigated in subsec:Objective-1:-Review and subsec:Objective-2:-Testing are applicable to producing micromechanical parts, at least in the context of small or prototype runs. This meets the objective and contributes to the overall aim of this work.

10.2.2 *Academic Impact of Research into WEDM*

The academic impact of this work manifests itself in the form of the provision of both data and techniques which can be used in their current form or developed further. This work has been disseminated to the scientific community through international conference communication (CIRP HPC 2018) and publication [274]. The premise that machining times can be improved provides a platform for further study (identified in subsection 10.2.5) both at the Advanced Manufacturing Research Centre (AMRC) and other institutions.

10.2.3 *Industrial Relevance and Impact of Research into WEDM*

Production of miniature gears and parts with complex geometries for small runs is particularly appropriate in industrial applications for small-scale production of parts or prototyping of new geometries. This is useful for industrial R&D as well as manufacturers for whom it is not appropriate to invest in larger-scale technologies such as hobbing. Examples of such companies are a small watch company, the Bremont Watch Company, who are looking to prototype novel gear geometries for their watches and will continue to do so in order to provide the novelty that the market requests. Being able to reduce machining times and produce small runs successfully allows such R&D. These outputs strengthen the reputation of The University of Sheffield and the University of Sheffield's Advanced Manufacturing Research Centre.

10.2.4 *Limitations*

There are both limitations in the existing work that has been carried out, and also considerations to be made when applying the technology investigated to industry. Primary limitations with the work carried out thus far have been machine-based. WEDM itself is limited by wire size in terms of the small sizes of gear that can be produced and thus it has not been possible to produce gears below diameter 6 mm. Micro-WEDM exists and has been researched in literature (chapter 2). The primary barrier to small companies carrying out R&D using WEDM is purchase of equipment and training. The latter has less significance, since typically WEDM are comparatively simple to program and work with. Equipment purchase costs are high and a model such as that employed by the AMRC presents a possible solution: an area with membership fees which provides shared resources. The AMRC currently has no WEDM capability which presents difficulty with this.

Technologically, the primary issue with WEDM is the low speed of machining which results in low productivity. On the other hand, set-up times are slow for faster production methods such as hobbing and stamping and thus WEDM provides an excellent compromise for prototyping of small runs of gears. However, it is likely to be many years before WEDM presents itself as an appropriate method for large-scale machining of gears and complex mechanical parts.

10.2.5 *Future Work*

Early work in WEDM identified that WEDM had the capability to produce the type of surface finish required for very small gears (chapter 2). The results identified a need to relate part geometry to surface finish, and in so doing transfer the research applicability from a research environment to an industrial environment. Investigations into the modified geometries yielded a methodology for reducing machining time while maintaining an acceptable surface finish for small gears (chapter 8). An immediate area for future work would be to investigate further the production of these gears, reducing the size of them. 0.3 mm gears are suitably small for use in micro-mechanical gearboxes, but the diameter should be reduced to below 5 mm, and the thickness to 0.3 mm. Further to this, there is progress to be made with the surface finish of the gears.

To achieve the above, a smaller wire diameter is required. This would not only enable smaller geometries to be created, but also would raise the question as to the effect that wire diameter has on machining stability (in this instance probability of sparking). As micromechanical parts get smaller, it will be necessary to use smaller wire diameters to meet requirements and in spite of the continual replacement of wire, there is inevitably wear to the wire in the form of material melting and removal. The rate at which the wire is replaced (wire speed) is limited by machine capabilities and work should take place on smaller diameter machines to establish the speed at which micro-EDM can take place and to maximise this.

From a tribological point of view, it would be valuable to investigate the properties of different lubricants, both liquid and solid (for example, light synthetic oils or dry lubricants such as PTFE or graphite), as the latter is more appropriate on the very small scale. These will depend on the topology of the machined surface which can be closely controlled by the machining parameters and could provide opportunities for increasing efficiency and lifetime of miniature gears. The difficulties optimising machining parameters in WEDM 4 continues to provide research motivation in the field.

10.3 MICRO-MILLING - KEY OUTCOMES AND CONCLUSIONS

10.3.1 *Outcomes*

As with WEDM, each objectives and the corresponding outcomes are identified herein, to determine the extent to which the project aim, defined in chapter 1 has been met.

10.3.1.1 *Objective 1: Review into the micro-milling process*

Review into the micro-milling process revealed that whereas on the macro-scale tool wear studies follow ISO standards (such as ISO8688-1 and ISO8688-2 [153, 154]) which determine parameters which can be used and make tool studies comparable, these are not appropriate for micro studies. Since it was clear from literature that micro-tool wear is poorly characterised which leads to unstable machining and difficulty predicting tool life, there was identification of a clear need for a standardised tool wear measurement protocol.

It was clear that although there has been some investigation into tool life enhancement through specialist coatings and investigation of geometries, there was insufficient understanding of the tribological behaviour of the tools and coatings when compared with macro-scale tools. Thus, a need to identify novel coatings and analyse their tribological behaviour (objective 3) was identified.

10.3.1.2 *Objective 2: Micro–milling wear methodology*

Based on the measurements that are taken for macro-sized tools and the relevant standards, measurement methods were identified in order to produce a protocol for measuring micro tool wear. This has enabled unification of research into micro-milling tool wear and measurement therein, thus enabling more collaborative work and sharing of results/building on existing research to increase common understanding. The ability to repeatedly characterise wear curves for different tools has can be used to maximise process efficiency in industry.

Tests used to validate the protocol indicated that it allows the wear curve of sub-millimetre micro end mills to be plotted. Furthermore, a novel method of measuring machining distance was proposed: whereas normally cutting time or distance are used, sliding distance and it's conversion factors have been introduced. This has provided a much more appropriate measure of reporting micro end mill wear since it accounts for different cutting speeds and feed rates, allowing comparison between coatings.

These investigations determined the appropriateness of techniques such as SEM, including use of backscattered electrons, and examining the chips for examining wear mechanisms. Thus suggested that it is possible to understand the wear mechanisms taking place, which is useful when designing coatings for micro end mills and enabled objective 3 to be undertaken.

10.3.1.3 *Objective 3: Use of methodology to investigate novel coatings and geometries, with a view to increasing tool life*

Having achieved objective 2, two studies took place: the first on investigating novel coatings as a means of extending tool life; the second on modified tool geometries. Three sets of carbide tools were tested for three different materials: brass, titanium and Hastelloy. For each material, two types of coating were tested: TiB2 and AlTiN for brass, and AlTiN vs two proprietary coatings for titanium and Hastelloy. A method for evaluating the improvement of tools was devised and published [275]: the elongation of the steady-state region (SRR) of the tool wear curves for micro-milling was considered as a means to improve the prediction of the evolution of tool wear. The ratio between run-in period (RIP) and SSR was developed. This novel metric (RIP:SSR) ratio proved to be effective in assessing the performance of tools. For each material investigated, one of the coatings yielded a longer SSR. It was concluded that coating design can be used to extend the length of the steady state wear region and not simply reduce overall tool wear. This allowed optimal coatings to be selected to reduce the length of tool run-in, thus allowing the SSR to be reached more quickly.

Wear was observed using SEM and pin-on-disc testing of discs coated with each material took place. This enabled further understanding of the differences between wear on the macro-scale and the micro-scale, in terms of milling. It was determined that the very small sizes of the tools meant that a small cutting-edge radius, corresponding high temperatures and stresses conspired to add wear mechanisms seen much less for macro-tools. Whereas abrasive and adhesive mechanisms are known to be dominant in macro-milling, at the micro-scale the effects of impact wear and cracking are exacerbated due to relatively large workpiece grain size and very high stresses where tool-workpiece contact is small.

For micro-tools cutting edge radius is typically significant compared with tooth size which compromises geometrical accuracy of parts. It was seen that wear is steadier and easier to predict for the radiused tools, but sharper tools should be used where high precision is required.

10.3.1.4 *Objective 4: Application of fundamental research to and industrial context*

A significant requirement in any piece of work whose purpose is to have industrial applications is to increase its technology readiness level (as discussed in section). Using a standard testpiece, both face and flank wear for two of the tool coatings measured followed a traditional wear curve, which supported the results from chapter 6. This verified that tool lives exhibited for straight line cuts can be related to tool lives seen in a machining context and supports the success of Objective 3. A challenge is presented in comparing straight cuts to longer, more continuous cuts since abrupt, interrupted cuts exert extreme forces at the start of the slot which wears the tools faster than a longer, continuous tool path.

10.3.2 *Academic Impact of Micro-milling Research*

The publication of a tool wear measurement protocol for micro mills allows the scientific community to produce comparable studies which significantly facilitates advancement of the field. Two international conferences (STLE Tribology Frontiers 2019, Euromat 2019) have communicated this work to the scientific community. Data for analysis on micro-tool wear has been obtained for numerous materials with application in aerospace. This provides opportunity for further analysis of the wear curves of micro-tools [13, 276]. Furthermore, the coatings studies carried out can be compared with existing studies to broaden the existing knowledge base on appropriate tool coatings on the small scale, since novel coatings and material-coating combinations were investigated.

The application of micro-tool wear measurement techniques has not previously taken place for real-life industrial parts, and the work carried out herein presents a novel perspective on tool wear and facilitates the integrating of existing micro-milling research into industry. As much motivation and indeed external funding for work into micro-tooling comes from industry, this is essential.

10.3.3 *Industrial Relevance and Impact of Micro-milling Research*

The research into tribological characteristics of different coatings on the micro-scale has resulted in Kyocera being able to determine more appropriate coatings than have been used previously in industry. This has allowed selection of the most appropriate coatings to maximise the life of their micro-sized machine tools, delivering a competitive advantage by potentially enabling customers to significantly increase the time between tool changes.

Important results have been presented here that demonstrate a decrease in tool wear and thus improvements to machining accuracy and reduced production costs. In doing so, this work has resulted in significant elongation of the SSR of the tool wear curve for micro-milling as a means to improve the prediction of the evolution of tool wear. This allows cutting processes to be modified to maximise geometrical accuracy as the tool wears and to measure the efficacy of applying different coatings to micro tools.

10.3.4 *Limitations*

Primary limitations in the results that have been obtained in this work relate to size: smaller tools could not be investigated using the machining centre available at the AMRC and the result of this was that the smallest tools measured were 0.5 mm in diameter. There are also limitations in investigating micro-mill wear using visual analysis and removing tools in the sense that too removal and replacement by eye can result in significant disturbance to tool position and run-out and as this process of tool removal and measurement cannot be automated, currently, errors are inherently quite high.

10.3.5 *Future Work*

Micro-milling has both large uptake currently and a huge amount of potential as a leading process in micro-engineering.There is value in further investigating both the novel application of coatings that have previously only be used in a macro-milling and in modifying the design of these coatings to increase the SSR of the tools.

Typically, micro-milling tools are designed to cut at speeds in the order of 100,000 rev/min. Typically, these high speeds reduce chip size, which reduces machining forces and the temperature at the tool-workpiece interface which is very significant for micro tools. Furthermore, the smaller chips tend to be more easily evacuated from between the flutes and therefore chip clogging (which can cause catastrophic failure) is less likely. A spindle speed of 50,000 RPM as used here was able to give a representative idea of how the micro-milling tools wear and also represents a speed that would be used in industry; but it is at the slow end of the scale. A higher spindle speed would enable tests to be run for longer with reduced tool breakage and studies into the relationship between spindle speed and tool wear rates would in themselves be useful and could be used to support (or improve) current manufacturer recommendations.

Future analysis of workpieces to plot surface finish with tool wear in order to determine whether SF deteriorates less rapidly for tools with cutting edge radius would be interesting. This could be used to characterise the relationship between surface finish and number of teeth, which has significance in both macro- and micro-machining, and how this changes on the micro-scale.

10.4 FORMAL STATEMENT OF NOVELTY

The aim of this work was to improve process outcomes in advanced manufacturing of micro parts. This primarily came about by reduction of wear in micro tools which in turn led to improved MRR and SF. The field of WEDM is vast and well-researched, and can be abstract. Thus it is important to identify research areas with direct application or at least wherein the novelty of the research has potential application. On the other hand, micro-milling research can often be very applied and there are not standardised procedures for measuring micro-tool wear.

Novelty in both the field of WEDM and micro-milling has been achieved. This is supported by publication in both areas, as described in the following paragraphs.

In WEDM, a novel application of multi-pass methods was used to produce ultra-thin micro gears [274]. The optimisation of the machining parameters based on part geometry which has not been explained in detail can be applied to future research and industrial work. Very little work in WEDM has focussed on very thin parts due to difficulty with maintaining a steady sparking rate, and the micro-gears produced present a new body of research into this.

For micro-milling, it was clear that there was a key issue with unifying the research into the measurement of tools, making it difficult to compare studies across the field as takes place on the macro scale. To solve this issue, a novel method of measuring tool wear has developed [13]. Previously, no such protocol existed. This took into account the results from literature and early studies carried out during the course of the PhD. The novel protocol enables micro-milling tools to be measured to a high-standard as with macro-milling, in such a way that similar studies are comparable. This is important because a coherent body of literature allows research into micro-milling tool design and lifespan to progress faster than sporadic study.

The investigation of novel coatings for micro-mills and their impact on tool wear [277] allows coatings which had previously not been applied to macro-mills to be used on the micro-scale. It is necessary to study coatings for micro-tools since typically in industry only one or two coating options are provided, which has restricted some studies into the efficacy of micro-tools.

A more in-depth understanding of the wear mechanisms involved in micro-mill wear has been achieved by studying the wear mechanisms on a micro-scale for tools used in a workshop environment and coated discs in a laboratory environment. This identified links between the wear of micro and macro tools which has not previously been considered in detail. Furthermore, previous work has investigated primarily straight slots or shoulder cuts in mulling, due to the described difficulties in measuring micro-tool wear. While this has been important for fundamental investigations, there is a need to increase the technology readiness level of existing wear studies so that the results can be applied directly to industry. The authors present, for the first time, a comparison between fundamental tool wear studies and tool wear observed when producing testpieces representative to micro-industrial parts. This presents a novel perspective on tool wear and facilitates the integrating of existing micro-milling research into industry.

Part IV

BIBLIOGRAPHY

BIBLIOGRAPHY

[1] A. Kilpatrick and T. Lawson. 'On the nature of industrial decline in the UK.' In: *Cambridge Journal of Economics* 4.1 (1980), pp. 85–102 (cit. on p. 3).

[2] D. E. Keeble. 'Industrial decline, regional policy and the urban - rural manufacturing shift in the United Kingdom.' In: *Environment and Planning A* 12.8 (1980), pp. 945–962 (cit. on p. 3).

[3] F. Jovane, E. Westkämper, and D. Williams. *The ManuFuture Road: Towards Competitive and Sustainable High-Adding-Value Manufacturing*. Springer Berlin Heidelberg, 2008 (cit. on p. 3).

[4] K. Jemielniak and P. Arrazola. 'Application of AE and cutting force signals in tool condition monitoring in micro-milling.' In: *CIRP Journal of Manufacturing Science and Technology* 1.2 (2008), pp. 97–102 (cit. on pp. 3, 33, 121).

[5] A. Aramcharoen and P. Mativenga. 'Size effect and tool geometry in micromilling of tool steel.' In: *Precision Engineering* 33.4 (2009), pp. 402–407 (cit. on pp. 3, 185).

[6] W. J. Endres and R. K. Kountanya. 'The effects of corner radius and edge radius on tool flank wear.' In: *Journal of Manufacturing Processes* 4.2 (2002), pp. 89–96 (cit. on pp. 3, 119, 155).

[7] J. Fulemova and Z. Janda. 'Influence of the cutting edge radius and the cutting edge preparation on tool life and cutting forces at inserts with wiper geometry.' In: *Procedia Engineering* 69 (2014), pp. 565–573 (cit. on pp. 3, 4, 26, 119, 155).

[8] K. Yang, Y.-c. Liang, K.-n. Zheng, Q.-s. Bai, and W.-q. Chen. 'Tool edge radius effect on cutting temperature in micro-end-milling process.' In: *The International Journal of Advanced Manufacturing Technology* 52.9-12 (2011), pp. 905–912 (cit. on pp. 3, 4, 156).

[9] İ. Ucun, K. Aslantas, and F. Bedir. 'An experimental investigation of the effect of coating material on tool wear in micro milling of Inconel 718 super alloy.' In: *Wear* 300.1-2 (2013), pp. 8–19 (cit. on pp. 4, 12, 93, 125, 185).

[10] A. Aramcharoen, P. Mativenga, S. Yang, K. Cooke, and D. Teer. 'Evaluation and selection of hard coatings for micro milling of hardened tool steel.' In: *International Journal of Machine Tools and Manufacture* 48.14 (2008), pp. 1578–1584 (cit. on pp. 4, 93, 121, 125, 185).

[11] K.-D. Bouzakis, N. Michailidis, G. Skordaris, S. Kombogiannis, S. Hadjiyiannis, K. Efstathiou, G. Erkens, S. Rambadt, and I. Wirth. 'Effect of the cutting edge radius and its manufacturing procedure, on the milling performance of PVD coated cemented carbide inserts.' In: *CIRP Annals-Manufacturing Technology* 51.1 (2002), pp. 61–64 (cit. on p. 4).

[12] Y. Wang, B. Zou, C. Huang, Z. Liu, and P. Yao. 'The micro-cutting performance of cermet and coated WC micro-mills in machining of TC4 alloy micro-grooves.' In: *The International Journal of Advanced Manufacturing Technology* (2018) (cit. on pp. 4, 93, 124, 126, 127).

[13] L. Alhadeff, M. Marshall, D. Curtis, and T. Slatter. 'Protocol for tool wear measurement in micro-milling.' In: *Wear* 420 (2019), pp. 54–67 (cit. on pp. 4, 124, 125, 131, 187, 210, 212).

[14] N. Tosun, C. Cogun, and A. Inan. 'The effect of cutting parameters on workpiece surface roughness in wire EDM.' In: *Machining Science and Technology* 7.2 (2003), pp. 209–219 (cit. on pp. 4, 26, 31, 57, 69, 86, 88, 169).

[15] R. Kumar and S. Singh. 'Current research trends in wire electrical discharge machining: an overview.' In: *International Journal on Emerging Technologies* 3.1 (2012), pp. 33–40 (cit. on pp. 4, 26, 57, 78, 167).

[16] K. Ho, S. Newman, S. Rahimifard, and R. Allen. 'State of the art in wire electrical discharge machining (WEDM).' In: *International Journal of Machine Tools and Manufacture* 44.12 (2004), pp. 1247–1259 (cit. on pp. 4, 13, 16, 31, 57, 58, 70, 167).

[17] J. Huang, Y. Liao, and W. Hsue. 'Determination of finish-cutting operation number and machining-parameters setting in wire electrical discharge machining.' In: *Journal of Materials Processing Technology* 87.1 (1999), pp. 69–81 (cit. on pp. 4, 16, 17, 26, 29, 167, 181).

[18] K. K. Jangra. 'An experimental study for multi-pass cutting operation in wire electrical discharge machining of WC-5.3% Co composite.' In: *The International Journal of Advanced Manufacturing Technology* 76.5-8 (2015), pp. 971–982 (cit. on pp. 4, 28, 30, 69, 81, 84, 88).

[19] S. Sarkar, K. Ghosh, S. Mitra, and B. Bhattacharyya. 'An integrated approach to optimization of WEDM combining single-pass and multipass cutting operation.' In: *Materials and Manufacturing Processes* 25.8 (2010), pp. 799–807 (cit. on pp. 4, 69, 84, 88).

[20] X. Yang and C. Richard Liu. 'Machining titanium and its alloys.' In: *Machining Science and Technology* 3.1 (1999), pp. 107–139 (cit. on pp. 4, 5).

[21] D. Stephenson and J. Agapiou. *Metal Cutting Theory and Practice, Third Edition*. CRC Press, 2016 (cit. on p. 5).

[22] ArcamEBM system. *Grade 2 Titanium*. Oct. 2015 (cit. on p. 5).

[23] A. Hosseini and H. A. Kishawy. 'Cutting tool materials and tool wear.' In: *Machining of Titanium Alloys*. Ed. by J. P. Davim. Springer, 2014, pp. 31–56 (cit. on p. 5).

[24] F. Campbell. *Manufacturing Technology for Aerospace Structural Materials*. Aerospace engineering materials science. Elsevier Science, 2011 (cit. on pp. 5, 6).

[25] E. Ezugwu and Z. Wang. 'Titanium alloys and their machinability - a review.' In: *Journal of materials processing technology* 68.3 (1997), pp. 262–274 (cit. on pp. 5–7, 126, 139).

[26] A. Machado and J. Wallbank. 'Machining of titanium and its alloys - a review.' In: *Proceedings of the Institution of Mechanical Engineers, Part B: Journal of Engineering Manufacture* 204.1 (1990), pp. 53–60 (cit. on p. 5).

[27] A. Pramanik. 'Problems and solutions in machining of titanium alloys.' In: *The International Journal of Advanced Manufacturing Technology* 70.5-8 (2014), pp. 919–928 (cit. on pp. 5–7).

[28] K. Maekawa, T. Obikawa, Y. Yamane, and T. Childs. *Metal Machining: Theory and Applications*. Elsevier Science, 2013 (cit. on p. 5).

[29] S. Bhaumik, C. Divakar, and A. Singh. 'Machining Ti-6Al-4V alloy with a wBN-cBN composite tool.' In: *Materials & Design* 16.4 (1995), pp. 221–226 (cit. on p. 5).

[30] R. Komanduri and B. Von Turkovich. 'New observations on the mechanism of chip formation when machining titanium alloys.' In: *Wear* 69.2 (1981), pp. 179–188 (cit. on pp. 6, 7).

[31] J. Barry, G. Byrne, and D. Lennon. 'Observations on chip formation and acoustic emission in machining Ti–6Al–4V alloy.' In: *International Journal of Machine Tools and Manufacture* 41.7 (2001), pp. 1055–1070 (cit. on p. 6).

[32] M. Rahman, Z.-G. Wang, and Y.-S. Wong. 'A review on high-speed machining of titanium alloys.' In: *JSME International Journal Series C* 49.1 (2006), pp. 11–20 (cit. on p. 7).

[33] J. Pérez, J. Llorente, J. Sanchez, et al. 'Advanced cutting conditions for the milling of aeronautical alloys.' In: *Journal of Materials Processing Technology* 100.1 (2000), pp. 1–11 (cit. on p. 7).

[34] J. Davis and A. Committee. *Nickel, Cobalt, and Their Alloys*. ASM specialty handbook. ASM International, 2000 (cit. on p. 7).

[35] H. S. Mali and D. R. Unune. 'Machinability of Nickel-Based Superalloys: An Overview.' In: (2014) (cit. on p. 7).

[36] D. Zhu, X. Zhang, and H. Ding. 'Tool wear characteristics in machining of nickel-based superalloys.' In: *International Journal of Machine Tools and Manufacture* 64 (2013), pp. 60–77 (cit. on pp. 7, 129).

[37] Copper Development Association. *Cost-Effective Manufacturing: Machining Brass, Copper and its Alloys*. Oct. 1992 (cit. on p. 8).

[38] E. Trent. 'Metal Cutting: Fourth Edition.' In: Butterworth Heinmann, 2000. Chap. 9, p. 190 (cit. on pp. 8, 10).

[39] P. Hoffman, E. Hopewell, and B. Janes. *Precision Machining Technology*. Cengage Learning, 2014 (cit. on p. 8).

[40] M. Bauccio and A. Metals. *ASM Metals Reference Book, 3rd Edition:* ASM International, 1993 (cit. on p. 8).

[41] K. Medicus, M. Davies, B. Dutterer, C. Evans, and R. Fielder. 'Tool wear and surface finish in high speed milling of aluminum bronze.' In: (2001) (cit. on pp. 8, 34, 92).

[42] H. Meigh. *Cast and Wrought Aluminium Bronzes: Properties, Processes and Structure*. Book (Institute of Materials (Great Britain))). IOM Communications, 2000 (cit. on p. 8).

[43] Y. Li, T. L. Ngai, W. Xia, Y. Long, and D. Zhang. 'A study of aluminum bronze adhesion on tools during turning.' In: *Journal of materials processing technology* 138.1 (2003), pp. 479–483 (cit. on p. 8).

[44] O. Mendes, R. Avila, A. Abrao, P. Reis, and J. Paulo Davim. 'The performance of cutting fluids when machining aluminium alloys.' In: *Industrial Lubrication and Tribology* 58.5 (2006), pp. 260–268 (cit. on p. 10).

[45] M. Nouari, G. List, F. Girot, and D. Coupard. 'Experimental analysis and optimisation of tool wear in dry machining of aluminium alloys.' In: *Wear* 255.7 (2003), pp. 1359–1368 (cit. on p. 10).

[46] F. Klocke and G. Eisenblätter. 'Dry cutting.' In: *CIRP Annals-Manufacturing Technology* 46.2 (1997), pp. 519–526 (cit. on p. 10).

[47] Sandvik Cormoront UK. 'Machining Aluminium Alloys.' In: *Aircraft Engineering and Aerospace Technology* 61.1 (Jan. 1989), p. 12014 (cit. on p. 10).

[48] B. Boswell and M. N. Islam. 'Feasibility study of adopting minimal quantities of lubrication for end milling aluminium.' In: *Proceedings of the World Congress on Engineering*. Vol. 3. 2012, pp. 1–5 (cit. on p. 10).

[49] C. Tsao. 'Grey–Taguchi method to optimize the milling parameters of aluminum alloy.' In: *The International Journal of Advanced Manufacturing Technology* 40.1-2 (2009), pp. 41–48 (cit. on p. 10).

[50] J. Kelly and M. Cotterell. 'Minimal lubrication machining of aluminium alloys.' In: *Journal of Materials Processing Technology* 120.1 (2002), pp. 327–334 (cit. on p. 10).

[51] C. Reymondin, R. Bandi-Tebbutt, G. Monnier, D. Jeanneret, E. technique de la Vallée de Joux (Le Sentier), and U. Pelaratti. *The Theory of Horology*. Swiss Federation of Technical Colleges, 1999 (cit. on pp. 11, 94, 129, 141).

[52] L. Défossez. *Théorie Générale de l'Horlogerie*. Ed. by C. S. de le horlogerie La Chaux-de-Fonds. Vol. 1. Ecoles suisses d'horlogerie, 1950 (cit. on p. 11).

[53] H. El-Hofy. *Fundamentals of Machining Processes: Conventional and Nonconventional Processes, Second Edition*. Taylor & Francis, 2013 (cit. on p. 13).

[54] E. Jameson. 'Electrical Discharge Machining.' In: Society of Manufacturing Engineers, 2001. Chap. 7, p. 140 (cit. on pp. 13, 16, 26).

[55] J. A. McGeough. *Advanced methods of machining*. Springer Science & Business Media, 1988 (cit. on p. 13).

[56] K. Gupta and N. Jain. 'Manufacturing of high quality miniature gears by wire electric discharge machining.' In: *Chapter* 40 (2013), pp. 679–696 (cit. on pp. 13, 32).

[57] M. Kunleda, Y. Miyoshi, T. Takaya, N. Nakajima, Y. ZhanBo, and M. Yoshida. 'High speed 3D milling by dry EDM.' In: *CIRP Annals-Manufacturing Technology* 52.1 (2003), pp. 147–150 (cit. on p. 13).

[58] G. Levy and F. Maggi. 'WED machinability comparison of different steel grades.' In: *CIRP Annals-Manufacturing Technology* 39.1 (1990), pp. 183–185 (cit. on p. 13).

[59] K. Ho and S. Newman. 'State of the art electrical discharge machining (EDM).' In: *International Journal of Machine Tools and Manufacture* 43.13 (2003), pp. 1287–1300 (cit. on p. 13).

[60] M. Kunieda, B. Lauwers, K. P. Rajurkar, and B. Schumacher. 'Advancing EDM through fundamental insight into the process.' In: *CIRP Annals-Manufacturing Technology* 54.2 (2005), pp. 64–87 (cit. on pp. 13, 15, 27).

[61] P. T. Eubank, M. R. Patel, M. A. Barrufet, and B. Bozkurt. 'Theoretical models of the electrical discharge machining process. III. The variable mass, cylindrical plasma model.' In: *Journal of applied physics* 73.11 (1993), pp. 7900–7909 (cit. on p. 14).

[62] Engineers Edge, LLC. *Electrical Discharge Machining (EDM) Design Consideration Process Capabilities | Engineers Edge*. Engineersedge.com. 2009 (cit. on p. 14).

[63] J. Portt. *What is Wire EDM?* Oct. 1992 (cit. on p. 14).

[64] R. G. H. Singh. 'Effects of process parameters on material removal rate in WEDM.' In: *Journal of Achievements in Materials and Manufacturing Engineering* 32.1 (2009) (cit. on pp. 14, 25, 79).

[65] G. Boothroyd and A. Winston. 'Non-conventional machining processes.' In: *Fundamentals of Machining and Machine Tools, Marcel Dekker, Inc, New York* 491 (1989) (cit. on p. 15).

[66] K. Gupta, N. Jain, and R. Laubscher. 'Spark erosion machining of miniature gears: a critical review.' In: *The International Journal of Advanced Manufacturing Technology* 80.9-12 (2015), pp. 1863–1877 (cit. on pp. 15, 32, 168).

[67] E. Guitreau. 'Basic Theory - Electrical Discharge Machining.' In: *EDM Today* (1991) (cit. on pp. 15, 26, 27, 70, 77).

[68] J. Singh, M. R. Singh, and M. R. Kumar. 'Review on Effects of Process Parameters in Wire Cut EDM and Wire Electrode Development.' In: *International Journal for Innovative Research in Science and Technology* 2.11 (2016), pp. 701–706 (cit. on pp. 15, 17, 26, 77).

[69] E. Uhlmann, S. Piltz, and U. Doll. 'Machining of micro/miniature dies and moulds by electrical discharge machining - recent development.' In: *Journal of Materials Processing Technology* 167.2 (2005), pp. 488–493 (cit. on pp. 15–17).

[70] S. Kuriakose and M. Shunmugam. 'Characteristics of wire-electro discharge machined Ti6Al4V surface.' In: *Materials Letters* 58.17 (2004), pp. 2231–2237 (cit. on pp. 15, 16, 26, 27, 30).

[71] D. Scott, S. Boyina, and K. P. Rajurkar. 'Analysis and optimization of parameter combinations in wire electrical discharge machining.' In: *The International Journal Of Production Research* 29.11 (1991), pp. 2189–2207 (cit. on pp. 16, 27, 32, 33, 70, 168).

[72] A. Goswami and J. Kumar. 'Optimization in wire-cut EDM of Nimonic-80A using Taguchi's approach and utility concept.' In: *Engineering Science and Technology, an International Journal* 17.4 (2014), pp. 236–246 (cit. on pp. 16, 26, 27, 70, 77, 78).

[73] B. K. Lodhi and S. Agarwal. 'Optimization of machining parameters in WEDM of AISI D3 Steel using Taguchi Technique.' In: *Procedia CIRP* 14 (2014), pp. 194–199 (cit. on pp. 16, 26, 70, 77, 169).

[74] V. K. Pasam, S. B. Battula, P. Madar Valli, and M. Swapna. 'Optimizing surface finish in WEDM using the Taguchi parameter design method.' In: *Journal of the Brazilian Society of Mechanical Sciences and Engineering* 32.2 (2010), pp. 107–113 (cit. on pp. 16, 25–27, 70, 169).

[75] Y. Liao, J. Huang, and Y. Chen. 'A study to achieve a fine surface finish in Wire-EDM.' In: *Journal of Materials Processing Technology* 149.1 (2004), pp. 165–171 (cit. on pp. 16, 17, 26–28, 70, 75, 77, 78).

[76] F. Han, J. Jiang, and D. Yu. 'Influence of machining parameters on surface roughness in finish cut of WEDM.' In: *The International Journal of Advanced Manufacturing Technology* 34.5-6 (2007), pp. 538–546 (cit. on pp. 16, 25, 70, 78).

[77] H. Singh and A. Singh. 'Effect of pulse on/pulse off time on machining of AISI D3 die steel using copper and brass electrode in EDM.' In: *Int. J. of Engg. and Science* 1.9 (2012), pp. 19–22 (cit. on pp. 16, 26).

[78] L. Gillespie. 'Troubleshooting Manufacturing Processes: Adapted from the Tool and Manufacturing Engineers Handbook : a Reference Book for Manufacturing Engineers, Managers, and Technicians.' In: Society of Manufacturing Engineers, 1988. Chap. 2, p. 89 (cit. on p. 16).

[79] M. Manjaiah, R. F. Laubscher, A. Kumar, and S. Basavarajappa. 'Parametric optimization of MRR and surface roughness in wire electro discharge machining (WEDM) of D2 steel using Taguchi-based utility approach.' In: *International Journal of Mechanical and Materials Engineering* 11.1 (2016), p. 7 (cit. on pp. 16, 26, 169).

[80] M.-T. Yan and P.-H. Huang. 'Accuracy improvement of wire-EDM by real-time wire tension control.' In: *International Journal of Machine Tools and Manufacture* 44.7 (2004), pp. 807–814 (cit. on p. 17).

[81] A. Nee, S. Ong, and Y. Wang. 'Computer Applications in Near Net-Shape Operations.' In: Advanced Manufacturing. Springer London, 2012. Chap. 2, p. 84 (cit. on p. 17).

[82] M. P. Groover. *Fundamentals of modern manufacturing: materials processes, and systems*. John Wiley & Sons, 2007 (cit. on pp. 18, 57, 110, 121).

[83] M. Groover. *Groover's Principles of Modern Manufacturing: Materials, Processes, and Systems*. Wiley, 2016 (cit. on p. 18).

[84] M. Alauddin, M. El Baradie, and M. Hashmi. 'Optimization of surface finish in end milling Inconel 718.' In: *Journal of Materials Processing Technology* 56.1-4 (1996), pp. 54–65 (cit. on p. 21).

[85] E. Kuljanic. 'An investigation of wear in single-tooth and multi-tooth milling.' In: *International Journal of Machine Tool Design and Research* 14.1 (1974), pp. 95–109 (cit. on p. 21).

[86] P. Mativenga. 'Micromachining.' In: *CIRP Encyclopedia of Production Engineering*. Ed. by L. Laperrière and G. Reinhart. Berlin, Heidelberg: Springer Berlin Heidelberg, 2014, pp. 873–877 (cit. on p. 21).

[87] G. Bram and C. Downs. *Manufacturing Technology*. Macmillan Education, Limited, 1975 (cit. on p. 21).

[88] A. Mian, N. Driver, and P. Mativenga. 'Identification of factors that dominate size effect in micro-machining.' In: *International Journal of Machine Tools and Manufacture* 51.5 (2011), pp. 383–394 (cit. on pp. 22, 123).

[89] C.-J. Kim, M. Bono, J. Ni, et al. 'Experimental analysis of chip formation in micro-milling.' In: *TECHNICAL PAPERS-SOCIETY OF MANUFACTURING ENGINEERS-ALL SERIES-* (2002) (cit. on pp. 22, 34, 35).

[90] J. Chae, S. Park, and T. Freiheit. 'Investigation of micro-cutting operations.' In: *International Journal of Machine Tools and Manufacture* 46.3 (2006), pp. 313–332 (cit. on pp. 22, 33, 123, 126).

[91] I. Tansel, O. Rodriguez, M. Trujillo, E. Paz, and W. Li. 'Micro-end-milling - I. Wear and breakage.' In: *International Journal of Machine Tools and Manufacture* 38.12 (1998), pp. 1419–1436 (cit. on pp. 22, 34, 121–123, 139).

[92] M. Camara, J. C. Rubio, A. Abrão, and J. Davim. 'State of the art on micromilling of materials, a review.' In: *Journal of Materials Science & Technology* 28.8 (2012), pp. 673–685 (cit. on pp. 22, 33, 123, 124).

[93] K. Kanlayasiri and P. Jattakul. 'Simultaneous optimization of dimensional accuracy and surface roughness for finishing cut of wire-EDMed K460 tool steel.' In: *Precision Engineering* 37.3 (2013), pp. 556–561 (cit. on pp. 24, 26, 28, 78).

[94] C. Sommer and S. Sommer. *Complete EDM Handbook*. Advance Pub, 2005 (cit. on pp. 24, 30).

[95] M. Manjaiah, S. Narendranath, S. Basavarajappa, and V. Gaitonde. 'Investigation on material removal rate, surface and subsurface characteristics in wire electro discharge machining of Ti50Ni50-xCux shape memory alloy.' In: *Proceedings of the Institution of Mechanical Engineers, Part L: Journal of Materials: Design and Applications* 232.2 (2018), pp. 164–177 (cit. on p. 25).

[96] Y. Suziki and M. Kishi. 'Improvement of Surface Roughness in wire EDM.' In: *Proceedings of the Ninth International Symposium for Electro-Machining (ISEM-9), Nagoya, Japan*. 1989 (cit. on p. 25).

[97] R. Bobbili, V. Madhu, and A. Gogia. ‘An experimental investigation of wire electrical discharge machining of hot-pressed boron carbide.’ In: *Defence Technology* 11.4 (2015), pp. 344–349 (cit. on p. 26).

[98] S. Sarkar, S. Mitra, and B. Bhattacharyya. ‘Parametric analysis and optimization of wire electrical discharge machining of γ-titanium aluminide alloy.’ In: *Journal of Materials Processing Technology* 159.3 (2005), pp. 286–294 (cit. on pp. 26, 28, 30, 77, 78).

[99] S. S. Mahapatra and A. Patnaik. ‘Parametric optimization of wire electrical discharge machining (WEDM) process using Taguchi method.’ In: *Journal of the Brazilian Society of Mechanical Sciences and Engineering* 28.4 (2006), pp. 422–429 (cit. on pp. 26, 27, 169).

[100] D. Gimpert. ‘An ’Elementary’ Guide to Gear Inspection.’ In: *Gear Solutions* (June 2005), pp. 32–38 (cit. on pp. 26, 49).

[101] A. A. Khan, M. B. M. Ali, and N. B. M. Shaffiar. ‘Relationship of surface roughness with current and voltage during wire EDM.’ In: *Journal of Applied Sciences* 6.10 (2006), pp. 2317–2320 (cit. on pp. 26, 28, 78).

[102] Y. Liao, J. Huang, and H. Su. ‘A study on the machining-parameters optimization of wire electrical discharge machining.’ In: *Journal of materials processing technology* 71.3 (1997), pp. 487–493 (cit. on p. 27).

[103] J.-T. Huang and Y.-S. Liao. ‘Optimization of machining parameters of wire-EDM based on grey relational and statistical analyses.’ In: *International Journal of Production Research* 41.8 (2003), pp. 1707–1720 (cit. on p. 27).

[104] S. Balasubramanian and S. Ganapathy. ‘Grey relational analysis to determine optimum process parameters for wire electro discharge machining (WEDM).’ In: *International journal of engineering Science and Technology* 3.1 (2011), pp. 95–101 (cit. on p. 27).

[105] R. K. Fard, R. A. Afza, and R. Teimouri. ‘Experimental investigation, intelligent modeling and multi-characteristics optimization of dry WEDM process of Al–SiC metal matrix composite.’ In: *Journal of Manufacturing Processes* 15.4 (2013), pp. 483–494 (cit. on p. 27).

[106] R. B. Azhiri, R. Teimouri, M. G. Baboly, and Z. Leseman. ‘Application of Taguchi, ANFIS and grey relational analysis for studying, modeling and optimization of wire EDM process while using gaseous media.’ In: *The International Journal of Advanced Manufacturing Technology* 71.1-4 (2014), pp. 279–295 (cit. on p. 27).

[107] S. Hashmi. ‘Comprehensive Materials Finishing.’ In: Elsevier Science, 2016. Chap. 1.10, p. 279 (cit. on p. 28).

[108] T. R. Newton, S. N. Melkote, T. R. Watkins, R. M. Trejo, and L. Reister. ‘Investigation of the effect of process parameters on the formation and characteristics of recast layer in wire-EDM of Inconel 718.’ In: *Materials Science and Engineering: A* 513 (2009), pp. 208–215 (cit. on pp. 28, 30, 70, 167).

[109] R. Chalisgaonkar and J. Kumar. 'Investigation of the machining parameters and integrity of the work and wire surfaces after finish cut WEDM of commercially pure titanium.' In: *Journal of the Brazilian Society of Mechanical Sciences and Engineering* 38.3 (2016), pp. 883–911 (cit. on pp. 29, 30).

[110] M. Antar, S. Soo, D. Aspinwall, M. Cuttell, R. Perez, and A. Winn. 'WEDM of aerospace alloys using 'Clean Cut' generator technology.' In: *ISEM XVI, Shanghai* (2010), pp. 285–290 (cit. on pp. 29, 30, 69, 84, 88, 167).

[111] F. Balleys and C. Piantchenko. 'Surface integrity of materials machined by wire EDM machines.' In: *EDM Technology* 4 (1996), pp. 3–6 (cit. on pp. 30, 65, 167).

[112] T. A. Spedding and Z. Wang. 'Study on modeling of wire EDM process.' In: *Journal of Materials Processing Technology* 69.1 (1997), pp. 18–28 (cit. on p. 30).

[113] J. V. Jose and M. Shunmugam. 'Investigation into white layer formed on wire electrical discharge machined Ti6Al4V surface.' In: *International Journal of Machining and Machinability of Materials* 6.3-4 (2009), pp. 234–249 (cit. on pp. 30, 70).

[114] P. S. Rao, K. Ramji, and B. Satyanarayana. 'Experimental investigation and optimization of wire EDM parameters for surface roughness, MRR and White Layer in machining of aluminium alloy.' In: *Procedia Materials Science* 5 (2014), pp. 2197–2206 (cit. on pp. 30, 70).

[115] J.-P. Kruth, L. Stevens, L. Froyen, and B. Lauwers. 'Study of the white layer of a surface machined by die-sinking electro-discharge machining.' In: *CIRP Annals-Manufacturing Technology* 44.1 (1995), pp. 169–172 (cit. on p. 30).

[116] G. Cusanelli, A. Hessler-Wyser, F. Bobard, R. Demellayer, R. Perez, and R. Flükiger. 'Microstructure at submicron scale of the white layer produced by EDM technique.' In: *Journal of Materials Processing Technology* 149.1 (2004), pp. 289–295 (cit. on pp. 30, 65).

[117] D. Dudley and D. Townsend. *Dudley's gear handbook*. McGraw-Hill, 1991 (cit. on p. 31).

[118] H. Moser and W. Boehmert. 'Trends in EDM.' In: *Modern Machine Shop(USA)* 72.9 (2000), pp. 70–77 (cit. on p. 31).

[119] A. Kruusing, S. Leppävuori, A. Uusimäki, B. Petrêtis, and O. Makarova. 'Micromachining of magnetic materials.' In: *Sensors and Actuators A: Physical* 74.1 (1999), pp. 45–51 (cit. on p. 31).

[120] A. Neville, A. Morina, T. Haque, and M. Voong. 'Compatibility between tribological surfaces and lubricant additives - how friction and wear reduction can be controlled by surface/lube synergies.' In: *Tribology International* 40.10 (2007), pp. 1680–1695 (cit. on p. 31).

[121] A. Erdemir. 'Review of engineered tribological interfaces for improved boundary lubrication.' In: *Tribology International* 38.3 (2005), pp. 249–256 (cit. on p. 31).

[122] International Standards Organisation. *ISO/TR 10064-2: Cylindrical gears - Code of inspection practice - Part 2: Inspection related to radial composite deviations, runout, tooth thickness and backlash*. International Standards Organisation, 2006 (cit. on pp. 31, 44).

[123] British Standards Institution. *Spur and helical gears. Basic rack form, pitches and accuracy (diametral pitch series) [withdrawn december 2005]*. Oct. 1967 (cit. on p. 31).

[124] Deutsches Institut für Normung. *DIN3961 Tolerances for Cylindrical Gear Teeth*. Deutsches Institut für Normung, Aug. 1978 (cit. on pp. 31, 44).

[125] K. Hori and Y. Murata. 'Wire electrical discharge machining of microinvolute gears.' In: *Transactions of the Japan Society of Mechanical Engineers, Part C* 60 (1994), pp. 3957–3962 (cit. on pp. 32, 58, 168).

[126] M. Y. Ali, A. M. Karim, E. Y. T. Adesta, A. F. Ismail, A. A. Abdullah, and M. N. Idris. 'Comparative study of conventional and micro WEDM based on machining of meso/micro sized spur gear.' In: *International Journal of Precision Engineering and Manufacturing* 11.5 (2010), pp. 779–784 (cit. on pp. 32, 58, 65, 69, 86, 88, 173).

[127] A. Schoth, R. Förster, and W. Menz. 'Micro wire EDM for high aspect ratio 3D microstructuring of ceramics and metals.' In: *Microsystem technologies* 11.4-5 (2005), pp. 250–253 (cit. on p. 32).

[128] K. Takahata, N. Shibaike, and H. Guckel. 'High-aspect-ratio WC-Co microstructure produced by the combination of LIGA and micro-EDM.' In: *Microsystem Technologies* 6.5 (2000), pp. 175–178 (cit. on p. 32).

[129] K. Gupta and N. K. Jain. 'On micro-geometry of miniature gears manufactured by wire electrical discharge machining.' In: *Materials and Manufacturing Processes* 28.10 (2013), pp. 1153–1159 (cit. on pp. 32, 65).

[130] Y.-S. Liao, S.-T. Chen, and C.-S. Lin. 'Development of a high precision tabletop versatile CNC wire-EDM for making intricate micro parts.' In: *Journal of micromechanics and microengineering* 15.2 (2004), p. 245 (cit. on p. 32).

[131] G. Benavides, L. Bieg, M. Saavedra, and E. Bryce. 'High aspect ratio mesoscale parts enabled by wire micro-EDM.' In: *Microsystem Technologies* 8.6 (2002), pp. 395–401 (cit. on pp. 32, 33, 58).

[132] S. Di, R. Huang, and G. Chi. 'Study on micro-machining by micro-WEDM.' In: *2006 1st IEEE International Conference on Nano/Micro Engineered and Molecular Systems*. IEEE. 2006, pp. 615–619 (cit. on p. 32).

[133] D. Sari, D. Welling, C. Löpenhaus, F. Klocke, and A. Klink. 'Adjusting Surface Integrity of Gears Using Wire EDM to Increase the Flank Load Carrying Capacity.' In: *Procedia CIRP* 45 (2016), pp. 295–298 (cit. on pp. 32, 60, 176).

[134] K. Gupta and N. K. Jain. 'Comparative Study of Wire-EDM and Hobbing for Manufacturing High-Quality Miniature Gears.' In: *Materials and Manufacturing Processes* 29.11-12 (2014), pp. 1470–1476 (cit. on pp. 32, 58, 69, 176).

[135] H. Takeuchi, K. Nakamura, N. Shimizu, and N. Shibaike. 'Optimization of mechanical interface for a practical micro-reducer.' In: *Micro Electro Mechanical Systems, 2000. MEMS 2000. The Thirteenth Annual International Conference on*. IEEE. 2000, pp. 170–175 (cit. on pp. 32, 58).

[136] T. Özel, T. Thepsonthi, D. Ulutan, and B. Kaftanoğlu. 'Experiments and finite element simulations on micro-milling of Ti–6Al–4V alloy with uncoated and cBN coated micro-tools.' In: *CIRP Annals-Manufacturing Technology* 60.1 (2011), pp. 85–88 (cit. on p. 33).

[137] W. Bao and I. Tansel. 'Modeling micro-end-milling operations. Part I: analytical cutting force model.' In: *International Journal of Machine Tools and Manufacture* 40.15 (2000), pp. 2155–2173 (cit. on p. 33).

[138] O. Ohnishi, H. Onikura, S.-K. Min, M. Aziz, and S. Tsuruoka. 'Characteristics of grooving by micro end mills with various tool shapes and approach to their optimal shape.' In: *Memoirs of the Faculty of Engineering, Kyushu University* 67.4 (2007), pp. 143–151 (cit. on p. 33).

[139] M. Rahman, A. S. Kumar, and J. Prakash. 'Micro milling of pure copper.' In: *Journal of Materials Processing Technology* 116.1 (2001), pp. 39–43 (cit. on pp. 34, 185).

[140] Z. Yuan, M. Zhou, and S. Dong. 'Effect of diamond tool sharpness on minimum cutting thickness and cutting surface integrity in ultraprecision machining.' In: *Journal of Materials Processing Technology* 62.4 (1996), pp. 327–330 (cit. on p. 34).

[141] H. Li, X. Lai, C. Li, J. Feng, and J. Ni. 'Modelling and experimental analysis of the effects of tool wear, minimum chip thickness and micro tool geometry on the surface roughness in micro-end-milling.' In: *Journal of Micromechanics and Microengineering* 18.2 (2007), p. 025006 (cit. on p. 34).

[142] S. Filiz, C. M. Conley, M. B. Wasserman, and O. B. Ozdoganlar. 'An experimental investigation of micro-machinability of copper 101 using tungsten carbide micro-endmills.' In: *International Journal of Machine Tools and Manufacture* 47.7 (2007), pp. 1088–1100 (cit. on pp. 34, 92–94, 124).

[143] A. A. Elkaseer, S. Dimov, K. Popov, and R. Minev. 'Tool Wear in Micro-Endmilling: Material Microstructure Effects, Modeling, and Experimental Validation.' In: *Journal of Micro and Nano-Manufacturing* 2.4 (2014), p. 044502 (cit. on pp. 34, 35, 92, 93).

[144] D. L. Wissmiller and F. E. Pfefferkorn. 'Micro end mill tool temperature measurement and prediction.' In: *Journal of Manufacturing Processes* 11.1 (2009), pp. 45–53 (cit. on p. 35).

[145] A. Dhanorker, X. Liu, and T. Özel. 'Micromilling process planning and modeling for micromold manufacturing.' In: *ASME 2007 International Manufacturing Science and Engineering Conference*. American Society of Mechanical Engineers. 2007, pp. 759–769 (cit. on p. 35).

[146] N. Ikawa, S. Shimada, and H. Tanaka. 'Minimum thickness of cut in micromachining.' In: *Nanotechnology* 3.1 (1992), p. 6 (cit. on p. 35).

[147] M. Malekian, M. Mostofa, S. Park, and M. Jun. 'Modeling of minimum uncut chip thickness in micro machining of aluminum.' In: *Journal of Materials Processing Technology* 212.3 (2012), pp. 553–559 (cit. on p. 35).

[148] Y. Kita, M. Ido, and S. Hata. 'The mechanism of metal removal by an abrasive tool.' In: *Wear* 47.1 (1978), pp. 185–193 (cit. on p. 35).

[149] R. Lekkala, V. Bajpai, R. K. Singh, and S. S. Joshi. 'Characterization and modeling of burr formation in micro-end milling.' In: *Precision Engineering* 35.4 (2011), pp. 625–637 (cit. on pp. 35, 125).

[150] T.-R. Lin. 'Experimental study of burr formation and tool chipping in the face milling of stainless steel.' In: *Journal of Materials Processing Technology* 108.1 (2000), pp. 12–20 (cit. on p. 35).

[151] G.-L. Chern. 'Experimental observation and analysis of burr formation mechanisms in face milling of aluminum alloys.' In: *International Journal of Machine Tools and Manufacture* 46.12 (2006), pp. 1517–1525 (cit. on p. 35).

[152] D. Dornfeld, S. Min, and Y. Takeuchi. 'Recent advances in mechanical micromachining.' In: *CIRP Annals-Manufacturing Technology* 55.2 (2006), pp. 745–768 (cit. on pp. 35, 98, 105, 117, 188).

[153] International Standards Organisation. *ISO 8688-1: Tool life testing in milling- Part 1: Face milling*. International Standards Organisation, 1989 (cit. on pp. 35, 91, 208).

[154] International Standards Organisation. *ISO 8688-2: Tool life testing in milling - Part 2: End milling*. International Standards Organisation, 1989 (cit. on pp. 35, 91, 97, 187, 208).

[155] B. H. T. Baharudin, N. Dimou, and K. Hon. 'Tool wear behaviour of micro-tools in high speed CNC machining.' In: *Proceedings of the 34th International MATADOR Conference*. Springer. 2004, pp. 111–118 (cit. on pp. 35, 92, 107, 110, 124, 185, 187).

[156] Mitsubishi Electric. *MV4800 MACHINING CHARACTERISTICS DATA BOOK*. Verson 3.0. Mar. 2015 (cit. on p. 39).

[157] OnDrives. *Precision Gears: Spur Gears*. Tech. rep. 2015 (cit. on p. 44).

[158] G. Goch. 'Gear metrology.' In: *CIRP Annals-Manufacturing Technology* 52.2 (2003), pp. 659–695 (cit. on pp. 44, 45).

[159] American Gear Manufacturers Association. *Gear Classification and Inspection Handbook: Tolerances and Measuring Methods for Unassembled Spur and Helical Gears (including Metric Equivalents)*. AGMA standard. American Gear Manufacturers Association, 1988 (cit. on p. 45).

[160] R. Moderow. 'Gear inspection and measurement.' In: *Gear Technology* (1992), pp. 44–49 (cit. on pp. 45, 46).

[161] E. Reiter and F. Eberle. 'Practical Considerations for the Use of Double-Flank Testing for the Manufacturing Control of Gearing-Part I.' In: *Gear Technol* 31.February (2014), pp. 44–51 (cit. on p. 46).

[162] M. Pueo, J. Santolaria, R. Acero, and A. Gracia. 'A review of tangential composite and radial composite gear inspection.' In: *Precision Engineering* 50 (2017), pp. 522–537 (cit. on p. 46).

[163] J. Tang, J. Jia, Z. Fang, and Z. Shi. 'Development of a gear measuring device using DFRP method.' In: *Precision Engineering* 45 (2016), pp. 153–159 (cit. on p. 46).

[164] K. Ni, Y. Peng, D. Stöbener, and G. Goch. 'Cylindrical Gear Metrology. In: Gao W. (eds) Metrology. Precision Manufacturing.' In: Jan. 2019, pp. 1–29. DOI: `10.1007/978-981-10-4912-5_9-1` (cit. on p. 46).

[165] M. M. Auerswald, A. von Freyberg, and A. Fischer. 'Laser line triangulation for fast 3D measurements on large gears.' In: *The International Journal of Advanced Manufacturing Technology* 100.9-12 (2019), pp. 2423–2433 (cit. on p. 46).

[166] F. Balzer, M. Schäfer, I. Lindner, A. Günther, D. Stöbener, and J. Westerkamp. 'Recent advances in optical gear measurements-a new approach for fast measurements of large gears.' In: *6th International Conference on Gears, Garching, VDI-Berichte*. Vol. 2255. 2015, pp. 655–666 (cit. on p. 46).

[167] J. Seewig, M. Eifler, F. Schneider, B. Kirsch, and J. C. Aurich. 'A model-based approach for the calibration and traceability of the angle resolved scattering light sensor.' In: *Surface Topography: Metrology and Properties* 4.2 (2016), p. 024010 (cit. on p. 46).

[168] H. Muhamedsalih, F. Gao, and X. Jiang. 'Comparison study of algorithms and accuracy in the wavelength scanning interferometry.' In: *Applied optics* 51.36 (2012), pp. 8854–8862 (cit. on p. 46).

[169] B. Zhang, J. Ziegert, F. Farahi, and A. Davies. 'In situ surface topography of laser powder bed fusion using fringe projection.' In: *Additive Manufacturing* 12 (2016), pp. 100–107 (cit. on p. 47).

[170] Y. Qu, D. He, J. Yoon, B. Van Hecke, E. Bechhoefer, and J. Zhu. 'Gearbox tooth cut fault diagnostics using acoustic emission and vibration sensors - A comparative study.' In: *Sensors* 14.1 (2014), pp. 1372–1393 (cit. on p. 47).

[171] R. B. Sharma, A. Parey, and N. Tandon. 'Modelling of acoustic emission generated in involute spur gear pair.' In: *Journal of sound and vibration* 393 (2017), pp. 353–373 (cit. on p. 47).

[172] R. L. Thoen. 'Measuring Base Helix Error on a Sine Bar.' In: *Gear Technology* (2001), pp. 25–27 (cit. on p. 48).

[173] P. Russell, D. Batchelor, and J. Thornton. 'SEM and AFM: complementary techniques for high resolution surface investigations.' In: *Veeco Instruments Inc., AN46, Rev A* 1 (2001), p. 2004 (cit. on p. 55).

[174] P. Goodhew, J. Humphreys, and R. Beanland. *Electron Microscopy and Analysis, Third Edition*. Taylor & Francis, 2000 (cit. on p. 55).

[175] G. Kibria, M. Jahan, and B. Bhattacharyya. *Micro-electrical Discharge Machining Processes: Technologies and Applications*. Materials Forming, Machining and Tribology. Springer Singapore, 2018 (cit. on p. 57).

[176] D. Zhu. 'Elastohydrodynamic Lubrication (EHL).' In: *Encyclopedia of Tribology*. Ed. by Q. J. Wang and Y.-W. Chung. Boston, MA: Springer US, 2013, pp. 874–889 (cit. on p. 57).

[177] K. Johnson, J. Greenwood, and S. Poon. 'A simple theory of asperity contact in elastohydro-dynamic lubrication.' In: *Wear* 19.1 (1972), pp. 91–108 (cit. on p. 57).

[178] K. Gupta and N. K. Jain. 'Analysis and optimization of micro-geometry of miniature spur gears manufactured by wire electric discharge machining.' In: *Precision Engineering* 38.4 (2014), pp. 728–737 (cit. on p. 57).

[179] R. Williams and K. P. Rajurkar. 'Study of wire electrical discharge machined surface characteristics.' In: *Journal of materials processing technology* 28.1-2 (1991), pp. 127–138 (cit. on p. 60).

[180] Alicona. *Alicona's Guide to Optical Roughness Measurement*. Alicona Imaging GmbH. Dr.-Auner-Strasse 21a, 8074 Raaba/Graz, Austria, 2015 (cit. on pp. 65, 72, 79, 86).

[181] G. F. Royo. *Improvement of electro-discharge machining performance by radio frequency control and orbital motion movement*. 1988 (cit. on p. 65).

[182] Mitsubishi. *WIRE-CUT EDM SYSTEMS MV4800 - MACHINING CHARACTERISTICS DATA BOOK*. Version 3.0. Mitsubishi Electric. Mitsubishi Electric Corporation, Nagoya Works, EDM Systems Dept., EDM Application Technology Section, Mar. 2015 (cit. on p. 72).

[183] N. Tague. *The Quality Toolbox, Second Edition*. ASQ Quality Press, 2005. URL: `https://books.google.co.uk/books?id=G3c6S0mzLQgC` (cit. on p. 74).

[184] J. D. Brown. 'Standard error vs. Standard error of measurement.' In: *JALT Testing & Evaluation SIG Newsletter* 3.1 (Apr. 1999), pp. 20–25 (cit. on p. 78).

[185] Ł. Orzech. 'Acoustic effects of single electrostatic discharges.' In: *Journal of Physics: Conference Series*. Vol. 646. 1. IOP Publishing. 2015, p. 012040 (cit. on p. 79).

[186] Y. Lok and T. Lee. 'Processing of advanced ceramics using the wire-cut EDM process.' In: *Journal of Materials Processing Technology* 63.1-3 (1997), pp. 839–843 (cit. on p. 81).

[187] C. Li, X. Lai, H. Li, and J. Ni. 'Modeling of three-dimensional cutting forces in micro-end-milling.' In: *Journal of Micromechanics and Microengineering* 17.4 (2007), p. 671 (cit. on p. 92).

[188] H. Li, X. Lai, C. Li, J. Feng, and J. Ni. 'Modelling and experimental analysis of the effects of tool wear, minimum chip thickness and micro tool geometry on the surface roughness in micro-end-milling.' In: *Journal of micromechanics and microengineering* 18.2 (2007), p. 025006 (cit. on p. 92).

[189] M. Malekian, S. S. Park, and M. B. Jun. 'Tool wear monitoring of micro-milling operations.' In: *Journal of Materials Processing Technology* 209.10 (2009), pp. 4903–4914 (cit. on pp. 93, 155, 185).

[190] K.-M. Li and S.-Y. Chou. 'Experimental evaluation of minimum quantity lubrication in near micro-milling.' In: *Journal of materials processing technology* 210.15 (2010), pp. 2163–2170 (cit. on p. 93).

[191] H. Ding, N. Shen, and Y. C. Shin. 'Experimental evaluation and modeling analysis of micromilling of hardened H13 tool steels.' In: *Journal of Manufacturing Science and Engineering* 133.4 (2011), p. 041007 (cit. on p. 93).

[192] J. Bai, Q. Q Bai, and Z. Tong. 'Experimental and multiscale numerical investigation of wear mechanism and cutting performance of polycrystalline diamond tools in micro-end-milling of titanium alloy Ti-6Al-4V.' In: *International Journal of Refractory Metals and Hard Material* (2018) (cit. on p. 93).

[193] X. Teng, D. Huo, I. Shyha, W. Chen, and E. Wong. 'An experimental study on tool wear behaviour in micro milling of nano Mg/Ti metal matrix composites.' In: *International Journal of Advanced Manufacturing Technology* (2018) (cit. on pp. 93, 124).

[194] G. Strnad and J. Buhagiar. 'Latest developments in PVD coatings for tooling.' In: *Scientific Bulletin of the" Petru Maior" University of Targu Mures* 7.1 (2010), p. 32 (cit. on p. 94).

[195] K. A. Vikram, C. Ratnam, K. S. Narayana, and B. S. Ben. 'Assessment of surface roughness and MRR while machining brass with HSS tool and carbide inserts.' In: (2015) (cit. on p. 94).

[196] V. P. Astakhov and J. P. Davim. 'Tools (geometry and material) and tool wear.' In: *Machining: Fundamentals and Recent Advances* (2008), pp. 29–57 (cit. on p. 94).

[197] T. Masuzawa. 'State of the art of micromachining.' In: *CIRP Annals-Manufacturing Technology* 49.2 (2000), pp. 473–488 (cit. on pp. 98, 188).

[198] N. Taniguchi. 'Current status in, and future trends of, ultraprecision machining and ultrafine materials processing.' In: *CIRP Annals-Manufacturing Technology* 32.2 (1983), pp. 573–582 (cit. on p. 98).

[199] F. Fang, H. Wu, X. Liu, Y. Liu, and S. Ng. 'Tool geometry study in micromachining.' In: *Journal of Micromechanics and Microengineering* 13.5 (2003), p. 726 (cit. on p. 105).

[200] J. Fleischer, M. Deuchert, C. Ruhs, C. Kühlewein, G. Halvadjiysky, and C. Schmidt. 'Design and manufacturing of micro milling tools.' In: *Microsystem Technologies* 14.9-11 (2008), pp. 1771–1775 (cit. on p. 105).

[201] S. Afazov, D. Zdebski, S. Ratchev, J. Segal, and S. Liu. 'Effects of micro-milling conditions on the cutting forces and process stability.' In: *Journal of Materials Processing Technology* 213.5 (2013), pp. 671–684 (cit. on p. 116).

[202] P. Mativenga and K. Hon. 'An experimental study of cutting forces in high-speed end milling and implications for dynamic force modeling.' In: *Journal of Manufacturing Science and Engineering* 127.2 (2005), pp. 251–261 (cit. on p. 117).

[203] D. Kim and D. Jeon. 'Fuzzy-logic control of cutting forces in CNC milling processes using motor currents as indirect force sensors.' In: *Precision Engineering* 35.1 (2011), pp. 143–152 (cit. on p. 117).

[204] W. Knight and G. Boothroyd. *Fundamentals of Metal Machining and Machine Tools, Third Edition*. Manufacturing engineering and materials processing. Taylor & Francis, 2005 (cit. on p. 118).

[205] V. P. Astakhov. *Tribology of metal cutting*. Vol. 52. Elsevier, 2006 (cit. on p. 121).

[206] X. Liu, R. DeVor, S. Kapoor, and K. Ehmann. 'The mechanics of machining at the microscale: assessment of the current state of the science.' In: *Journal of manufacturing science and engineering* 126.4 (2004), pp. 666–678 (cit. on p. 123).

[207] X. Lai, H. Li, C. Li, Z. Lin, and J. Ni. 'Modelling and analysis of micro scale milling considering size effect, micro cutter edge radius and minimum chip thickness.' In: *International Journal of Machine Tools and Manufacture* 48.1 (2008), pp. 1–14 (cit. on p. 123).

[208] J. Saedon, S. Soo, D. Aspinwall, A. Barnacle, and N. H. Saad. 'Prediction and optimization of tool life in micromilling AISI D2 (62 HRC) hardened steel.' In: *Procedia Engineering* 41 (2012), pp. 1674–1683 (cit. on p. 123).

[209] A. Sarhan, R. Sayed, A. Nassr, and R. El-Zahry. 'Interrelationships between cutting force variation and tool wear in end-milling.' In: *Journal of Materials Processing Technology* 109.3 (2001), pp. 229–235 (cit. on p. 124).

[210] B. H. T. Baharudin, N. Dimou, and K. Hon. 'Tool wear behaviour of micro-tools in high speed CNC machining.' In: *Proceedings of the 34th International MATADOR Conference*. Springer. 2004, pp. 111–118 (cit. on p. 124).

[211] A. Rajabi, M. J. Ghazali, J. Syarif, and A. Daud. 'Development and application of tool wear: a review of the characterization of TiC-based cermets with different binders.' In: *Chemical Engineering Journal* 255 (2014), pp. 445–452 (cit. on pp. 124, 138).

[212] S. N. B. Oliaei and Y. Karpat. 'Influence of tool wear on machining forces and tool deflections during micro milling.' In: *The International Journal of Advanced Manufacturing Technology* 84.9-12 (2016), pp. 1963–1980 (cit. on pp. 124, 141).

[213] Y.-J. Lin, A. Agrawal, and Y. Fang. 'Wear progressions and tool life enhancement with AlCrN coated inserts in high-speed dry and wet steel lathing.' In: *Wear* 264.3-4 (2008), pp. 226–234 (cit. on p. 125).

[214] A. Zareena and S. Veldhuis. 'Tool wear mechanisms and tool life enhancement in ultra-precision machining of titanium.' In: *Journal of Materials Processing Technology* 212.3 (2012), pp. 560–570 (cit. on pp. 125, 139).

[215] M. Lahres, P. Müller-Hummel, and O. Doerfel. 'Applicability of different hard coatings in dry milling aluminium alloys.' In: *Surface and Coatings Technology* 91.1-2 (1997), pp. 116–121 (cit. on p. 125).

[216] R. Bian, N. He, W. Ding, and S. Liu. 'A study on the tool wear of PCD micro end mills in ductile milling of ZrO 2 ceramics.' In: *The International Journal of Advanced Manufacturing Technology* 92.5-8 (2017), pp. 2197–2206 (cit. on p. 125).

[217] F. Dweiri, M. Al-Jarrah, and H. Al-Wedyan. 'Fuzzy surface roughness modeling of CNC down milling of Alumic-79.' In: *Journal of Materials Processing Technology* 133.3 (2003), pp. 266–275 (cit. on p. 125).

[218] H. Prengel, W. Pfouts, and A. Santhanam. 'State of the art in hard coatings for carbide cutting tools.' In: *Surface and Coatings Technology* 102.3 (1998), pp. 183–190 (cit. on p. 126).

[219] D. Neves, A. E. Diniz, and M. S. F. Lima. 'Microstructural analyses and wear behavior of the cemented carbide tools after laser surface treatment and PVD coating.' In: *Applied Surface Science* 282 (2013), pp. 680–688 (cit. on p. 126).

[220] D. Biermann, M. Steiner, and E. Krebs. 'Investigation of different hard coatings for micromilling of austenitic stainless steel.' In: *Procedia Cirp* 7 (2013), pp. 246–251 (cit. on p. 126).

[221] G. Fox-Rabinovich, A. Kovalev, M. Aguirre, B. Beake, K. Yamamoto, S. Veldhuis, J. Endrino, D. Wainstein, and A. Rashkovskiy. 'Design and performance of AlTiN and TiAlCrN PVD coatings for machining of hard to cut materials.' In: *Surface and coatings technology* 204.4 (2009), pp. 489–496 (cit. on pp. 126, 141).

[222] M. Faga, G. Gautier, R. Calzavarini, M. Perucca, E. A. Boot, F. Cartasegna, and L. Settineri. 'AlSiTiN nanocomposite coatings developed via Arc Cathodic PVD: Evaluation of wear resistance via tribological analysis and high speed machining operations.' In: *Wear* 263.7-12 (2007), pp. 1306–1314 (cit. on p. 126).

[223] X. Sui, G. Li, X. Qin, H. Yu, X. Zhou, K. Wang, and Q. Wang. 'Relationship of microstructure, mechanical properties and titanium cutting performance of TiAlN/TiAlSiN composite coated tool.' In: *Ceramics International* 42.6 (2016), pp. 7524–7532 (cit. on pp. 126, 147).

[224] L. Dobrzański and D. Pakuła. 'Comparison of the structure and properties of the PVD and CVD coatings deposited on nitride tool ceramics.' In: *Journal of Materials Processing Technology* 164 (2005), pp. 832–842 (cit. on p. 127).

[225] P. Hedenqvist and M. Olsson. 'Sliding wear testing of coated cutting tool materials.' In: *Tribology International* 24.3 (1991), pp. 143–150 (cit. on p. 127).

[226] D. Jianxin, L. Jianhua, Z. Jinlong, S. Wenlong, and N. Ming. 'Friction and wear behaviors of the PVD ZrN coated carbide in sliding wear tests and in machining processes.' In: *Wear* 264.3-4 (2008), pp. 298–307 (cit. on pp. 127, 138).

[227] L. Aihua, D. Jianxin, C. Haibing, C. Yangyang, and Z. Jun. 'Friction and wear properties of TiN, TiAlN, AlTiN and CrAlN PVD nitride coatings.' In: *International Journal of Refractory Metals and Hard Materials* 31 (2012), pp. 82–88 (cit. on pp. 127, 143).

[228] H. Shao, L. Liu, and H. Qu. 'Machinability study on 3% Co–12% Cr stainless steel in milling.' In: *Wear* 263.1-6 (2007), pp. 736–744 (cit. on p. 128).

[229] Q. Chen and G. A. Thouas. 'Metallic implant biomaterials.' In: *Materials Science and Engineering: R: Reports* 87 (2015), pp. 1–57 (cit. on p. 129).

[230] C. Elias, J. Lima, R. Valiev, and M. Meyers. 'Biomedical applications of titanium and its alloys.' In: *Jom* 60.3 (2008), pp. 46–49 (cit. on p. 129).

[231] J. R. Davis. *Handbook of materials for medical devices*. ASM international, 2006 (cit. on p. 129).

[232] C. Nobel, F. Klocke, D. Lung, and S. Wolf. 'Machinability enhancement of lead-free brass alloys.' In: *Procedia CIRP* 14 (2014), pp. 95–100 (cit. on pp. 138, 143).

[233] N. Corduan, T. Himbart, G. Poulachon, M. Dessoly, M. Lambertin, J. Vigneau, and B. Payoux. 'Wear mechanisms of new tool materials for Ti-6AI-4V high performance machining.' In: *CIRP Annals* 52.1 (2003), pp. 73–76 (cit. on p. 138).

[234] X. Cheng, Z. Wang, K. Nakamoto, and K. Yamazaki. 'A study on the micro tooling for micro/nano milling.' In: *The International Journal of Advanced Manufacturing Technology* 53.5-8 (2011), pp. 523–533 (cit. on p. 138).

[235] M. Nouari and H. Makich. 'On the physics of machining titanium alloys: interactions between cutting parameters, microstructure and tool wear.' In: *Metals* 4.3 (2014), pp. 335–358 (cit. on p. 139).

[236] A. Ginting and M. Nouari. 'Surface integrity of dry machined titanium alloys.' In: *International Journal of Machine Tools and Manufacture* 49.3-4 (2009), pp. 325–332 (cit. on p. 139).

[237] A.-S. Dehlinger, F. Lapostolle, S. Lamy, O. Rapaud, C. Meunier, V. Brien, D. Klein, and C. Coddet. 'Influence of Cr and Si addition on structural and mechanical properties of TiAlN coatings reactively sputter deposited.' In: *Plasma Processes and Polymers* 4.S1 (2007), S588–S592 (cit. on p. 140).

[238] C. Feng, S. Hu, Y. Jiang, N. Wu, M. Li, L. Xin, S. Zhu, and F. Wang. 'Effects of Si content on microstructure and mechanical properties of TiAlN/Si3N4-Cu nanocomposite coatings.' In: *Applied Surface Science* 320 (2014), pp. 689–698 (cit. on p. 140).

[239] I. Ucun, K. Aslantas, and F. Bedir. 'An experimental investigation of the effect of coating material on tool wear in micro milling of Inconel 718 super alloy.' In: *Wear* 300.1 (2013), pp. 8–19 (cit. on pp. 141, 149).

[240] M. Faga, G. Gautier, R. Calzavarini, M. Perucca, E. A. Boot, F. Cartasegna, and L. Settineri. 'AlSiTiN nanocomposite coatings developed via Arc Cathodic PVD: Evaluation of wear resistance via tribological analysis and high speed machining operations.' In: *Wear* 263.7-12 (2007), pp. 1306–1314 (cit. on pp. 143, 147).

[241] N. Corduan, T. Himbart, G. Poulachon, M. Dessoly, M. Lambertin, J. Vigneau, and B. Payoux. 'Wear mechanisms of new tool materials for Ti-6AI-4V high performance machining.' In: *CIRP Annals* 52.1 (2003), pp. 73–76 (cit. on p. 145).

[242] Y. Altintas and X. Jin. 'Mechanics of micro-milling with round edge tools.' In: *CIRP Annals-Manufacturing Technology* 60.1 (2011), pp. 77–80 (cit. on p. 156).

[243] T. Özel and T. Altan. 'Process simulation using finite element method - prediction of cutting forces, tool stresses and temperatures in high-speed flat end milling.' In: *International Journal of Machine Tools and Manufacture* 40.5 (2000), pp. 713–738 (cit. on pp. 156, 163).

[244] G. Bissacco, H. N. Hansen, and J. Slunsky. 'Modelling the cutting edge radius size effect for force prediction in micro milling.' In: *CIRP Annals-Manufacturing Technology* 57.1 (2008), pp. 113–116 (cit. on pp. 156, 163).

[245] M. N. Nasr, E.-G. Ng, and M. Elbestawi. 'Modelling the effects of tool-edge radius on residual stresses when orthogonal cutting AISI 316L.' In: *International Journal of Machine Tools and Manufacture* 47.2 (2007), pp. 401–411 (cit. on pp. 156, 163).

[246] R. Khurmi and J. Gupta. *Machine Design*. Eurasia Publishing House, 2005 (cit. on p. 156).

[247] T. Özel and T. Altan. 'Determination of workpiece flow stress and friction at the chip–tool contact for high-speed cutting.' In: *International Journal of Machine Tools and Manufacture* 40.1 (2000), pp. 133–152 (cit. on p. 156).

[248] J. Jam and V. Fard. 'A novel method to determine tool-chip thermal contact conductance in machining.' In: *IJEST* 3.12 (2011) (cit. on p. 156).

[249] A. Torres, I. Puertas, and C. Luis. 'Modelling of surface finish, electrode wear and material removal rate in electrical discharge machining of hard-to-machine alloys.' In: *Precision Engineering* 40 (2015), pp. 33–45 (cit. on p. 168).

[250] S. Enache and C. Opran. 'Dynamic stability of the technological machining system in EDM.' In: *CIRP annals* 42.1 (1993), pp. 209–214 (cit. on p. 168).

[251] R. Ramakrishnan and L. Karunamoorthy. 'Multi response optimization of wire EDM operations using robust design of experiments.' In: *The International Journal of Advanced Manufacturing Technology* 29.1-2 (2006), pp. 105–112 (cit. on p. 169).

[252] K. Zakaria, Z. Ismail, N. Redzuan, and K. Dalgarno. 'Effect of wire EDM cutting parameters for evaluating of Additive Manufacturing Hybrid Metal Material.' In: *Procedia Manufacturing* 2 (2015), pp. 532–537 (cit. on p. 169).

[253] A. Ikram, N. A. Mufti, M. Q. Saleem, and A. R. Khan. 'Parametric optimization for surface roughness, kerf and MRR in wire electrical discharge machining (WEDM) using Taguchi design of experiment.' In: *Journal of Mechanical Science and Technology* 27.7 (2013), pp. 2133–2141 (cit. on p. 169).

[254] J. Antony. *Design of Experiments for Engineers and Scientists*. Elsevier Science, 2003 (cit. on p. 169).

[255] D. Montgomery. *Design and Analysis of Experiments, Minitab Manual*. Student solutions manual. John Wiley & Sons, 2010 (cit. on pp. 169, 170).

[256] R. Roy. *Design of Experiments Using The Taguchi Approach: 16 Steps to Product and Process Improvement*. A Wiley-Interscience publication. Wiley, 2001 (cit. on p. 170).

[257] P. Ross. *Taguchi Techniques for Quality Engineering: Loss Function, Orthogonal Experiments, Parameter and Tolerance Design*. McGraw-Hill, 1996 (cit. on p. 171).

[258] B. D. H. *Total Quality Management, (Revised Edition)*. Pearson, 2011 (cit. on p. 171).

[259] R. Fisher. *Statistical Methods for Research Workers*. Hafner, Collier-Macmillan, 1970. URL: https://books.google.co.uk/books?id=sx8utAEACAAJ (cit. on p. 174).

[260] L. Li, Y. Guo, X. Wei, and W. Li. 'Surface integrity characteristics in wire-EDM of Inconel 718 at different discharge energy.' In: *Procedia CirP* 6 (2013), pp. 220–225 (cit. on p. 176).

[261] K. Gupta, S. K. Chaube, and N. Jain. 'Exploring wire-EDM for manufacturing the high quality meso-gears.' In: *Procedia Materials Science* 5 (2014), pp. 1755–1760 (cit. on p. 176).

[262] I. Ucun, K. Aslantas, and F. Bedir. 'The performance of DLC-coated and uncoated ultra-fine carbide tools in micromilling of Inconel 718.' In: *Precision Engineering* 41 (2015), pp. 135–144 (cit. on p. 185).

[263] R. Piquard, A. D'Acunto, P. Lahuerte, and D. Dudzinski. 'Micro-end milling of NiTi biomedical alloys, burr formation and phase transformation.' In: *Precision Engineering* 38.2 (2014), pp. 356–364 (cit. on p. 185).

[264] M. B. Sorte and H. Shaikh. 'Optimisation of the Cutting Parameters of Milling - A Review.' In: *International Journal of Engineering Sciences and Management Research* 2.10 (Oct. 2015), pp. 126–131 (cit. on p. 185).

[265] N. Yusup, A. M. Zain, and S. Z. M. Hashim. 'Evolutionary techniques in optimizing machining parameters: Review and recent applications (2007–2011).' In: *Expert Systems with Applications* 39.10 (2012), pp. 9909–9927 (cit. on p. 185).

[266] A. Aggarwal and H. Singh. 'Optimization of machining techniques - a retrospective and literature review.' In: *Sadhana* 30.6 (2005), pp. 699–711 (cit. on p. 185).

[267] B. J. Sauser, J. E. Ramirez-Marquez, D. Henry, D. DiMarzio, et al. 'A system maturity index for the systems engineering life cycle.' In: *International Journal of Industrial and Systems Engineering* 3.6 (2008), p. 673 (cit. on p. 186).

[268] B. Sick. 'On-line and indirect tool wear monitoring in turning with artificial neural networks: a review of more than a decade of research.' In: *Mechanical systems and signal processing* 16.4 (2002), pp. 487–546 (cit. on p. 186).

[269] A. Ghasempoor, T. Moore, and J. Jeswiet. 'On-line wear estimation using neural networks.' In: *Proceedings of the Institution of Mechanical Engineers, Part B: Journal of Engineering Manufacture* 212.2 (1998), pp. 105–112 (cit. on p. 186).

[270] T. Vorburger and E. Teague. 'Optical techniques for on-line measurement of surface topography.' In: *Precision Engineering* 3.2 (1981), pp. 61–83 (cit. on p. 186).

[271] D. Dimla Sr and P. Lister. 'On-line metal cutting tool condition monitoring.: I: force and vibration analyses.' In: *International Journal of Machine Tools and Manufacture* 40.5 (2000), pp. 739–768 (cit. on p. 186).

[272] J.-S. Kim, M.-C. Kang, B.-J. Ryu, and Y.-K. Ji. 'Development of an on-line tool-life monitoring system using acoustic emission signals in gear shaping.' In: *International Journal of Machine Tools and Manufacture* 39.11 (1999), pp. 1761–1777 (cit. on p. 186).

[273] R. Pavel, I. Marinescu, M. Deis, and J. Pillar. 'Effect of tool wear on surface finish for a case of continuous and interrupted hard turning.' In: *Journal of Materials Processing Technology* 170.1-2 (2005), pp. 341–349 (cit. on p. 201).

[274] L. Alhadeff, D. Curtis, M. Marshall, and T. Slatter. 'The Application of Wire Electrical Discharge Machining (WEDM) in the Prototyping of Miniature Brass Gears.' In: *Procedia CIRP* 77 (2018), pp. 642–645 (cit. on pp. 206, 211).

[275] L. Alhadeff, M. Marshall, and T. Slatter. 'The influence of tool coating on the length of the normal operating region (steady-state wear) for micro end mills.' In: *Precision Engineering* (2019) (cit. on p. 209).

[276] L. Alhadeff, M. Marshall, and T. Slatter. 'Wear data for trials machining brass, titanium grade 2 and Hastelloy in order to characterize wear of micro-tools.' In: *Data in Brief* (2018) (cit. on p. 210).

[277] L. Alhadeff, M. Marshall, D. Curtis, and T. Slatter. ‘Protocol for tool wear measurement in micro-milling.’ In: *Wear* 420 (2019), pp. 54–67 (cit. on p. 212).